Engineering the Catalysis of Selected Metals in the Oxidation of Biomass Derivatives using DFT Calculations

Toyese Oyegoke

Numéro National de Thèse : 2023ENSL0011

THESE

en vue de l'obtention du grade de Docteur, délivré par

l'ECOLE NORMALE SUPERIEURE DE LYON

Ecole Doctorale N° 206

Ecole Doctorale Chimie (Chimie, Procédés et Environnement)

Discipline : Chimie

Soutenue publiquement le 24/03/2023, par :

Toyese OYEGOKE

Engineering the Catalysis of Selected Metals in the Oxidation of Biomass Derivatives Using DFT Calculations

Ingénierie de la catalyse de métaux sélectionnés dans l'oxydation des dérivés de la biomasse à l'aide de calculs DFT

Devant le jury composé de :

Anne MILET	Professeure des Universités, Université Grenoble Alpes, Département de Chimie Moléculaire, Grenoble, France	Rapporteure
Jean-François PAUL	Professeur des Universités, Université de Lille, Unité de Catalyse et Chimie du Solide Modélisation et Spectroscopie, Lille, France	Rapporteur
Pascal FONGARLAND	Professeur des Universités, Université Claude Bernard, Catalyse, Polymérisation, Procédés et Matériaux (CP2M), Lyon, France	Membre du Jury
Carine MICHEL	Chargée de Recherche-HDR, Laboratoire de Chimie, ENS de Lyon, France.	Directrice de Thèse
Baba El-Yakubu JIBRIL	Professeur, Université Ahmadu Bello, Département de Génie Chimique, Centre de Recherche en Catalyse PTDF, Zaria, Nigeria.	Co-directeur de Thèse

My heartfelt thanks go to Almighty God ("Balogun Ọkọ Mi, Olugbeja Mi, Ọlọrun Alaileyipada, ati Aduro Tini"), who created me, guided me, and ensured the success of this research and the entire doctoral degree program. I am grateful to God for making me the son of uneducated parents from a humble background and the holder of the highest degree from a prestigious French university. The journey has not been smooth. There was a COVID-19 crisis, lockdown, front & back, roundabout, up & down, and much more, but His grace and strength eased it and made the journey successful, with a bunch of knowledge and experience gained in the course to show for the success of the research journey.

For those reasons, I return all honor and adoration to the God of gods. Moreover, I dedicate this thesis to Almighty God for the abundance of His grace, mercy, and favor that have kept me moving throughout my life and the program.

Acknowledgment

With a grateful heart, I would like to acknowledge the tremendous academic motherly support, direction, guidance, patience, and understanding of my thesis director, Dr. Carine MICHEL, who spends her time both day and night despite her tight schedule to ensure that this research reaches a successful completion stage, as well as a lot more that I cannot mention here. In addition, the support, guidance, and patience of my international co-supervisor, Prof. Baba El-Yakubu JIBRIL, and my other team member, Dr. Stephane STEINMANN, cannot be overemphasized, for their availability, professional guidance, recommendations, innovation, and support, which have resulted in the successful completion of the study. Also, I want to acknowledge the support of my CST committee, jury committee, and thesis examiners for giving their precious time and interest in contributing to the success of the thesis, despite their busy schedules. I appreciate them all.

Moreover, I cannot go further without acknowledging the great support and guidance my parents (Mr. Mathew & Mrs. Rebecca OYEGOKE) have given me since high school, including investing their hard-earned money to ensure that my younger siblings and I get highly educated, even though they were themselves uneducated. This was because, without their readiness to finance my earlier studies (Primary, SSCE, BEng, and MSc), this program would have just ended up as a dream without becoming a reality. I appreciate them all, and may God keep them to enjoy the fruit of their hard labor, in Jesus' name (Amen).

Furthermore, I would like to appreciate the financial support of the Petroleum Technology Development Fund Overseas Scholarship (PTDF Abuja, Nigeria), the ENS de Lyon International Doctoral Co-Fund (ENS de Lyon, France), the Agence Nationale de la Recherche (ANR - iNGENCAT Group Project Fund, France), the Complementary Funding (Laboratoire de Chimie, ENS de Lyon, France), and Ahmadu Bello University Zaria, Nigeria for giving me the time to go for study, which has helped my doctoral program attain a successful completion. In addition, they provided financial support for several conferences where I presented. I count it as a huge privilege and cannot

underestimate its value. I am also grateful to the management of the Pôle Scientifique de Modélisation Numérique (PSMN) for letting me use their computing resources. This support lets me do all my calculations using a wide range of nodes, CPUs, and memories.

Also, I would like to acknowledge the support of the laboratory head (Stéphane PAROLA), respected permanent researchers (Dr. David LOFFREDA and Dr. Tangui LE BAHERS), post-doctoral researchers (Dr. Carles MARTI and Dr. Sarit DUTTA), and other fellow doctoral students (Nawras ABIDI, Laleh ALLAHKARAM, and Sarah BLANCK) of the theoretical axes of Laboratoire de Chimie (ENS de Lyon) for their contributions during my doctoral program. I cannot move on without appreciating the support of lab administration & IT staff, especially Christian MELKONIAN (for his IT support and some other subjects) and Edwige ROYBOZ (for her hospitality, patience, guidance, kindness, and administrative support).

Ultimately, I would like to acknowledge the support of Prof. Albert B. OGUNKOYA, Prof. Adegboyega S. OLAWALE, Prof. Joseph. O. ODIGURE, Prof. Sunday M. OLAKUNLE, Prof. Adamu UZAIRU, Dr. Umaru MUSA (lecturer that gave me a sound foundation in research and communication for public speaking during my undergraduate research as my first project supervisor), and other respected professors for their academic advice; my dear wife (Dr. Ayandunmola F. OYEGOKE), my younger ones (Folashade OYEGOKE, Ademola OYEGOKE, and Adepeju A. OYEGOKE), the Pencil Team members, and other vessels (Mrs. Victoria OMOTOSHO, Engr. Caleb SAMBO, Engr. Gideon MARCUS, Pastor Ben HARDIN, Engr. John OLOTU, Mr. Adeolu R. ADENIYI, Dr. Olumide OWOADE, Rev. Paul ADEYEMO, Mr. Sunday OLUWASANMI, Mr. & Mrs. Simon ADEDIRAN, Mr. Maxwell KODUA, Engr. Ruth AWUKUBOAHEMAA, and others) that have contributed to the success of my program in one way or another. I sincerely pray that Almighty God blesses and richly rewards you all accordingly, in Jesus' name (Amen).

Table of Contents

Abstract

Hydroxymethyl furfural (HMF) and furfural (FF) have been identified as key bio-refinery platforms for the synthesis of new materials. The conversion of these platform molecules into intermediates increasingly relies on heterogeneous catalysis rather than the enzymatic approach in recent years. One of these catalytic processes is the oxidation of HMF and FF to 2,5-furan dicarboxylic acid (FDCA) and furoic acid (FA), using O_2 as oxidant and supported gold catalysts. However, oxidation faces degradation challenges when using heterogeneous catalysts, leading to low yield and poor selectivity for FDCA and FA. In this thesis, we proposed a redesign strategy of the Au catalyst to retard the degradation activities reported in the oxidation of biomass derivatives (HMF and FF) on Au. Our study uses a theoretical approach based on the periodic density functional theory. First, we showed that the activation of O_2 when working in a liquid water environment is metal dependent: OH forms on Au, while O forms on Pt and Pd. Then, the oxidation and degradation pathways of HMF and FF on Au were identified by computing the stability of possible surface intermediates. This study shows that the alcohol function is more difficult to oxidize than the aldehyde function in HMF and this step is probably the rate-determining step. Regarding degradation, the furan ring's C-H is the most sensitive to oxidation compared with other routes examined. Analysis of the same reaction on Pt and Pd shows the mechanism to be the same, with greater stability of intermediates leading to higher activity but also higher degradation. Finally, the effect of alloying on Au catalysis was evaluated, showing that AuPd alloy improves the kinetics, while AuPt alloy improves HMF oxidation selectivity and delays degradation activity. Our study suggests alloying Pt and Au to retard HMF degradation, the main threat. Alternatively, alloying Pt and Pd with Au to form a trimetallic alloy would improve kinetics and retard HMF degradation.

Keywords: Heterogeneous Catalysis, Reaction Engineering, Green Chemistry, Oxidation, Degradation, Selectivity.

Resume

L'hydroxyméthyl furfural (HMF) et le furfural (FF) ont été identifiés comme des plateformes clés de bio-raffinage permettant la synthèse de nouveaux matériaux. La conversion de ces molécules plateformes en intermédiaires repose de plus en plus sur la catalyse hétérogène plutôt que l'approche enzymatique ces dernières années. L'un de ces procédés catalytiques est l'oxydation du HMF et du FF en acide 2,5-furane dicarboxylique (FDCA) et en acide furoïque (FA), en utilisant O_2 comme oxydant et des catalyseurs d'or supportés. Cependant, contrôler finement l'oxydation est difficile et ces procédés souffrent généralement de dégradation lors de l'utilisation de catalyseurs hétérogènes, conduisant à un faible rendement et une mauvaise sélectivité pour le FDCA et le FA. Dans cette thèse, nous cherchons à proposer une stratégie de reconception du catalyseur Au pour retarder les activités de dégradation rapportées dans l'oxydation des dérivés de la biomasse (HMF et FF) sur Au. Nous utilisons une approche théorique basée sur la théorie fonctionnelle de la densité périodique. Tout d'abord, nous avons montré que l'activation de O_2 lorsque l'on travaille dans un environnement d'eau liquide dépend du métal : OH se forme sur Au, tandis que O se forme sur Pt et Pd. Ensuite, les voies d'oxydation et de dégradation de HMF et FF sur Au ont été identifiées en calculant la stabilité des intermédiaires de surface possibles. Cette étude montre que la fonction alcool est plus difficile à oxyder que la fonction aldéhyde dans le HMF et cette étape est probablement l'étape cinétiquement déterminante. En ce qui concerne la dégradation, les liaisons C-H du cycle furane du HMF sont les plus sensibles à l'oxydation par rapport aux autres voies examinées. L'analyse de la même réaction sur Pt & Pd montre que le mécanisme est le même, avec une plus grande stabilité des intermédiaires conduisant à une plus grande activité mais aussi à une dégradation plus importante. Enfin, l'effet d'alliage sur la catalyse Au a été évalué, ce qui montre que l'alliage AuPd améliore la cinétique, tandis que l'alliage AuPt améliore la sélectivité de l'oxydation du HMF et retarde l'activité de dégradation. Notre étude suggère d'allier Pt et Au pour retarder la dégradation du HMF, la principale menace. Sinon, l'alliage de Pt et Pd avec Au pour former un alliage trimétallique améliorerait la cinétique et retarderait la dégradation du HMF.

Mots-clés: *Catalyse hétérogène, Ingénierie des réactions, Chimie verte, Oxydation, Dégradation, Sélectivité.*

Notations, Descriptions, and Structures

Notations	Descriptions	2-D Molecular Structure
AC or C	Activated carbon, charcoal, or carbonaceous material,	-
'el'	Electron	-
'nu'	Nucleus	-
AuX	Au catalyst alloy, where the X denote the new metal alloyed with the Au catalyst in Au:X ratio of 63:1	-
C-C (C-CH2OH)	Scission of C-C bond in C-CH2OH in HMF/HMFCA	-
C-C (C-CO(H))	Scission of C-C bond in C-COH in HMF	-
C-C (C-COOH)	Scission of C-C bond in C-COOH in HMFCA	-
C-H (H-CHOH)	Abstraction of H from the C-H in an alcohol function(H-CHOH)	-
C-H (H-CO)	Abstraction of H from the C-H in the aldehyde (H-CO)	-
C-H (H-RingCH2OH)	Abstraction of H from the C-H on furan ring's carbon close to alcohol (H-RingCH2OH)	-
C-H (H-RingCO(H))	Abstraction of H from the C-H on furan ring's carbon close to aldehyde (H-RingCO(H))	-
C-H (H-RingCOOH)	Abstraction of H from the C-H on furan ring's carbon close to acid (H-RingCOOH)	-
CNF	Carbon nanofibers	-
CNT	Carbon nanotubes	-
C-O (OpenRing)	Opening of the ring via the C-O bond breaking	-
DFF	Diformylfuran in gas-phase	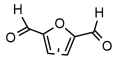
E	Electronic energy	-

Ef	Energies of the final (f) reaction step	-
Ei	Energies of the initial (i) reaction step	-
FA	Furoic acid in gas-phase unadsorbed	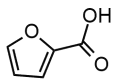
FF	Furfural in gas-phase unadsorbed	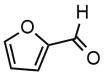
G	Gibbs free energy	-
H	Enthalpy	-
PBE	Perdew-Burke-Ernzerhof	
PDFT	Periodic density functional theory	-
RDS	Rate-determining step	-
S-E or SE	Schrodinger Equation	-
X or Slab	Catalyst which could be represent any metal studied.	
xCH2OH	Surface alcohol, a product of C-C scission in HMF or HMFCA via C-CH_2OH	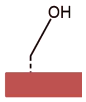
xCOH	Surface aldehyde, a product of C-C scission in HMF via C-CH_2OH	
xCOOH	Surface acid or surface COOH, a product of C-C scission in HMF via C-COOH	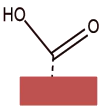
xDFF	Surface Diformylfuran adsorbed on a catalyst	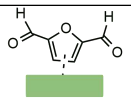
xFA	Surface furoic acid adsorbed on a solid catalyst surface	
xFDCA	Surface 2,5-Furandicarboxylic acid adsorbed on a catalyst	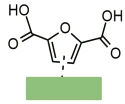

xFF	Surface furfural adsorbed on a solid catalyst surface	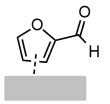
xFFCA	Surface 5-Formyl-2-furan carboxylic Acid adsorbed on a catalyst	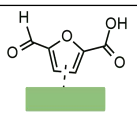
xFFdiO	Surface furan dioxide or carbonate (xFFdiO), an undesired species in furfural oxidation mechanism	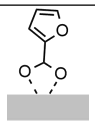
xFFdiOH	Surface furan diol (xFFdiOH), an undesired species in furfural oxidation mechanism	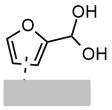
xFFO	Surface furan ketone or furan oxide (xFFO), an intermediate species in furfural oxidation mechanism	
xFFO(H)O or xFFHdiO	Surface furan hydrogen dioxide or carbonate, an intermediate species in furfural oxidation mechanism	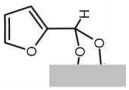
xFFO(OH)H or xFFOOHH	Surface furan carboxylate, an intermediate species in furfural oxidation mechanism	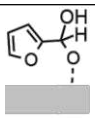
xFFOH	Surface furan alcohol specie in furfural oxidation mechanism	
xFFtriOH	Surface furan triol in furfural oxidation mechanism	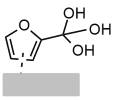
xH	Surface hydrogen (adsorbed hydrogen specie on solid catalyst surface)	
xH2O	Surface water (adsorbed water on solid catalyst surface)	
xHMF	Surface 5-hydroxymethylfurfural adsorbed on a catalyst	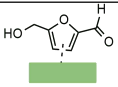
xHMF_CH2OH	Surface HMF_CH2OH, a product of C-C scission in HMF via C-COH	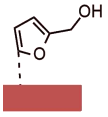

xHMF_COH	Surface HMF_COH, a product of C-C scission in HMF via C-CH_2OH	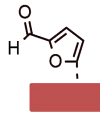
xHMF_deH_CO	Surface HMF_deH_CO, an intermediate of oxidizing HMF to HMFCA (via the dehydrogenation of H-CO in aldehyde)	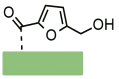
xHMF_deH_ringCH2OH	Surface HMF_deH_ringCH2OH, a furan ring C-H scission in HMF via the carbon close to alcohol	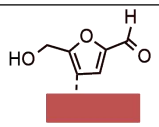
xHMF_deH_ringCOH	Surface HMF_deH_ringCOH, a furan ring C-H scission in HMF via the carbon close to aldehyde	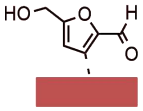
xHMF_ringbreak	Surface HMF_ringbreak via O-C (that is, C closed to alcohol, CH_2OH)	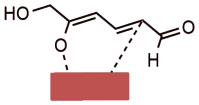
xHMF_ringbreak	Surface HMF_ringbreak via O-C (that is, C closed to aldehyde, COH)	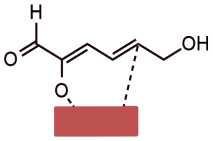
xHMFCA	Surface HMFCA adsorbed on catalyst	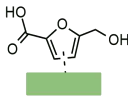
xHMFCA_CH2OH	Surface HMFCA_CH2OH, a product of C-C scission in HMFCA via C-COOH	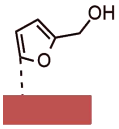
xHMFCA_COOH	Surface HMFCA_COOH, a product of C-C scission in HMFCA via C-CH_2OH	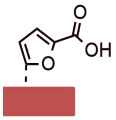
xHMFCA_deH_CH2O	Surface HMFCA_deH_CH2O, an intermediate of oxidizing HMFCA to FFCA (via the dehydrogenation of CH_2O-H in alcohol)	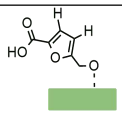
xHMFCA_deH_CHOH	Surface HMFCA_deH_CHOH, an intermediate of oxidizing HMFCA to FFCA (via the dehydrogenation of H-CH_2O in alcohol)	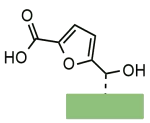

xHMFCA_deH_COO	Surface HMFCA_deH_COO, a product of H abstraction from COO-H	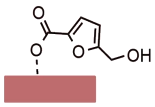
xHMFCA_deH_ringCH2OH	Surface HMFCA_deH_ringCH2OH, a furan ring C-H scission in HMFCA via the carbon close to alcohol	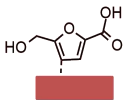
xHMFCA_deH_ringCOOH	Surface HMFCA_deH_ringCOOH, a furan ring C-H scission in HMFCA via the carbon close to acid	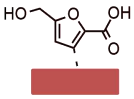
xHMFCA_ringbreak	Surface HMFCA_ringbreak via O-C (that is, C closed to CH2OH)	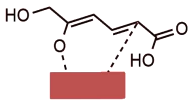
xHMFCA_ringbreak	Surface HMFCA_ringbreak via O-C (that is, C closed to COOH)	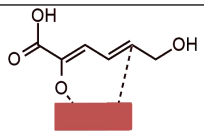
xO	Surface oxygen atom (adsorbed oxygen specie on solid catalyst surface)	
xO2	Surface oxygen gas (adsorbed oxygen gas on solid catalyst surface)	
xOH	Surface hydroxyl (adsorbed hydroxyl species on solid catalyst surface)	
XXact	Activation energy in any defined quantity, XX = E, G, or H	-
XXads	Adsorption energy in any defined quantity, XX = E, G, or H	-
XXrxn	Reaction energy in any defined quantity, XX = E, G, or H	-

Introduction

1 Introduction

Chapter 1 Introduction

1.1 Background Information

Most countries across the globe are blessed mainly with vast biomass resources, especially countries with low population densities [1]. The bulk of the biomass is sourced from agricultural wastes (like maize cob, rice husk, sugarcane straws, sugarcane bagasse, bean shell, ground shells, maize stalk, etc.) [2,3] and domestic wastes, which includes food wastes (like unused parts of food, rotten or uneaten food, e.g., yam peels, potatoes peels, fruit peels, and many others from various homes, food industries, and restaurants[4,5]. Most of these resources are on the rise during the harvest season when most farmers harvest their crops. Tenenbaum's report [6] further indicates that biomass and waste would continue to rise and were estimated to grow to 368 million dry tons by 2030. This includes developing and developed countries. Some of these countries, especially the developing ones [7,8], are yet to explore the best[9,10] out of these resources as most of their current explorations are generally for heating to warm, cooking their meals, and housing.

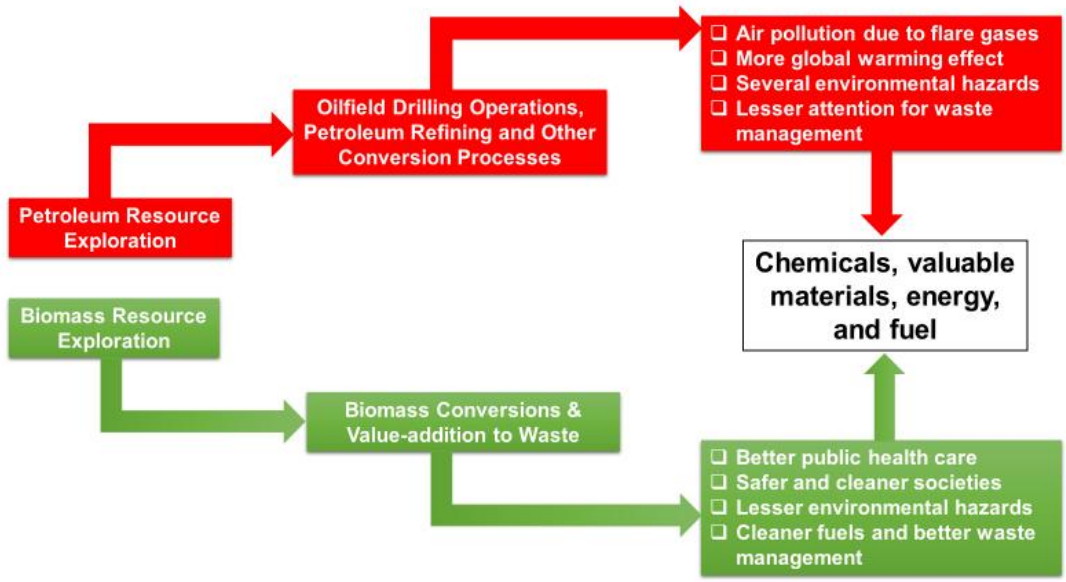

Figure 1-1 *Implications of promoting petroleum exploration, the current practice of biomass wastes, and conversions to valuable materials, energy, and fuel.*

And for age-long, the world has been striving to meet the global needs of energy generation, material resources, and fuels. Currently, material production in the markets is primarily obtained from petroleum, despite the possibility of their derivability from these biomass resources [11–13]. This practice of relying on petroleum-based products has largely contributed to the ongoing global warming, and sudden changes (as shown in Figure 1- 1) reported in several countries' climatic conditions [13,14]. Due to the ongoing environmental challenges, significant attention is now given to decarbonizing all this in our manufacturing sector via the promotion of greener technologies. The considerable role biomass resource exploration would play in achieving a more sustainable environment cannot be overemphasized[15], especially in developing countries where biomass resources are poorly managed.

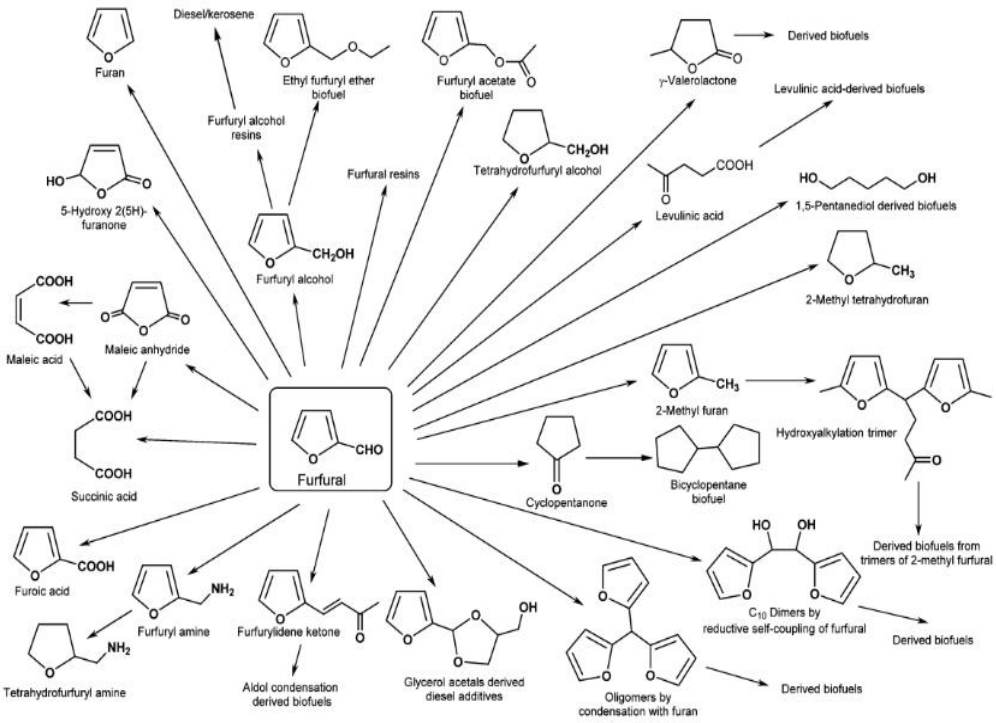

Figure 1- 2 Graphical scheme presenting different derivable chemicals and other valuable materials from furfural. Adopted from Literature [26,27].

Biomass materials are often managed by disposal on dumpsites (traditional landfills), and open burning process methods since the government needs better attention to community waste management. The practice has been primarily reported in the

literature that it exposes community health to danger [16,17]. Some of the dangers could be exposure of the habitants of such communities to poisonous gases released during the combustion processes, which can result in chronic illness, climatic change, and global warming [18,19]. The rising concern about the wastes generated and the nuisance caused by poorly managed wastes raises concern about the need to be developed a better approach to managing the present and future biomass wastes. The initiative of exploration of biomass resources to obtain valuable materials like glucose, xylose, furfural, and hydroxymethyl furfural (HMF) [20] would go a long way to attract the interest of countries' government and private sectors toward investment in the technology, which would further result to better management of biomass resource and their wastes in communities.

Furfural (FF) and hydroxymethyl furfural (HMF) are among the top fourteen essential biomass-derived platform chemicals classified by the US Department of Energy's report [21]. They were important due to the presence of the functional groups (such as an aldehyde group, and hydroxyl group attached to the 2-position of furan structure) in their structures. Other factors that contributed to its emergence in the list include the ease of obtaining them from widely available lignocellulosic materials. It can further be used to produce other vital chemicals for the production of essentials, such as fuel additives, lubricants, furoic acid (FA), furan dicarboxylic acid (FDCA), resins, pharmaceuticals, and bio-plastics [22–25]. Some of the valuable products derivable from furfural are pictorially represented in Figure 1- 2. This wide range of areas for its applications significantly motivated the interest of significant industries and researchers to improve its conversions and product distributions. In addition, it has been established that furfural and HMF, as biomass-platform molecules, would provide a safer and environmentally friendly method of producing most of our practical daily needs in the communities and industries.

A further survey of existing reports in the literature has established different approaches that can aid in efficient biomass resource management and their waste for maximum benefits. Some of the reported methods include bioenergy generation (that is, biomass to green energy or heat and power generation)[28,29], biofuel synthesis (that is, biomass to green fuels)[30,31], and material production via biomass conversion process (that is, biomass to valuable materials)[32–35]. These approaches were identified as better and safer ways of managing biomass resource and their wastes in communities due to the environmental and economic advantages they offer if invested in.

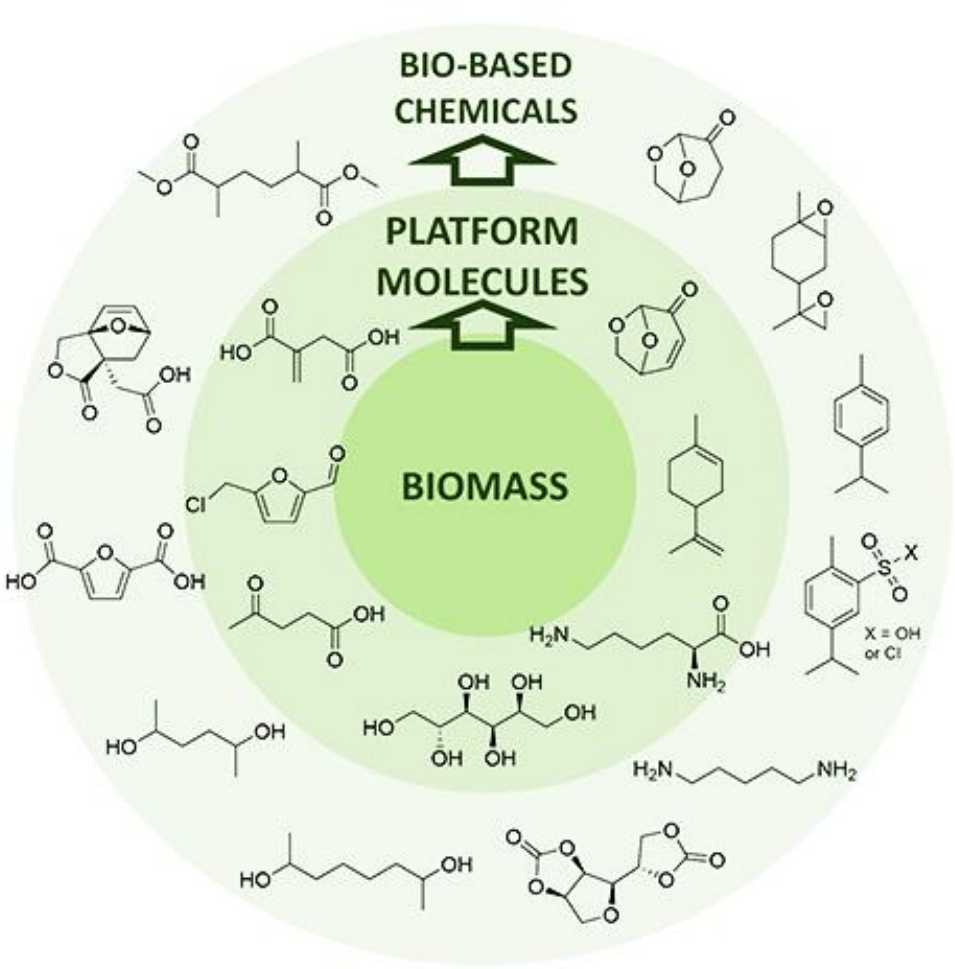

Figure 1- 3 *Potential derivatives obtained from the exploration of biomass conversion processes. Source: Clean Synthesis*[36]

Notably, the worldwide study focuses more on exploring the biomass conversion processes (illustrated in Figure 1- 3) that could aid in transforming biomass resources

into valuable materials as a better alternative to petroleum-based. These biomass conversion processes include hydrolysis, oxidation, dehydrogenation, hydrogenation, isomerization, dehydration, hydration, and other processes. Some of the resulting key intermediate products include furfural, 5-hydroxymethylfurfural (HMF), glucose, and xylose [33,34] . Of which the furfural (obtained from cellulose) and HMF (obtained from hemicellulose) are well-known biomass or bio-refinery platform molecules due to their vast range of areas. They find applications in chemical and petrochemical process industries for producing valuable materials like chemicals, polymers, fuels, and others.

Our studies majorly investigate the oxidation of biomass derivatives like furfural and hydroxymethyl furfural (HMF). And a survey of the literature indicates that research works have been exploring the benefit or impact of deploying the use of enzymes [37] and heterogeneous catalysts [38–44] in their search for efficient means of converting the HMF to valuable materials like 5-hydroxymethyl-2-furan carboxylic acid (HMFCA), diformylfuran (DFF), 5-Formyl-2-furan carboxylic Acid (FFCA) and 2,5-Furandicarboxylic acid (FDCA). In the use of heterogeneous catalysts, some works explore the use of metallic oxides, metals, and other forms of catalysts (like zeolites) in search of one that would aid in promoting the efficiency of the conversion process. A good number of the existing works deployed experimental approaches, and a few deployed the use of the computational approach in this search for an efficient way of deriving valuable materials from HMF (Note that Chapter 2 of this report presented details of the work done). Several studies with our current study have derived motivation towards the search for understanding of the pathways leading to degradation during the oxidation of HMF to FDCA. As a way of alleviating the degradation challenge that often leads to low yield and poor selectivity in the oxidation process.

This conversion process for synthesizing the FDCA from HMF and furfural is highly important due to its wide range of applications in different materials, pharmaceutical productions, and other valuable chemicals. The use of a computational approach can aid in unraveling details on the various routes promoting the degradation activity, which is competing with the oxidation activity for the production of FDCA on Au.

1.2 Key Goal of this Thesis

In this study, we employed the computational approach using periodic density functional theory (DFT) calculation to analyze, re-design, and simulate the catalyst for the prevention of degradation experimentally observed in Furfural and HMF oxidation to FDCA over gold (Au). As a measure of engineering the Au and its alloys, AuX (where X = Au, Pd, and Pt) performance in the oxidation of HMF to FDCA, to understand the best approach to hinder or retard the degradation of the catalyst.

1.3 Overview of the Thesis Report's Framework

To achieve the research goal, this thesis was structured into seven chapters, which are presented here (excluding the introduction chapter) as follows:

Chapter 2 reviews literature presenting general information on the oxidation of HMF, the available mechanisms involved in its oxidation processes, and the significance of its derivatives (like HMFCA, DFF, FFCA, and FDCA). The existing works in the literature reported on HMF oxidation to FDCA in the presence of heterogeneous catalysts were reviewed. The survey included works for experimental and computational studies focusing on the use of metals and their alloys. From this, a summary of the current issues is obtained from the literature and the key research problem that this recent thesis report investigated. And further information on the thesis's studies objectives for addressing the challenge experimentally reported the use of Au and the specific strategy design deployed in this thesis's studies were presented.

Moreover, Chapter 3 highlighted details and literature on molecular modeling and various available approaches involved in carrying out computational studies as reported in the literature. Further information on density functional theory (DFT) calculation deployment in studying solid surfaces was reported. The relevant parameters involved in DFT calculation, transition state search methods, and thermodynamic properties calculation methods were presented.

Three specific studies on the oxidation process on Au surfaces were reported in Chapters 4 to 6. Chapter 4 presents the report of the findings made for the Study of mechanism & possible competition pathways in oxidizing furfural to furoic acid on Au catalyst as a preliminary study for HMF oxidation on Au. Where the significance of water to the process and possible products competing with the desired product were reported. And Chapter 5 presented the report of the findings made for the investigation of pathways promoting degradation in oxidizing HMF to FDCA on Au were reported. Whereas Chapter 6 showcases the deduction for evaluating Au-alloys' effects on the degradation pathway in HMF Oxidation, where the capacity of AuX (X = Au, Pd, and Pt) alloy to retard degradation was reported.

To end the entire report, Chapter 7 was used to summarize all the deductions made for the three studies reported in Chapters 4 to 6. And also presented areas that further studies can look into in advancing the catalytic performance of Au catalyst in the oxidation of furfural and HMF to furoic acid and FDCA.

1.4 List of References Cited

1. IEA. (2021, November). IEA Bioenergy Countries' Report – Update 2021 | Bioenergy. IEA Bioenergy Report. https://www.ieabioenergy.com/blog/publications/iea-bioenergy-countries-report-update-2021/

2. Tripathi, N., Hills, C. D., Singh, R. S., & Atkinson, C. J. (2019). Biomass waste utilisation in low-carbon products: harnessing a major potential resource. Npj Climate and Atmospheric Science 2019 2:1, 2(1), 1–10. https://doi.org/10.1038/s41612-019-0093-5

3. Duque-Acevedo, M., Lancellotti, I., Andreola, F., Barbieri, L., Belmonte-Ureña, L. J., & Camacho-Ferre, F. (2022). Management of agricultural waste biomass as raw material for the construction sector:

an analysis of sustainable and circular alternatives. Environmental Sciences Europe, 34(1), 1–23. https://doi.org/10.1186/S12302-022-00655-7/TABLES/6

4. Carpenter, D., Westover, T. L., Czernik, S., & Jablonski, W. (2014). Biomass feedstocks for renewable fuel production: a review of the impacts of feedstock and pretreatment on the yield and product distribution of fast pyrolysis bio-oils and vapors. Green Chemistry, 16(2), 384–406. https://doi.org/10.1039/C3GC41631C

5. Saleem, M. (2022). Possibility of utilizing agriculture biomass as a renewable and sustainable future energy source. Heliyon, 8(2), e08905. https://doi.org/10.1016/J.HELIYON.2022.E08905

6. Tenenbaum, D. J. (2005). Harvesting the Potential of BIOMASS. Environmental Health Perspectives, 113(11), A750. https://doi.org/10.1289/EHP.113-A750

7. Kidmo, D. K., Deli, K., & Bogno, B. (2021). Status of renewable energy in Cameroon. Renewable Energy and Environmental Sustainability, 6, 2. https://doi.org/10.1051/REES/2021001

8. Oyedepo, S. O. (2012). Energy and sustainable development in Nigeria: The way forward. Energy, Sustainability and Society, 2(1), 1–17. https://doi.org/10.1186/2192-0567-2-15/TABLES/9

9. Research and Data. (2020). 2,5-Furandicarboxylic Acid (FDCA) Market | Size & Analysis. https://www.reportsanddata.com/report-detail/2-5-furandicarboxylic-acid-fdca-market

10. Grand View Research. (2014). Furandicarboxylic Acid Market Size, Share & Trends Analysis Report By Application (PET, Polyamides, Polycarbonates, Plasticizers, Polyester Polyols), By Region, And Segment Forecasts, 2015 - 2020. https://www.grandviewresearch.com/industry-analysis/fdca-industry

11. Ugwu, C. O., Ozor, P. A., Ozoegwu, C. G., Ndukwe, A., & Mbohwa, C. (2022, April 7). Biomass Resources in Nigeria and the Conversion Pathways. Proceedings of the International Conference on Industrial Engineering and Operations Management Nsukka, Nigeria,. https://ieomsociety.org/proceedings/2022nigeria/142.pdf

12. Oyegoke, T., & Dabai, F. (2018). Techno-economic feasibility study of bioethanol production from a combined cellulose and sugar feedstock in Nigeria: 1-modeling, simulation and cost evaluation. Nigerian Journal of Technology, 37(4), 913–920. https://doi.org/10.4314/njt.v37i4.8

13. Okafor, C., Madu, C., Ajaero, C., Ibekwe, J., Bebenimibo, H., Nzekwe, C., Okafor, C., Madu, C., Ajaero, C., Ibekwe, J., Bebenimibo, H., & Nzekwe, C. (2021). Moving beyond fossil fuel in an oil-exporting and emerging economy: Paradigm shift. AIMS Energy , 9(2), 379–413. https://doi.org/10.3934/ENERGY.2021020

14. DSTI. (2016). Biomass for a sustainable bioeconomy: Technology and governance. https://one.oecd.org/document/DSTI/STP/BNCT(2016)7/en/pdf

15. Scarlat, N., Dallemand, J. F., Monforti-Ferrario, F., & Nita, V. (2015). The role of biomass and bioenergy in a future bioeconomy: Policies and facts. Environmental Development, 15, 3–34. https://doi.org/10.1016/J.ENVDEV.2015.03.006

16. Ogundele, O. M., Opeagbe, &, Rapheal, M., & Abiodun, A. M. (2018). Effects of Municipal Waste Disposal Methods on Community Health in Ibadan - Nigeria. Polytechnica, 1(1), 61–72. https://doi.org/10.1007/S41050-018-0008-Y

17. Oluranti, I., & Omosalewa, E. (2012). Health and Economic Implications of Waste Dumpsites in Cities: The Case of Lagos, Nigeria. International Journal of Economics and Finance, 4(4), 239–251. https://doi.org/10.5539/ijef.v4n4p239

18. Adejumo, I. O., & Adebiyi, O. A. (2020). Agricultural Solid Wastes: Causes, Effects, and Effective Management. Strategies of Sustainable Solid Waste Management, 1–19. https://doi.org/10.5772/INTECHOPEN.93601

19. Onyekwelu, I. L., & Aghamelu, O. P. (2019). Impact of organic contaminants from dumpsite leachates on natural water sources in the Enugu Metropolis, southeastern Nigeria. Environmental Monitoring and Assessment 2019 191:9, 191(9), 1–20. https://doi.org/10.1007/S10661-019-7719-2

20. Takkellapati, S., Li, T., & Gonzalez, M. A. (2018). An Overview of Biorefinery Derived Platform Chemicals from a Cellulose and Hemicellulose Biorefinery. Clean Technologies and Environmental Policy, 20(7), 1630. https://doi.org/10.1007/S10098-018-1568-5

21. Aden, A., Bozell, J., Holladay, J., White, J., & Amy, M. (2004). Top Value Added Chemicals from Biomas: Results of Screening for Potential Candidates from Sugars and Synthesis Gas Produced by the Staff at Pacific Northwest National Laboratory (PNNL) National Renewable Energy Laboratory (NREL) Office of Biomass Program (EERE) For the Office of the Energy Efficiency and Renewable Energy (T. Werpy & G. Petersen, Eds.; Vol. 1). http://www.osti.gov/bridge

22. Yang, Z., Zhang, J., Qian, G., Duan, X., & Zhou, X. (2021). Production of biomass-derived monomers through catalytic conversion of furfural and hydroxymethylfurfural. Green Chemical Engineering, 2(2), 158–173. https://doi.org/10.1016/J.GCE.2020.11.001

23. Wikipedia. (2022, September 25). Furfural. Wikipedia Encyclopedia; Springer New York LLC. https://en.wikipedia.org/wiki/Furfural

24. Adams, R., & Voorhees, V. (1921). Furfural. Organic Syntheses, 1, 49. https://doi.org/10.15227/orgsyn.001.0049

25. Jessica, E. (2022). Furfural: Future Feedstock for Fuels and Chemicals | Biomassmagazine.com. Biomass Magazine. https://biomassmagazine.com/articles/1950/furfural-future-feedstock-for-fuels-and-chemicals

26. PubChem. (2022, September 25). Furfural. National Library of Medicine; Nature Publishing Groups. https://doi.org/10.1038/SDATA.2018.125

27. Mariscal, R., Maireles-Torres, P., Ojeda, M., Sádaba, I., & López Granados, M. (2016). Furfural: a renewable and versatile platform molecule for the synthesis of chemicals and fuels. Energy & Environmental Science, 9(4), 1144–1189. https://doi.org/10.1039/C5EE02666K

28. Piotr, B., & Jeremy, M. (2021, November). Bioenergy Power Generation – Analysis. IEA Report. https://www.iea.org/reports/bioenergy-power-generation

29. Uddin, M. N., Siddiki, S. Y. A., Mofijur, M., Djavanroodi, F., Hazrat, M. A., Show, P. L., Ahmed, S. F., & Chu, Y. M. (2021). Prospects of Bioenergy Production From Organic Waste Using Anaerobic Digestion Technology: A Mini Review. Frontiers in Energy Research, 9, 33. https://doi.org/10.3389/FENRG.2021.627093/BIBTEX

30. Singh, A. R., Singh, S. K., & Jain, S. (2022). A review on bioenergy and biofuel production. Materials Today: Proceedings, 49, 510–516. https://doi.org/10.1016/J.MATPR.2021.03.212

31. Alalwan, H. A., Alminshid, A. H., & Aljaafari, H. A. S. (2019). Promising evolution of biofuel generations. Subject review. Renewable Energy Focus, 28, 127–139. https://doi.org/10.1016/J.REF.2018.12.006

32. Réocreux, R., & Michel, C. (2018). Rational design of heterogeneous catalysts for biomass conversion – Inputs from computational chemistry. Current Opinion in Green and Sustainable Chemistry, 10, 51–59. https://doi.org/10.1016/J.COGSC.2018.02.004

33. Li, X., Jia, P., & Wang, T. (2016). Furfural: A Promising Platform Compound for Sustainable Production of C4 and C5 Chemicals. ACS Catalysis, 6(11), 7621–7640. https://doi.org/10.1021/ACSCATAL.6B01838/ASSET/IMAGES/MEDIUM/CS-2016-01838C_0017.GIF

34. Jiang, Z., Hu, D., Zhao, Z., Yi, Z., Chen, Z., & Yan, K. (2021). Mini-Review on the Synthesis of Furfural and Levulinic Acid from Lignocellulosic Biomass. Processes, 9(7), 1234. https://doi.org/10.3390/PR9071234

35. Chang, H., Motagamwala, A. H., Huber, G. W., & Dumesic, J. A. (2019). Synthesis of biomass-derived feedstocks for the polymers and fuels industries from 5-(hydroxymethyl)furfural (HMF) and acetone. Green Chemistry, 21(20), 5532–5540. https://doi.org/10.1039/C9GC01859J

36. Clean Synthesis. (2022, October 3). Clean synthesis technology platform. Green Chemistry Centre of Excellence Report; American Chemical Society. https://www.york.ac.uk/chemistry/research/green/clean-synthesis/

37. Lalanne, L., Nyanhongo, G. S., Guebitz, G. M., & Pellis, A. (2021). Biotechnological production and high potential of furan-based renewable monomers and polymers. Biotechnology Advances, 48, 107707. https://doi.org/10.1016/J.BIOTECHADV.2021.107707

38. Chai, X., Jiang, K., Wang, J., Ren, Z., Liu, X., Chen, L., Zhuang, X., & Wang, T. (2022). Efficient Catalytic Conversion of 5-Hydroxymethylfurfural to 2,5-Furandicarboxylic Acid over Ruthenium Cluster-Embedded Ni(OH)2 Catalyst. ChemSusChem, 15(16), e202200863. https://doi.org/10.1002/CSSC.202200863

39. Ardemani, L., Cibin, G., Dent, A. J., Isaacs, M. A., Kyriakou, G., Lee, A. F., Parlett, C. M. A., Parry, S. A., & Wilson, K. (2015). Solid base catalysed 5-HMF oxidation to 2,5-FDCA over Au/hydrotalcites: fact or fiction? Chemical Science, 6(8), 4940–4945. https://doi.org/10.1039/C5SC00854A

40. Deshan, A. D. K., Atanda, L., Moghaddam, L., Rackemann, D. W., Beltramini, J., & Doherty, W. O. S. (2020). Heterogeneous Catalytic Conversion of Sugars Into 2,5-Furandicarboxylic Acid. Frontiers in Chemistry, 8, 659. https://doi.org/10.3389/FCHEM.2020.00659/BIBTEX

41. Jin, Y., Sarina, S., Liu, H., Martens, W., Waclawik, E. R., Peiris, E., Jia, J., Shang, J., Kou, L., Guo, C., & Zhu, H.-Y. (2022). Aerobic Oxidation of 5-Hydroxymethyl-furfural to 2,5-Furandicarboxylic Acid at 20 °C by Optimizing Adsorption on AgPd Alloy Nanoparticle Catalysts. ACS Catalysis, 11226–11238. https://doi.org/10.1021/ACSCATAL.2C03457

42. ElMetwally, A. E., Sayed, M. S., Zhou, Y., Domena, J. B., Shim, J.-J., Leblanc, R. M., Knecht, M. R., & Bachas, L. G. (2022). Photocatalytic Partial Oxidation of 5-Hydroxymethylfurfural to 2,5-Diformylfuran Using Exfoliated g-C 3 N 4 /Pd Nanoarchitectures. The Journal of Physical Chemistry C, 126(37), 15671–15684. https://doi.org/10.1021/ACS.JPCC.2C04186

43. Zhao, D., Su, T., Wang, Y., Varma, R. S., & Len, C. (2020). Recent advances in catalytic oxidation of 5-hydroxymethylfurfural. Molecular Catalysis, 495, 111133. https://doi.org/10.1016/J.MCAT.2020.111133

44. Xu, S., Zhou, P., Zhang, Z., Yang, C., Zhang, B., Deng, K., Bottle, S., & Zhu, H. (2017). Selective Oxidation of 5-Hydroxymethylfurfural to 2,5-Furandicarboxylic Acid Using O2 and a Photocatalyst of Co-thioporphyrazine Bonded to g-C3N4. Journal of the American Chemical Society, 139(41), 14775–14782. https://doi.org/10.1021/JACS.7B08861/SUPPL_FILE/JA7B08861_SI_001.PDF

Review of Literature

2 Review of Literature

Chapter 2 Review of Literature

2.1 Overview

The rising demand for bio-based means of manufacturing different chemicals and materials in the process industries is significantly attracting the attention of researchers and industries' experts towards exploring several biomass-based platform molecules (like furfural and HMF) and other valuable derivatives like FDCA[1,2]. Being an excellent alternative to the patronage of petroleum-based means, which are significantly contributing to global warming. Considering bio-based production methods is necessary, especially with the over-dependence or monopoly of petroleum-based production methods, which is diminishing and is predicted to be finished soon. FDCA, a derivative obtained from biomass, is also known as "YXY building blocks" or furanic [3] and is also referred to as a "sleeping giant" due to the vast range of areas where it can find application in the manufacturing industries. Other YXY building block molecules include Furfuryl Ethyl Ether, Ethoxymethyl Tetrahydrofuran Ether, and Bisethoxy methyl furan[4].

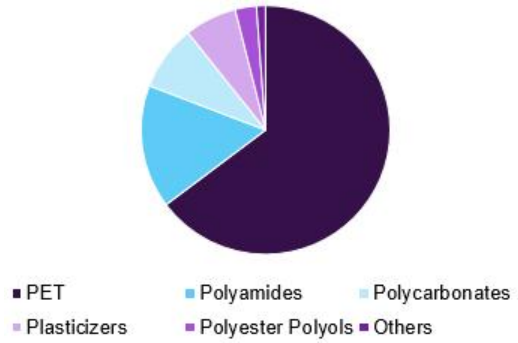

Figure 2- 1 FDCA's global market revenue share by application in 2020 (in %). Source: Grand View Research [5]

Some areas where it finds applications include the production of chemicals, green materials, and fuel upgrades [3,4]. The YXY molecules are generally used to build new materials and improve diesel quality [4]. However, among all these YXY building blocks or furanics, FDCA is well-known for being the most versatile due to its feature of furan

and carboxylic acid functional groups. It enables FDCA to find application in a vast range of polymer productions like polyesters (e.g., polyethylene terephthalate - PET, polyethylene 2,5-furandicarboxylate-PEF), poly-amides, and other new materials synthesis [6–8] as shown in Figure 2- 1.

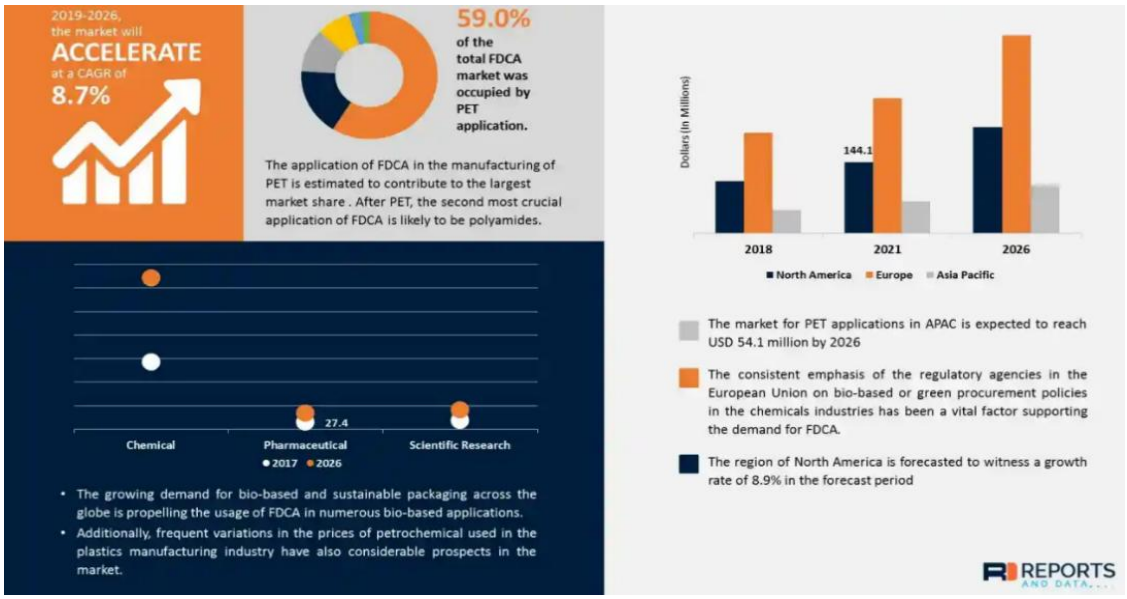

Figure 2- 2 Market report for the FDCA demand. Source: Research and Data [9]

A survey of the market demand for the FDCA indicates that its global market value is worth 88.2 million dollars as of 2014, according to Grand View Research [5]. It was also projected to grow about 33.5 % in its market demand from 2015 to 2020, where the need for poly-ether polyols production claims a large share of the FDCA market demand [5]. A recent report by Research and Data [9] for the FDCA market indicated that the market value has risen to 441.5 million dollars in 2020, which agrees with the projected rise indication reported by Grand View Research[5]. And have been launched to increase by 8.70 % from 2020 to 2028. According to Research and Data [9], Pacific Asia, Europe, and North America are the only continents currently exploring the market. And Europe has the largest market share (Figure 2- 2).

Findings from these reports raise the need to re-design and optimize its production method to upgrade the production yield due to the rising FDCA market demands. A

further survey of literature [5,9] indicates that extreme rules placed on the deployment of petroleum-based methods of production materials like polymers in industries are one of the primary drives attracting significant attention to this market as an approach to promoting bio-based production of materials globally.

Methods deployed in the production of the FDCA include the oxidation of HMF to FDCA, the transformation of galactonic acid into FDCA in the presence of acidic conditions; the production of FDCA from furoic acid; synthesizing FDCA from furan via haloform reaction; and the production of FDCA via dimethyl diglycolate from diglycolic acid, in the presence of catalysts [10]. The approach of synthesizing FDCA from the oxidation of HMF is more deployed than other methods, claiming a large percent of FDCA sold in the market by the literature [5,8,9].

This review of literature, therefore, focuses on understanding the HMF oxidation to FDCA. The literature survey includes exploring the reported mechanisms said to be involved in the process and the experimental and computational studies of the HMF oxidation to FDCA in the presence of metals and alloys. The review enables us to identify possible areas where further studies contribute to advancing the synthesis of FDCA from biomass derivatives in the presence of a solid catalyst.

2.2 Catalytic Oxidation of Biomass Derivatives

This process of oxidizing biomass derivatives has produced several ranges of valuable chemicals, polymers, and other essential materials that find applications in different aspects of our daily lives. Some of the biomass derivatives often oxidized into valuable resources in the literature include sugars (glucose, fructose, sucrose, lactose, xylose, and others)[11–24], alcohols (ethanol, glycerol, phenol, propanol, and others)[25–35], furan-based compounds (furfural, HMF, HMFCA, DFF, and others) [36–47] , and many other derivatives.

Several approaches to oxidizing these biomass derivatives into valuable materials are currently being explored in the literature. Especially with the rising interest in the promotion of green technologies across the globe due to the harm over-dependence on petroleum resources has caused our environment. These researchers have been exploring the measures of improving the transformation of the derivatives in valuable materials. At the same time, some of these studies examine the use of enzymes (that is, biological means) and other reaction-catalytic approaches like radiation (in photo-catalysis) and voltage (in electrocatalysis). Some concentrate on using solid catalysts, also known as heterogeneous catalysts. Solid catalysts are receiving better attention than other methods due to the ease of their recovery (after use) and their ease of facilitating continuous production when such a process is scale-up. Some of these solid catalysts whose capabilities are currently explored can either be classified as metals (Au, Pt, Ni, Ru, Pd, Co, and others)[32,34,48]; metal alloys (AuPd, PtPd, and many others) [34,42,44,48,49] ; metal oxides and zeolites (ZSM-5, NaX-zeolite, NaY-zeolite, Au-betazeolite)[50–53]. Other works explore the capability of the catalyst's support (such as ZSM-5, metallic oxides, and others) influencing the activity of the catalyst. This current report primarily focused on its survey of the literature that explores the capability of metals and alloys (bi-metals) to influence the oxidation of biomass derivatives processes.

2.2.1 Metal catalysis of biomass derivatives

The report of the existing works is generally summarized in Table 2- 1. The respective catalysts' performances are presented along with the operating condition deployed in the individual studies.

2.2.1.1 Overview of sugars oxidation in the presence of a metallic catalyst

Oxidation of other sugars like lactose [24], xylose [23], arabinose [13], and many others studied in the presence of metal catalysts like Au, Pt, and Pd is summarized in Table

2- 1. The literature survey on the oxidation of sugar into valuable materials indicates that many studies are exploring the potential of solid catalysts (Experimental reports for the use of metals and their alloys are presented in Table 2- 1) in the optimization of production yield. Some of the works that used pure metal include the work of Lee et al. [12], which demonstrated that Pt supported by activated carbon (AC) would yield 74 % glucaric acid in the absence of a base.

Table 2- 1 *Some experimental studies that investigated the benefits of using pure metals (M = Metals) on a support in the study of biomass derivative oxidation processes [Note: XC-72 = commercial carbon materials, AC= Activated carbon or Charcoal, HAP-LDH = hydroxyapatite & Ca–Al layered double hydroxide.]*

Ref	M	Support	T (°C)	P (bar)	Base	Feed	Yield, %	Products
[32]	Au	Graphite	60	1	NaOH	Glycerol	S=100	Glyceric Acid
[29]	Pd	XC-72	130	-	-	Benzyl Alcohol	S=99, C=90	Benzaldehyde
[34]	Pd	AC	50	3	NaOH	Glycerol	S=99.5	Glyceric & Tartronic Acid
[21]	Au	HAP-LDH	110	5	-	Glucose	>98	Gluconic Acid
[15]	Au	TiO_2	110	10	-	Glucose	95-97	Gluconic Acid
[54]	Au	CeO_2	120	1	-	1-Phenylethanol	>95	Ketone
[54]	Au	CeO_2	120	1	-	3-Octanol	>95	Ketone
[54]	Pd	CeO_2	160	1	-	1-Phenylethanol	>95	Ketone
[24]	Pt	AC	70	-	NaOH	Lactose	S=83	Lactobionic Acid
[34]	Au	AC	30	3	NaOH	Glycerol	S=82.5	Glyceric & Tartronic Acid
[28]	Pd	TiO_2	120	3	-	Cinnamyl Alcohol	C=81	Cinnam Aldehyde
[15]	Au	AC	110	10	-	Glucose	78	Gluconic Acid
[48]	Pd	AC	120	1	NaOH	Benzyl Alcohol	S=78.7 , C=30	Benzaldehyde
[12].	Pt	AC	80	13.8	-	Glucose	74	Glucaric Acid
[13]	Pt	AC	60	6	-	Xylose	64	Xylaric Acid
[15]	Pd	AC	110	10	-	Glucose	52	Gluconic Acid
[34]	Pt	AC	50	3	NaOH	Glycerol	S=48.3	Glyceric & Tartronic Acid
[54]	Pd	apatite	120	1	-	3-Octanol	45	Ketone
[28]	Au	TiO_2	120	3	-	Cinnamyl Alcohol	C=10	Cinnam Aldehyde

Guo et al. [15] also confirmed that base-free glucose oxidation on Au/TiO_2 would favor a high yield (i.e., 95-97 %) of gluconic acid. The authors [15] further established that substituting the Au/AC reduces the yield to about 78 % gluconic acid. Other reports, such as Franz et al. [13], further confirmed a good gluconic & arabinonic acid yield for

using Au/Al_2O_3 in base-free oxidation of glucose and arabinose. Using Pd/AC [24] in the base oxidation of lactose results in the selectivity of 83 % for lactobionic acid.

Generally, the report for the oxidation of different sugar molecules has shown a high yield with lesser degradation. This implies that the use of the metallic catalyst significantly favors the oxidation activity over the degradation one, which leads to undesired products.

2.2.1.2 Overview of metallic catalysis of alcohols and other biomass-derivatives oxidation

Many other studies have also demonstrated the applicability of metallic catalysts in the oxidation of biomass derivatives like alcohols and other multi-functional molecules. Some include the works of Wang et al. [29], where 90 % conversion and 99 % selectivity for the formation of benzaldehyde from benzyl alcohol in the presence of Pd/XC-72 was demonstrated to be good, especially for the catalyst synthesized with the use of glycerine (that exhibit multiple OH functional groups) unlike other solvents like ethanol (that has one OH). It was reported that the number of OH from the glycerine aid in dispersing the Pd nanoparticle to avoid sintering on the catalyst. The capability of the Pd influencing the oxidation of 1-phenylethanol [54] in the presence of CeO_2 support was confirmed to have yielded 95% ketones. However, the study [54] further established that the use of Pd-supported by apatite showed a lower yield of 45 % ketone, unlike the use of CeO_2 [54] . Other investigations for using Pd further confirmed a high yield for the benefit of Pd/AC in oxidizing glycerol into glyceric acid [34] and in oxidizing benzyl alcohol on the same catalyst (Pd/AC) yield of 78.70 % benzaldehyde [34].

The influence of other metals like Au and Pt in the oxidation of biomass derivatives was further explored in the literature. A report summary for the use of the metals is presented in Table 2- 1. Where it was established that Au had been identified to have

effectively catalyzed different oxidation processes like the case of glycerol to glyceric acid with a yield of 82.5 % on an AC support [34] ; 1-phenylethanol to yield >95 % ketones with a catalyst supported by CeO_2 [54]; oxidation of octanol into ketone with a yield of >95 % on catalyst supported by CeO_2 and others [54]. A report in the literature[15] established that the stability of Au-catalyst is more effective than other metals in oxidation reactions (as demonstrated in the oxidation of glucose into glucaric and gluconic acid).

The survey reveals that catalyst support like XC-72, CeO_2, apatite, and many other materials used in the experimental works significantly influenced the catalysis of the active component of a catalyst matrix. In addition, it was established that the Au catalyst showed higher stability than others in the literature[15]. This is evident with the quantity of yield its oxidation of glucose does yield, unlike other catalysts like Pt and Pd in Table 2- 1 that show a lower yield and favor the degradation of the species into undesired products. However, the high cost of the catalyst is another challenge.

2.2.2 Alloying effects on the catalysis of biomass derivative oxidation

Outside the study of metallic catalysis in biomass derivative oxidation, many other works are also significantly investigating the alloying effect of combining two or more metals in this catalysis oxidation process. The results are summarized in Table 2- 2. Some of these studies that investigated the use of alloy in the catalysis of sugar oxidation into valuable materials include the work of Solmi et al.[11], which explored the alloy of Au with Bi on activated carbon (AuBi/AC) for the oxidation of glucose that yields 31% glucaric acid and 18% gluconic acid in a base in Figure 2- 3. Moreover, Guo et al. report a higher yield of 34 % gluconic acid for using PdBi/AC than for using AuBi/AC [11] . Findings from their reports indicate that the AuBi/AC and PdBi/AC alloys favor the formation of undesired products (that is, degradation) over desired products (that is, the oxidation of glucose to produce gluconic and glucaric acid over

other routes). In general, introducing the Bi on the metal in the oxidation of glucose favors the production of gluconic acids. The oxidation mechanism reported in the study shows that gluconic acid is the intermediate through which the D-glucose gets oxidized to glucaric acid. This implies that introducing Bi eases the oxidation of the aldehyde group of the glucose to gluconic acid (due to the increase in yield of gluconic acid reported). At the same time, the Au site favors the oxidation of the hydroxyl to give carboxylic acid (gluconic acid than glucaric acid).

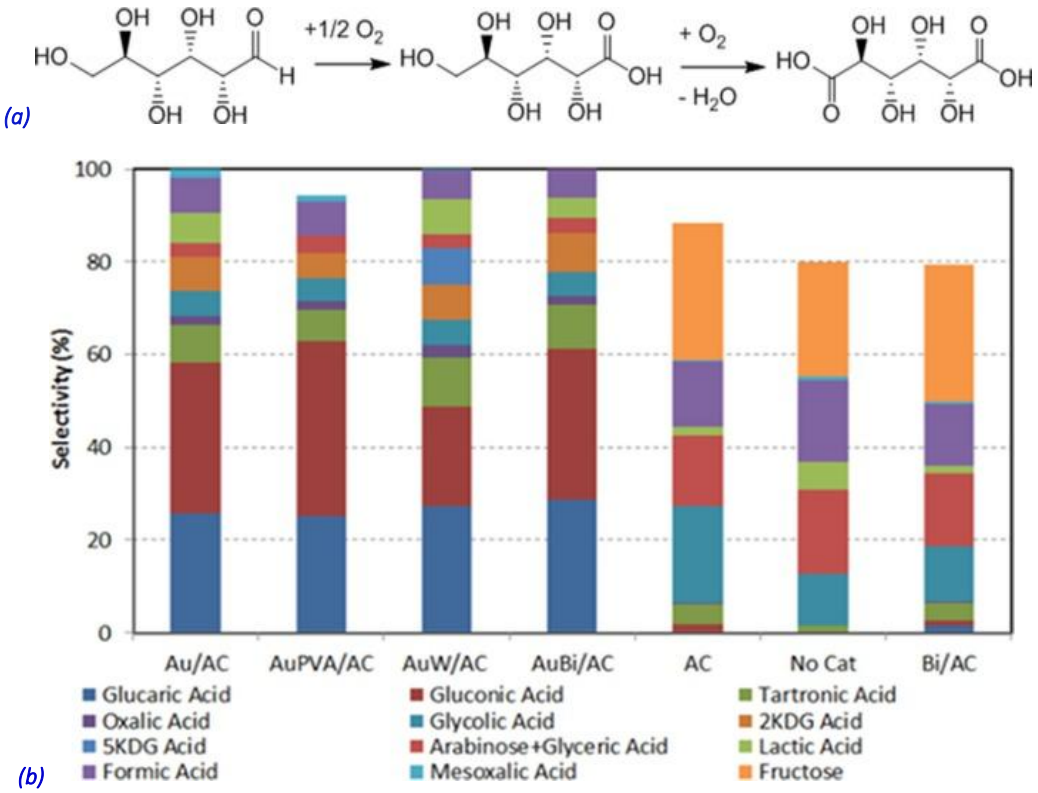

Figure 2- 3 (a) *Oxidation of d-Glucose to Glucaric Acid Using Au/AC Catalysts,* ***(b)*** *Selectivity profile (below figure) for the oxidation of d-glucose to glucaric acid [Source: Solmi et al.[11] reports]*

Another effect that the alloying effect results in the oxidation of the biomass derivative are the promotion of the reaction route or diversion of the reaction route (or pathway). Like the oxidation of glucose that has been earlier reported by Solmi et al.[11] and Guo et al.[15] to have yielded gluconic and glucaric acids in the presence of AuBi/AC or PdBi/AC, unlike the report of Liu et al.[18], where alloying of Au with Pt on a support TiO_2 (in $AuPt/TiO_2$ in Figure 2- 3) was confirmed to have yielded 50% tartaric

acid via base-free oxidation of glucose. This difference in the resulting products (gluconic, glucaric, and tartaric acids) indicated a change of reaction route, which later led to the production of different products (tartaric acid). This was due to the high selectivity of the Pt site for forming tartaric acid and xylonic acid over other Au sites. The transformation of gluconic acid into tartaric acid involves the oxidation of hydroxyl and the formation of carbon dioxide. The AuPt/TiO_2 alloy effect yielded a better selectivity for tartaric acid. It has further shown that using Au/TiO_2 (68 %)

Table 2- 2 *Some experimental studies investigated the benefits of using alloys (M = Metals) in the study of biomass derivative oxidation processes in the presence of oxygen and water [Note: AC= Activated carbon or Charcoal, SBA-15 = Santa Barbara Amorphous-15, X is the promoter in the catalyst, and M:X is the alloy ratio].*

Ref	M	X	M:X	Support	T (°C)	P (bar)	Base	Feed	Yield, %	Products
[55]	Au	Ir	1:3	Silica	180	-	-	Ethanol	S=92, C=56	Acetaldehyde
[34]	Au	Pd	-	AC	30	3	NaOH	Glycerol	S=97	Glyceric & Tartronic acid
[26]	Au	Pd	-	SBA-15	80	1	Na_2CO_3	Benzyl alcohol	S=97, C=39	Benzaldehyde
[28]	Au	Pd	3:1	TiO_2	120	3	-	Cinnamyl alcohol	C=~97	Cinnam aldehyde
[48]	Au	Pd, Pt	-	AC	120	1	NaOH	Benzyl alcohol	S=87, C=30	Benzaldehyde
[48]	Au	Pd	-	AC	120	1	NaOH	Benzyl alcohol	S=82, C=30	Benzaldehyde
[34]	Au	Pt	-	AC	50	3	NaOH	Glycerol	S=80	Glyceric & Tartronic acid
[14]	Pt	Cu	-	TiO_2	90	15	-	Glucose	S=60	Glucaric acid
[16]	Au	Pt	-	TiO_2	110	20	-	Glucose	50	Tartaric acid
[15]	Pd	Bi	-	AC	110	10	-	Glucose	34	Gluconic acid
[11]	Au	Bi	3:1	AC	60	10	NaOH	D-glucose	31	Glucaric acid
[11]	Au	Bi	3:1	AC	60	10	NaOH	D-glucose	18	Gluconic acid

yielded more gluconic acid than Au/AC (18 %). Comparing the report of other authors that use AC support with this one reveals that TiO_2 support aid in influencing the oxidation of the aldehyde group of the glucose to gluconic acid, unlike AC.

Moreover, Shi et al. [14] also confirmed 60% selectivity for glucaric acid in base-free glucose oxidation on PtCu/TiO_2. The study shows that introducing Cu in the catalyst results in a high glucaric acid yield. This implies that the Cu site facilitates the

oxidation of the hydroxyl group in gluconic acid (the intermediate) into glucaric acid on Au. Similarly, adding Au to Ir (1:3) supported by SiO_2 also enhances the catalyst selectivity for acetaldehyde to 92 % (at 56 % conversion) in the base-free oxidation of ethanol[55]. The Au aid in binding ethanol well to the catalyst, while the Ir site covered with O aid in catalyzing the C-H bond breaking (in the alcohol) to yield aldehyde.

(a)

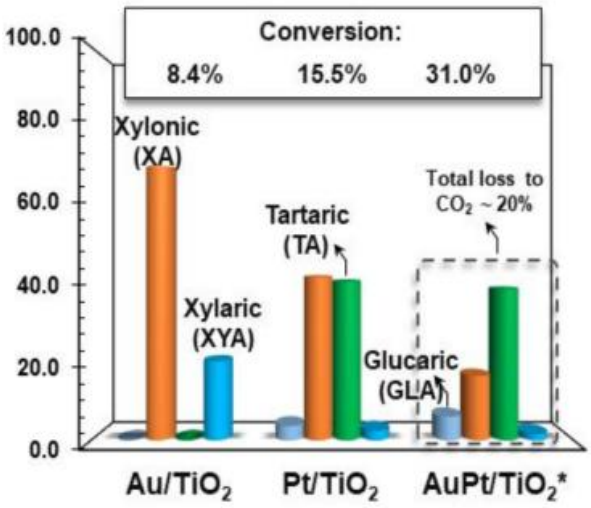

(b)

Entry	T (°C)	O_2 (MPa)	Substrate	conversion (%)	Selectivity (%)				
					TA	XYLA	XA	GLA	Others
1[a]	110	0.5	Gluconic	50.4	48.9	15.6	8.7	6.7	8.4
2[a]	110	1.0	Gluconic	47.1	45.8	14.7	8.4	7.1	8.0
3[a]	110	2.0	Gluconic	59.4	43.4	14.4	8.3	9.9	8.5
4[a]	110	3.0	Gluconic	40.7	44.4	16.0	10.9	9.1	9.2
5[a]	100	1.0	Gluconic	40.7	52.4	12.6	9.9	7.5	4.2
6[a]	120	1.0	Gluconic	76.8	32.5	9.9	3.5	13.3	9.4
7[b]	110	2.0	Glucose	100.0	50.1	10.2	3.2	0.0	15.7

a: $AuPt/TiO_2$-7.5 catalyst; b: $AuPt/TiO_2$-8.4 catalyst; TA: tartaric acid, XYLA: xylaric acid, XA: xylonic acid, GLA: glucaric acid, GA: gluconic acid. Reaction conditions: $C_{GA,0}$ ($C_{glucose,0}$): 0.3 M, catalyst amount: 0.05 g

(c)

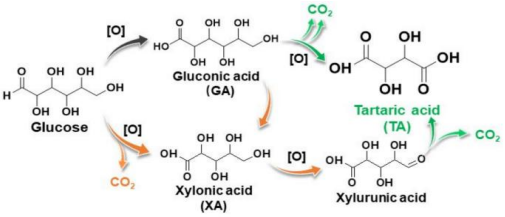

Figure 2- 4 (a & b) *Selected experimental results for Gluconic acid (GA) oxidation over Au/TiO_2 and Pt/TiO_2, showing the alloying effect on the catalysis of the process and selectivity for tartaric acid (TA), using C_{GA0} = 0.3M, cat. amount = 0.05g, T =110°C, 10bar O_2, 4h.* ***(c)*** *The oxidation routes for glucose to tartaric acid and other products [Source: Liu et al. report[18]]*

Other works that investigative the alloying effect include benzyl alcohol to benzaldehyde on AuPd/SBA-15 (97 % selectivity, 39 % conversion at 353 K, 1 atm) [26]; AuPd/AC (81 % selectivity, 30 % conversion at 393K, 1 bar) [48] ; AuPdPt/AC (86.7 % selectivity, 30 % conversion at 393K, 1 bar)[48]; glycerol to glyceric and tartaric acid on AuPd/AC (97.1 % selectivity) and AuPt/AC (80.4 % selectivity) [34]; glycerol to glyceric and tartaric acid on AuPd/AC [34] ; and many others [56] . Table 2- 2 summarizes the operating conditions, yield, catalyst type (for alloys), feedstock, and products.

2.2.3 Key remarks on the catalytic, support and alloy effects on the process

The findings from the survey of the existing works on biomass derivatives oxidation on a solid catalyst show that the alloying effects are a function of their constituent

metals and the support. This was because the nature of the metal used in alloy another one influences the resulting material behavior; the same applies to the support. And their resulting behavior influences the yield, conversion, and selectivity for desired products. This implies that the alloying effect of some bimetallic catalysts can favor some undesired routes (degradation activities) over their desired ones on their surfaces. Like, Cu-in-Au eases the oxidation of OH to carboxylic acid, Ir-in-Au eases the breaking of C-H, Pt-in-Au eases the oxidation of OH to carboxylic acid with CO_2 release, and in many other cases. The AuPd was the alloy found to be a promising catalyst due to its better catalytic performance in benzyl alcohol (97 % selectivity) and glucose (97.1 % selectivity) oxidation. Moreover, the experiment report indicates that some pure metals better hinder degradation than their respective alloys [11,15]. These findings indicating a significant and careful choice is required when screening materials to obtain the best performance.

2.3 Overview of Catalytic Oxidation Furfural and HMF to Acids

Oxidation of furfural and HMF to acids (furoic acid and FDCA, respectively) involves removing hydrogen atoms and accepting oxygen or hydroxyl. The oxygen is often obtained for the activating oxygen gas to the oxygen atom (specie) on the catalyst surfaces. In the presence of water, the activation of the oxygen gas results in the production of surface hydroxyl species (instead of an surface oxygen atom). After successful removal of the hydrogen atoms and acceptance of hydroxyl or oxygen results in the conversion of the aldehyde and hydroxyl functional groups of the HMF into FDCA, a product with two carboxylic acid functionals production. Figure 2-5 diagrammatically displayed a primary mechanism of oxidizing furfural and HMF into acids. The oxidation process can be done in the presence or absence of a base. Ones held in the presence of a base are referred to as alkaline oxidation. While the oxidation carried out in the absence of base is referred to as base-free oxidation [44].

Base-free oxidation methods have been reported to have been less toxic than the other approach of oxidizing furfural and HMF in the presence of a base to obtain furoic acid and FDCA, respectively.

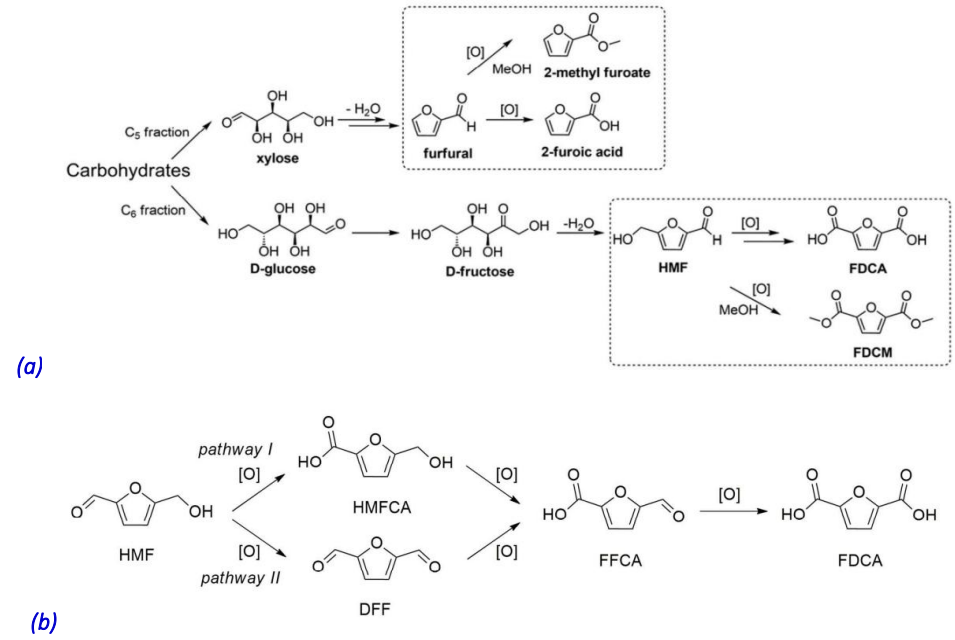

*Figure 2- 5 Schematic diagram showing **(a)** the synthesis of furoic acid and FDCA from biomass and possible degradation (oxidative esterification) routes, and **(b)** the general oxidation mechanism for transforming HMF into FDCA*

Moreover, the furfural and HMF oxidation process involves several steps over a heterogeneous catalyst surface. The state of each step tends to vary from one type of catalyst surface to another due to the varying affinity of the different catalyst surfaces for the species involved in the oxidation process. The presence of water in the oxidation process also changes the mechanisms involved in catalytic activities over the heterogeneous catalyst (whether they are metals, alloys, or metal oxides). The possible mechanisms involved in the conversion process are presented in detail for different situations (in the presence or absence of water) for the oxidation and degradation route in furoic acid (from furfural) and FDCA (from HMF) production. The possible mechanism involved in conversion is presented in Figure 2- 5. The scheme displayed the general mechanism involved in synthesizing furoic acid and FDCA from biomass (that is, carbohydrates), including a possible side reaction (a case of oxidative

esterification). The generic oxidation mechanism for transforming HMF into FDCA via the aldehyde oxidation (pathway I) and hydroxyl oxidation (pathway II) routes was also presented in Figure 2- 5.

We further reviewed the existing studies on the oxidation of furfural and HMF to acids such as furoic acid and formyl furan dicarboxylic acid (FDCA) in the presence of metals or their alloys. The works include both experimental and computational investigations. Our research into the diverse methods of obtaining FDCA in the literature unravels that the bulk of the existing FDCA consumed in the markets is largely produced from the oxidation of HMF. Likewise, the furoic acid from furfural is attracting the attention of both industries and researchers. Due to its wide range of applications in chemical, material, and pharmaceuticals productions using bio-based feedstock [57] . This significant drive of attention towards this method was due to its possibility of synthesizing it from biomass resources amidst this huge campaign against further exploration of petroleum resources [58]. Much research has attempted to synthesize different kinds of metal and alloy catalysts that would yield a higher yield for the production of FDCA. Any possible high-yield catalyst identified would significantly aid the industries in meeting the market's rising demand for FDCA. Some of these industries requiring these FDCA as feedstock [8,59,60] are presented earlier in this report's introduction. Similarly, furoic acid [38,59,61–63] also finds a wide range of applications in the market for the production of FDCA.

Some of these works have considered the study of single metal catalysts (such as Pt, Au, Ag, Pd, Ni, Ru, Co, and many others)[37,58,64–66], bimetallic materials or alloyed-metal catalysts (such as AuPd, AuCu, AuPt, PtPd, RuNi, RuPt, PdBi, AuAg, PtBi, and many others) [40,42,44,45,67–71], while some investigated the use of other catalytic materials [38,72] in the oxidation of furfural and HMF into acids. Other works attempt to explore the chances that different support in the catalyst design has on the formulation

performance while seeking a way to optimize the yield for higher production feasibility. However, we limit our reviews (in this Chapter) to the studies on the use of metal catalysts in the literature with emphasis on the use of gold (Au), platinum (Pt), and palladium (Pd), and any bimetallic form of Au/Pt/Pd for the oxidation of furfural (in Section 2.3.1) and HMF (in Section 2.3.2 and 2.4).

2.3.1 Metal Catalytic & Support Effects in Furfural Oxidation into Furoic Acid

A survey of existing studies [37–41,43,62,63,69] indicates that the research focuses on identifying catalysts that effectively transform furfural into furoic acid with a high yield and good selectivity. Some of these studies include Bruno [73] investigation which revealed the influence of Au-supported catalysts. In the study, it was confirmed that the use of Au/HT (that is, hydrotalcite) support favored 78 % furoic acid yield and more degradation. In contrast, Au/VPP (that is, vanadyl pyrophosphate) favored the production of maleic acid (with 38 % yield) in base-free oxidation of furfural (as shown in Figure 2- 6). With the use of MgO-based support for the Au catalyst, Ferraz et al. [66] obtained a better yield of 100 % for furoic (in the absence of base), different from the finding made using HT and VPP support. Despite the high yield of furoic acid reported for the use of MgO, leaching was the key challenge that accounted for its use in the process.

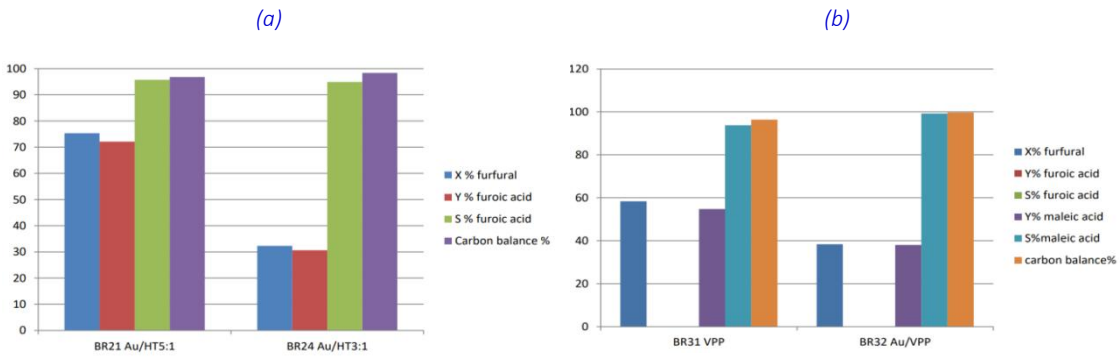

Figure 2- 6 (a) *Experimental results comparing different times of reaction 2h (BR24) and 6h (BR36) with Au/HT3:1* ***(b)*** *Effect of gold nanoparticle addition on the process.* ***Reaction conditions:*** *BR24 [Au/HT 3:1 (100mg), water (20mL), t=2h]; BR36 [Au/HT 3:1 (100mg), water(20mL), t=6h]; BR31 [VPP(100mg), water(20mL), t=2h]; and BR32 [Au/VPP(100mg), water(20mL), t=2h] at mass of furfural=50mg, P=15bar, T=110C. [Source: Bruno[73]].*

Moreover, Douthwaite et al.[69] experimentally confirmed that the alloying of Au with Pd supported by $Mg(OH)_2$ was found to have improved furoic acid yield from 63.30 to 93.20 % in a base (NaOH). Another study by Kumar et al.[38] experimentally identified an optimum yield of 81 % using alum-impregnated activated alumina in furoic acid production. Using titanium silicate[43] leads to higher selectivity for maleic acid than furoic acid. It was also established that the presence of an acid site on some support like Zeolite-templated carbons (ZTC) could aid in suppressing undesired side reactions, as reported by Papanikolaou et al.[41] for the use of Au/ZTC. The studies show that catalyst support significantly impacts the catalytic activity, which agrees with similar reports by Donoeva et al.[74] and other reports [39].

In another search to improve Au selectivity for the oxidation of furfural (FF) into furoic acid (FA), Al-Rawas et al.[40] explore the benefit of alloying Pt and Pd with Au/TiO_2. The study established that Au_3Pd has shown the highest selectivity for furoic acid (FA), while alloying Au with Pt favors better maleic acid (MA) selectivity. It is also found that the improvement significantly depended on the metal ratios, similar to an earlier study,[68] which also showed the impact of the metal ratio. A recent study by Sadier et al.[64] reported a 96 % furoic acid (FA) yield for using Ag/TiO_2 in a base. However, the recyclability study of the catalyst shows that catalyst activity easily deactivate due to the drastic drop in its activity after three runs. The study further established the loss of the activity to be associated with re-oxidation of the silver (Ag) particles.

Finally, there is a need to unravel more details on the activities of metals, especially Au, in the catalysis of the furfural oxidation to furoic. It helps to unravel why lower yield was obtained in the literature, especially in the report of Bruno favoring the production of undesired products. The insight gained from such an investigation would facilitate the design of a more effective and efficient catalyst.

2.3.2 Metal Catalytic & Support Effects in the Oxidation of HMF to FDCA

Here, we present survey works showcasing the effect of different metals and their catalyst support in the catalysis of the oxidation processes involved in the production of FDCA on Au, Pt, and Pd. The findings are summarized in Table 2- 3 to Table 2- 5.

2.3.2.1 Gold (Au) in HMF oxidation: Catalytic and support effects

Several studies in the literature (in Table 2- 3) have highlighted the implications of deploying several forms of metals in the oxidation process's catalysis for producing valuable products from HMF.

Table 2- 3 *Report of experimental studies on HMF oxidation studies using Au-catalyst [M=Metal, HT=hydrotalcite, AC= Activated carbon or Charcoal, ZTC=ZTC replica of BETA zeolite (β-ZTC), VPP=vanadyl pyrophosphate $(VO)_2P_2O_7$, Cp = Sibunit carbon, FA = furoic acid, MFA = methyl-2-furoate, MA = maleic acid].*

Ref	Au Support	Ratio	Oxidant	P (bar)	Base Used	T (°C)	Time (h)	X(HMF) %	Y (FDCA) %
[75]	TiO_2	150	air	10	NaOH	130	8	100	99
[76]	Al_2O_3	100	O_2	3	NaOH	70	4	100	99
[77]	HT	40	O_2	50 $^{mL}/_{min}$	Base free	93	7	99	99
[75]	CeO_2	640	Air	10	NaOH	130	5	100	96
[78]	CeO_2	53	O_2	5	Na_2CO_3	140	15	99	91
[79]	MgO	50	O_2	16	Base free	110	2	99	91
[80]	ZrO_2	384	air	50	NaOH	125	5	100	89
[81]	TiO_2-MgO	200	O_2	3	NaOH	60	2	99	87(HMFCA)
[82]	TiO_2	110	O_2	3	NaOH	60	6	99	85
[81]	TiO_2-CeO_2	200	O_2	3	NaOH	60	2	99	84(HMFCA)
[81]	AlOOH-S	200	O_2	3	NaOH	60	2	100	80(HMFCA)
[81]	Cp	200	O_2	3	NaOH	60	2	100	79(HMFCA)
[83]	SiO_2	72	O_2	10	$NaHCO_3$	90	5	99	74
[84]	TiO_2	100	O_2	10	NaOH	30	18	100	71
[85]	TiO_2	100	O_2	3.4	NaOH	25	22	100	69
[86]	CeO_2	100	O_2	10	NaOH	70	4	100	52
[71]	AC	200	O_2	3	NaOH	60	2	100	36
[81]	Cp	200	O_2	3	NaOH	60	2	100	21
[87]	PVP-HT	-	O_2	40 mL/min	Base free	95	3	69	1

One of the works uses Au/MgO in HMF oxidation [79], where a conversion of 99% and FDCA yield of 91 % in the absence of base was obtained. Despite recording a lower degradation, the result for oxidation showed that MgO support got leached. The

leaching challenge makes catalyst recycling difficult. To address the challenge, the author synthesis a composite made up of MgO-MgF_2 to serve as a support of Au.

Using the composite resulted in less FDCA yield, with degradation accounted for in carbon loss. In the presence of a base, a similar kind of higher effect (99 % conversion and 91 % FDCA yield) was obtained for the use of Au/CeO_2 catalyst[78]. Although there is no report of leaching for using CeO_2, but the toxicity of the basic environment is a subject of concern. In oxidizing HMFCA to FDCA, the yield obtained for the use of Au/MgO [78] (with leaching problem) and Au/CeO_2 [78] (in the basic environment) is relatively higher than that obtained for using activated carbon (AC) support [71] that yields 36 % FDCA (at 100 % conversion in a base); TiO_2 [84] that yields 71 % FDCA in a base (at 100% conversion); and Cp (Sibunit carbon) support [81] with a yield of 21 % (at 100 % conversion in a basic environment). With different kinds of varying yields reported for the use of other supports, it is essential to computationally explore details on the activities of Au catalysis in the oxidation of HMF to acids to understand better how it influences the reaction. It has been established that supports like MgO [79] and HT [77], significantly influences the activity in a catalyst. And the like of such supports used for the Au has shown a good yield. However, the catalyst has often been reported to suffer the challenge of leaching.

Differently from the behavior of the previously used support for Au catalyst, the use of ZrO_2 [88] resulted in the production of the new product, DMF, with a yield of 78.5 %. The catalyst was found to have promoted the oxidative esterification route that led to the new products. Tianqi et al. report further unravel that AC support promotes hydroxyl oxidation to produce DFF. On the way, HT support promotes the aldehyde oxidation to produce HMFCA. It shows that the support not only provides a good surface area for the metal activities but also competes with its in influencing the reaction route and product selectivity. Table 2- 3 further presents other parameters

(operating conditions), the kind of materials used for catalyst synthesis, and other details for our existing works on the deployment of pure Au in the oxidation of HMF.

The literature has largely established the significant impact of catalyst support choice, as existing works (displayed in Figure 2- 7 and Figure 2- 8) have shown that the choice has contributed to improving the Au's catalytic activity on the surface. Some of these influences include the kind of product distribution, conversion, yield, and other parameters of the reaction kinetics. Many experimental studies have established the

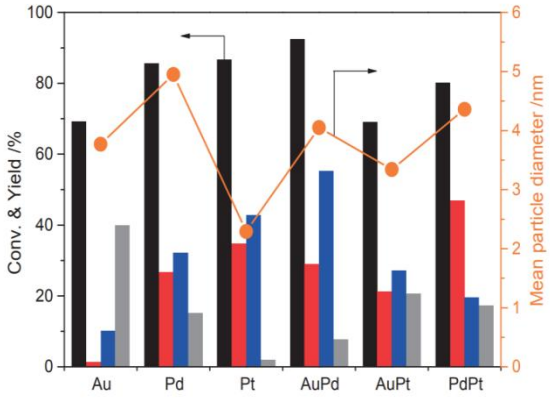

Figure 2- 7 Experimental reports collated by Choudhary et al.[87] Study of the pure form and alloying effect of Au, Pd, and Pt supported by PVP-HT in base-free oxidation (using 0.5mmol HMF, Catalyst (Metal load on HT is 1wt %; 70mg), 5mL water, 3h, 95°C, oxygen flow of 40mL/min, with metal alloy ratio of 1:1. [Note that HMF conversion (black bar), Yields of FDCA (red bar), FFCA (blue bar), and HMFCA (gray bar)].

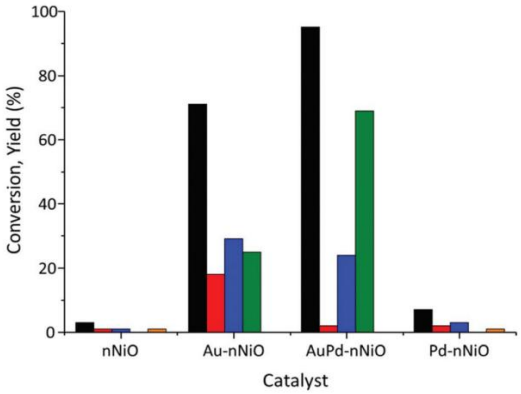

Figure 2- 8 Impact of pure Au and its alloy effect on the catalysis of HMF oxidation using nNiO support reported by Bonincontro et al.[87] at 90°C, 6h, 10 bar O2, HMF/metal is = 100. [Note that HMF conversion (Black bar), HMFCA yield (Red bar), FFCA yield (Blue bar), FDCA yield (Green bar), and DFF yield (Gold bar)].

impact of support alone on the reaction activities in the absence of the metal, but no effects of unsupported metal activity on HMF oxidation have been reported experimentally. However, the survey of the works in the literature indicates how significant Au catalytic activities are faced with the degradation favoring the production of HMFCA more than FDCA (the desired product) relative to other metals (Pd and Pt), as shown in Figure 2- 7. There is a need to understand the influence of the metal alone on the catalysis of the oxidation pathways leading to the acids (that is, furoic acid and FDCA) using a computational approach. Such investigation would help to unravel factors hindering the production of FDCA over Au. Moreover, leaching has

also been identified as one of the major challenges reported for using some reducible basic supports, like MgO, HT, and others, although they showed a higher yield.

2.3.2.2 Platinum (Pt) in HMF oxidation: Catalytic and support effects

The use of platinum (Pt) catalyst in the literature has been largely evaluated similarly to the level of attention that the use of Au is also receiving. Similar to the report obtained for the use of pure Au over a different range of supports, a good range of support investigated in the literature for the use of the Pt is highly beneficial, resulting in a yield ranging from 95 to 100 % FDCA with a good conversion in most of these supports.

Table 2-4 *The existing experimental studies on the use of Pt in the oxidation of HMF to valuable products [RGO=Reduced Graphene Oxide, GO = Graphene Oxide, CTF = covalent triazine framework, HT = hydrotalcite, CNT = carbon nanotubes, AC or C = Activated carbon or Charcoal, PVP=poly (N-vinyl-2-pyrrolidone), Cp = Sibunit carbon, EDA = ethylenediamine, C-EDA = nitrogen-containing carbons EDA, Feed/Metal Ratio = F/M]*

Ref	Pt Support	F/M	Oxidant	P (bar)	Base Used	T (° C)	Time (h)	X (HMF) %	Y (FDCA) %
[89]	110-Fe_3O_4 @C@Pt	24	O_2	100 $^{mL}/_{min}$	Na_2CO_3	90	4	100	100
[90]	PVP-ACS-800	125	O_2	10	Base free	110	5	100	100
[91]	NC-CeO_2	163	O_2	4	Base free	150	4	100	99
[92]	CNTs	100	O_2	5	Base free	95	14	100	98
[93]	Dowex-Na resin	62	O_2	20	Base free	120	22	100	98
[94]	$Ce_{0.8}Bi_{0.2}O_2$-δ	200	O_2	10	NaOH	23	0.5	100	98
[95]	C-O-Mg	50	O_2	10	Base free	110	12	100	97
[96]	ZrO_2-ALD-30	70	O_2	4	Base free	100	12	100	97
[92]	HT	100	O_2	5	Base free	95	14	100	97
[97]	CNT	200	O_2	30	Base free	100	12	100	97
[96]	CeCP@Pt	50	O_2	30 $^{mL}/_{min}$	NaOH	70	12	100	96
[95]	C-EDA-4.1	50	O_2	10	Base free	110	12	100	96
[94]	α-Al_2O_3	43	O_2	1	Na_2CO_3	140	12	96	96
[92]	GO	100	O_2	5	Base free	95	14	100	95
[98]	TiO_2	100	Air	40	Na_2CO_3	100	6	99	84
[99]	RGO	40	O_2	50	NaOH	25	24	100	84
[98]	AC	100	Air	40	Na_2CO_3	100	6	100	69
[87]	PVP-HT	-	O_2	40 $^{mL}/_{min}$	Base free	95	3	87	35
[92]	Al_2O_3	100	O_2	5	Base free	95	14	94	26
[94]	CeO_2	200	O_2	10	NaOH	23	0.5	100	20
[92]	ZrO_2	100	O_2	5	Base free	95	14	81	8

Moreover, Some of these supports are proven to be a good yield in the presence of a base, while some are in the absence of a base. Some of those catalyst supports that have positively influenced the catalytic activity of the Pt catalysts to include NC-CeO_2 [91] with 99 %; Dowex-Na Resin [92] with 98 %; CNT [97, 92] with 97-98 %; 100-Fe_3O_4@C [89] with 97 %; HT [92] with 97 %; Al_2O_3 [92] with 96 % in a base; GO [92] with 95 %; and many others [90,95,96,] whose details are presented in Table 2- 4.

Some of the other catalysts support that show lower yields include the use of AC [98] with a yield of 69% FDCA in a base; CeO_2 in base yields 20 % FDCA [94]; Al_2O_3 with a yield of 26 % FDCA in the absence of a base; and ZrO_2 with an 8 % yield of FDCA [92] Similar to reports [71] for the use of Au/AC (with 36 % FDCA yield), the use of pure AC support for Pt [98] in the oxidation of HMF has also been proven to have a negatively (with a yield of 69 %) impact on its activity in the oxidation of HMF into FDCA. Moreover, the yield obtained for Pt/AC [98] in oxidizing HMF into FDCA was much better than that obtained using Au/AC [71], with both carried out in a base. In contrast, other supports showed poorer yields for the FDCA production in the presence of the Pt catalyst. And some of these supports, like CeO_2, Al_2O_3, and ZrO_2, were established in the previous report (in Table 2- 4) to have positively influenced the yield of FDCA when supporting Au-catalysts, unlike that of the Pt.

This implies that the impact of the support used in synthesizing a metallic catalyst varies from one metal to the other. A good number of reports presented in Table 2- 4 for the use of Pt indicated that a good number of base-free oxidation over Pt-supported catalysts showed a higher acid yield (furoic acid and FDCA), with a few cases showing lower yields.

2.3.2.3 Palladium (Pd) in HMF oxidation: Catalytic and support effects

A further survey of the findings reported on the use of pure palladium (Pd) catalysts and how the choice of support materials in their synthesis has impacted the resulting yield for the oxidation of HMF into valuable products reveals that a lot has been reported. Out of which, a few sets of catalyst supports has been proven to be highly efficient in promoting the Pd activity. Some of these few support materials include Pd/PVP, which shows a 90 % FDCA yield [100]; Pd/KF-Al_2O_3, which shows a 91 % FDCA yield [100]; Pd/ZrO_2-La_2O_3 which shows a 90 % FDCA yield [100]; Pd/HAP@Fe_2O_3 shows a yield of 93 % FDCA [101]; Pd/HT yields 100% FDCA [102], and many other supports which presented in Table 2- 5.

Table 2- 5 *The existing experimental studies on the use of Pd in the oxidation of HMF to valuable products [Note: CNT=carbon nanotubes, AC = Activated carbon, charcoal, or carbonaceous material, FLG = few-layers graphene, CNF= carbon nanofibers, HPGSs = highly porous nitrogen- and phosphorus- co-doped graphene sheets, PVP = poly (N-vinyl-2-pyrrolidone), PVP = polyvinylpyrrolidone, Cp = Sibunit carbon, M = Metal, F = Feed].*

Ref	Pd Support	F/M Ratio	Oxid-ant	P (bar)	Base Used	T (°C)	Time (h)	X (HMF) %	Y (FDCA) %
[102]	HT	21	O_2	100 $^{mL}/_{min}$	Base free	100	8	100	100
[103]	$CaMn_2O_4$	25	O_2	100 $^{mL}/_{min}$	Base free	100	12	100	99
[101]	γ-Fe_2O_3@HAP-Pd(0)	43	O_2	30 $^{mL}/_{min}$	K_2CO_3	100	6	97	93
[100]	KF-Al_2O_3	100	O_2	1	NaOH	90	8	100	91
[104]	AC-Fe_2O_3	56	O_2	1	K_2CO_3	80	4	98	91
[100]	PVP	100	O_2	1	NaOH	90	6	100	90
[100]	ZrO_2 -La_2O_3	100	O_2	1	NaOH	90	8	100	90
[105]	C@Fe_3O_4	27	O_2	20 $^{mL}/_{min}$	K_2CO_3	80	6	99	87
[106]	FLG	83	O_2	5	K_2CO_3	160	5	100	85
[107]	AC	16	O_2	20 $^{mL}/_{min}$	K_2CO_3	140	30	100	85
[108]	HPGSs	60	O_2	500 $^{mL}/_{min}$	NaOH	50	6	100	83
[103]	$CaMn_3O_6$	25	O_2	100 $^{mL}/_{min}$	Base free	100	12	100	79
[100]	Al_2O_3	100	O_2	1	NaOH	90	8	100	78
[85]	AC	150	O_2	7	NaOH	70	4	100	71
[103]	$Ca_2Mn_3O_8$	25	O_2	100 $^{mL}/_{min}$	Base free	100	12	100	70
[106]	CNF	83	O_2	5	K_2CO_3	160	5	100	70
[106]	CNT	83	O_2	5	K_2CO_3	160	5	100	60
[103]	$CaMnO_3$	25	O_2	100 $^{mL}/_{min}$	Base free	100	12	100	59
[81]	Cp	200	O_2	3	NaOH	60	2	99	55
[100]	TiO_2	100	O_2	1	NaOH	90	8	100	52
[81]	AlOOH-S	200	O_2	3	NaOH	60	2	97	50
[87]	PVP-HT	-	O_2	40 $^{mL}/_{min}$	Base free	95	3	87	35

However, the catalyst supports that showed lower yields for using Pd include PVP-HT yielded 35 % FDCA; AlOOH-S showed a yield of 50 % FDCA; TiO_2, with a 52 % FDCA yield [100], and CNT, with a yield of 60 % FDCA [106]. The yield obtained for the use of Pt/TiO_2 [98] in the oxidation of HMF into FDCA showed a higher yield of 84 % FDCA unlike that case of Pd/TiO_2 [100] which was reported to be 52 % yield, with both cases in a base.

The survey reveals that some metal activities in catalysis could strongly influence the reaction output more than the support effect, like the case of Pt/TiO_2, unlike the case of Pd/TiO_2, where a lower yield would obtain. It was also identified that using reducible supports like HT and others has strongly influenced the higher FDCA yield obtained on Pd-supported catalysts.

2.3.3 Key remarks on the catalytic and support material effects

The use of platinum catalysts has been largely reported to be effective, with higher conversion and selectivity compared to the use of palladium and gold-supported catalyst. The catalyst supports have also been established to influence the catalysis of the reaction progresses in the oxidation of the furfural and HMF into acid. In an absence base, the non-basic support materials have largely shown lower acid yield with a production of undesired products. The basic support materials have generally shown a better yield and selectivity for acid during oxidation, but those supports are not stable in the solution that is increasingly acidic with the generation of carboxylic acid which favors leaching in the process. It is, therefore, vital to investigate how to improve Au activity and selectivity for acid using non-basic support that cannot be exposed to leaching.

2.4 Alloying effects in the catalysis of furfural and HMF oxidation

The previous section established the efforts of the research works on the promotion of pure metal usage in the oxidation of furfural and HMF (Where the impact of how their supports influences their yields were reported). However, other research tends to give further attention to exploring the metal alloying effect on the catalysis of the oxidation processes in transforming the furfural and HMF oxidation into valuable products. Details of some findings reported in the literature on using Au-alloys, Pt-alloys, and Pd-alloys are reviewed from the existing reports.

Table 2- 6 *Report of experimental studies on Furfural (FF) and HMF oxidation studies using Au-alloys [CNT=carbon nanotubes, ZOC = Zinc hydroxycarbonate, AC= Activated carbon or Charcoal, nNiO=Nanosized-NiO, PECN = hydrophilic mesoporous ionic copolymer,, IRA-734 = commercial IX resin Amberlite, Feed/Metal = F/M].*

Ref	Au Promo-ter	Support	F/M	Oxid-ant	P (bar)	Base Used	T (°C)	Time (h)	X (HMF) %	Y (FDCA) %
[111]	Pd	La-CaMgAl-LDH	68	O_2	5	Base free	100	4	100	99
[70]	Pd	nNiO	100	O_2	10	Base free	90	14	100	99
[112]	Pd	PECN	100	O_2	1	K_2CO_3	90	12	100	99
[113]	0.33Cu	TiO_2	100	O_2	10	NaOH	95	4	100	99
[114]	Pd	ZOC	100	O_2	3	$NaHCO_3$	80	4	99	99
[115]	Cu	TiO_2	100	O_2	10	NaOH	95	4	100	95
[71]	Pd	AC	200	O_2	3	NaOH	60	2	100	95
[44]	Pd	CNT	100	O_2	5	Base free	100	18	100	91
[67]	Pd	IRA-743	100	air	10	Na_2CO_3	100	4	100	93
[116]	(3/7)Ag	ZrO_2	100	Air	10	NaOH	120	5	100	75
[71]	Pt	AC	200	O_2	3	NaOH	60	2	100	62
[116]	(1/9)Ag	ZrO_2	100	Air	10	NaOH	120	5	100	31
[116]	(5/5)Ag	ZrO_2	100	Air	10	NaOH	120	5	100	29
[87]	Pd	PVP-HT	-	O_2	40 $^{mL}/_{min}$	Base free	95	3	33	29
[87]	Pt	PVP-HT	-	O_2	40 $^{mL}/_{min}$	Base free	95	3	69	21
[116]	(7/3)Ag	ZrO_2	100	Air	10	NaOH	120	5	100	10
[116]	(9/1)Ag	ZrO_2	100	Air	10	NaOH	120	5	100	1

2.4.1 Au-alloy effects on the catalysis of furfural and HMF oxidation

Some of the reported alloys for Au include AuPd, AuPt, AuAg, AuCu, and many others [44,67,71,81,109,110] summarized in Table 2- 6. A Survey of the impact of these Au alloys on the catalysis of the oxidation processes studied by Churchil et al. [67] work which

confirmed a yield of 93 % FDCA using AuPd/IRA-743 in a base; Danilo et al. [70] confirmed 99 % FDCA yield for AuPd/nNiO; Alberto et al. [71] confirms 95 % FDCA yield in a base; and many other works [112]. This confirms that the use of AuPd alloy for the oxidation of HMF into FDCA has been reported to have shown a good FDCA yield better than using some pure Au-supported catalysts. Although some of these works that deployed AuPd alloys largely use base in their oxidation processes with only a few works, consider the use of base-free ones.

The use of the Au-alloys has shown 62 % FDCA yield using AuPt/AC in a base[71]; 75% FDCA yield using AuPd/ZrO_2 with base in 3:7 ratio[116]; and AuCu/TiO_2 in a base 95-99% FDCA [113,115]. A smaller ratio of Pd or Cu in the Au-alloy was demonstrated to have shown better FDCA yield in the oxidation of HMF, unlike a higher ratio. The effect of alloying Pd and Pt with Au/AC was found to have reduced degradation and yielded 95 % and 62 % FDCA, respectively, compared to using a pure metal, Au/AC, which shows a lower yield (36 %).

2.4.2 Pt-alloy effects on the catalysis of furfural and HMF oxidation

A few of the research works that investigated the use of Pt-alloys in the catalysis of furfural and HMF oxidation into valuable products are presented in Table 2- 7.

Table 2- 7 *The existing experimental studies on the use of pt in the oxidation of furfural and HMF to valuable products [Note: AC= Activated carbon or Charcoal, FA=Furoic acid, Feed/metal = F/M].*

Ref	Cat.	Support	Feed type	F/ M	Oxid- ant	P (bar)	Base Used	T (° C)	Time (h)	X (HMF) %	Y (FDCA) %
[98]	PtBi	AC	HMF	100	Air	40	Na_2CO_3	100	6	100	99
[98]	PtBi	TiO_2	HMF	100	Air	40	Na_2CO_3	100	6	99	99
[117]	PtPb	AC	FF	-	O_2	5 $^{mL}/s$	NaOH	65	1	93	89 (FA)
[87]	PtPd	PVP-HT	HMF	-	O_2	40 $^{mL}/_{min}$	Base free	95	3	81	47

This includes Hichan et al., [98] whose attempt to alloyed Bi with Pt goes a long way to improving the FDCA production with a yield of 99 % in a base. The authors [98] further

established that no significant difference in yield and conversion was obtained for using AC or TiO_2 in support PtBi alloy due to similar yield reported for supports.

In the presence of a base, Verdeguer et al. [117] further explored the impact of alloying Pt with Pb (using charcoal (AC) as the support in the catalyst matrix) in the oxidation of furfural into furoic acid. Findings from study [117] indicate that the PtPb/AC yielded 89 % (at 93 % conversion) furoic acid. This reveals that the introduction of Pb and Bi in Pt/AC has significantly improved its FDCA yield from 69 % (Pt/AC) to 89 % (PtPd/AC) and 99 % (PtBi/AC), respectively, in the catalysis of HMF oxidation.

2.4.3 Pd-alloy effects on the catalysis of furfural and HMF oxidation

Some of the Pd-based alloys (in Table 2- 8) explored in the literature include PdAu [81], PdPt-PVP [87], $PdNi_{0.9}Pd_{0.1}$ [118], PdBiTe, [119] and many other alloys. One of the Pd-alloy is the PdAu that was investigated by German et al., whose introduction of Au into the Pd catalyst matrix significantly appreciated the FDCA yield from 54 % (on Pd only) to 74 % on the alloy (as shown in Figure 2- 9).

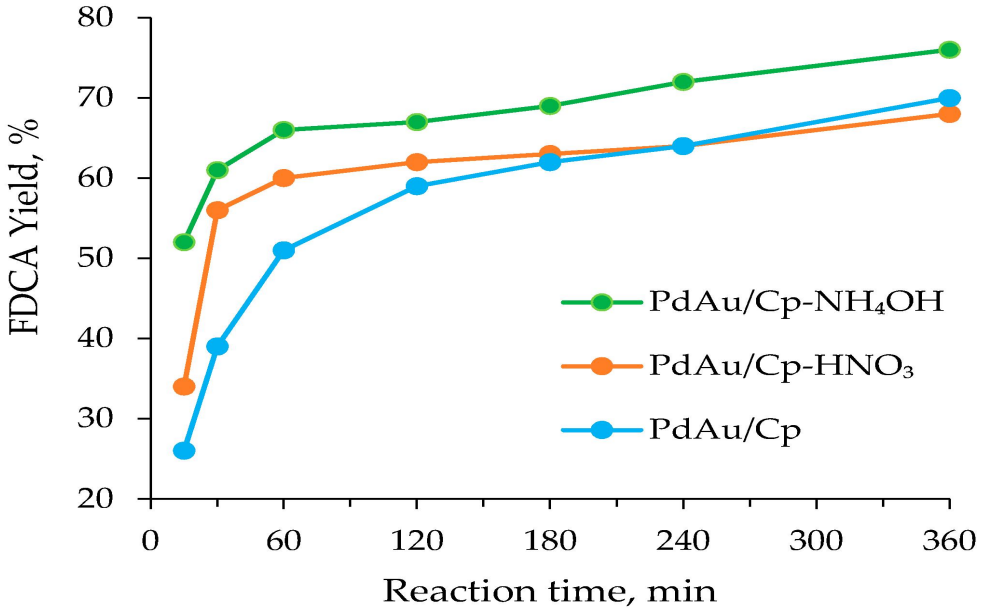

Figure 2- 9 *A production-time plot for FDCA showing the effect of Sibunit (Cp) support treatments in HMF oxidation on Pd-Au catalysts using 0.15 M HMF (H_2O, 0.15 L), NaOH/HMF = 2, T = 60 °C, $P_{(O2)}$ 3 atm, R = 200. (Source: German et al.[81])*

Further evaluation of the support impact or influence on the catalytic performance of the catalyst was seen to have improved with the replacement of Sibunit carbon (Cp) support with Cp-NH_4OH (81 % FDCA yield) in a base. Whereas the alloyed of the Pd

Table 2- 8 *The existing experimental studies on using Pd in the oxidation of furfural and HMF to valuable products [Note: HT=hydrotalcite, AC= Activated carbon or Charcoal, PVP = polyvinylpyrrolidone, Cp = Sibunit carbon, Feed/metal = F/M].*

Ref	Pd Promo-ter	Support	Feed type	F/M	Oxid-ant	P (bar)	Base Used	T (°C)	Time (h)	X (HMF) %	Y (FDCA) %
[87]	Pt-PVP	HT	HMF	75	O_2	40 $^{mL}/_{min}$	Base free	95	11.5	100	100
[119]	Bi-Te	AC	HMF	100	O_2	1	KOH	50	6	100	95
[118]	$Ni_{0.9}Pd_{0.1}$	Nil	HMF	20	Air	Nil	Na_2CO_3	80	4	100	86
[81]	Au	Cp-NH_4OH	HMF	200	O_2	3	NaOH	60	6	99	81
[81]	Au	Cp-HNO_3	HMF	200	O_2	3	NaOH	60	6	99	74
[81]	Au	Cp	HMF	200	O_2	3	NaOH	60	6	99	71

with Pt-PVP on HT support results in a yield of 100 % in the absence of base. Other works confirm a yield of 95 % FDCA for using $PdNi_{0.9}Pd_{0.1}$ [118], and 86 % yield for using PdBiTe [119] on AC support. They indicate that trimetallic alloys can also aid in improving the catalytic performance of metal, like the case of $PdNi_{0.9}Pd_{0.1}$ [118].

The survey of works done reveals that the introduction of Au in Pd/Cp(German et al., 2021) (PdAu/Cp) and Bi and Te in Pd (PdBiTe/AC) significantly improves the FDCA yield obtained from the oxidation process. The catalyst support and the kind of treatment were established that have also affected the selectivity and yield for FDCA, in line with the reported works in the literature. No report was found for the base-free oxidation using an alloy-based catalyst.

2.4.4 Key remarks on the alloying effects

The survey of work reveals that significant attention is given to the experimental investigation of the Au alloy effect on the catalysis of HMF oxidation into FDCA compared to Pt and Pd. The lesser attention (with few reports in the literature) given

to the study of the alloying effect on Pt and Pd could be due to good activities reported for using their pure form compared to that of Au. Moreover, the alloying of metal with a new one has been demonstrated to have significantly improved the yield of FDCA from the oxidation of HMF across the Au, Pt, and Pd. It was also shown that with the use of an alloy-based catalyst in oxidation, the support effect on the catalysis of the reaction is observed. However, the impact of introducing new metal in the catalyst matrix has yielded varying outputs. This insight suggests the use of extra care in screening the metals before considering them for alloying another one. The use of a computational approach can help aid the screening metals of the alloys for existing metals to improve their catalytic activity in oxidation while inhibiting the degradation activities on the catalyst surface.

2.5 Theoretical Study for the Roles of Metals & their Alloys

Here, the reports of existing works on the deployment of theoretical approaches in the search for an innovative idea for the synthesis or design of high-performance metal-based catalysts are presented in this section. The survey of the literature includes both alloys and pure metals. The earlier section of this report presents the existing findings on deploying a computational approach to design better catalysts for the oxidation of different biomass derivatives (such as sugars, alcohols, furan-based compounds, and many others). The later part of the report presents existing works on the use of Au, Pt, and Pd (including any alloy of such metals) in the oxidation of furfural and HMF into valuable products such as furoic acid, FDCA, and any others.

2.5.1 Catalysis of the oxidizing wide range of biomass derivatives on metals

With the use of the DFT (GGA/PBE) calculation method, Li et al. [18] show that the yield (50 % tartaric acid) obtained experimentally for the alloying of the Pt with Au on TiO_2 in the oxidation of glucose was found to be a function of the synergistic activity of Pt and Au on the catalyst surface created by alloying of Au with Pt. The Pt-Au alloy on

the TiO_2 contributed to influencing the kinetics of the C-H and C-C cleavage reaction in the oxidation process. Caglar et al.[20] further investigation into $PtAu/TiO_2$ catalysis of glucose oxidation confirms that the interaction of the surface hydroxyl (xOH) interaction with glucose was much better on the Pt site than Au and DFT (B3LYP). This was contrary to the report of Amaniampong et al. [19] and Gu et al.[109], which confirms that the presence of surface xOH aid in easing oxidation processes. Gu et al. [109] demonstrated the impact of surface xOH in the oxidation of ethanol into ethanoic acid on Au and Pt to be advantageous using DFT-dDsC (GGA/PBE) shown in Figure 2- 10(a). The study established the benefits of alloying Au with Pt in the oxidation process. And it confirmed the oxidation in the presence of water (generating xOH) to benefit the process. The author[120] unraveled that the co-adsorption of xO and xOH could facilitate the production of carbon dioxide from xCOOH, unlike HCOOx, which was found to be more challenging. The works of Gu et al.[109] (shown in Figure 2- 10b), Amaniampong et al.[19], Wang & Liu[121] and Scaranto & Mavrikakis[120], and many others works were able to establish the significance of having water present in the base-free oxidation, especially for the surface like Au and its alloys.

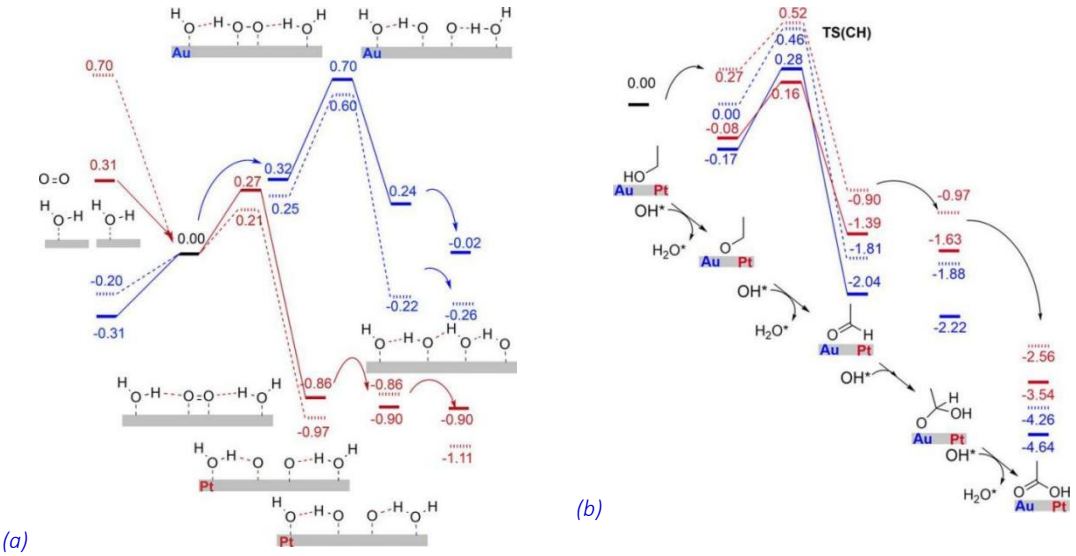

(a) *(b)*

Figure 2- 10 *The profiles showing* ***(a)*** *the water oxidation over Au and Pt,* ***(b)*** *the ethanol oxidation over Au alloyed with Pt in presence of water, where dash line represent basic while straight line represented neutral pH. (Source: Gu et al.[109] report)*

Other works' findings for investigating alloying metal with another on the catalysis of the oxidation process are presented in Table 2- 10 (for the use of alloys). One of the works that investigated the alloy effects include, Monyoncho et al. [122] , which evaluated the electrocatalysis influence of Pd_3Au, Pt_3Au, and Pt_3Ga in promoting ethanol oxidation into carbon dioxide and hydrogen using DFT (GGA/PBE). From this, it was confirmed that none of the alloys evaluated were found to be promising. Similarly, Wang & Liu [121] and Scaranto & Mavrikakis [120] further computationally investigated the feasibility of synthesizing carbon dioxide and hydrogen from formic acid oxidation. Wang & Liu [121] showed that Pt(111) in water, the C-H barrier was one higher barrier hindering the reaction progress, but with the increased appearance of formate coverages, formic acid oxidation go accelerated in the presence of an electric field. In agreement with the report of Wang & Liu [121] that C-H scission is difficult on Pt(111), the report of Scaranto & Mavrikakis [120] similarly indicated that the HCOO-H scission, which confirms to be easier than H-COOH on Pd(111).

Monyoncho et al. [120] unraveled that the co-adsorption of xO and xOH could facilitate the production of carbon dioxide from xCOOH, unlike HCOOx, which was found to be more challenging. The works of Gu et al.[27] (shown in Figure 2- 10b), Amaniampong et al.[19], Wang & Liu [121] and Scaranto & Mavrikakis [120], and many others works were able to establish the significance of having water present in the base-free oxidation, especially for the surface like Au and its alloys.

Table 2- 9 *Other biomass derivative oxidation processes investigated using metals only in DFT calculation.*

Ref	Code	Method	Metals	Feedstock	Product	Findings made
[123]	GWAP	PAW / BEEF / vdW	Au(111)	Alcohol (Ethanol)	Acetald-ehyde	The molecular oxygen activation was assisted by a hydrogen-bond-donor species (ethanol). This led to hydrogen abstraction from the bond donor to form an xOOH intermediate, followed by its facile dissociation.
[124]	VASP	PAW / PW91	Au(111), Au(511), Au-rod, Au_{38}	Alcohol (Ethanol)	Aldehydes	Oxidative dehydrogenation of alcohol into carbonyl compounds is structure dependent and the activity of the Au site accessible would be subject to its CN. The higher the CN, the lower the Au activity.
[27]	VASP	PAW / PBE / dDsC	Au (111), and Pt (111)	Ethanol	Ethanoic acid	The important role played by water for OH generation in oxidation was demonstrated to be significant, and the benefit of alloy Pt with Au was confirmed to be impressive for oxidation rate improvement.
[120]	DACAPO	Ultrasoft Vanderbilt Pseudopote ntials / PW91	Pd (111)	Formic acid	Carbon dioxide, hydrogen gas	HCOO-H scission is easier than H-COOH scission on Pd (111). Also, further breaking of HCOO is more challenging than COOH. However, co-adsorption of O and OH aided CO_2 production from COOH, unlike HCOO, which was still difficult.
[121]	SIESTA	Troullier-Martins norm-conservin Pseudopote ntials / PBE	Pt (111)	Formic acid	Carbon dioxide, hydrogen gas	C-H bond breaking was found to be of high barrier (1eV). Moreover, the increased appearance of formate coverage accelerates formic acid oxidation in the presence of an electric field & water

[31]	VASP	PAW / PBE / vdW	Pt (111)	MeOH, EtOH, 1-PrOH, 2-PrOH, & 2-BuOH	Valuable products	Pt showed insignificant impact on the surface activity with/without water.
[125]	Quantum Espresso	Ultrasoft pseudopotentials (USPP) / PBE / empirical Grimme-D3 method	Au/TiO_2	Methanol	Valuable products	Rate-determining step (RDS) was identified as methoxy oxidation.
[35]	DMol3 / Material Studio	Double Numerical Plus Polarization (DNPP) / PBE / vdW - Grimme-D2 method	Pt(111)	Glycerol	Tartronic & glyceric acid	The stable glyceric acid promotes the cracking of the C-C bond resulting in lower selectivity for desired products. Promoters like Cu and Co were suggested to present C-C bond cracking, leading to glycolic acid production instead of tartronic acid.
[126]	VASP	PAW / PBE with plane wave	Au(111)	Methanol	Formald-ehyde & other valuables	Sufficiency of surface oxygen, the slab in methanol oxidation was critical to influencing product distribution (in the absence of water)
[127]	Gaussian	MO6 / 6-31++G (d,p), LANDL2DZ for metals	Au_8^- (Cluster model)	Methanol	Formic acid	RDS is the 1st step (H abstraction of methoxy species).
[20]	Gaussian	B3LYP / 6-31G(d,p), LANDL2DZ for metals	Au and Pt (Cluster model)	Glucose	Valuable products	Interaction of the glucose with surface OH was stronger on Pt than Au via thermodynamic analysis

Table 2- 10 Other biomass derivative oxidation processes investigated using alloys in DFT calculation.

Ref	Code	Method	Metals	Feedstock	Product	Findings made
[27]	VASP	PAW / PBE / dDsC	Au-Pt	Alcohol (ethanol)	Carboxylic acid	O_2 activation in a base shows a lower energy barrier than a neutral one on Au, but the reverse was the case of Pt. Au-alloyed with Pt yield better properties.
[128]	DMol3	Localized double-numerical quality basis set with polarization functions (DNP) / PBE	Au-Pd (111), Au-Pd (100)	Alcohol (methanol)	Formal-dehyde	The study finds an unusual O_2 activation via an OOH route in place of direct dissociation on Au–Pd catalysts (i.e., Pd aids co-adsorption of xO_2 & xCH_3OH to yield *OOH). Which enhanced its activity and selectivity.
[129]	DMOL	DFT Semi-core Pseudopots (DSPP) / PBE / Grimme's D3 approach	Pd (111), PdZn (110)	Ethanol	Ethanoic acid	The addition of Zn to the Pd slab enables the surface to have two sites with a good affinity for OH and ethanol compared to a pure Pd slab in the presence electric field.
[122]	VASP	PAW / PBE	Pd_3Au (100), Pt_3Au(100), Pt_3Ga(100)	Ethanol	Carbon dioxide	The study was not able to identify a promising electrocatalyst for the process.
[130]	VASP	PAW / PBE / Grimme's D3 approach	Pt (111), Pd, Au	Ethanol	Valuable product	Pt(111), Pt/Pd(111), Pt/Au(111), and Pd/Pt(111) were confirmed to have improved adsorption characteristics and good prospective catalysts for oxidizing ethanol.
[131]	VASP	PAW / PBE / dDsC	$AuCu/CeO_2$	Fatty alcohol ethoxylates	Alkyl ether carboxylic acids	Higher Cu atoms' density over-stabilizes the intermediates, leading to a higher energetic span compared to pure metals and low Cu-alloy, indicating that the isolation or dispersal of Cu on the Au-Cu alloy would facilitate catalysis.
[18]	CASTEP	PBE with plane wave	Pt(111) PtAu(111)	Glucose	Tartaric acid	The additional defect created on Pt with the introduction of Au on it alters the kinetics involved in the oxidation process.
[17]	Gaussian	B3LYP / 6-31G(d,p) / LANDL2DZ for metals	Au, Cu, Ni, Pd, Pt and Zn	Glucose	glucono-lactone	Cu, Au, and Pt supported by graphene were found to be more effective in the presence of an electric field.

[49]	DMOL	Density functional semicore pseudopotential (DSPP) / PBE	PtPd (111)	Methanol	Formic acid	Adding Pd to Pt was demonstrated to have improved catalyst efficiency and reduced CO poisoning.

Contrary to the works that have shown the importance of water to the oxidation process on Au-catalyst, Li et al. [31] have established that the oxidation of alcohols such as methanol, ethanol, propanol, 2-propanol and 2-butanol to valuable products on Pt(111) in water result to no any different with its absence in the process. This implies that the presence of water in the oxidation processes on the Pt surface has no significant impact on its catalytic characteristics (or behavior). Which was similar to the Gu et al. [27] report that shows poor Pd's affinity for xOH (obtainable from water oxidation) compared to Pd alloyed with Zn, which displayed a better affinity for the xO due to the presence of Zn on the slab in the simulation. These different metals' behavior reported for the presence of water and their affinity for surface xOH implies that there is no global relationship or interaction mode for the surface xOH with all kinds of metals or alloys. Other computational studies on the catalytic oxidation of biomass derivatives into valuable products presented in Table 2- 9 and Table 2- 10 include the oxidation of glucose into glucono-lactone; methanol into formaldehyde; ethanol, and methanol to other useful materials on different metals and some alloys [17,125,130].

2.5.2 Catalysis of furfural and HMF oxidation on metals

Among the studies that deployed the density functional theory (DFT) calculation to computationally explored the mechanism involved in the aerobic oxidation of furfural and HMF into FDCA is Lei et al.[132] work. With DFT (GGA-PBE), this work[132] established that Pd facets have varying impacts on HMF oxidation. Where it was confirmed that Pd(111) facet showed a better catalytic influence for the oxidation of the alcohol group (of HMF), unlike the Pd(100) that favor that of the aldehyde groups. Moreover, Lei et al. study[132] reveals a lower energy barrier for the transformation of HMFCA's

alcohol function into FFCA (aldehyde) on Pd(111) than Pd(100), as shown in Figure 2- 11. The study [132] further showed that oxidation of the O-H bond in HMFCA is relatively easier than the C-H bond on both Pd facets due to relatively lower energy barrier obtained for O-H than the C-H bond. This implies that HMFCA feasibly oxidizes to FFCA via its O-H bond rather than C-H. In general, the barrier obtained for Pd(100) was found to be higher than for Pd(111). The analysis of reaction barriers and energies in the mechanism shows that the reaction barrier exhibits a direct relationship with the reaction energies, except for the alcohol (O-H) oxidation step in HMFCA, which was slightly different. Pd(111) would be more effective in catalyzing the oxidation of HMFCA to FFCA than Pd(100).

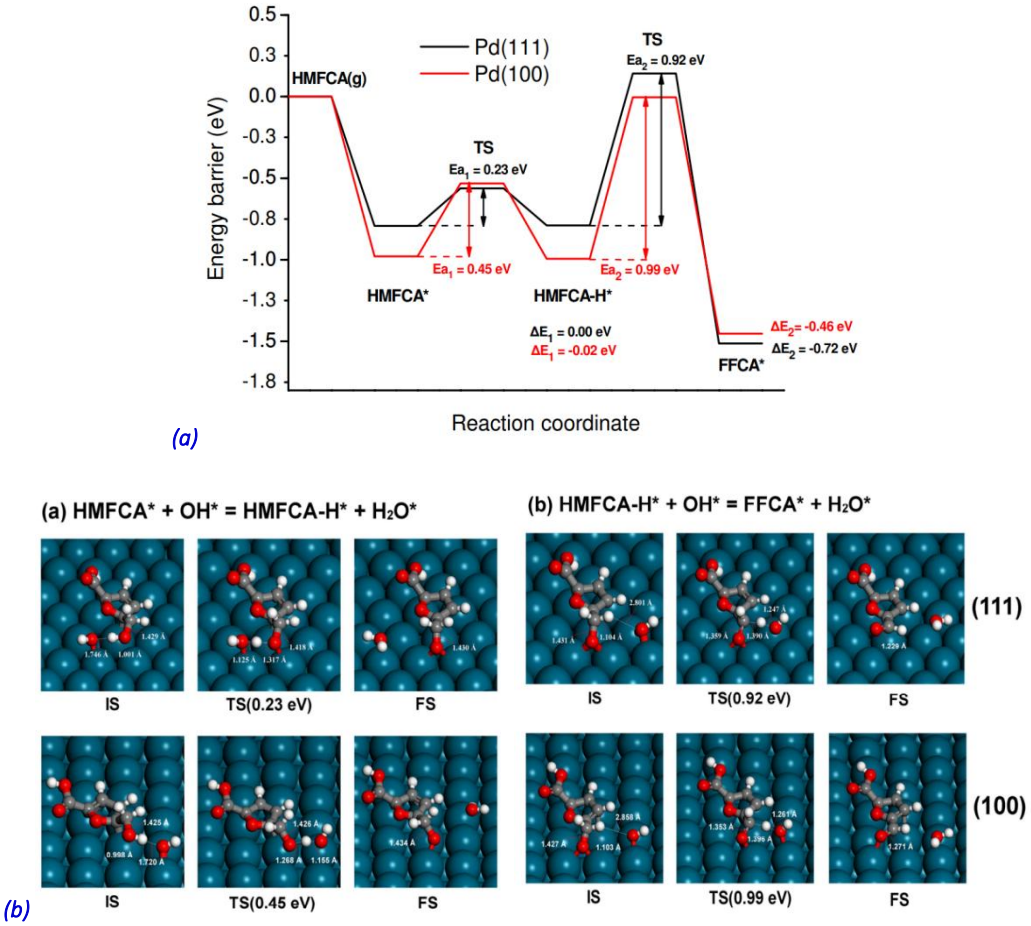

Figure 2- 11 (a) *Energy profile showing the oxidation of HMFCA to FFCA on Pd (111) and Pd (100),* ***(b)*** *Geometrical Structure of the intial state (IS), transition state (TS), and final state (FS). (Source: Lei et al.[132] report)*
Note: *HMFCA(g) = HMFCA before adsorption, HMFCA* = adsorbed HMFCA, HMFCA-H* = product of oxidizing O-H of HMFCA, and FFCA* = product of oxidizing C-H of HMFCA.*

Following the previous experimental findings on the impact of support on the catalytic properties of the catalyst, Yang et al.[103] using the DFT (GGA-PW91) method, the author explored the reducibility of $Ca_xMn_yO_z$ surface when supporting Pd. From this, it was shown that the order of reducibility (using their reduction temperature) was $CaMn_2O_4$ (396 ^oC) > $CaMn_3O_6$ (430 ^oC) > $Ca_2Mn_3O_8$ (438 ^oC) > $CaMnO_3$ (472 ^oC), which was confirmed to have shown good agreement with H_2-TPR experiment[103]. The study further establishes that surfaces with a lower coordination number and longer M-O bond showed higher reducibility [103] . The report further reveal that $CaMnO_3$ displayed the least the reducibility among the $Ca_xMn_yO_z$ surfaces, showing the highest reduction temperature, while $CaMn_2O_4$ show the least reduction temperature. Reverse order was the case of the oxidizability trend ($CaMn_2O_4$ (510 ^oC) < $CaMn_3O_6$ (426 ^oC) < $Ca_2Mn_3O_8$ (376 ^oC) < $CaMnO_3$ (362 ^oC) using their oxidation temperature) of the $Ca_xMn_yO_z$ surfaces, which agreed with O_2-TPO experiment[103].

Moreover, the Liaoi et al.[133] study for using Pd_x/MnO_2 confirmed that the use of Pd single site (Pd_1/MnO_2) showed better binding affinity and more accessible activation pathways for the HMF oxidation compared to the use of Pd_{13}/MnO_2(1110). Pd_1/MnO_2 showed a lower oxygen vacancy formation energy (-0.21 eV) than Pd_{13}/MnO_2 (1.78 eV). Liao et al. study[133] further reveal why more oxygen vacancies were reported from the XPS and O_2-TPD analysis, showing that an atomic Pd would favor more oxygen vacancy formation on Pd/MnO_2 than Pd_{13}/MnO_2. Findings from study[133] indicated that the atomic dispersion of Pd not only increases the atomic efficiency but also maximizes metal-support interactions and effectivity tuning of the electronic properties (which do result in better catalytic performance). To further understand the influence of Pd(111) in furfural conversion, Vassil et al.[36] also use DFT (PBE-D3) to evaluate the furfural transformation into valuable products (furan, furfuryl alcohol

(FAL) and 2-methyl furan(MF)) on a Pd(111) slab. Findings from study [36] indicate that it would favor the production of furan and CO more than MF and FAL.

Some studies investigated the role of other metals influencing the catalysis of furfural and HMF oxidation processes. The use of CdS was explored by Afrox et al. [134] in the oxidation of HMF into FFCA using DFT (LDA) method. Afrox et al. [134] evaluated the binding energies of HMF with the CdS surface, exploring the facet (111) and (001). Results from the author [134] studies reveal binding energies of 12.58 kcal/mol (nanosheet) for CdS (111) and 43.92 kcal/mol (nanorod) for CdS(001), which correlated well with the experimental yield obtained as 65 % and 90 %, FFCA respectively, despite the low precision of LDA relative to other the use of other functionals. The findings from Afrox et al. [134] reports further indicate that the adsorption or binding energies of a feedstock can be used as a catalyst descriptor for the prediction of the catalytic capacities or performance.

With the use of DFT (GGA/PBE-D3), other reports (in Figure 2- 12) on the use of Pt catalyst, like Liu et al. [135], computationally predict the presence of oxygen gas on the surface aid in lowering barriers on Pt. Study [135] further reveals that the use of Pt(100) favors the formation of xOH on the surface more than Pt (111) and that Pt(100) promotes liquid-phase oxidation in the transformation of furfural (FF) into furoic acid (FA). Zhen et al. [136] further reveal that the negatively-charged Pt site on Pt-catalyst-supported by MgO in the oxidation of furfural (FF) into furoic acid (FA) served as the intrinsic active site. The site aid in oxidizing FF via the adsorption of the C=O bond and oxygen activation [136].

Also, Gong et al.[37] use DFT to study electrocatalytic means of oxidizing furfural in the presence of Pt (111) and show that selectivity to FA was high. The study also predicted the use of Pt to be prone to side reactions (degradation) to other products,

Table 2- 11. *DFT studies on the oxidation of FF and HMF oxidation to produce valuable products using solid catalysts*

Ref	Software Used	DFT	Catalyst Studied	Feed type	Material Produced	Key findings made
[134]	Quantum ESPRESSO	LDA	CdS	HMF	FFCA	HMF firmly binds to CdS. The CdS(111) and CdS(001) with a binding energy of -12.58kcal/mol (nanosheet) and -43.92kcal/mol (nanorod) correlate with the expt FFCA yield obtained as 65 % and 90 %, respectively.
[132]	VASP	PAW / PBE	Pd(111) Pd(100)	HMF	FDCA	Pd(111) facet exhibited better catalytic behavior in the oxidation of the alcohol group, while Pd(100) performed effectively in the oxidation of aldehyde groups, where Pd(111) showed a lower barrier for alcohol oxidation (HMFCA to FFCA) than Pd(100) facets.
[36]	VASP	PBE-D3	Pd(111)	FF	FAL, furan, 2-methyl furan	It shows that furfural and furfuryl alcohol would easily undergo decarbonylation to furan and CO.
[136]	VASP	PAW / PBE-D3	Pt/MgO	FF	Furoic acid	The negatively-charged Pt site serves as the intrinsic active site, which aids in facilitating furfural oxidation via the unique adsorption of the C=O bond and activation of O_2.
[135]	VASP	PAW / PBE	Pt(100) Pt(111)	HMF	FDCA	O_2 presence on the surface significantly lowers the barrier compared to a clean surface. Pt(100) was showed produces more xOH due to the stronger bond it has for O_2 and lowers the barrier for xOH production compared to Pt(111). Other findings also indicated that Pt(100) favors the liquid-phase oxidation process.
[133]	VASP	PBE / PAW	Pd-MnO_2 (1110) Pd13-MnO_2 (1110)	HMF	FDCA	The Pd single site has a stronger binding affinity and an easier activation path for HMF than other Pd13-MnO_2(1110). Pd-MnO_2 showed a lower oxygen vacancy formation energy (−0.21 eV) than Pd_{13}/MnO_2 (1.78 eV). Suggesting the atomic dispersion of Pd to be highly beneficial for better catalytic performance

[103]	VASP	PW91	$Pd/Ca_xMn_yO_z$	HMF	FCDA	With the use of oxygen vacancy formation energy as the reducibility of surface lattice oxygen descriptor, the order of the reducibility of the surfaces was found to be $CaMn_2O_4$ > $CaMn_3O_6$ > $Ca_2Mn_3O_8$ > $CaMnO_3$, which was in agreement with the H2-TPR experiment results. Where it was identified that surfaces with lower coordination numbers and longer M-O bond lengths displayed the highest reducibility.

such as succinic acid. Mark et al. [137] explore possible pathways leading to the degradation of furanic compounds into other low molecular weight compounds over Pt (111), where the presence of O_2 on Pt was observed to facilitate their oxidation into CO_2 and other smaller furanic compounds. Pt (111) in furfural oxidation facilitates the C-C scission leading to the production of smaller furanic compounds.

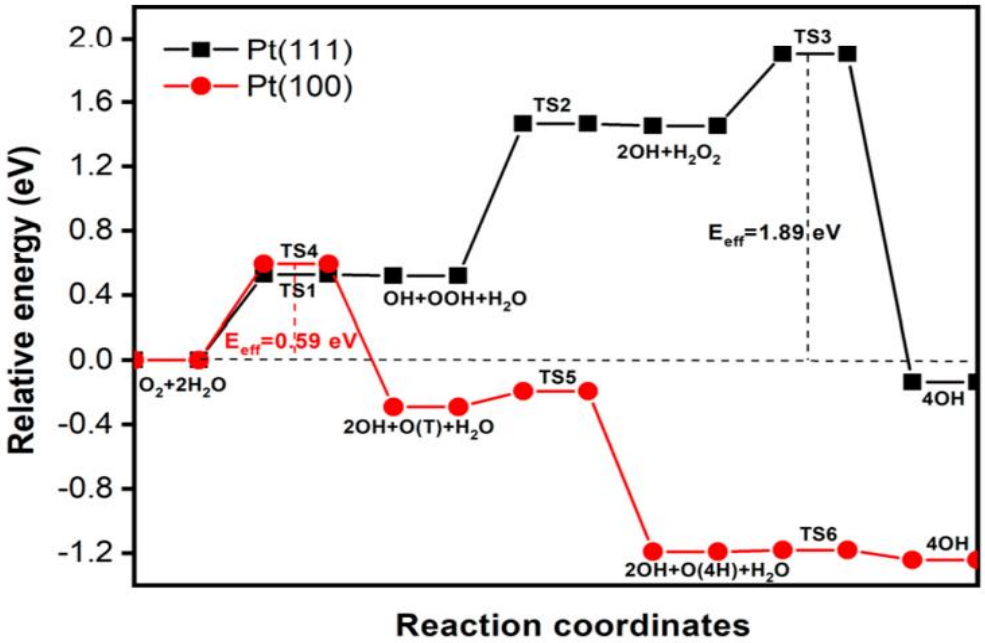

Figure 2- 12 *Energy profiles for water oxidation in the presence of oxygen on Pt(100) and Pt(111). (Source: Liu et al.[135] reports).*

Moreover, Vorotnikov et al. [36] also predicted the reaction of the furfural into furan and carbon monoxide in the presence of Pd (111). The study [36] established that the production of furan and CO would be more feasible on Pd(111) than the production

of furfuryl alcohol (FAL) and methyl furan (MF). The report of Mark et al. [137] and Vorotnikov et al.[36] confirms that using pure Pt and Pd for the oxidation of furfural into furoic acid would not be efficient due to their promotion of several degradation pathways on their surface. Other studies, such as by Jenness et al. [138] showed the kinetics involved in furfural conversion to other valuable materials like 2-methyl furan (MF) over RuO_2(110). The author[138] identified the rate-determining step (RDS) as the scission of the side chain's C-O bond. However, there is a need to investigate further the factors promoting degradation during the oxidation of furfural on metals, especially Au.

2.5.3 Key remarks on the theoretical studies

The survey of the existing works in the literature that computationally investigate the oxidation of several biomass derivatives, especially the alcohols. The literature has primarily investigated the oxidation of alcohols like methanol, ethanol, glycerol, and many others over Au, Pt, and Pd, limited computational studies evaluated the oxidation of furfural and HMF on metals. Most furfural and HMF studies focus on investigating the use of Pt and Pd. With no report on the impact of Au in the catalysis of furfural and HMF oxidation, despite the low yield and poor selectivity reported in some existing experimental studies, which needs insight for redesigning the Au catalyst for improved performance. It is, therefore, essential to investigate the factors promoting the production of undesired products via the identification of degradation routes feasible on Au during the oxidation of furfural and HMF.

2.6 Summary, Key Research Problem, Objectives & Study Strategy

2.6.1 Summary of Existing Findings Made in the Literature

The literature survey has revealed the impact of the different pure metals, their supports, and alloy effects. Some of the metals recording lower yield during the oxidation of either furfural or HMF as a result of the degradation holding on their

surfaces (Au, Pt, and Pd) were reported to have been improved via the use of replacement of support, and some via the approach of alloying the metal with a new metal (promoter). The ratio has also been a serious subject of alloying effect research works reviewed in the literature. The report of computational studies for the oxidation of furfural so far is generally found to be much lower than that of the HMF oxidation, especially for the use of metal-based catalysts. However, there needs to explore details of the mechanism involved in the oxidation of furfural into furoic acid on metals like Au, which is fairly reported in the literature, unlike Pt and Pd. And the exploration of the possible factors or paths promoting the degradation of the furfural oxidation intermediates and furoic acid on Au.

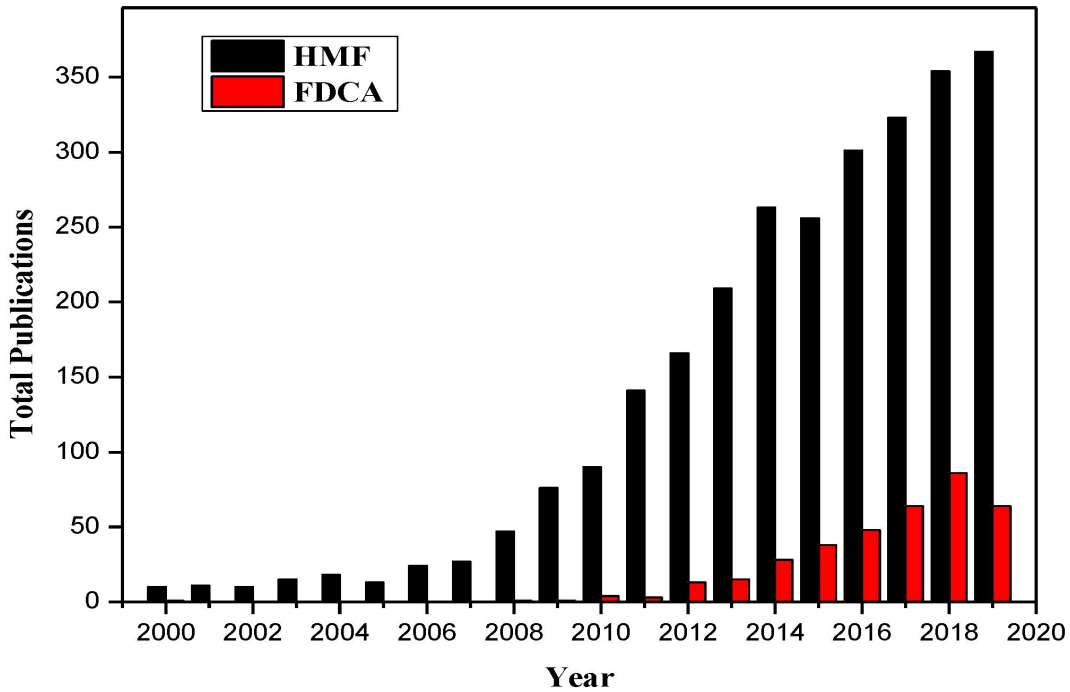

Figure 2- 13 The trend of research work exploring the HMF and FDCA from 2000 to 2019 reported by Hameed et al. [139]

The review unravels that many experimental studies have been carried out on using metals (Au, Pd, and Pt) in the catalysis of HMF oxidation. With the majority being base oxidation and a few of them being base-free. These studies reported include metals and their alloys. Many of these studies have focused mainly on other valuable products other than FDCA. With the shift in the chemical industries [5] toward a

greener process, FDCA is gradually receiving better attention. Recent research works are now largely researching the science and technologies involved in synthesizing FDCA. This is evident in FIGURE 2-5, collated by Hameed et al.[139]

The literature further indicates that the bulk of the studies reported on using DFT in the study of HMF oxidation is largely in the presence of pure metal. Few or no reports on the theoretical exploration of details involved in the catalysis of HMF oxidation in the presence of alloys with/without a base. It would be necessary to provide detailed information on the varying reaction routes competing with the desired reaction path. And more information on how to address the challenge of degradation that is often experimented with using some pure metals can be addressed. The understanding would aid in redesigning the metal catalyst to obtain a better catalytic performance

2.6.2 Key Research Problem of Focus in this Thesis

With a different kind of varying yield reported for the use of different supports for the competition with degradation, it is important to computationally explore details on the activities of Au catalysis in the oxidation of furfural and HMF to acids to understand better how it behaves in the absence of support. A theoretical explanation for the alloy effects on the retardation or hindrance of the degradation routes during HMF oxidation to FDCA is insignificantly investigated. And it is necessary for theoretical studies to be carried out to unfold details on why some alloys failed to perform above the pure form of their metals in promoting HMF oxidation routes over the degradation ones. This would go a long way to facilitating high yield to meet the FDCA market demands.

Some of the recent results collected by our experimental partner for the oxidation of HMF into FDCA in the presence of Au-supported catalyst are presented in Figure 2- 14 and other results. The result showed a huge carbon loss in the carbon balance trend. The carbon loss indicates the degradation activities in the oxidation process leading to

undesired products that were not accounted for in the experiment. The result from the recycling tests showed that no regeneration was successfully achieved in the study due to some carbon loss which may have deactivated the active site on the

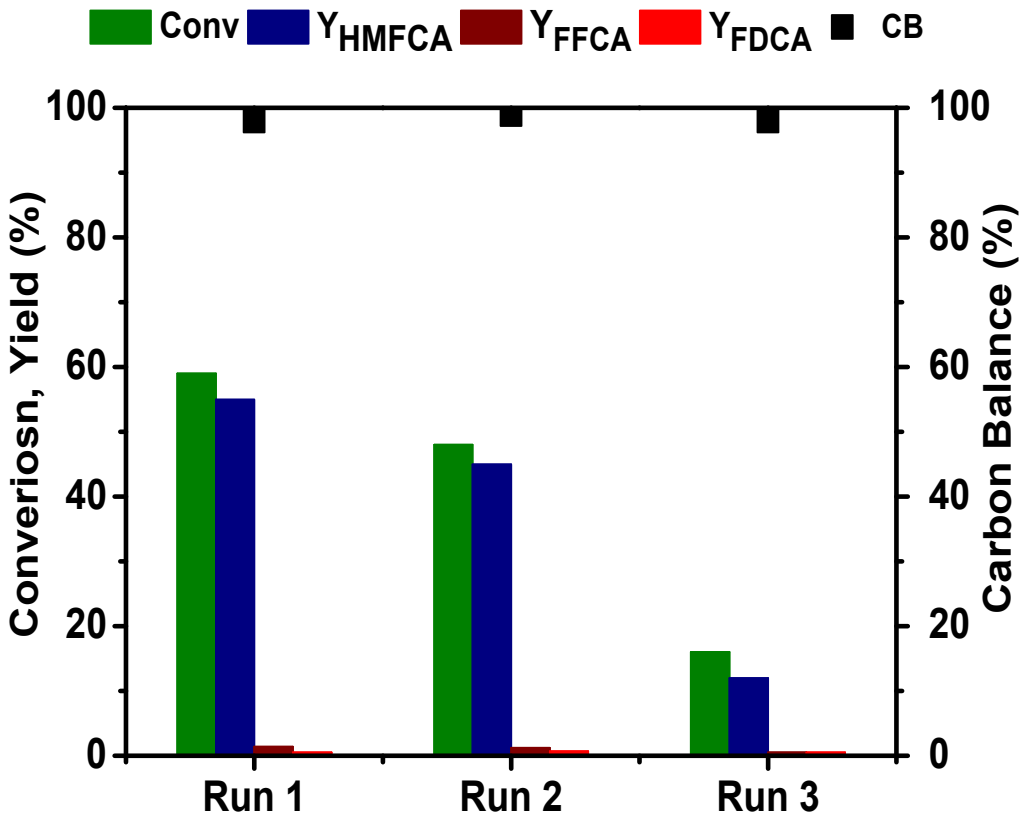

Figure 2- 14 *Recyclability results obtained for an investigation (pending for publication) on the oxidation of HMF over Au/TiO_2 SZ-61192: PVA:Au= 1.2 at a P(air) of 20bar, T = 50°C, nHMF/nAu = 500, C_0(HMF) = 45mM, nOH/nHMF = 3, and time = 1.5h for the reaction.*[140]

catalyst as the reaction progressed. Identifying the possible reaction routes promoting the degradation of the feedstock, intermediate, or products observed in the experiment is necessary. Knowing well that furoic acid synthesized from furfural can be further carboxylated to yield FDCA, it is, therefore, essential to unravel factor-promoting degradation (as reported in Figure 2- 6) during the oxidation of furfural into furoic acid on Au catalyst.

2.6.3 Thesis Objectives

In addressing the issues mentioned earlier regarding the use of Au and its alloys in the oxidation of furfural and HMF to valuable products and to facilitate better catalyst design for the process, this study therefore aimed:

1) To understand the mechanism involved in base-free furfural oxidation with/without water and the factors leading to the degradation of furfural intermediates and furoic acid (FA) during the FA production on Au-catalyst (in Chapter 4).
2) To investigate the mechanism involved in a base-free HMF oxidation into FDCA and explore possible reaction pathways that contribute to the degradation of HMF and HMFCA during the synthesis of FDCA on Au-catalyst (in Chapter 5).
3) To evaluate the impact of the other metals (Pt and Pd) on the activation of O_2 with or without water, to understand other metals' oxidation mechanisms for converting HMF to FDCA, and to explore the impact of Au-alloy on the retarding degradation pathway.

2.6.4 Study Strategy

In the thesis, we deployed the use of the DFT method and thermodynamic analysis to search for the feasible mechanism leading to the oxidation of furfural and HMF into furoic acid and FDCA on the metal. The study of furfural oxidation with and without water was used to identify the influence of water presence in the Au catalysis of the process. In the study of furoic acid production from furfural on Au, we investigate the influence of water on the oxidation process and seek some understanding of some degradation routes possibly competing with the production of the desired product (Furoic acid) in Chapter 4.

After that, the feasible condition (with/without water) was deployed to oxidize HMF into FDCA on Au. This is diagrammatically summarized in Figure 2- 15. We also explored a wide range of reaction routes leading to the degradation of HMF and HMFCA during the synthesis of FDCA on an Au catalyst. The reaction energies of the various degradation routes were used in identifying the most feasible route promoting degradation on the catalyst.

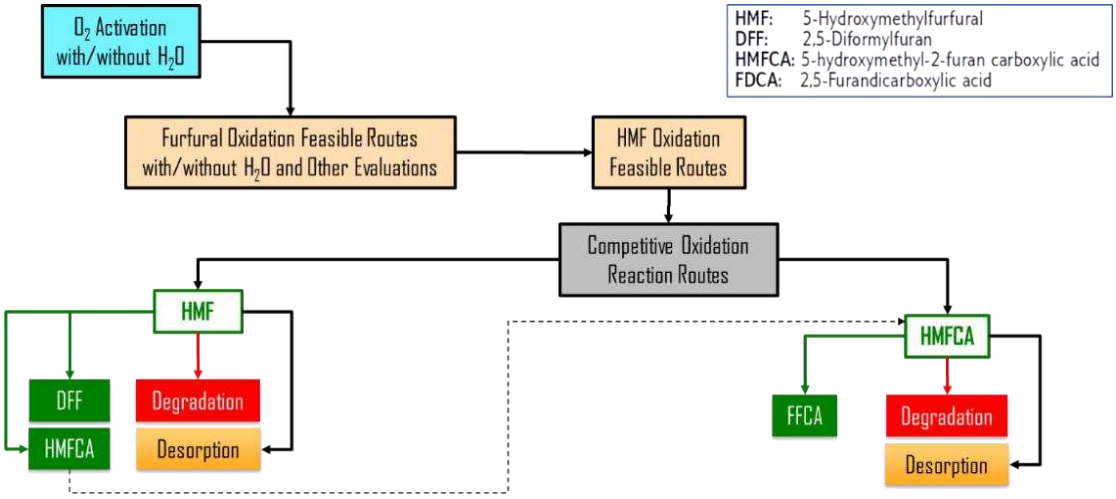

Figure 2- 15 Strategy deployed in our investigation in this report.

Various routes promoting degradation and oxidation were explored for the transformation of HMF into HMFCA and HMFCA into FFCA in the later part of this report (in Chapter 5). The routes explored include breaking or forming C-C, O-H, C-H, and C-O bonds across the furan ring and the other functional groups (like the hydroxyl and aldehyde groups). The species' desorption routes were also explored. The most energetically feasible degradation route, strongly competing with the oxidation route leading to the production of FDCA on Au, was investigated in Chapter 5.

2.7 List of references cited

1. Zhao, D., Su, T., Wang, Y., Varma, R. S., & Len, C. (2020). Recent advances in catalytic oxidation of 5-hydroxymethylfurfural. *Molecular Catalysis*, *495*, 111133. https://doi.org/10.1016/J.MCAT.2020.111133

2. Li, X., Jia, P., & Wang, T. (2016). Furfural: A Promising Platform Compound for Sustainable Production of C4 and C5 Chemicals. *ACS Catalysis*, *6*(11), 7621–7640. https://doi.org/10.1021/ACSCATAL.6B01838/ASSET/IMAGES/MEDIUM/CS-2016-01838C_0017.GIF

3. de Jong, E., Dam, M. A., Sipos, L., & Gruter, G. J. M. (2012). Furandicarboxylic acid (FDCA), A versatile building block for a very interesting class of polyesters. *ACS Symposium Series*, *1105*, 1–13. https://doi.org/10.1021/BK-2012-1105.CH001/ASSET/IMAGES/LARGE/BK-2011-00691K_G010.JPEG

4. de Jong, E., Vijlbrief, T., Hijkoop, R., Gruter, G. J. M., & van der Waal, J. C. (2012). Promising results with YXY Diesel components in an ESC test cycle using a PACCAR Diesel engine. *Biomass and Bioenergy*, *36*, 151–159. https://doi.org/10.1016/J.BIOMBIOE.2011.10.034

5. Grand View Research. (2014). *Furandicarboxylic Acid Market Size, Share & Trends Analysis Report By Application (PET, Polyamides, Polycarbonates, Plasticizers, Polyester Polyols), By Region, And Segment Forecasts, 2015 - 2020*. https://www.grandviewresearch.com/industry-analysis/fdca-industry

6. Terzopoulou, Z., Papadopoulos, L., Zamboulis, A., Papageorgiou, D. G., Papageorgiou, G. Z., & Bikiaris, D. N. (2020). Tuning the Properties of Furandicarboxylic Acid-Based Polyesters with Copolymerization: A Review. *Polymers*, *12*(6), 1209. https://doi.org/10.3390/POLYM12061209

7. Loos, K., Zhang, R., Pereira, I., Agostinho, B., Hu, H., Maniar, D., Sbirrazzuoli, N., Silvestre, A. J. D., Guigo, N., & Sousa, A. F. (2020). A Perspective on PEF Synthesis, Properties, and End-Life. *Frontiers in Chemistry*, *8*, 585. https://doi.org/10.3389/FCHEM.2020.00585/BIBTEX

8. de Jong, E., Visser, H. A., Dias, A. S., Harvey, C., & Gruter, G. J. M. (2022). The Road to Bring FDCA and PEF to the Market. *Polymers*, *14*(5), 943. https://doi.org/10.3390/POLYM14050943

9. Research and Data. (2020). *2,5-Furandicarboxylic Acid (FDCA) Market | Size & Analysis*. https://www.reportsanddata.com/report-detail/2-5-furandicarboxylic-acid-fdca-market

10. Cong, H., Yuan, H., Tao, Z., Bao, H., Zhang, Z., Jiang, Y., Huang, D., Liu, H., & Wang, T. (2021). Recent Advances in Catalytic Conversion of Biomass to 2,5-Furandicarboxylic Acid. *Catalysts*, *11*(9), 1113. https://doi.org/10.3390/CATAL11091113

11. Solmi, S., Morreale, C., Ospitali, F., Agnoli, S., & Cavani, F. (2017). Oxidation of d-Glucose to Glucaric Acid Using Au/C Catalysts. *ChemCatChem*, *9*(14), 2797–2806. https://doi.org/10.1002/CCTC.201700089

12. Lee, J., Saha, B., & Vlachos, D. G. (2016). Pt catalysts for efficient aerobic oxidation of glucose to glucaric acid in water. *Green Chemistry*, *18*(13), 3815–3822. https://doi.org/10.1039/C6GC00460A

13. Franz, S., Shcherban, N. D., Simakova, I. L., Peurla, M., Eränen, K., Wärnå, J., Salmi, T., & Murzin, D. Y. (2021). Oxidation of glucose and arabinose mixtures over Au/Al2O3. *Reaction Kinetics, Mechanisms and Catalysis*, *132*(1), 59–72. https://doi.org/10.1007/S11144-020-01901-W/TABLES/2

14. Shi, H., Thapa, P. S., Subramaniam, B., & Chaudhari, R. v. (2018). Oxidation of Glucose Using Mono- and Bimetallic Catalysts under Base-Free Conditions. *Organic Process Research and Development*, *22*(12), 1653–1662. https://doi.org/10.1021/ACS.OPRD.8B00302/SUPPL_FILE/OP8B00302_SI_001.PDF

15. Guo, S., Fang, Q., Li, Z., Zhang, J., Zhang, J., & Li, G. (2019). Efficient base-free direct oxidation of glucose to gluconic acid over TiO2-supported gold clusters. *Nanoscale*, *11*(3), 1326–1334. https://doi.org/10.1039/C8NR08143C

16. Liu, M., Jin, X., Zhang, G., Xia, Q., Lai, L., Wang, J., Zhang, W., Sun, Y., Ding, J., Yan, H., & Yang, C. (2020). Bimetallic AuPt/TiO2Catalysts for Direct Oxidation of Glucose and Gluconic Acid to Tartaric Acid in the Presence of Molecular O2. *ACS Catalysis*, *10*(19), 10932–10945. https://doi.org/10.1021/ACSCATAL.0C02238/SUPPL_FILE/CS0C02238_SI_001.PDF

17. Düzenli, D., Onal, I., & Tezsevin, I. (2022). Investigation of glucose electrooxidation mechanism over N-modified metal-doped graphene electrode by density functional theory approach. *Journal of Computational Chemistry*, *43*(26), 1793–1801. https://doi.org/10.1002/JCC.26981

18. Liu, M., Jin, X., Zhang, G., Xia, Q., Lai, L., Wang, J., Zhang, W., Sun, Y., Ding, J., Yan, H., & Yang, C. (2020). Bimetallic AuPt/TiO2Catalysts for Direct Oxidation of Glucose and Gluconic Acid to Tartaric Acid in the Presence of Molecular O2. *ACS Catalysis*, *10*(19), 10932–10945. https://doi.org/10.1021/ACSCATAL.0C02238/SUPPL_FILE/CS0C02238_SI_001.PDF

19. Amaniampong, P. N., Karam, A., Trinh, Q. T., Xu, K., Hirao, H., Jérôme, F., & Chatel, G. (2017). Selective and Catalyst-free Oxidation of D-Glucose to D-Glucuronic acid induced by High-Frequency Ultrasound. *Scientific Reports*, *7*(1), 1–8. https://doi.org/10.1038/srep40650

20. Caglar, A., Düzenli, D., Onal, I., Tezsevin, I., Sahin, O., & Kivrak, H. (2020). A comparative experimental and density functional study of glucose adsorption and electrooxidation on the Au-graphene and Pt-graphene electrodes. *International Journal of Hydrogen Energy*, *45*(1), 490–500. https://doi.org/10.1016/J.IJHYDENE.2019.10.163

21. Zhuge, Y., Fan, G., Lin, Y., Yang, L., & Li, F. (2019). A hybrid composite of hydroxyapatite and Ca–Al layered double hydroxide supported Au nanoparticles for highly efficient base-free aerobic oxidation of glucose. *Dalton Transactions*, *48*(25), 9161–9172. https://doi.org/10.1039/C9DT00985J

22. Gurgel, L. V. A., Marabezi, K., Zanbom, M. D., & Curvelo, A. A. da S. (2012). Dilute Acid Hydrolysis of Sugar Cane Bagasse at High Temperatures: A Kinetic Study of Cellulose Saccharification and Glucose Decomposition. Part I: Sulfuric Acid as the Catalyst. *Industrial and Engineering Chemistry Research*, *51*(3), 1173–1185. https://doi.org/10.1021/IE2025739

23. Sadula, S., & Saha, B. (2018). Aerobic Oxidation of Xylose to Xylaric Acid in Water over Pt Catalysts. *ChemSusChem*, *11*(13), 2124–2129. https://doi.org/10.1002/CSSC.201800494

24. Tokarev, A. v., Murzina, E. v., Eränen, K., Markus, H., Plomp, A. J., Bitter, J. H., Mäki-Arvela, P., & Murzin, D. Y. (2009). Lactose oxidation over palladium catalysts supported on active carbons and on carbon nanofibres. *Research on Chemical Intermediates 2009 35:2*, *35*(2), 155–174. https://doi.org/10.1007/S11164-008-0023-3

25. Miedziak, P. J., He, Q., Edwards, J. K., Taylor, S. H., Knight, D. W., Tarbit, B., Kiely, C. J., & Hutchings, G. J. (2011). Oxidation of benzyl alcohol using supported gold–palladium nanoparticles. *Catal Today*, *163*(1), 47–54. https://doi.org/10.1016/j.cattod.2010.02.051

26. Ma, C. Y., Dou, B. J., Li, J. J., Cheng, J., Hu, Q., Hao, Z. P., & Qiao, S. Z. (2009). Catalytic oxidation of benzyl alcohol on Au or Au–Pd nanoparticles confined in mesoporous silica. *Applied Catalysis B: Environmental*, *92*(1–2), 202–208. https://doi.org/10.1016/J.APCATB.2009.07.007

27. Gu, Q., Sautet, P., & Michel, C. (2018). Unraveling the Role of Base and Catalyst Polarization in Alcohol Oxidation on Au and Pt in Water. *ACS Catalysis*, *8*(12), 11716–11721. https://doi.org/10.1021/ACSCATAL.8B03494/SUPPL_FILE/CS8B03494_SI_001.PDF

28. Rucinska, E., Pattisson, S., Miedziak, P. J., Brett, G. L., Morgan, D. J., Sankar, M., & Hutchings, G. J. (2020). Cinnamyl Alcohol Oxidation Using Supported Bimetallic Au–Pd Nanoparticles: An Optimization of Metal Ratio and Investigation of the Deactivation Mechanism Under Autoxidation Conditions. *Topics in Catalysis*, *63*(1–2), 99–112. https://doi.org/10.1007/S11244-020-01231-0/FIGURES/13

29. Wang, F., Hao, G., Guo, Y., Ma, X., Yang, L., Wang, F., Hao, G., Guo, Y., Ma, X., & Yang, L. (2017). Solvent Effects on Preparation of Pd-Based Catalysts: Influence on Properties of Palladium and Its Catalytic Activity for Benzyl Alcohol Oxidation. *Open Journal of Metal*, *7*(4), 59–68. https://doi.org/10.4236/OJMETAL.2017.74005

30. Rucinska, E., Pattisson, S., Miedziak, P. J., Brett, G. L., Morgan, D. J., Sankar, M., & Hutchings, G. J. (2020). Cinnamyl Alcohol Oxidation Using Supported Bimetallic Au–Pd Nanoparticles: An Optimization of Metal Ratio and Investigation of the Deactivation Mechanism Under Autoxidation Conditions. *Topics in Catalysis*, *63*(1–2), 99–112. https://doi.org/10.1007/S11244-020-01231-0/FIGURES/13

31. Liu, F., Wang, H., Sapi, A., Tatsumi, H., Zherebetskyy, D., Han, H. L., Carl, L. M., & Somorjai, G. A. (2018). Molecular Orientations Change Reaction Kinetics and Mechanism: A Review on Catalytic Alcohol Oxidation in Gas Phase and Liquid Phase on Size-Controlled Pt Nanoparticles. *Catalysts*, *8*(6), 226. https://doi.org/10.3390/CATAL8060226

32. Carrettin, S., McMorn, P., Johnston, P., Griffin, K., & Hutchings, G. J. (2002). Selective oxidation of glycerol to glyceric acid using a gold catalyst in aqueous sodium hydroxide. *Chemical Communications*, *7*(7), 696–697. https://doi.org/10.1039/B201112N

33. Dai, C., Sun, L., Liao, H., Khezri, B., Webster, R. D., Fisher, A. C., & Xu, Z. J. (2017). Electrochemical production of lactic acid from glycerol oxidation catalyzed by AuPt nanoparticles. *Journal of Catalysis*, *356*, 14–21. https://doi.org/10.1016/J.JCAT.2017.10.010

34. Bianchi, C. L., Canton, P., Dimitratos, N., Porta, F., & Prati, L. (2005). Selective oxidation of glycerol with oxygen using mono and bimetallic catalysts based on Au, Pd and Pt metals. *Catalysis Today*, *102–103*, 203–212. https://doi.org/10.1016/J.CATTOD.2005.02.003

35. Yan, H., Yao, S., Liang, W., Feng, X., Jin, X., Liu, Y., Chen, X., & Yang, C. (2019). Selective oxidation of glycerol to carboxylic acids on Pt(111) in base-free medium: A periodic density functional theory investigation. *Applied Surface Science*, *497*, 143661. https://doi.org/10.1016/J.APSUSC.2019.143661

36. Vorotnikov, V., Mpourmpakis, G., & Vlachos, D. G. (2012). DFT study of furfural conversion to furan, furfuryl alcohol, and 2-methylfuran on Pd(111). *ACS Catalysis*, *2*(12), 2496–2504. https://doi.org/10.1021/CS300395A/SUPPL_FILE/CS300395A_SI_001.PDF

37. Gong, L., Agrawal, N., Roman, A., Holewinski, A., & Janik, M. J. (2019). Density functional theory study of furfural electrochemical oxidation on the Pt (1 1 1) surface. *Journal of Catalysis*, *373*, 322–335. https://doi.org/10.1016/J.JCAT.2019.04.012

38. Kumar, N. S., Srivastava, V. C., & Basu, S. (2013). Optimization and Kinetics of Furfural Oxidation to Furoic Acid Over Alum-impregnated Activated Alumina. *Indian Chemical Engineer*, *55*(3), 153–164. https://doi.org/10.1080/00194506.2013.829259

39. Ferraz, C. P., da Silva, A. G. M., Rodrigues, T. S., Camargo, P. H. C., Paul, S., & Wojcieszak, R. (2018). Furfural Oxidation on Gold Supported on MnO2: Influence of the Support Structure on the Catalytic Performances. *Applied Sciences*, *8*(8), 1246. https://doi.org/10.3390/APP8081246

40. al Rawas, H. K., Ferraz, C. P., Thuriot-Roukos, J., Heyte, S., Wojcieszak, R., & Paul, S. (2021). Influence of Pd and Pt Promotion in Gold Based Bimetallic Catalysts on Selectivity Modulation in Furfural Base-Free Oxidation. *Catalysts*, *11*(10), 1226. https://doi.org/10.3390/CATAL11101226

41. Papanikolaou, G., Lanzafame, P., Perathoner, S., Centi, G., Cozza, D., Giorgianni, G., Migliori, M., & Giordano, G. (2021). High performance of Au/ZTC based catalysts for the selective oxidation of bio-derivative furfural to 2-furoic acid. *Catalysis Communications*, *149*, 106234. https://doi.org/10.1016/J.CATCOM.2020.106234

42. Jin, Y., Sarina, S., Liu, H., Martens, W., Waclawik, E. R., Peiris, E., Jia, J., Shang, J., Kou, L., Guo, C., & Zhu, H.-Y. (2022). Aerobic Oxidation of 5-Hydroxymethyl-furfural to 2,5-Furandicarboxylic Acid at 20 °C by Optimizing Adsorption on AgPd Alloy Nanoparticle Catalysts. *ACS Catalysis*, 11226–11238. https://doi.org/10.1021/ACSCATAL.2C03457

43. Alonso-Fagúndez, N., Fagúndez, F., Agirrezabal-Telleria, I., Arias, P. L., Fierro, J. L. G., Mariscal, R., & L ´ Opez Granados, M. (2014). Aqueous-phase catalytic oxidation of furfural with H 2 O 2 : high yield of maleic acid by using titanium silicalite-1 †. *RSC Advances*, *4*, 54960–54972. https://doi.org/10.1039/c4ra11563e

44. Wan, X., Zhou, C., Chen, J., Deng, W., Zhang, Q., Yang, Y., & Wang, Y. (2014). Base-free aerobic oxidation of 5-hydroxymethyl-furfural to 2,5-furandicarboxylic acid in water catalyzed by functionalized carbon nanotube-supported au-pd alloy nanoparticles. *ACS Catalysis*, *4*(7), 2175–2185. https://doi.org/10.1021/CS5003096/SUPPL_FILE/CS5003096_SI_001.PDF

45. Campisi, S., Capelli, S., Motta, D., Trujillo, F. J. S., Davies, T. E., Prati, L., Dimitratos, N., & Villa, A. (2018). Catalytic Performances of Au–Pt Nanoparticles on Phosphorous Functionalized Carbon Nanofibers towards HMF Oxidation. *C 2018*, *4*(3), 48. https://doi.org/10.3390/C4030048

46. Ardemani, L., Cibin, G., Dent, A. J., Isaacs, M. A., Kyriakou, G., Lee, A. F., Parlett, C. M. A., Parry, S. A., & Wilson, K. (2015). Solid base catalysed 5-HMF oxidation to 2,5-FDCA over Au/hydrotalcites: fact or fiction? *Chemical Science*, *6*(8), 4940–4945. https://doi.org/10.1039/C5SC00854A

47. Gupta, K., Rai, R. K., & Singh, S. K. (2018). Metal Catalysts for the Efficient Transformation of Biomass-derived HMF and Furfural to Value Added Chemicals. *ChemCatChem*, *10*(11), 2326–2349. https://doi.org/10.1002/CCTC.201701754

48. Hutchings, G. J. (2014). Selective oxidation using supported gold bimetallic and trimetallic nanoparticles. *Catalysis Today*, *238*, 69–73. https://doi.org/10.1016/J.CATTOD.2014.01.033

49. Yang, T., Xue, Q., Yu, X., Qi, X., Wu, R., Lu, S., Gu, Z., Jiang, J., & Nie, Y. (2022). DFT Study on Methanol Oxidation Reaction Catalyzed by PtmPdn Alloys. *Coatings*, *12*(7), 918. https://doi.org/10.3390/COATINGS12070918

50. Shcherban, N. D., Barakov, R. Y., Sergiienko, S. A., Eränen, K., Wärnå, J., & Murzin, D. Y. (2021). Furfural Oxidation with Hydrogen Peroxide Over ZSM-5 Based Micro-Mesoporous Aluminosilicates. *Catalysis Letters*, *152*(10), 2920–2932. https://doi.org/10.1007/S10562-021-03899-9/TABLES/5

51. Kandasamy, P., Gogoi, P., Venugopalan, A. T., & Raja, T. (2021). A highly efficient and reusable Ru-NaY catalyst for the base free oxidation of 5-Hydroxymethylfurfural to 2,5-Furandicarboxylic acid. *Catalysis Today*, *375*, 145–154. https://doi.org/10.1016/J.CATTOD.2020.05.009

52. Wolska, J., Walkowiak, A., Sobczak, I., Wolski, L., & Ziolek, M. (2021). Gold-containing Beta zeolite in base-free glucose oxidation – The role of Au deposition procedure and zeolite dopants. *Catalysis Today*, *382*, 48–60. https://doi.org/10.1016/J.CATTOD.2021.05.020

53. Mirzai, J. I., Nadirov, P. A., Velieva, A. D., & Muradkhanli, V. G. (2017). Oxidation of ethanol on NaX zeolite modified with transition metals. *Russian Journal of Physical Chemistry A* , *91*(6), 1005–1009. https://doi.org/10.1134/S0036024417060164

54. Abad, A., Almela, C., Corma, A., & García, H. (2006). Efficient chemoselective alcohol oxidation using oxygen as oxidant. Superior performance of gold over palladium catalysts. *Tetrahedron*, *62*(28), 6666–6672. https://doi.org/10.1016/J.TET.2006.01.118

55. Guan, Y., & Hensen, E. J. M. (2013). Selective oxidation of ethanol to acetaldehyde by Au–Ir catalysts. *Journal of Catalysis*, *305*, 135–145. https://doi.org/10.1016/J.JCAT.2013.04.023

56. Carabineiro, S. A. C. (2019). Supported Gold Nanoparticles as Catalysts for the Oxidation of Alcohols and Alkanes. *Frontiers in Chemistry*, *7*, 702. https://doi.org/10.3389/FCHEM.2019.00702/BIBTEX

57. Menegazzo, F., Manzoli, M., di Michele, A., Ghedini, E., & Signoretto, M. (2018). Supported Gold Nanoparticles for Furfural Valorization in the Future Bio-based Industry. *Topics in Catalysis 2018 61:18*, *61*(18), 1877–1887. https://doi.org/10.1007/S11244-018-1003-5

58. Taarning, E., Nielsen, I. S., Egeblad, K., Madsen, R., & Christensen, C. H. (2008). Chemicals from Renewables: Aerobic Oxidation of Furfural and Hydroxymethylfurfural over Gold Catalysts. *ChemSusChem*, *1*(1–2), 75–78. https://doi.org/10.1002/CSSC.200700033

59. Drault, F., Snoussi, Y., Paul, S., Itabaiana, I., & Wojcieszak, R. (2020). Recent Advances in Carboxylation of Furoic Acid into 2,5-Furandicarboxylic Acid: Pathways towards Bio-Based Polymers. *ChemSusChem*, *13*(19), 5164–5172. https://doi.org/10.1002/CSSC.202001393

60. Pedroso, G. B., Philippsen, M. R., Saldanha, L. F., Araujo, R. B., & Martins, A. F. (2019). Strategies for Fermentable Sugar Production by Using Pressurized Acid Hydrolysis for Rice Husks. *Rice Science*, *26*(5), 319–330. https://doi.org/10.1016/J.RSCI.2019.08.006

61. Drault, F., Snoussi, Y., Paul, S., Itabaiana, I., & Wojcieszak, R. (2020). Recent Advances in Carboxylation of Furoic Acid into 2,5-Furandicarboxylic Acid: Pathways towards Bio-Based Polymers. *ChemSusChem*, *13*(19), 5164–5172. https://doi.org/10.1002/CSSC.202001393

62. Payne, K. A. P., Marshall, S. A., Fisher, K., Cliff, M. J., Cannas, D. M., Yan, C., Heyes, D. J., Parker, D. A., Larrosa, I., & Leys, D. (2019). Enzymatic Carboxylation of 2-Furoic Acid Yields 2,5-Furandicarboxylic Acid (FDCA). *ACS Catalysis*, *9*(4), 2854–2865. https://doi.org/10.1021/ACSCATAL.8B04862/ASSET/IMAGES/LARGE/CS-2018-048627_0008.JPEG

63. Cioc, R. C., Smak, T. J., Crockatt, M., van der Waal, J. C., & Bruijnincx, P. C. A. (2021). Furoic acid and derivatives as atypical dienes in Diels–Alder reactions. *Green Chemistry*, *23*(15), 5503–5510. https://doi.org/10.1039/D1GC01535D

64. Sadier, A., Paul, S., & Wojcieszak, R. (2022). Selective Oxidation of Furfural at Room Temperature on a TiO2-Supported Ag Catalyst. *Catalysts* , *12*(8), 805. https://doi.org/10.3390/CATAL12080805

65. Li, X., Ho, B., Lim, D. S. W., & Zhang, Y. (2017). Highly efficient formic acid-mediated oxidation of renewable furfural to maleic acid with H2O2. *Green Chemistry*, *19*(4), 914–918. https://doi.org/10.1039/C6GC03020C

66. Ferraz, C. P., da Silva, A. G. M., Rodrigues, T. S., Camargo, P. H. C., Paul, S., & Wojcieszak, R. (2018). Furfural Oxidation on Gold Supported on MnO2: Influence of the Support Structure on the Catalytic Performances. *Applied Sciences*, *8*(8), 1246. https://doi.org/10.3390/APP8081246

67. Antonyraj, C. A., Huynh, N. T. T., Park, S. K., Shin, S., Kim, Y. J., Kim, S., Lee, K. Y., & Cho, J. K. (2017). Basic anion-exchange resin (AER)-supported Au-Pd alloy nanoparticles for the oxidation of 5-hydroxymethyl-2-furfural (HMF) into 2,5-furan dicarboxylic acid (FDCA). *Applied Catalysis A: General*, *547*, 230–236. https://doi.org/10.1016/J.APCATA.2017.09.012

68. Ferraz, C. P., Costa, N. J. S., Teixeira-Neto, E., Teixeira-Neto, Â. A., Liria, C. W., Thuriot-Roukos, J., Machini, M. T., Froidevaux, R., Dumeignil, F., Rossi, L. M., & Wojcieszak, R. (2020). 5-Hydroxymethylfurfural and Furfural Base-Free Oxidation over AuPd Embedded Bimetallic Nanoparticles. *Catalysts* , *10*(1), 75. https://doi.org/10.3390/CATAL10010075

69. Douthwaite, M., Huang, X., Iqbal, S., Miedziak, P. J., Brett, G. L., Kondrat, S. A., Edwards, J. K., Sankar, M., Knight, D. W., Bethell, D., & Hutchings, G. J. (2017). The controlled catalytic oxidation of furfural to furoic acid using AuPd/Mg(OH)2. *Catalysis Science & Technology*, *7*(22), 5284–5293. https://doi.org/10.1039/C7CY01025G

70. Bonincontro, D., Lolli, A., Villa, A., Prati, L., Dimitratos, N., Veith, G. M., Chinchilla, L. E., Botton, G. A., Cavani, F., & Albonetti, S. (2019). AuPd-nNiO as an effective catalyst for the base-free oxidation of HMF under mild reaction conditions. *Green Chemistry*, *21*(15), 4090–4099. https://doi.org/10.1039/C9GC01283D

71. Villa, A., Schiavoni, M., Campisi, S., Veith, G. M., & Prati, L. (2013). Pd-modified Au on Carbon as an Effective and Durable Catalyst for the Direct Oxidation of HMF to 2,5-Furandicarboxylic Acid. *ChemSusChem*, *6*(4), 609–612. https://doi.org/10.1002/CSSC.201200778

72. Brandolese, A., Ragno, D., di Carmine, G., Bernardi, T., Bortolini, O., Giovannini, P. P., Pandoli, O. G., Altomare, A., & Massi, A. (2018). Aerobic oxidation of 5-hydroxymethylfurfural to 5-hydroxymethyl-2-furancarboxylic acid and its derivatives by heterogeneous NHC-catalysis. *Organic & Biomolecular Chemistry*, *16*(46), 8955–8964. https://doi.org/10.1039/C8OB02425A

73. Bruno, R. (2016). *Selective oxidation of furfural and 5-methyl furfural under green conditions*. http://amslaurea.unibo.it/13421/1/Tesi LM Bruno Reghizzi_RW_BR.pdf

74. Donoeva, B., Masoud, N., & de Jongh, P. E. (2017). Carbon Support Surface Effects in the Gold-Catalyzed Oxidation of 5-Hydroxymethylfurfural. *ACS Catalysis*, *7*(7), 4581–4591. https://doi.org/10.1021/ACSCATAL.7B00829/ASSET/IMAGES/LARGE/CS-2017-008292_0006.JPEG

75. Casanova, O., Iborra, S., & Corma, A. (2009). Biomass into Chemicals: Aerobic Oxidation of 5-Hydroxymethyl-2-furfural into 2,5-Furandicarboxylic Acid with Gold Nanoparticle Catalysts. *ChemSusChem*, *2*(12), 1138–1144. https://doi.org/10.1002/CSSC.200900137

76. Megías-Sayago, C., Lolli, A., Ivanova, S., Albonetti, S., Cavani, F., & Odriozola, J. A. (2019). Au/Al2O3 – Efficient catalyst for 5-hydroxymethylfurfural oxidation to 2,5-furandicarboxylic acid. *Catalysis Today*, *333*, 169–175. https://doi.org/10.1016/J.CATTOD.2018.04.024

77. Gupta, N. K., Nishimura, S., Takagaki, A., & Ebitani, K. (2011). Hydrotalcite-supported gold-nanoparticle-catalyzed highly efficient base-free aqueous oxidation of 5-hydroxymethylfurfural into 2,5-furandicarboxylic acid under atmospheric oxygen pressure. *Green Chemistry*, *13*(4), 824–827. https://doi.org/10.1039/C0GC00911C

78. Kim, M., Su, Y., Fukuoka, A., Hensen, E. J. M., & Nakajima, K. (2018). Aerobic Oxidation of 5-(Hydroxymethyl)furfural Cyclic Acetal Enables Selective Furan-2,5-dicarboxylic Acid Formation with CeO2-Supported Gold Catalyst. *Angewandte Chemie International Edition*, *57*(27), 8235–8239. https://doi.org/10.1002/ANIE.201805457

79. Ferraz, C. P., Zieliński, M., Pietrowski, M., Heyte, S., Dumeignil, F., Rossi, L. M., & Wojcieszak, R. (2018). Influence of Support Basic Sites in Green Oxidation of Biobased Substrates Using Au-Promoted Catalysts. *ACS Sustainable Chemistry and Engineering*, *6*(12), 16332–16340. https://doi.org/10.1021/ACSSUSCHEMENG.8B03330/ASSET/IMAGES/MEDIUM/SC-2018-03330P_0008.GIF

80. Schade, O. R., Kalz, K. F., Neukum, D., Kleist, W., & Grunwaldt, J. D. (2018). Supported gold- and silver-based catalysts for the selective aerobic oxidation of 5-(hydroxymethyl)furfural to 2,5-furandicarboxylic acid and 5-hydroxymethyl-2-furancarboxylic acid. *Green Chemistry*, *20*(15), 3530–3541. https://doi.org/10.1039/C8GC01340C

81. German, D., Pakrieva, E., Kolobova, E., Carabineiro, S. A. C., Stucchi, M., Villa, A., Prati, L., Bogdanchikova, N., Corberán, V. C., & Pestryakov, A. (2021). Oxidation of 5-Hydroxymethylfurfural on Supported Ag, Au, Pd and Bimetallic Pd-Au Catalysts: Effect of the Support. *Catalysts* , *11*(1), 115. https://doi.org/10.3390/CATAL11010115

82. Cai, J., Ma, H., Zhang, J., Song, Q., Du, Z., Huang, Y., & Xu, J. (2013). Gold Nanoclusters Confined in a Supercage of Y Zeolite for Aerobic Oxidation of HMF under Mild Conditions. *Chemistry – A European Journal*, *19*(42), 14215–14223. https://doi.org/10.1002/CHEM.201301735

83. Masoud, N., Donoeva, B., & de Jongh, P. E. (2018). Stability of gold nanocatalysts supported on mesoporous silica for the oxidation of 5-hydroxymethyl furfural to furan-2,5-dicarboxylic acid. *Applied Catalysis A: General*, *561*, 150–157. https://doi.org/10.1016/J.APCATA.2018.05.027

84. Gorbanev, Y. Y., Klitgaard, S. K., Woodley, J. M., Christensen, C. H., & Riisager, A. (2009). Gold-Catalyzed Aerobic Oxidation of 5-Hydroxymethylfurfural in Water at Ambient Temperature. *ChemSusChem*, *2*(7), 672–675. https://doi.org/10.1002/CSSC.200900059

85. Davis, S. E., Zope, B. N., & Davis, R. J. (2012). On the mechanism of selective oxidation of 5-hydroxymethylfurfural to 2,5-furandicarboxylic acid over supported Pt and Au catalysts. *Green Chemistry*, *14*(1), 143–147. https://doi.org/10.1039/C1GC16074E

86. Albonetti, S., Lolli, A., Morandi, V., Migliori, A., Lucarelli, C., & Cavani, F. (2015). Conversion of 5-hydroxymethylfurfural to 2,5-furandicarboxylic acid over Au-based catalysts: Optimization of active phase and metal–support interaction. *Applied Catalysis B: Environmental*, *163*, 520–530. https://doi.org/10.1016/J.APCATB.2014.08.026

87. Choudhary, H., & Ebitani, K. (2016). Hydrotalcite-supported PdPt-catalyzed Aerobic Oxidation of 5-Hydroxymethylfurfural to 2,5-Furandicarboxylic Acid in Water. *Chemistry Letters*, *45*(6), 613–615. https://doi.org/10.1246/CL.160178

88. Li, Z., Zhu, C., Wang, H., Liang, Y., Xin, H., Li, S., Hu, X., Wang, C., Zhang, Q., Liu, Q., & Ma, L. (2021). 5-Hydroxymethylfurfural hydrodeoxygenation coupled with water-gas shift reaction for 2,5-

dimethylfuran production over Au/ZrO2 catalysts. *ACS Sustainable Chemistry and Engineering*, *9*(18), 6355–6369. https://doi.org/10.1021/ACSSUSCHEMENG.1C00616/SUPPL_FILE/SC1C00616_SI_001.PDF

89. Zhang, Y., Xue, Z., Wang, J., Zhao, X., Deng, Y., Zhao, W., & Mu, T. (2016). Controlled deposition of Pt nanoparticles on Fe3O4@carbon microspheres for efficient oxidation of 5-hydroxymethylfurfural. *RSC Advances*, *6*(56), 51229–51237. https://doi.org/10.1039/C6RA06792A

90. Yu, H., Kim, K. A., Kang, M. J., Hwang, S. Y., & Cha, H. G. (2019). Carbon Support with Tunable Porosity Prepared by Carbonizing Chitosan for Catalytic Oxidation of 5-Hydroxylmethylfurfural. *ACS Sustainable Chemistry and Engineering*, *7*(4), 3742–3748. https://doi.org/10.1021/ACSSUSCHEMENG.8B03775/SUPPL_FILE/SC8B03775_SI_001.PDF

91. Ke, C., Li, M., Fan, G., Yang, L., & Li, F. (2018). Pt Nanoparticles Supported on Nitrogen-Doped-Carbon-Decorated CeO2 for Base-Free Aerobic Oxidation of 5-Hydroxymethylfurfural. *Chemistry – An Asian Journal*, *13*(18), 2714–2722. https://doi.org/10.1002/ASIA.201800738

92. Zhou, C., Deng, W., Wan, X., Zhang, Q., Yang, Y., & Wang, Y. (2015). Functionalized Carbon Nanotubes for Biomass Conversion: The Base-Free Aerobic Oxidation of 5-Hydroxymethylfurfural to 2,5-Furandicarboxylic Acid over Platinum Supported on a Carbon Nanotube Catalyst. *ChemCatChem*, *7*(18), 2853–2863. https://doi.org/10.1002/CCTC.201500352

93. Liguori, F., Barbaro, P., & Calisi, N. (2019). Continuous-Flow Oxidation of HMF to FDCA by Resin-Supported Platinum Catalysts in Neat Water. *ChemSusChem*, *12*(12), 2558–2563. https://doi.org/10.1002/CSSC.201900833

94. Miao, Z., Wu, T., Li, J., Yi, T., Zhang, Y., & Yang, X. (2015). Aerobic oxidation of 5-hydroxymethylfurfural (HMF) effectively catalyzed by a Ce0.8Bi0.2O2−δ supported Pt catalyst at room temperature. *RSC Advances*, *5*(26), 19823–19829. https://doi.org/10.1039/C4RA16968A

95. Han, X., Li, C., Guo, Y., Liu, X., Zhang, Y., & Wang, Y. (2016). N-doped carbon supported Pt catalyst for base-free oxidation of 5-hydroxymethylfurfural to 2,5-furandicarboxylic acid. *Applied Catalysis A: General*, *526*, 1–8. https://doi.org/10.1016/J.APCATA.2016.07.011

96. Gong, W., Zheng, K., & Ji, P. (2017). Platinum deposited on cerium coordination polymer for catalytic oxidation of hydroxymethylfurfural producing 2,5-furandicarboxylic acid. *RSC Advances*, *7*(55), 34776–34782. https://doi.org/10.1039/C7RA05427K

97. Sharma, P., Solanki, M., & Sharma, R. K. (2019). Metal-functionalized carbon nanotubes for biomass conversion: base-free highly efficient and recyclable catalysts for aerobic oxidation of 5-hydroxymethylfurfural. *New Journal of Chemistry*, *43*(26), 10601–10609. https://doi.org/10.1039/C9NJ01555H

98. Ait Rass, H., Essayem, N., & Besson, M. (2013). Selective aqueous phase oxidation of 5-hydroxymethylfurfural to 2,5-furandicarboxylic acid over Pt/C catalysts: influence of the base and effect of bismuth promotion. *Green Chemistry*, *15*(8), 2240–2251. https://doi.org/10.1039/C3GC40727F

99. Niu, W., Wang, D., Yang, G., Sun, J., Wu, M., Yoneyama, Y., & Tsubaki, N. (2014). Pt Nanoparticles Loaded on Reduced Graphene Oxide as an Effective Catalyst for the Direct Oxidation of 5-Hydroxymethylfurfural (HMF) to Produce 2,5-Furandicarboxylic Acid (FDCA) under Mild Conditions. *Bulletin of the Chemical Society of Japan*, *87*(10), 1124–1129. https://doi.org/10.1246/BCSJ.20140096

100. Siyo, B., Schneider, M., Radnik, J., Pohl, M. M., Langer, P., & Steinfeldt, N. (2014). Influence of support on the aerobic oxidation of HMF into FDCA over preformed Pd nanoparticle based materials. *Applied Catalysis A: General*, *478*, 107–116. https://doi.org/10.1016/J.APCATA.2014.03.020

101. Zhang, Z., Zhen, J., Liu, B., Lv, K., & Deng, K. (2015). Selective aerobic oxidation of the biomass-derived precursor 5-hydroxymethylfurfural to 2,5-furandicarboxylic acid under mild conditions

over a magnetic palladium nanocatalyst. *Green Chemistry*, *17*(2), 1308–1317. https://doi.org/10.1039/C4GC01833H

102. Wang, Y., Yu, K., Lei, D., Si, W., Feng, Y., Lou, L. L., & Liu, S. (2016). Basicity-Tuned Hydrotalcite-Supported Pd Catalysts for Aerobic Oxidation of 5-Hydroxymethyl-2-furfural under Mild Conditions. *ACS Sustainable Chemistry and Engineering*, *4*(9), 4752–4761. https://doi.org/10.1021/ACSSUSCHEMENG.6B00965/SUPPL_FILE/SC6B00965_SI_001.PDF

103. Yang, J., Yu, H., Wang, Y., Qi, F., Liu, H., Lou, L. L., Yu, K., Zhou, W., & Liu, S. (2019). Effect of the oxygen coordination environment of Ca–Mn oxides on the catalytic performance of Pd supported catalysts for aerobic oxidation of 5-hydroxymethyl-2-furfural. *Catalysis Science & Technology*, *9*(23), 6659–6668. https://doi.org/10.1039/C9CY01298B

104. Mei, N., Liu, B., Zheng, J., Lv, K., Tang, D., & Zhang, Z. (2015). A novel magnetic palladium catalyst for the mild aerobic oxidation of 5-hydroxymethylfurfural into 2,5-furandicarboxylic acid in water. *Catalysis Science & Technology*, *5*(6), 3194–3202. https://doi.org/10.1039/C4CY01407C

105. Liu, B., Ren, Y., & Zhang, Z. (2015). Aerobic oxidation of 5-hydroxymethylfurfural into 2,5-furandicarboxylic acid in water under mild conditions. *Green Chemistry*, *17*(3), 1610–1617. https://doi.org/10.1039/C4GC02019G

106. Espinosa, J. C., Contreras, R. C., Navalón, S., Rivera-Cárcamo, C., Álvaro, M., Machado, B. F., Serp, P., & Garcia, H. (2019). Influence of Carbon Supports on Palladium Nanoparticle Activity toward Hydrodeoxygenation and Aerobic Oxidation in Biomass Transformations. *European Journal of Inorganic Chemistry*, *2019*(14), 1979–1987. https://doi.org/10.1002/EJIC.201900190

107. Rathod, P. v., & Jadhav, V. H. (2018). Efficient Method for Synthesis of 2,5-Furandicarboxylic Acid from 5-Hydroxymethylfurfural and Fructose Using Pd/CC Catalyst under Aqueous Conditions. *ACS Sustainable Chemistry and Engineering*, *6*(5), 5766–5771. https://doi.org/10.1021/ACSSUSCHEMENG.7B03124/SUPPL_FILE/SC7B03124_SI_001.PDF

108. Chen, C., Li, X., Wang, L., Liang, T., Wang, L., Zhang, Y., & Zhang, J. (2017). Highly Porous Nitrogen- and Phosphorus-Codoped Graphene: An Outstanding Support for Pd Catalysts to Oxidize 5-Hydroxymethylfurfural into 2,5-Furandicarboxylic Acid. *ACS Sustainable Chemistry and Engineering*, *5*(12), 11300–11306. https://doi.org/10.1021/ACSSUSCHEMENG.7B02049/SUPPL_FILE/SC7B02049_SI_001.PDF

109. Gu, Q., Sautet, P., & Michel, C. (2018). Unraveling the Role of Base and Catalyst Polarization in Alcohol Oxidation on Au and Pt in Water. *ACS Catalysis*, *8*(12), 11716–11721. https://doi.org/10.1021/ACSCATAL.8B03494/SUPPL_FILE/CS8B03494_SI_001.PDF

110. de Oliveira Rocha, K., Marques, C. M. P., & Bueno, J. M. C. (2019). Effect of Au doping of Ni/Al2O3 catalysts used in steam reforming of methane: Mechanism, apparent activation energy, and compensation effect. *Chemical Engineering Science*, *207*, 844–852. https://doi.org/10.1016/j.ces.2019.06.049

111. Gao, Z., Xie, R., Fan, G., Yang, L., & Li, F. (2017). Highly Efficient and Stable Bimetallic AuPd over La-Doped Ca-Mg-Al Layered Double Hydroxide for Base-Free Aerobic Oxidation of 5-Hydroxymethylfurfural in Water. *ACS Sustainable Chemistry and Engineering*, *5*(7), 5852–5861. https://doi.org/10.1021/ACSSUSCHEMENG.7B00573/SUPPL_FILE/SC7B00573_SI_001.PDF

112. Wang, Q., Hou, W., Li, S., Xie, J., Li, J., Zhou, Y., & Wang, J. (2017). Hydrophilic mesoporous poly(ionic liquid)-supported Au–Pd alloy nanoparticles towards aerobic oxidation of 5-hydroxymethylfurfural to 2,5-furandicarboxylic acid under mild conditions. *Green Chemistry*, *19*(16), 3820–3830. https://doi.org/10.1039/C7GC01116D

113. Pasini, T., Piccinini, M., Blosi, M., Bonelli, R., Albonetti, S., Dimitratos, N., Lopez-Sanchez, J. A., Sankar, M., He, Q., Kiely, C. J., Hutchings, G. J., & Cavani, F. (2011). Selective oxidation of 5-hydroxymethyl-2-furfural using supported gold–copper nanoparticles. *Green Chemistry*, *13*(8), 2091–2099. https://doi.org/10.1039/C1GC15355B

114. Gui, Z., Cao, W., Saravanamurugan, S., Riisager, A., Chen, L., & Qi, Z. (2016). Efficient Aerobic Oxidation of 5-Hydroxymethylfurfural in Aqueous Media with Au–Pd Supported on Zinc Hydroxycarbonate. *ChemCatChem*, *8*(23), 3636–3643. https://doi.org/10.1002/CCTC.201600852

115. Albonetti, S., Pasini, T., Lolli, A., Blosi, M., Piccinini, M., Dimitratos, N., Lopez-Sanchez, J. A., Morgan, D. J., Carley, A. F., Hutchings, G. J., & Cavani, F. (2012). Selective oxidation of 5-hydroxymethyl-2-furfural over TiO2-supported gold–copper catalysts prepared from preformed nanoparticles: Effect of Au/Cu ratio. *Catalysis Today*, *195*(1), 120–126. https://doi.org/10.1016/J.CATTOD.2012.05.039

116. Schade, O. R., Stein, F., Reichenberger, S., Gaur, A., Saraçi, E., Barcikowski, S., & Grunwaldt, J. D. (2020). Selective Aerobic Oxidation of 5-(Hydroxymethyl)furfural over Heterogeneous Silver-Gold Nanoparticle Catalysts. *Advanced Synthesis & Catalysis*, *362*(24), 5681–5696. https://doi.org/10.1002/ADSC.202001003

117. Verdeguer, P., Merat, N., & Gaset, A. (1994). Lead/platinum on charcoal as catalyst for oxidation of furfural. Effect of main parameters. *Applied Catalysis A: General*, *112*(1), 1–11. https://doi.org/10.1016/0926-860X(94)80133-9

118. Gupta, K., Rai, R. K., Dwivedi, A. D., & Singh, S. K. (2017). Catalytic Aerial Oxidation of Biomass-Derived Furans to Furan Carboxylic Acids in Water over Bimetallic Nickel–Palladium Alloy Nanoparticles. *ChemCatChem*, *9*(14), 2760–2767. https://doi.org/10.1002/CCTC.201600942

119. Ahmed, M. S., Mannel, D. S., Root, T. W., & Stahl, S. S. (2017). Aerobic Oxidation of Diverse Primary Alcohols to Carboxylic Acids with a Heterogeneous Pd-Bi-Te/C (PBT/C) Catalyst. *Organic Process Research and Development*, *21*(9), 1388–1393. https://doi.org/10.1021/ACS.OPRD.7B00223/SUPPL_FILE/OP7B00223_SI_001.PDF

120. Scaranto, J., & Mavrikakis, M. (2016). Density functional theory studies of HCOOH decomposition on Pd(111). *Surface Science*, *650*, 111–120. https://doi.org/10.1016/J.SUSC.2015.11.020

121. Wang, H. F., & Liu, Z. P. (2009). Formic acid oxidation at Pt/H2O interface from periodic DFT calculations integrated with a continuum solvation model. *Journal of Physical Chemistry C*, *113*(40), 17502–17508. https://doi.org/10.1021/JP9059888/SUPPL_FILE/JP9059888_SI_001.PDF

122. Monyoncho, E. A., Steinmann, S. N., Sautet, P., Baranova, E. A., & Michel, C. (2018). Computational screening for selective catalysts: Cleaving the CC bond during ethanol electro-oxidation reaction. *Electrochimica Acta*, *274*, 274–278. https://doi.org/10.1016/J.ELECTACTA.2018.04.102

123. Behravesh, E., Melander, M. M., Wärnå, J., Salmi, T., Honkala, K., & Murzin, D. Y. (2021). Oxidative dehydrogenation of ethanol on gold: Combination of kinetic experiments and computation approach to unravel the reaction mechanism. *Journal of Catalysis*, *394*, 193–205. https://doi.org/10.1016/J.JCAT.2020.07.022

124. Boronat, M., Corma, A., Illas, F., Radilla, J., Ródenas, T., & Sabater, M. J. (2011). Mechanism of selective alcohol oxidation to aldehydes on gold catalysts: Influence of surface roughness on reactivity. *Journal of Catalysis*, *278*(1), 50–58. https://doi.org/10.1016/J.JCAT.2010.11.013

125. Belletti, G. D., Colombo, E., Cabana, N., Quaino, P., & Collins, S. (2022). Mechanistic Investigation of Methanol Oxidation on Au/TiO2: A Combined DRIFT and DFT Study. *Topics in Catalysis 2022 65:7*, *65*(7), 915–925. https://doi.org/10.1007/S11244-022-01620-7

126. Liu, S., Jin, P., Zhang, D., Hao, C., & Yang, X. (2013). Reaction mechanism for methanol oxidation on Au(1 1 1): A density functional theory study. *Applied Surface Science*, *265*, 443–451. https://doi.org/10.1016/J.APSUSC.2012.11.026

127. Karanjit, S., Bobuatong, K., Fukuda, R., Ehara, M., & Sakurai, H. (2013). Mechanism of the aerobic oxidation of methanol to formic acid on Au8−: A DFT study. *International Journal of Quantum Chemistry*, *113*(4), 428–436. https://doi.org/10.1002/QUA.24056

128. Chang, C. R., Long, B., Yang, X. F., & Li, J. (2015). Theoretical Studies on the Synergetic Effects of Au-Pd Bimetallic Catalysts in the Selective Oxidation of Methanol. *Journal of Physical Chemistry C*,

119(28), 16072–16081. https://doi.org/10.1021/ACS.JPCC.5B03965/SUPPL_FILE/JP5B03965_SI_001.PDF

129. Qiu, Y., Zhang, J., Jin, J., Sun, J., Tang, H., Chen, Q., Zhang, Z., Sun, W., Meng, G., Xu, Q., Zhu, Y., Han, A., Gu, L., Wang, D., & Li, Y. (2021). Construction of Pd-Zn dual sites to enhance the performance for ethanol electro-oxidation reaction. *Nature Communications 2021 12:1*, *12*(1), 1–9. https://doi.org/10.1038/s41467-021-25600-9

130. Pereira, A. O., & Miranda, C. R. (2014). Atomic scale insights into ethanol oxidation on Pt, Pd and Au metallic nanofilms: A DFT with van der Waals interactions. *Applied Surface Science*, *288*, 564–571. https://doi.org/10.1016/J.APSUSC.2013.10.074

131. Gu, Q., Fang, W. H., Wischert, R., Zhou, W. J., Michel, C., & Pera-Titus, M. (2019). AuCu/CeO2 bimetallic catalysts for the selective oxidation of fatty alcohol ethoxylates to alkyl ether carboxylic acids. *Journal of Catalysis*, *380*, 132–144. https://doi.org/10.1016/J.JCAT.2019.10.017

132. Lei, D., Yu, K., Li, M. R., Wang, Y., Wang, Q., Liu, T., Liu, P., Lou, L. L., Wang, G., & Liu, S. (2017). Facet Effect of Single-Crystalline Pd Nanocrystals for Aerobic Oxidation of 5-Hydroxymethyl-2-furfural. *ACS Catalysis*, *7*(1), 421–432. https://doi.org/10.1021/ACSCATAL.6B02839/SUPPL_FILE/CS6B02839_SI_001.PDF

133. Liao, X., Hou, J., Wang, Y., Zhang, H., Sun, Y., Li, X., Tang, S., Kato, K., Yamauchi, M., & Jiang, Z. (2019). An active, selective, and stable manganese oxide-supported atomic Pd catalyst for aerobic oxidation of 5-hydroxymethylfurfural. *Green Chemistry*, *21*(15), 4194–4203. https://doi.org/10.1039/C9GC01674K

134. Afroz, K., Ntambwe, M., & Nuraje, N. (2020). Experimental and DFT Study of Metal-Free Catalyst for Selective Oxidation of Biomass-Derived Molecule (HMF). *Inorganic Chemistry*, *59*(18), 13335–13342. https://doi.org/10.1021/ACS.INORGCHEM.0C01702/SUPPL_FILE/IC0C01702_SI_001.PDF

135. Liu, Y., Ma, H. Y., Lei, D., Lou, L. L., Liu, S., Zhou, W., Wang, G. C., & Yu, K. (2019). Active Oxygen Species Promoted Catalytic Oxidation of 5-Hydroxymethyl-2-furfural on Facet-Specific Pt Nanocrystals. *ACS Catalysis*, *9*(9), 8306–8315. https://doi.org/10.1021/ACSCATAL.9B02115/SUPPL_FILE/CS9B02115_SI_001.PDF

136. Ren, Z., Yang, Y., Wang, S., Li, X., Feng, H., Wang, L., Li, Y., Zhang, X., & Wei, M. (2021). Pt atomic clusters catalysts with local charge transfer towards selective oxidation of furfural. *Applied Catalysis B: Environmental*, *295*, 120290. https://doi.org/10.1016/J.APCATB.2021.120290

137. Mark, L. O., Agrawal, N., Román, A. M., Holewinski, A., Janik, M. J., & Medlin, J. W. (2019). Insight into the Oxidation Mechanism of Furanic Compounds on Pt(111). *ACS Catalysis*, *9*(12), 11360–11370. https://doi.org/10.1021/ACSCATAL.9B03983/SUPPL_FILE/CS9B03983_SI_001.PDF

138. Jenness, G. R., & Vlachos, D. G. (2015). DFT study of the conversion of furfuryl alcohol to 2-methylfuran on RuO2 (110). *Journal of Physical Chemistry C*, *119*(11), 5938–5945. https://doi.org/10.1021/JP5109015/SUPPL_FILE/JP5109015_SI_001.PDF

139. Hameed, S., Lin, L., Wang, A., & Luo, W. (2020). Recent Developments in Metal-Based Catalysts for the Catalytic Aerobic Oxidation of 5-Hydroxymethyl-Furfural to 2,5-Furandicarboxylic Acid. *Catalysts* , *10*(1), 120. https://doi.org/10.3390/CATAL10010120

140. Ferraz, C. P., & Wojcieszak, R. (2022). *Experimental Study of HMF Oxidation into FDCA over Gold-nanoparticle*.

Methodology

3 Methodology

Chapter 3 Methodology

3.1 Overview

Here, we present the background details on the computational methods deployed in our studies in general in the first section (Section 3.1), with reference to existing reports in the literature. And the later part of the section (Section 3.2) presents the specific computational details of the methods and the common specifications deployed in our studies, while the more peculiar specification deployed for some projects are given along with their results in the latter chapters. This study majorly focused on the modeling and simulation of solid system, to be precise, an heterogeneous catalyst.

3.2 Background Details on Computational Methods

3.2.1 Schrodinger Equation and Fundamental Principles

This Equation, popularly known as the Schrodinger Equation (S-E), forms the heart of quantum mechanics calculation. Quantum mechanics studies molecules using the interactions between nuclei and electrons with the minimum energy arrangement of nuclei for a given molecular geometry. Identifying an easy and accurate method of solving the Schrodinger equation is essential for enhancing theoretical prediction efficiency using quantum chemical calculation. The many-body Schrodinger Equation is presented in Equation 3- 1, composing muti-electron and multi-nuclei in its systems[1].

$$H\Psi = E_{tot}\Psi \qquad 3\text{-}1$$

In the many-body wavefunction, Ψ, is expressed as a function of positions $(r_1, r_2, \ldots, r_N)$. The Hamiltonian, H, is basically composed of kinetic and potential energies summation[1,2]. The summation of the potential and kinetic energies (i.e., PE

and KE) gives the Hamiltonian, H, which are expressed as in the below mathematical models in Equation 3- 2 and 3- 3.

$$H = KE_{el} + KE_{nu} + PE_{el,el} + PE_{el,el} + PE_{nu,nu} + PE_{el,nu} \quad 3\text{-}2$$

$$H = -\frac{\hbar^2}{2}\left(\sum_{i}^{el}\frac{\nabla_i^2}{m_e} + \sum_{A}^{nu}\frac{\nabla_A^2}{M_A}\right) + \frac{e^2}{4\pi\epsilon_o}\left(\frac{1}{2}\sum_{i<j}^{el}\frac{1}{|r_i - r_j|} + \frac{1}{2}\sum_{A<B}^{nu}\frac{Z_A Z_B}{|R_A - R_B|} - \sum_{i}^{el}\sum_{A}^{nu}\frac{Z_A}{|r_i - R_A|}\right) \quad 3\text{-}3$$

Here, the KE_{el} represent the electron's KE, the KE_{nu} is the nuclei's KE, the $PE_{el,el}$ is the electron-electron repulsion potential energy (i.e., the electrons coulomb interaction only), the $PE_{nu,\,nu}$ is the nuclei-nuclei repulsion potential energy (also known as nuclei-nuclei coulomb interaction), and the $PE_{el,nu}$ is the electron-nuclei interaction potential energy (also known as coulomb interaction between electron and nuclei)[2,3]. Using the above H expression, the Equation 3- 1 can be rewritten in the form presented in Equation 3- 4:

$$\left(KE_{el} + KE_{nu} + PE_{el,el} + PE_{el,el} + PE_{nu,nu} + PE_{el,nu}\right)\Psi = E_{tot}\Psi \quad 3\text{-}4$$

$$\left[-\frac{\hbar^2}{2}\left(\sum_{i}^{el}\frac{\nabla_i^2}{m_e} + \sum_{A}^{nu}\frac{\nabla_A^2}{M_A}\right) + \frac{e^2}{4\pi\epsilon_o}\left(\sum_{i<j}^{el}\frac{1}{|r_i - r_j|} + \sum_{A<B}^{nu}\frac{Z_A Z_B}{|R_A - R_B|} - \sum_{i}^{el}\sum_{A}^{nu}\frac{Z_A}{|r_i - R_A|}\right)\right]\Psi = E_{tot}\Psi \quad 3\text{-}5$$

The M_A is the ratio of the mass of nucleus A to be mass of an electron, Z is the nuclear charge, $|\mathrm{R_A} - R_B|$ is the spacing between the nuclei A and B, $|r_i - r_j|$ is the spacing existing between electron, i and j, and $|r_i - R_A|$ is the spacing between electron, i, and nucleus, A. The el and nu stand for the electron and nuclei,

respectively. The ∇^2 is a Laplacian operator, which can be expressed as: $\frac{\partial^2}{\partial x^2} + \frac{\partial^2}{\partial y^2} + \frac{\partial^2}{\partial z^2}$, and the position vector, r or R, can be also expressed as $(x^2 + y^2 + z^2)^{\frac{1}{2}}$.

Reports in the literature [1] has established that search for solution of the many-electron or many-body Schrodinger equation is high complicated to solved. Hence, there is need to consider the introduction of some reasonable approximation as a way of reducing the possible number of degrees of freedom involved in the calculation.

3.2.2 Born-Oppenheimer Approximation Model to Schrödinger Equation

One of the proposed approximations was the Born-Oppenheimer (BO) Approximation model [1] which aids in simplifying the solution of the Schrodinger Equation in a many-body systems. The BO approximation model facilitates the separation of electronic motion from nuclear motion. The approximation, in line with the knowledge that nuclei are more massive than electrons, considers that nuclear motion is slower (almost stationary) than that of electrons, which are mostly in motion. Although nuclei actually move, their movement is not fast compared to the speed of an electron.. This approximation was use to reform the Schrodinger Equation into becoming electronic Schrodinger Equation generally expressed in Equation 3- 6.

$$H^{el}\Psi^{el} = E^{el}\Psi^{el} \qquad 3\text{-}6$$

The electronic Hamiltonian, H^{el} is re-expressed to the form presented in Equation 3-7. The new expression for Hamiltonian omits the terms describing the nuclear kinetic energy (since it was assumed that nuclei is not in motion), and the nuclear-nuclear Coulomb term.

$$H_{el} = -\frac{1}{2}\sum_{i}^{el}\nabla_i^2 + V_{el-nu} + \frac{1}{2}\sum_{i>J}^{el}\frac{1}{r_{ij}} \qquad 3\text{-}7$$

The V_{el-nu} denote the potential accounting for the interaction that exists between the electrons and the atomic nuclei in Equation 3- 8.

$$V_{el-nu} = -\sum_{i}^{el}\sum_{A}^{nu}\frac{Z_A}{r_{iA}} \qquad 3\text{-}8$$

$$E_{tot} = E_{el} + \sum_{A<B}^{nu}\frac{Z_A Z_B}{R_{AB}} \qquad 3\text{-}9$$

The modification gives a new expression for computing total energy, where it was shown that the addition of the nuclear-nuclear Coulomb term to the electronic energy gives the total energy, E_{tot} expressed in Equation 3- 9.

Our study deployed the use of the density functional theory method in our evaluations which are presented in the later section.

3.2.3 DFT and Hohenberg, Kohn and Sham Theorems

DFT, a theory of Hohenberg, Kohn, and Sham[2,4,5] which is based on the summation of exchange and correlation energies of a uniform electron gas can be defined exactly knowing only its density. It is a widely used theory and is known as a theory of electronic structure [6]. The theory was derived from the N-particle of the Schrodinger equation (S-E) and is presented as a function of the electronic density distribution of the ground state. The method reduces the calculation of the ground state properties (of systems of interacting particles) to the solution of a single Hatree-type equation. This improvement has attracted much research into its usage for systems with many electrons. And this advantage has made it a good alternative approach to the traditional methods of quantum chemistry, which are often expressed in terms of the many-electron wave function. These other theoretical methods are largely more approximate, whereas, in principle, DFT provides an exact solution. The DFT methods find application problems involving molecules, atoms, and solids.

The journey to the discovery of the DFT method starts from the theorem of the Thomas-Fermi (T-F) Model, which first established the possibility of expressing energy in terms of electronic density in the 1920s. The kinetic energies, E_{KE} accounted in the model were obtained using quantum statistic theory of uniform electron gas. Whereas, other terms that account for other interactions like electron-electron, $\mathrm{E_{el-}}_{el}$, and electron-nuclear, $\mathrm{E_{el-nu}}$ were modeled classically as expressed in the Equation 3- 10 . $\mathrm{C_F}$ is 2.871.

$$E_{T-F}(\rho) = E_{KE} + E_{el-nu} + E_{el-el} = C_F \int \rho^{\frac{5}{3}}(r)dr - Z\int \frac{\rho(r)}{r}\, dr + \frac{1}{2}\int\int \frac{\rho(r_1)\rho(r_2)}{|r_1 - r_2|}\, dr_1 dr_2 \qquad 3\text{- }10$$

The nuclear charge of the particle was denoted as Z, the distance between the electron (el) and nucleus (nu) in the system was taken as r, and the distance between two electrons (el-el) at position 1 and 2 is $|r_1 - r_2|$. Moreover, Hohenberg-Kohn further built on the idea of the T-F theorem to derive a theorem that enables us to express electronic Hamiltonian as a function of electron density. Their theorem which states that there is existence a correspondence between external potential and electronic density and that the electronic density at ground state can also be obtained using variational principle. From which, DFT draws its basis expressing its energy, E_{H-K} as a function of electron density, $\rho(\mathrm{r})$ in Equation 3- 11.

$$E_{H-K}(\rho) = E_{KE}(\rho) + E_{el-nu}(\rho) + E_{el-el}(\rho) = \int \rho(r) v_{ext}(r)\, dr + F_{H-K} \qquad 3\text{- }11$$

The F_{H-K} term, als known as universal functional of electronic density, $\rho(\mathrm{r})$. And it is also referred to as the summation of the kinetic and electron-electron interaction energy, which is not dependent on external potential, $v_{ext}(\mathrm{r})$. Solving the computational of the F_{H-K} term has been reported to challenging especially for many-electron body problems.

The Kohn-Sham theorem[1], was later developed to address the challenge. From which, K-S theorem established that the wrong descriptions of kinetic energy in T-F theorem contribute to this failure. And to get this addressed corrected, we need to introduce the non-interacting election moving in the effective field. This would imply re-writing F_{H-K} in Equation 3- 11 to form Equation 3- 12, with the inclusion of non-interacting kinetic energy, E_{nKE}, Hartree energy, $\mathrm{E_H}$, and exchange and correlation energy, E_{XC}.

$$E = E_{ext} + E_{nKE} + E_H + E_{XC} = E_{known} + E_{XC} = \int \rho(r) v_{ext}(r)\, dr + E_{nKE}[\rho(r)] + E_H[\rho(r)] + E_{XC}[\rho(r)] \quad 3\text{- }12$$

It is easy to compute the first three terms, that is, why they were summed up as known energy terms $\mathrm{E_{known}}$. Computation of the $\mathrm{E_{XC}}$ term is the most challenging out of the four terms and sometime denoted as the unknown energy term, $\mathrm{E}_{unknown}$. The total electronic density, $\rho(r)$ is expressed in the form:

$$\rho(r) = 2 \sum_{i}^{orbitals} |\Psi_i(r)|^2 \quad 3\text{- }13$$

Whereas, the summation of the electrons, N is expressed is computed as follows:

$$N = \int \rho(r)\, dr \quad 3\text{- }14$$

The effective potential, V_{eff} in the electronic structure problems was then expressed in the form:

$$V_{eff} = v_{ext}(r) + \int \frac{\rho(r')}{|r - r'|}\, dr' + v_{XC}(r) \quad 3\text{- }15$$

The second term in the above equation is the Hartree potential, v_H. And the exchange and correlation potential, v_{XC} and energy, E_{XC} are presented in the form:

$$v_{XC}(r) = \delta E_{XC} \frac{[\rho(r)]}{\delta \rho(r)} \quad 3\text{- }16$$

$$E_{XC} = E_X + (E_C^{int} + E_{kin}^{int}) = E_X + E_C = \int f(\rho(r), \nabla\rho(r), \ldots)dr$$

3- 17

The term, $\mathrm{E_C^{int}}$ represent the interacting correlation energy and the $\mathrm{E_{kin}^{int}}$ is the interacting kinetic energy. The summation of the terms is the correlation energy, $\mathrm{E_C}$. The term, E_{XC}, is accounts for the summation of the exchange energy, and the correlation energy of the electrons. The K-S equation can be expressed in Equation 3- 18 for a one-electron Schrodinger equation.

$$\left[-\frac{1}{2}\nabla^2 + V_{eff}\right]\Psi_i(r) = \varepsilon\,\Psi_i(r)$$

3- 18

The Ψ_i in the above Equation denotes the Kohn-Sham orbitals. It is used in the summation which is carried out over pairs of electrons within a finite basis set which is analogous to the LCAO approximation for the HF models). And the ground-state electronic energy E, is presented in Equation 3- 19.

$$E = \sum_i^N \varepsilon_i - \frac{1}{2}\int\int \frac{\rho(r)\rho(r')}{|r-r'|}\,drdr' + E_{XC}[\rho(r)] - \int v_{XC}(r)\rho(r)\,dr$$

3- 19

It can said that V_{eff} is a function of electronic density and the equations 3- 14, 3- 15, and 3- 19 formed that key basis for solving DFT problems which are largely celebrated in the literature. The Kohn-Sham equation is expected to be solved self-consistently.

In solving the Kohn-Sham equations, it often began with the provision of initial guess electron density, which is used in constructing the V_{eff}, and the obtained the K-S orbitals. With the use of the orbitals, a new density is then computed and then a new K-S orbital, $\mathrm{\Psi_i}$ is obtained (using equations 3- 14, 3- 15, and 3- 19). The computation loop is been repeated until the set convergence is attained. After which, the total energy is then computed using the last electron density obtained from the computation. So, when we are able to be obtain all the relevant terms provided in the K-S energy equation, we can then obtain the exact ground-state density and total

energy with an excellent or perfect prediction. At present, it is not possible due to the presence of an unknown energy term, better referred to as Exchange and correlation energy, E_{XC}. The energy do account for the non-classical electron-electron interaction along with the component of kinetic energy of a real system different from the non-fictitious (unrealistic) non-interacting system. Several research works have been reviews better ways of addressing the challenge.

3.2.4 Exchange and Correlation Functionals

Exchange and Correlation (XC) functionals [2] present in the Kohn-Sham's Schrodinger Equation do account for all the quantum effect in a given system studied. It is known to be composed of two parts, exchange and correlation energy that exist in a system [1,7,8]. The exchange energy has association with Pauli Exclusion principle which tries to ensure that electron with same spin do not stay in same orbital unlike the electron with different spins that can fill same orbital. The term, E_{XC} is an unknown term whose exact value is unknown in the K-S energy equation. The search for the expressions or models that could effectively computing the term give birth to development of different functional for computing an approximate value for the term. Some of the functionals are developed using physical rule (that is, non-empirical approach) while some are by fitting to a known result of atomic properties (that is, empirical approach). The various approximations in the literature [9] are general group in the categories which are diagrammatically presented in Figure 3-1.

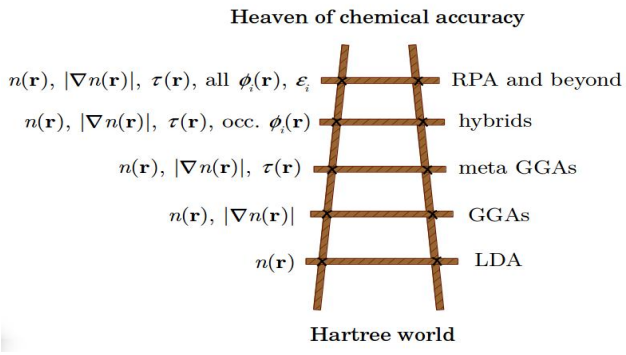

Figure 3-1 The Jacob Ladder of DFT showing different approximations[9].

Generally, there are many reported functionals in the literature with respective pros and cons (in terms of computational time and accuracy) [2,5] . However, the most populous functionals widely used in the existing reports includes, functionals based on the local spin density approximation (LDA); functionals based on the generalized gradient approximation (GGA); and hybrid functionals. The LDA is often referred to as local density models, while the other functional like GGA and the one that employed the use of H-F exchange as a component is commonly known as gradient-corrected models.

The choice of what functional to use in a defined study plays a vital role on the accuracy of modeling and simulation outputs. This vitality of the functional choice was due its high level of significance in computational studies which include: the role of connecting the 1-electron system to the n-electron systems; modeling of the electrons activities in the system; and vital for defining materials properties. So, wrong choice can lead to disconnect and yield false predictions. Unlike DFT that account for exchange and correlation energies, Hartree Fock method only accounts for the exchange energies. It is important to note that when the exact exchange/correlation functional is known, then the density functional approach can then be said to be "exact"[1].

3.2.4.1 Local Density Approximation (LDA)

In this approximation model for the computation of the exchange and correlation energies, it was assumed that all the electrons see the overall landscape in same way like they see locally. This idea implies that complex system can be converted into uniform volumes of electrons, whose electron density of each volume is assume to be constant with varying values[2]. The initiative confirms that one can compute XC energy for each electron using their electron densities and that the energies obtained from the locals (each volume) can be put together to yield the total XC energy, E_{xc}^{LDA}.

$$E_{xc}^{LDA}[\rho(r)] = E_{x}^{LDA}[\rho(r)] + E_{c}^{LDA}[\rho(r)] = \int \rho(r)\varepsilon_{xc}^{homo}[\rho(r)]dr$$

3- 20

The LDA exchange and correlation energy mathematical expression is presented in Equation 3- 20. The use of this approximation model for the exchange and correlation energy has been reported to have overestimate $E_{x}^{LDA}[\rho(r)]$ and underestimated, $E_{c}^{LDA}[\rho(r)]$. LDA was also found to be efficient when charge densities varies slowly relatively. LDA have shown to be applicable to systems involving molecules, atom, and solids like metals too. However, LDA was reported have underestimated the correlation energy and overestimated the exchange energy.

3.2.4.2 Generalized Gradient Approximation (GGA)

GGA is a family or group of functional which is more accurate than LDA in terms of prediction accuracy. This functional form depends on density and its gradient [7]. The functional was developed to address the limitation of LDA which was designed to be capture both the local and semi-local information like the electron density and their gradient at a specified point [2]. It has been reported that much better results have been reported for the use of GGA compared to LDA.

$$E_{xc}^{GGA}[\rho(r)] = \int \rho(r)\varepsilon_{xc}^{GGA}[\rho(r), \nabla\rho(r)]dr$$

3- 21

$$E_{xc}^{GGA}[\rho(r), s] = \int \varepsilon_{xc}^{LDA}[\rho(r)]\rho(r)F(s)dr$$

3- 22

Equation 3- 21 show cases GGA exchange and correlation (XC) energy model. When expressed in terms of LDA using extra factor, F(s) which directly changes the LDA, the GGA XC energy would be expressed in form presented in Equation 3- 22. The 's' in the integral is a function of electron density and their gradient as shown in Equation 3- 23.

$$s = C\frac{|\rho(r)|}{\rho^{\frac{3}{4}}(r)}$$

3- 23

The ‘s’ values range from 0 to 3 for electron density in solids. F(s) also known as enhancement factors of different GGAs for the exchange ranging from 1 to 1.6. It is important to note that when F(s) = 1, the model return to LDA. The use of GGA has been receiving a wide range of attention for its applications in several computational material studies in the literature[2]. Example these functionals include Becke 88 (B88), Lee-Yang-Parr (LYP), Perdew-Wang 91 (PW91), Perdew-Burke-Ernzerhof (PBE) and other ones[2,8].

3.2.4.3 Meta-GGA

GGA is a functional form which depends on semi-local information in the Laplacian of the local kinetics energy and spin density[7]. It is known as one of the third generation functionals which uses second derivatives of electron density, $\nabla^2\rho(r)$ and electron kinetic energy, τ. Such form of functionals are often expressed:

$$E_{xc}^{mGGA}[\rho(r)] = \int \rho(r)\varepsilon_{xc}^{GGA}[\rho(r), \nabla\rho(r), \nabla^2\rho(r), \tau]dr \qquad 3\text{-}24$$

The symbol, τ, denotes the kinetic energy density. The method provides a more efficient and accurate output compared to LDA and GGA. Although, it would required more computational time compared to LDA and GGA.

3.2.4.4 The Hybrid Approximation

This is a family or category of functionals which do deployed a combination of the GGA kinds of functions with the Hartree-Fock (H-K) ones[7,10]. Examples of such kind of functionals includes B3LYP (that combine the use of B88 and LYP) and others. It has reported to have good applications in the computations of transition-state barriers, bond energies, and many others.

Other families of functionals in the literature includes hyper-GGA, double hybrids, etc. The higher one go in the Jacob ladder to more accurate it becomes due to the

inclusion of more parameters. The computational time would be also increase as well. However, in our study, we deployed the use of GGA-PBE functionals in computing our exchange-correlation energies in our DFT calculations, due to its reported prediction effectiveness obtained for its applications in several computational material design studies. Example of such work is Gu et al.[11] that used it to investigate the catalysis of Au in ethanol oxidation.

3.2.5 Dispersion Correction Models

Dispersion interactions described empirically as the attractive component of a van der Waals (vdW)-type of interaction potential existing in between molecules or atoms that are not chemically bonded to each other [12] . The application of the post-self-consistent dispersion correction is now the norm of the day when employing the used density-functional theory in the study of a material systems where non-covalent interactions play an important role [13]. It was so in order to ensure good accuracy for non-bonded repulsion and dispersion attraction present in a system evaluated.

The dispersion corrections were classified into 3 groups (as shown in Figure 3- 2) which includes: non-local density-based (which mostly include a correction to the electronic potential V); semi-classical (C6-based) schemes (which often apply corrections only to the total energy E); and effective one-electron potentials. Almost all of the current dispersion corrections include empirical elements in various ways.

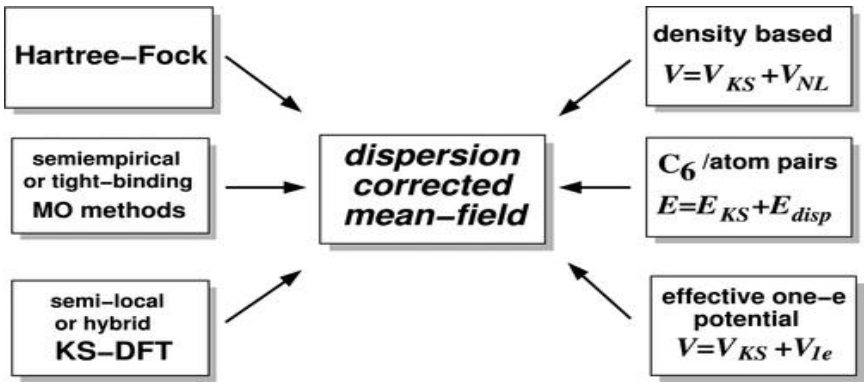

Figure 3- 2 Overview of the dispersion-corrections to mean-field quantum chemical approaches[12].

Examples the methods include the D3[14], D4[15], density-dependent correction (dDsC)[16], and many other ones. Irrespective of the method of dispersion correction used in a study, the dispersion energy is always added to the base DFT energy result as a post self-consistent-field (post-SCF) correction to yield the DFT total energy as show in Equation 3- 25.

$$E_{DFT} = E_{base} + E_{disp} \qquad 3\text{-}25$$

The E_{DFT} , E_{base} , and E_{disp} denotes the total energy (obtained from DFT), base-functional energy, and dispersion correction, respectively. Moreover, the non-local dispersion methods is an alternative for the use of post-SCF methods, which uses the van der Waals (vdW) density functional [17] with many variations [18,19] . These methods are of high accuracy. However, they are more computationally expensive than the post-SCF models due to their non-locality[13]. Our study, therefore, resolved to employ post-SCF model (using dDsC) due to the range of existing related studies that have deployed it and its simplification in term of computational cost, unlike the non-local dispersion methods.

3.2.6 K-points

It is an important computational parameter that defined describes the different energy levels in any periodic structure. When using VASP package [20,21] , it is normally prepared as input file tagged as KPOINT. The KPOINTS file for computation does specifies the Bloch vectors (k-points) employed in sampling the Brillouin zone. Converging this sampling is essential tasks in many calculations concerning the electronic minimization. It can be generated use gamma-centered mesh, Monkhorst-Pack mesh, and some of other approaches.

To select the K-point to use in an analysis, a range of K-points values used in a bulk (using a unit cell) was employed in identifying the best value and its corresponding

computational time, as the electronic energy changes, until it gets to a static value. Findings from the analysis is often used in deciding the K-points to use in studying a solid system.

3.3 Computational Details for This Study

3.3.1 DFT Calculations

In our study, density functional theory (DFT) calculations were performed using density-dependent dispersion correction (dDsC) and the Vienna Ab initio Simulation Package (VASP) package [21–23] to obtain energies. Using the VASP package, our computational work flow for the DFT calculation was structured in the pattern presented in Figure 3- 3.

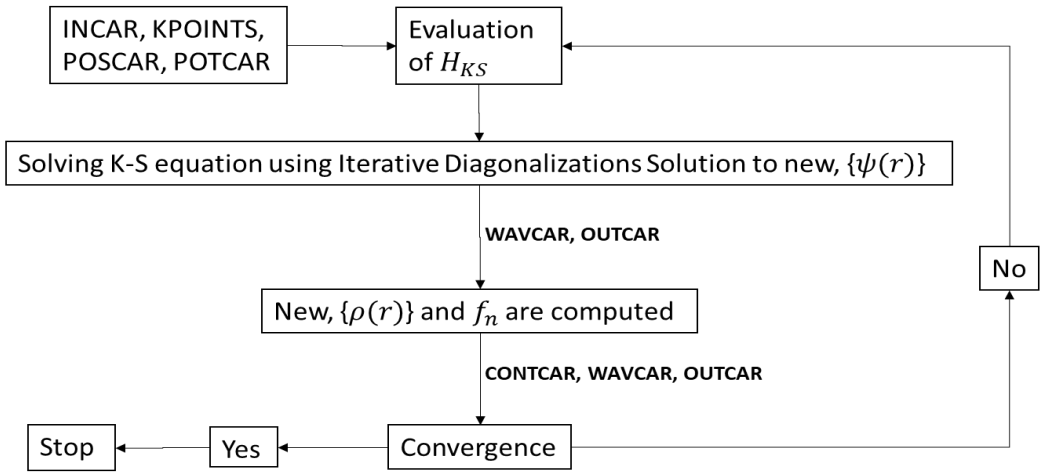

Figure 3- 3 A generic flow diagram for a DFT calculation used in VASP for our study.

The exchange and correlation terms were obtained using the Perdew–Burke–Ernzerhof (PBE) form of Generalized Gradient Approximation (GGA) functional [21,24] similar to the one used in previous studies [25] . It existing report for its efficiency in structural properties computation with a range of 7.9 % mean absolute error (m.a.e.)[9,26], and 1-3 % error[2] (for structural properties computations) also motivated our choice for the functional in order yield effective predictions. In this study, we

deployed the projector-augmented wave (PAW) pseudo-potentials in our computations using a cutoff energy of 400 eV and SCF convergence of 10^{-6} eV.

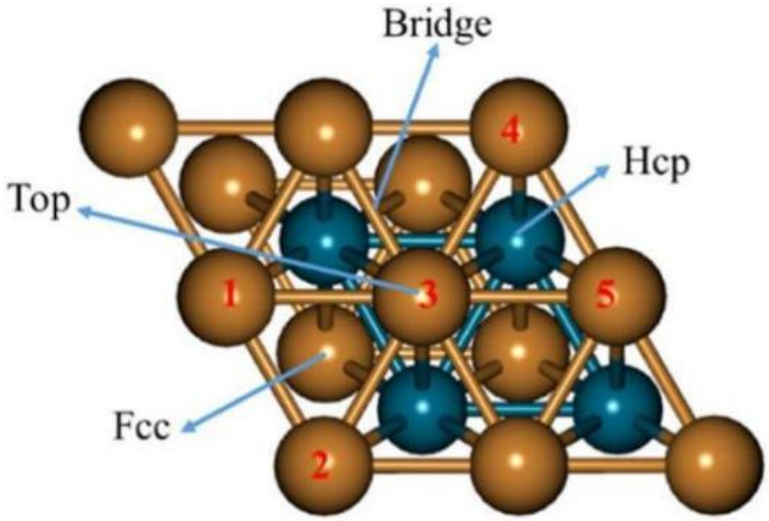

Figure 3-4 *A slab structure (a top view) showing the different adsorption sites present on the slab that were explored in our study in VASP.*

In general, all the slabs were modeled to be 4-layers, where the last two layers were frozen while the first two layers were kept free to adjust. For geometry optimization, the convergence of the forces acting on atoms was set to equal or less than 0.02 eV/Å using the Conjugate-gradient algorithm approach. A Monkhorst-Pack mesh K point was used for the 2D Brillouin zone integration. Dimension, number of the layer of the supercell, lattices of the metals, and other supercell information, are provided in the later chapters (where the results are discussed). To select the K-point to use in an analysis, a range of K-points values was employed in the bulk analysis (using a unit cell) to identify the best value and its corresponding computational time, as the electronic energy changes, until it gets to a static value. Findings from the analysis is often used in deciding the K-points to use in studying a solid system. An approach similar to one deployed in selecting K-points was also employed in the selection of cutoff energy (ENCUT) and lattice parameter in our study.

Various positions like top, bridge, FCC, and HCP sites on the metal slab were explored in the search for the most energetically stable optimized structure for all the species involved (as shown in Figure 3- 4). In this study, the structure with the most negative electronic energy identified from the overall energy evaluation for different positions is confirmed as the most stable optimized structure.

In this study, all the slabs modeled with surface specie (adsorbate) were mono-adsorbed on a slab singly, except for the case of the transition state (TS) computation were the reacting surface species are co-adsorbed on a single slab. This approach was employed in the study of furfural and HMF oxidation and degradation activity on a slab.

3.3.1.1 Transition State Geometry Search

In the study, we deployed the use of climbing images nudged elastic band (NEB)[27–29] in our transition state search between two stable states (initial and final state of the reaction step), where the forces are less than 0.5 eV/Å. After which, the image with the highest energy in the NEB steps were further use in running a DIMER calculation[30–32]. The resulting geometry images from the DIMER calculation was then subjected to the frequency calculation, in order to ensure that there exist a single imaginary frequency with the vibration mode corresponding to with the expected reaction coordinates.

3.3.2 Statistical Thermodynamic Calculations

We first made a code that we tagged, "PyThermoProperty," in Python for estimating thermodynamic properties so that our statistical calculations could be done automatically. The code was designed to automatically extract the atom positions, masses, electronic energies, cell lattices, and other relevant parameters from the optimized geometry results (in CONTCAR and OUTCAR files) from the VASP package. The extracted data from the DFT calculation output files were used in the code for

computing various contributions (like electronic, translation, and many others) that could be required in the calculation of various thermodynamic properties (like Gibbs energy, enthalpy, heat capacity, and many others) as shown in Figure 3-5. The computation structure in the "PyThermoProperty" code was written using relevant statistical thermodynamic models reported in the literature[33–35].

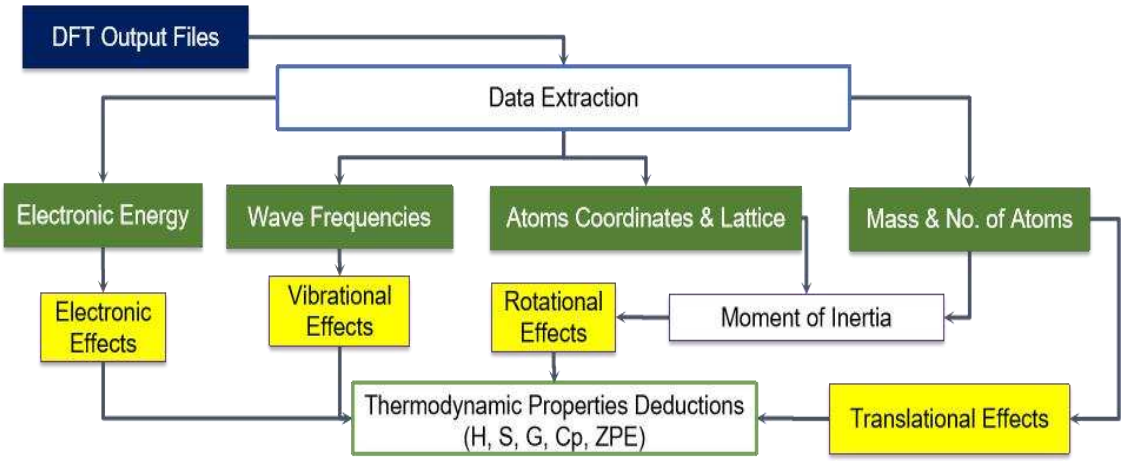

Figure 3-5 *A flow diagram scheme used in the design of the python-based thermodynamic properties estimation ("PyThermoProperty") code, using DFT output files.*

In our study, we used the code to compute the different species' free energies accounting majorly for translational, rotational, and electronic contributions. A generic form of the model for the estimation of the Gibbs free energy (G_i) is generally expressed as:

$$G_i = H_i(elec, trans, rot, ..) - T\,S_i(elec, trans, rot, ..) \qquad 3\text{-}26$$

Where the H_i denoted the Enthalpy, S_i is the entropy, T is the reaction temperature, $elec$ is the electronic contribution, $trans$ is the translational contribution, and rot is the rotational contribution in the simplified model (in Equation 3-26). The calculations were done using rigid rotator, harmonic vibration and perfect gas approximations[33,34,36,37]. Other details on the thermodynamic models used in the code are presented in the Supplementary Information of this Chapter. In addition, it is essential to note that the approximation used in the computation Gibb's energy for

the gas-phase species accounts for the electronic, translation, and rotation (with zero vibriation) contributions; while the approximation employed in solid-phase species accounts for only electronic contributions.

3.3.3 Adsorption, Activation, and Reaction Energies Calculations

Here, the energy quantity was general denoted as XX, which can be electronic energy,($XX = E$) or Gibbs energy ($XX = G$). Other analysis computed in this study includes the analysis of the adsorption energy (XX_{ads}), activation energy (XX_{act}), and reaction energies (XX_{rxn}) for different adsorbates and reaction steps. These energies were computed using the mathematical relations presented in Equation 3- 27 to 3- 29.

$$XX_{ads} = XX_{xs} - XX_x - XX_s \quad 3\text{-}27$$

$$XX_{act} = XX_{ts} - XX_i \quad 3\text{-}28$$

$$XX_{rxn} = XX_f - XX_i \quad 3\text{-}29$$

Where XX_x is the energies of the slab, XX_s is the energy of the specie, XX_{xs} is the energy of the slab with the specie adsorbed on it, XX_{ts} is the energies of the transition state (ts), XX_i is the energies of the initial (i) reaction step, and XX_f is the energies of the final (f) reaction step.

In this study, we deployed approximated that reaction step with the lowest exothermic (or highest endothermic) reaction energy (XX_{rxn}) as the slowest, otherwise known as rate-determining step (RDS). In contrast, one with the highest exothermic reaction energy was approximated to be the fastest step, since show reaction energies a direct linear relation with activation barrier. So, the step with the highest energy barrier (XX_{act}) known as the RDS [38] was approximated as the step with the least exothermic reaction energy (XX_{rxn}) in our analysis for rate control; following the principle of Brønsted–Evans–Polanyi Relation (BEP) and other linear

relations which establishes a direct relationship of reaction energies with their corresponding barriers[38–40]. This implies that when energy barrier (XX_{act}) is high, the corresponding reaction energy (XX_{rxn}) would be more endothermic and less exothermic relative to other cases analyzed. Although, it is not best approximation, but can be used to rapidly screen reaction steps to identify a RDS in a reaction mechanism using reaction energies.

3.4 List of Cited References

1. Warren, J. H. (2013). *A Guide to Molecular Mechanics and Quantum Chemical Calculations*. Wavefun Inc.

2. Lee, J. G. (2017). *Computational materials science : an introduction* (2nd ed.). CRC Press.

3. Giustino, Feliciano. (2014). *Materials modelling using density functional theory : properties and predictions*. Oxford University Press. https://books.google.com/books/about/Materials_Modelling_Using_Density_Functi.html?id=FzOTAwAAQBAJ

4. Keller, J. (1986). On the formulation of the Hohenberg–Kohn–Sham theory. *International Journal of Quantum Chemistry*, *30*(S20), 767–768. https://doi.org/10.1002/QUA.560300766

5. Yu, H. S., Li, S. L., & Truhlar, D. G. (2016). Perspective: Kohn-Sham density functional theory descending a staircase. *The Journal of Chemical Physics*, *145*(13), 130901. https://doi.org/10.1063/1.4963168

6. Kohn, W., Becke, A. D., & Parr, R. G. (1996). Density functional theory of electronic structure. *Journal of Physical Chemistry*, *100*(31), 12974–12980. https://doi.org/10.1021/JP960669L/ASSET/IMAGES/MEDIUM/JP960669LE00037.GIF

7. Harrison, N. M. (2000). *An Introduction to Density Functional Theory*.

8. Sholl, D. S., & Steckel, J. A. (2009). Density Functional Theory: A Practical Introduction. In *Density Functional Theory: A Practical Introduction*. John Wiley and Sons. https://doi.org/10.1002/9780470447710

9. Perdew, J. P., & Schmidt, K. (2001). Jacob's ladder of density functional approximations for the exchange-correlation energy. *AIP Conference Proceedings*, *577*(1), 1. https://doi.org/10.1063/1.1390175

10. Argaman, N., & Makov, G. (2000). Density functional theory: An introduction. *American Journal of Physics*, *68*(1), 69. https://doi.org/10.1119/1.19375

11. Gu, Q., Sautet, P., & Michel, C. (2018). Unraveling the Role of Base and Catalyst Polarization in Alcohol Oxidation on Au and Pt in Water. *ACS Catalysis*, *8*(12), 11716–11721. https://doi.org/10.1021/ACSCATAL.8B03494/SUPPL_FILE/CS8B03494_SI_001.PDF

12. Grimme, S., Hansen, A., Brandenburg, J. G., & Bannwarth, C. (2016). Dispersion-Corrected Mean-Field Electronic Structure Methods. *Chemical Reviews*, *116*(9), 5105–5154. https://doi.org/10.1021/ACS.CHEMREV.5B00533/ASSET/IMAGES/LARGE/CR-2015-00533M_0011.JPEG

13. Price, A. J. A., Bryenton, K. R., & Johnson, E. R. (2021). Requirements for an accurate dispersion-corrected density functional. *The Journal of Chemical Physics*, *154*(23), 230902. https://doi.org/10.1063/5.0050993

14. Grimme, S., Ehrlich, S., & Goerigk, L. (2011). Effect of the damping function in dispersion corrected density functional theory. *Journal of Computational Chemistry*, *32*(7), 1456–1465. https://doi.org/10.1002/JCC.21759

15. Caldeweyher, E., Ehlert, S., Hansen, A., Neugebauer, H., Spicher, S., Bannwarth, C., & Grimme, S. (2019). A generally applicable atomic-charge dependent London dispersion correction. *The Journal of Chemical Physics*, *150*(15), 154122. https://doi.org/10.1063/1.5090222

16. Steinmann, S. N., & Corminboeuf, C. (2011). Comprehensive benchmarking of a density-dependent dispersion correction. *Journal of Chemical Theory and Computation*, *7*(11), 3567–3577. https://doi.org/10.1021/CT200602X/SUPPL_FILE/CT200602X_SI_001.PDF

17. Andersson, Y., Andersson, D. C., & Lundqvist, B. I. (1996). van der Waals Interactions in Density-Functional Theory. *Physical Review Letters*, *76*(1), 102. https://doi.org/10.1103/PhysRevLett.76.102

18. Sabatini, R., Gorni, T., & de Gironcoli, S. (2013). Nonlocal van der Waals density functional made simple and efficient. *Physical Review B - Condensed Matter and Materials Physics*, *87*(4), 041108. https://doi.org/10.1103/PHYSREVB.87.041108/FIGURES/3/MEDIUM

19. Dion, M., Rydberg, H., Schröder, E., Langreth, D. C., & Lundqvist, B. I. (2004). Van der Waals density functional for general geometries. *Physical Review Letters*, *92*(24), 246401. https://doi.org/10.1103/PHYSREVLETT.92.246401/FIGURES/4/MEDIUM

20. VASP. (2021, October 30). *VASP - Vienna Ab initio Simulation Package*. VASP Report. https://www.vasp.at/

21. Hafner, J. (2008). Ab-initio simulations of materials using VASP: Density-functional theory and beyond. *Journal of Computational Chemistry*, *29*(13), 2044–2078. https://doi.org/10.1002/JCC.21057

22. Sun, G., Kürti, J., Rajczy, P., Kertesz, M., Hafner, J., & Kresse, G. (2003). Performance of the Vienna ab initio simulation package (VASP) in chemical applications. *Journal of Molecular Structure: THEOCHEM*, *624*(1–3), 37–45. https://doi.org/10.1016/S0166-1280(02)00733-9

23. VASP. (2022, September 25). *The VASP Manual - Vaspwiki*. Vienna Ab Initio Simulation Package (VASP). https://www.vasp.at/wiki/index.php/The_VASP_Manual

24. Fabiano, E., Constantin, L. A., & della Sala, F. (2010). Generalized gradient approximation bridging the rapidly and slowly varying density regimes: A PBE-like functional for hybrid interfaces. *Physical Review B - Condensed Matter and Materials Physics*, *82*(11), 113104. https://doi.org/10.1103/PHYSREVB.82.113104/FIGURES/5/MEDIUM

25. Qingyi, G., Sautet, P., & Michel, C. (2018). Unraveling the Role of Base and Catalyst Polarization in Alcohol Oxidation on Au and Pt in Water. *ACS Catalysis*, *8*(12), 11716–11721. https://doi.org/10.1021/ACSCATAL.8B03494/SUPPL_FILE/CS8B03494_SI_001.PDF

26. Giese, T. J., & York, D. M. (2010). Density-functional expansion methods: Evaluation of LDA, GGA, and meta-GGA functionals and different integral approximations. *The Journal of Chemical Physics*, *133*(24), 244107. https://doi.org/10.1063/1.3515479

27. Henkelman, G., & Jónsson, H. (2000). Improved tangent estimate in the nudged elastic band method for finding minimum energy paths and saddle points. *Journal of Chemical Physics*, *113*(22), 9978–9985. https://doi.org/10.1063/1.1323224

28. VASP. (2022). *Nudged Elastic Band — Transition State Tools for VASP*. VTST Tools. https://theory.cm.utexas.edu/vtsttools/neb.html

29. Henkelman, G., Uberuaga, B. P., & Jónsson, H. (2000). A climbing image nudged elastic band method for finding saddle points and minimum energy paths. *The Journal of Chemical Physics*, *113*(22), 9901. https://doi.org/10.1063/1.1329672

30. VASP. (2022). *THE DIMER METHOD — Transition State Tools for VASP*. VTST Tools. https://theory.cm.utexas.edu/vtsttools/dimer.html

31. Henkelman, G., & Jónsson, H. (1999). A dimer method for finding saddle points on high dimensional potential surfaces using only first derivatives. *The Journal of Chemical Physics*, *111*(15), 7010. https://doi.org/10.1063/1.480097

32. Heyden, A., Bell, A. T., & Keil, F. J. (2005). Efficient methods for finding transition states in chemical reactions: Comparison of improved dimer method and partitioned rational function optimization method. *The Journal of Chemical Physics*, *123*(22), 224101. https://doi.org/10.1063/1.2104507

33. Terrell, L. H. (1960). *An Introduction to Statistical Thermodynamics*. Dover Publications Inc.

34. Normand, M. L. (2005). *Statistical Thermodynamics: Fundamentals and Applications*. Cambridge University Press.

35. Donald, A. M. (1976). *Statistical Mechanics*. Haper and Row Publishers. https://vuquangnguyen2016.files.wordpress.com/2017/12/339279795-donald-a-mcquarrie-statistical-mechanics-bookzz-org.pdf

36. Laurendeau, N. M. (2005). Statistical Thermodynamics. In *Statistical Thermodynamics*. Cambridge University Press. https://doi.org/10.1017/cbo9780511815928

37. Serdaroglu, G., & Durmaz, S. (2010). DFT and statistical mechanics entropy calculations of diatomic and polyatomic molecules. *Indian Journal of Chemistry*, *49*, 861–866.

38. Zaffran, J., Michel, C., Auneau, F., Delbecq, F., & Sautet, P. (2014). Linear energy relations as predictive tools for polyalcohol catalytic reactivity. *ACS Catalysis*, *4*(2), 464–468. https://doi.org/10.1021/CS4010503/SUPPL_FILE/CS4010503_SI_001.PDF

39. Zaffran, J. (2014). *Linear energy relations for biomass transformation under heterogeneous catalysis: A fast prediction of polyalcohol dehydrogenation on transition metals* [ENS de Lyon]. https://theses.hal.science/tel-00992665/document

40. Cheng, J., Hu, P., Ellis, P., French, S., Kelly, G., & Lok, C. M. (2008). Brønsted-Evans-Polanyi relation of multistep reactions and volcano curve in heterogeneous catalysis. *Journal of Physical Chemistry C*, *112*(5), 1308–1311. https://doi.org/10.1021/JP711191J/SUPPL_FILE/JP711191J-FILE003.PDF

3.5 Supplementary Information for Chapter 3

3.5.1 Other Details On Statistical Thermodynamic Computation

3.5.1.1 Computation of Exact Positions of Atoms

The was done with the use of Python programming from which the following code was written to provide the followings:

(A) Number of Atoms in the Structure:

The total number of atoms in the structure was calculated with the list of atoms' numbers in a structure obtained from the VASP is expressed:

$$N = \Sigma n_i = n_1 + n_2 + \ldots + n_i \quad 3\text{-}30$$

where N is the total number of atoms in the structure, n_i is the number of atom (i).

(B) Total Mass of the Structure:

The total mass of the structure was calculated with the list of atomic masses for the atoms present in a structure obtained from the VASP is expressed:

$$M = \Sigma m_i n_i = m_1 n_1 + m_2 n_2 + \ldots + m_i n_i \quad 3\text{-}31$$

where M is the total mass of the structure, m_i is the mass of the atom (i), and n_i is the number of atoms (i).

(C) Center of Mass Computation

The center of mass of the structures [35] were computed via the use of the mathematical expression presented below:

$$X_{\text{com}} = \frac{\Sigma m_i X_i}{\Sigma m_i} \quad 3\text{-}32$$

$$Y_{\text{com}} = \frac{\Sigma m_i Y_i}{\Sigma m_i}$$

3- 33

$$Z_{\text{com}} = \frac{\Sigma m_i Z_i}{\Sigma m_i}$$

3- 34

where X_{com}, Y_{com} and Z_{com} is the X, Y and Z coordinate center of mass position, X_i, Y_i and Z_i is the direct lattice positions of the atoms in the structure respectively while m_i is the individual masses of the atoms present in the structure.

(D) Actual Position of Atoms with Scale-up in the Structure

The actual position of atoms with the scale-up in the structure was calculated with the lattice scale-up factor and the cell lattices matrix obtained from the VASP is expressed:

$$X_{sf,i} = X_i * L_{sf} * X_{cL}$$

3- 35

$$Y_{sf,i} = Y_i * L_{sf} * Y_{cL}$$

3- 36

$$Z_{sf,i} = Z_i * L_{sf} * Z_{cL}$$

3- 37

where $X_{sf,i}, Y_{sf,i}, Z_{sf,i}$ is the scale up X,Y,Z-coordinate of the different atoms, L_{sf} is the scale up factor for cell lattice, X_{cL}, Y_{cL}, Z_{cL} is the cell lattice matrix X,Y,Z-coordinates while X_i, Y_i, Z_i is the X,Y,Z direct coordinates for the different atoms.

3.5.1.2 Moment of Inertia

The moment of inertia computations was carried out with the use of the masses collected from the VASP file positions in their respective positions in the matrix.

(A) Moment of Inertia Tensor Computation

The moment of inertia tensors for the structures[35] was computed via the use of the mathematical expression presented below:

$$I_{XX} = \Sigma m_i * \left(Y_i^2 + Z_i^2\right) \quad 3\text{-}38$$

$$I_{YY} = \Sigma m_i * \left(X_i^2 + Z_i^2\right) \quad 3\text{-}39$$

$$I_{ZZ} = \Sigma m_i * \left(Y_i^2 + X_i^2\right) \quad 3\text{-}40$$

$$I_{XY} = I_{YX} = -\Sigma m_i * X_i * Y_i \quad 3\text{-}41$$

$$I_{ZY} = I_{YZ} = -\Sigma m_i * Z_i * Y_i \quad 3\text{-}42$$

$$I_{XZ} = I_{ZX} = -\Sigma m_i * X_i * Z_i \quad 3\text{-}43$$

where, I is the moment of inertia tensors for the respective $XX, YY, ZZ, XY, YX, ZY, YZ, XZ$, and XZ coordinates.

(B) Principal Moment of Inertia Computation

The principal moment of inertia tensors[35,38] for the structures was computed via the use of the result obtained for the calculation of the moment of inertia tensors and the use of mathematical expression presented below in Equation:

$$I = \begin{bmatrix} I_{XX} & I_{XY} & I_{XZ} \\ I_{YX} & I_{YY} & I_{YZ} \\ I_{ZX} & I_{ZY} & I_{ZZ} \end{bmatrix}$$

3- 44

The diagonalization of the above matrix for the moment of inertia was done via the use of python code which employed the use of the expression shown below in Equation:

$$U\, I \;=\; \lambda U$$

3- 45

$$I \;=\; \lambda U(1/U)$$

3- 46

$$I_m =\; U(1/U)$$

3- 47

$$I \;=\; \lambda I_m$$

3- 48

$$|I \;-\; \lambda I_m| = 0$$

3- 49

where I is the moment of inertia tensor matrix, I_m is the identity matrix, λ is the eigenvalue, U is the eigenvector. The diagonalized form gives rise to the matrix presented in Equation:

$$\lambda = \begin{bmatrix} I_a & 0 & 0 \\ 0 & I_b & 0 \\ 0 & 0 & I_c \end{bmatrix}$$

3- 50

where, I_a, I_b and I_c are principal moment of inertia computed.

3.5.1.3 Thermodynamic Properties Calculation

Using computed output collected from the previous model presented above like moment of inertia, total mass, and wave-numbers of the structure.

(A) Translation Effect Contribution on Thermodynamic Properties

The effect of translation on the thermodynamic properties[33–35] were estimated using perfect gas approximation:

a. Enthalpy, $\boldsymbol{dH_t}$:

$$dH_t(T) = \frac{5}{2}RT$$

3- 51

b. Entropy, $\boldsymbol{S_t}$:

$$s_t(T) = R\left[ln\frac{\left(\frac{2\pi m}{h^2}\right)^{\frac{3}{2}}(k_BT)^{\frac{5}{2}}}{P_o} + \frac{5}{2}\right]$$

3- 52

c. Partition function, $\boldsymbol{q_t}$:

$$q_{\mathrm{t}}(T) = \frac{(2\pi m\, k_{\mathrm{B}}T)^{\frac{3}{2}}V}{h^3}$$

3- 53

Where $\boldsymbol{m}$ is the mass of the molecule or specie, $\boldsymbol{V}$ is volume express as $\frac{RT}{P_o}$ for the calculation of its contribution, and P_o is the taken to be 1 atm (or 101.3 kPa). The translation effect contribution for adsorbed species is considered to be negligible (that is, zero) especially for entropy, enthalpy, and specific heat capacity which were in agreement with the literature[33–35,39] .

(B) Rotation Effect Contribution on Thermodynamic Properties

The effect of rotation on the thermodynamic properties was estimated using classical mechanical rigid rotator approximation:

a. Enthalpy, $\boldsymbol{dH_r}$:

$$dH_{r,linear}(T) = RT$$

3- 54

$$dH_{r,non-linear}(T) = \frac{3}{2} * RT$$

3- 55

b. Entropy, $\boldsymbol{S_r}$:

$$s_{r,linear}(T) = R\left[\ln\left(\frac{8\pi^2 k_B T I_{r,linear}}{h^2 \rho_r}\right) + 1\right]$$

3- 56

$$s_{r,non-linear}(T) = R\left[\ln\left(\frac{8\pi^2 (2\pi K_B T)^{\frac{3}{2}} (I_a I_b I_c)^{\frac{1}{2}}}{h^3 \rho_r}\right) + \frac{3}{2}\right]$$

3- 57

where,

$$I_{r,linear} = I_b = I_c, I_a = 0$$

c. Partition function, $\boldsymbol{q_r}$:

$$q_{r,linear}(T) = \frac{8\pi^2 I k_B T}{h^2 \rho_r}$$

3- 58

$$q_{r,non-linear}(T) = \frac{8\pi^2}{h^3 \rho_r} (I_a I_b I_c)^{\frac{1}{2}} (2\pi k_B T)^{\frac{3}{2}}$$

3- 59

Where, the I_a, I_b, I_c are principal moment of inertia, $\rho_{\{r\}}$ is the symmetry number of the structure. The translation effect contribution for the adsorbed species is

considered to be negligible (that is, zero) especially for entropy, enthalpy, and specific heat capacity which were in agreement with the literature[33–35,39] .

(C) Vibration Effect Contribution on Thermodynamic Properties

The effect of vibration on the thermodynamic properties [33–35] were estimated using quantum mechanical harmonic oscillators (QMHO) approximation:

a. Enthalpy, $\boldsymbol{dH}_v$:

$$dH_v(T) = R\,T \sum_i \left(\frac{hv_i}{k_B T}\right)^2 * \frac{e^{-\frac{hv_i}{k_B T}}}{\left(1 - e^{\frac{hv_i}{k_B T}}\right)}$$

3- 60

b. Entropy, $\boldsymbol{S}_v$:

$$s_v(T) = R \sum_i \frac{\frac{hv_i}{k_B T}}{e^{\frac{hv_i}{k_B T}} - 1} - R \sum_i In\left(1 - e^{\frac{hv_i}{k_B T}}\right)$$

3- 61

c. Partition function, $\boldsymbol{q}_v$:

$$q_v(T) = \prod_i \left(\frac{1}{1 - e^{-\left(\frac{hv_i}{k_B * T}\right)}}\right)$$

3- 62

Where, v_i is wave frequency in s^{-1} obtained from the conversion of wave number (i.e. $v_{n,i}$) in cm^{-1} via the use of the expression:

$$v_i = v_{n,i} c$$

3- 63

The c represents the speed of light, while all other variables' definitions remain the same as earlier defined.

d. Zero point energy, $\boldsymbol{ZPE}$

Zero-point energy (ZPE) is said to be the lowest possible energy that a quantum physical system could possess which corresponds to its ground state energy, that is to say when any other kind of energy has been eliminated. This energy can be mathematically presented in the form:

$$ZPE = \frac{1}{2}\sum v_{n,i}$$

3- 64

Where, $v_{n,i}$ is the wave numbers of the species in cm^{-1}, ZPE is the zero point energy which was to be converted from cm^{-1} to $\frac{J}{mol}$.

3.5.1.4 Overall Thermodynamic Properties

The Equations used are summarized below:

(A) Enthalpy, $\boldsymbol{H}$:

$$H(T) = dH(T) + E_{elect} + ZPE$$

3- 65

where, $dH(T) = dH_t + dH_r + dH_v$ which indicates the contributions of translation (t), rotational (r) and vibration (v) effects to the enthalpy of the structure computed. E_{elect} is the electronic energy which were in agreement with reports from literature[40].

(B) Entropy, $\boldsymbol{S}$:

$$S(T) = s_t + s_r + s_v$$

3- 66

where, s_t, s_r and s_v which indicates the contributions of translation (t), rotational (r) and vibration effects to the entropy of the structure computed[37,41].

(C) Gibbs free energy, $\boldsymbol{G}$:

$$G(T) = H(T) - T\,S(T)$$

3- 67

where, $H(T)$ is overall enthalpy, $S(T)$ is the overall entropy while T is temperature.

(D) Overall partition function, $\boldsymbol{Q}$:

$$Q(T) = q_t\, q_r\, q_v$$

3- 68

where, q_t, q_r, and q_v which indicates the contributions of translation (t), rotational (r), and vibration effects to the overall partition function of the structure computed.

Study of Mechanism & Competition Pathways in Oxidizing Furfural to Furoic Acid on Au

4 Study of Mechanism & Competition Pathways in Oxidizing Furfural to Furoic Acid on Au

Chapter 4 Study of mechanism & competition pathways in oxidizing furfural to furoic acid on Au

4.1 Overview

A survey of the literature in Chapter 2 (Section 2.3.1) has unraveled the need to investigate factors promoting the production of undesired products during the production of furoic acid from furfural over Au catalyst. Currently, more literature still needs to unveil details on the impact of Au on the catalysis of the process (that is, furfural (FF) oxidation to furoic acid (FA)). Unlike its application in the catalysis of ethanol [1–4], methanol [5–8], and glucose [9,10] oxidation into valuable products, which has been computationally studied to gain insight for redesigning Au-based catalysts. It was known well that furoic acid (FA) is a valuable feedstock for synthesizing FDCA, which has a wide range of applications and high market value[11–13].

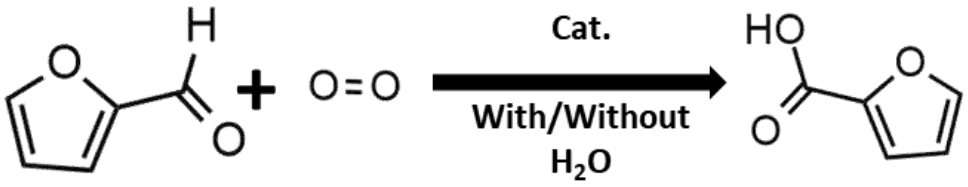

***Figure 4-1**. A scheme for the furfural oxidation reaction to yield furoic acid with the participation of water and a case when water does not participate.*

With the use of density functional theory (DFT) calculation and thermodynamic analysis, we studied molecular details on the mechanisms involved in the oxidation of furfural into furoic acid (as shown in Figure 4-1) in the presence of an Au catalyst and a further exploration of the pathway promoting degradation routes. The insight gained from this study provides better guidance for redesigning the Au catalyst to favor high furoic acid (FA) yield in furfural (FF) oxidation.

4.2 Computational Methodology

A thermodynamic feasibility study was deployed to understand furfural (FF) oxidation and the routes leading to the degradation of intermediates and furoic acid (FA) into undesired products that compete selectively with the oxidation of FF into FA. It was studied on Au(111) facet in modeling its slab for the simulation.

Details on the computational methods deployed in this study for computing the specie energies involved are presented earlier in Chapter 3. The peculiar specifications for this chapter include the p(3x3) supercell used as its slab in the study with four layers (Au-Au inter-atomic distances of 2.93 Å). The Monkhorst-Pack mesh was taken 3x3x1 K points, which was used for the 2D Brillouin zone integration. The total height of the periodic supercell was set at 23.92 Å, which takes 70 % of the supercell height to be a vacuum above the metal slab.

4.3 Results and Discussions

In this study, we investigate the impact of having water present and absent in furfural oxidation to furoic acid on Au (111). This ascertains the role of water in the furfural oxidation processes as a means of confirming the significant role of water accounted by Gu et al. in ethanol oxidation to ethanoic acid on metal. We resolve to structure the findings on:

1. the furfural oxidation on Au with and without the participation of water,
2. the influence of water in the synthesis of furoic acid from furfural on Au,
3. the influence of adsorption energies on the furfural oxidation, and
4. the possible competition pathways leading to undesired products.

In the overall evaluation of the entire reaction network's reaction energy, the reaction energy (E_{rxn}) obtained for oxidizing the furfural into furoic acid as -2.59 eV was found not to be closely related to one obtained as -3.13 eV from the use of experimental

thermochemical data in NIST[14–16] database, as shown in Table 4- 1. The difference in the result obtained could likely be due to the limitation of the functional (PBE-dDSc) used in our study in the computation of oxygen gas.

Table 4- 1 Reaction energy calculated using NIST thermochemistry data

Species	Symbols	Stochiometric Coefficient	Average Standard Enthalpy (ΔH)	Ref.
Furfural	FF	-1	-199.03 kJ/mol	15,17–19
Furoic acid	FA	1	-500.74 kJ/mol	14,19,20
Oxygen gas	O_2	-0.5	0	16,21
Reaction energy	E_{rxn}	-	-301.71 kJ/mol	-
Reaction energy	E_{rxn}	-	-3.13 eV	-

4.3.1 Evaluation of the furfural oxidation to furoic acid on Au

4.3.1.1 Oxidation without the Participation of Water

The mechanism involved transforming furfural into furoic acid on a Au (111) slab catalyst in the presence of oxygen without the participation of water. The scheme in Figure 4- 2 diagrammatically summarizes the reaction mechanism investigated in this study. Moreover, two reaction pathways investigated without the participation of water oxidize the surface furfural (xFF).

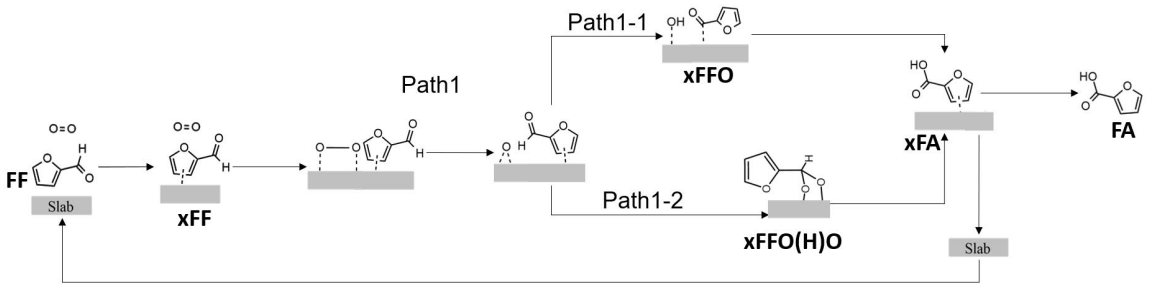

Figure 4- 2 The scheme for the oxidation reaction pathways for transforming furfural into furoic without the participation of water on Au. Note that "Path 1-1" is the C-H oxidation path, "Path 1-2" is the C-O oxidation path, FF is furfural, x is catalyst surface, FA is furoic acid, FFO is furan oxide, and FFHdiO is furan hydrogen dioxide. All surface species are singly mono-adsorbed (not co-adsorbed) on a slab.

The first route is via the initial C-H bond breaking to form xOH with xO (producing furan oxide, xFFO) for Path 1-1, and the later formation of the C-O bond using xOH to produce the surface furoic acid (xFA). Such reaction route, Path 1-1, is the "C-H oxidation path." The second reaction route of the pathway is the "C-O oxidation path" (Path 1-2) oxidizes via the initial formation of a C-O bond (using xO to yield furan hydrogen dioxide, xFFO(H)O), and the breaking of C-H bond to form O-H bond to give surface furoic acid (xFA) as shown in Figure 4- 2.

The corresponding energy diagram for oxidizing furfural (FF) into furoic acid (FA) on the Au (111) slab without the participation of water is presented in Figure 4- 3. All elementary reaction steps are exothermic. The adsorption of oxygen gas (O_2) and furoic acid (FA) desorption are endothermic, with the reaction energy (E_{rxn}) of +0.32 eV and +0.68 eV, reported for each step, respectively.

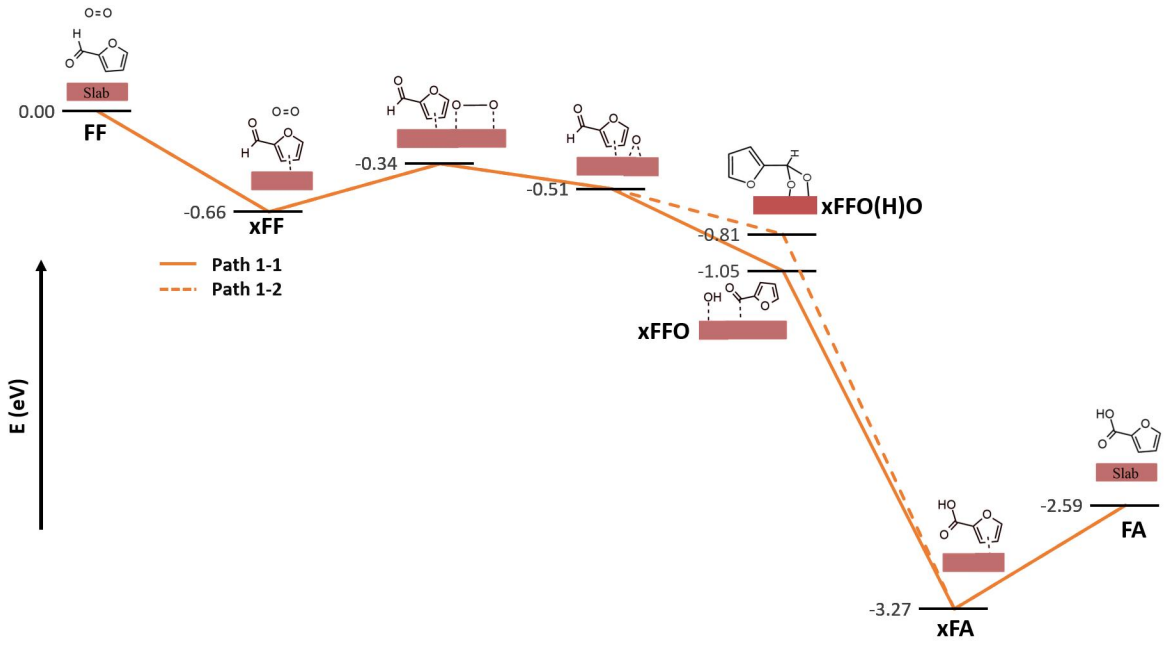

Figure 4- 3 The oxidation reaction energy profile for converting furfural to furoic acid without water participation on Au (111) using the electronic energies (in eV) computed, showing C-H (Path 1-1) and C-O (Path 1-2) oxidation pathways. Note: FF is furfural, x is catalyst surface, FA is furoic acid, FFO is furan oxide, and FFHdiO is furan hydrogen dioxide. All surface species are singly mono-adsorbed (not co-adsorbed) on a slab.

The overall reaction energy (in Figure 4- 3) was generally negative, indicating the process would be largely exothermic (E_{rxn} = -2.59 eV). The results suggest that the furfural oxidation was not overall a highly energy-requiring (that is, endothermic) process, despite the existence of two endothermic elementary steps. The analysis of the oxidation mechanism further confirms that the oxidation of furfural (in Figure 4-4) on Au(111) in the absence of water would be feasible via the pathway (the C-H oxidation path, that is, Path 1-1) involving the furan oxide (xFFO) formation (an intermediate), which later transforms into furoic acid (xFA). The pathway for the C-H oxidation path (E_{rxn} = -0.54 eV) was confirmed to be more feasible than the other pathway (E_{rxn} = -0.30 eV) due to its higher exothermic reaction energy. The findings agreed with the report of Gu et al. [2] for the oxidation of ethanol, where it was also demonstrated that the reaction energy of C-H oxidation was higher than that of the C-O oxidation (CH_3CHO to CH_3CO, similar to xFF to xFFO) reaction steps. Likewise, the identified feasible reaction pathway was found to be similar to the one reported by Li et al. [22] for the use of Au(111) and Roman et al. [23] on Au(111) and Pt(111) in the electrochemical oxidation of furfural into furoic acid. The findings show that the presence of the electrocatalytic effect also favors furfural oxidation via the C-H oxidation path on Au and Pt.

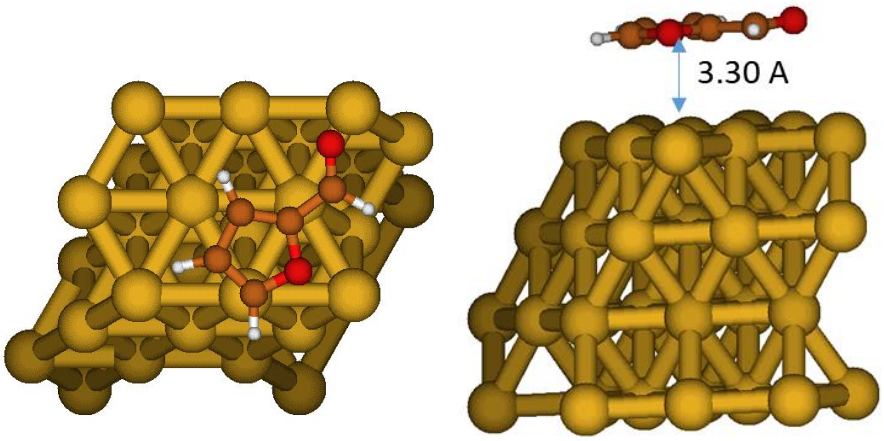

Figure 4-4 *Structural geometry of the furfural (xFF) (distance from the surface, H-Au is 3.30A).*

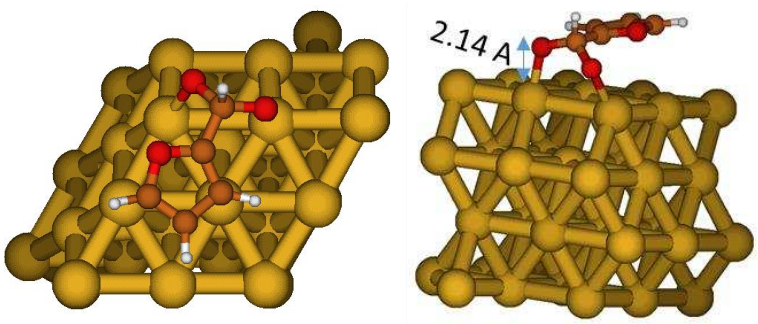

Figure 4-5 *Structural geometry of the resulting products of oxidizing furfural (FF) via the O-H oxidation routes: FFO(H)O (distance from the surface, O-Au is 2.14A).*

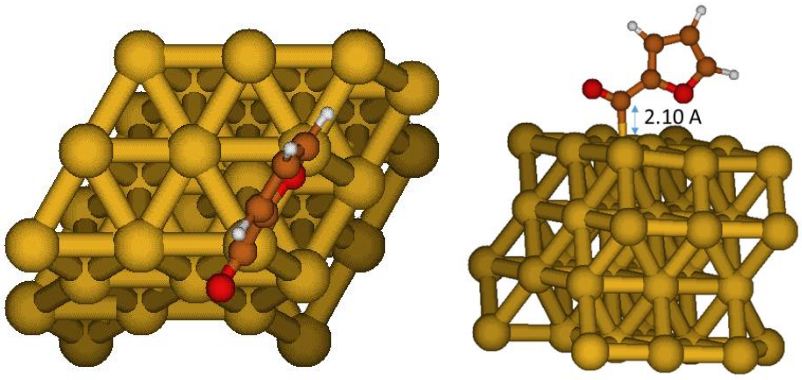

Figure 4-6 *Structural geometry of the resulting products of oxidizing furfural (FF) via the C-H oxidation routes: FFO (distance from the surface, C-Au is 2.10A)*

Moreover, the later step (after adsorption) of oxidizing furfural (xFF in Figure 4-4) to yield furan oxide (xFFO in Figure 4-5) or furan hydrogen dioxide (xFFO(H)O in Figure 4-6), which shows a shorter distance to the Au surface than the furfural (xFF). Comparison of the distance of the intermediates surface species with the Au surface confirms that furan oxide (xFFO) shows the shortest distance of 2.10A compared to others, as shown in Figure 4-4 to Figure 4-6.

4.3.1.2 Oxidation with the Participation of Water

In the presence of water, we further investigated the mechanism involved in transforming furfural into furoic acid on Au (111) slab catalyst. The scheme in Figure 4- 7 diagrammatically displayed the reaction mechanism employed in our study with the participation of water.

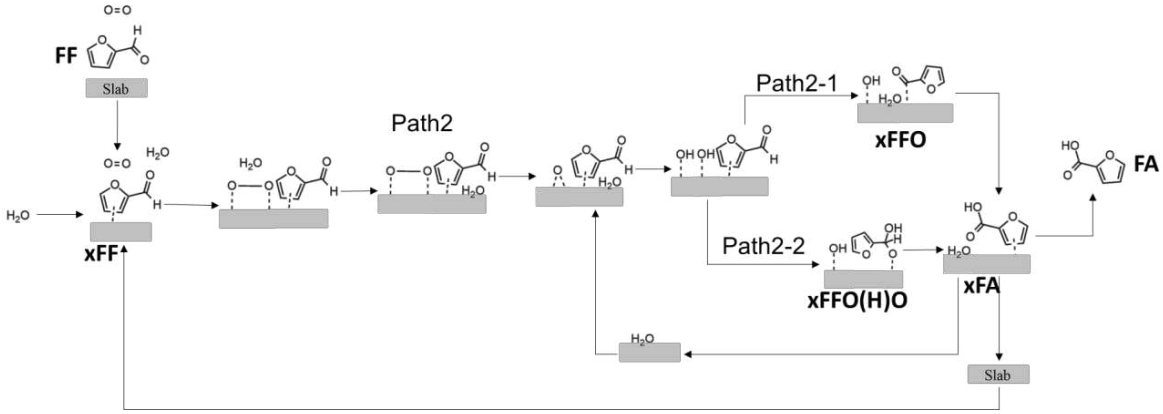

Figure 4- 7 The oxidation reaction pathways for transforming furfural into furoic with the participation of water are investigated in this report on Au. Note that "Path 2-1" is the C-H oxidation path, "Path 2-2" is the C-O oxidation path, FF is furfural, x is catalyst surface, FA is furoic acid, FFO is furan oxide, and FFHdiO is furan hydrogen dioxide. All surface species are singly mono-adsorbed (not co-adsorbed) on a slab.

The reaction pathways are generally divided into two routes (as shown in Figure 4- 7), which include one (that is, Path 2-1 with water) that oxidizes the surface furfural (xFF) via the initial C-H bond breaking (to form water with xOH to yield furan oxide, xFFO, and water) and the later formation of C-O bond (using xOH) to produce the surface furoic acid (xFA). This first route is the "C-H oxidation path." Whereas the other route of the pathway is the "C-O oxidation path" (that is, Path 2-2 with water) oxidizes via the initial formation of a C-O bond (using xOH to form furan carboxylate, xFFO(OH)H), and later breaking of C-H bond to form C=O (on Path 2-2 in Figure 4- 7) to give surface furoic acid (xFA).

Further exploration of the impact of water participation in the oxidation of furfural (FF) into furoic acid (FA) on the Au (111) slab was also investigated. The results are presented in Figure 4- 8. We investigated the pathway involved in the oxidation of the furfural via the pathway leading to the formation of furan oxide (xFFO, Path 2-1) and furan carboxylate (xFFO(OH)H, Path 2-2) intermediates into furoic acid (xFA), as shown in Figure 4- 7.

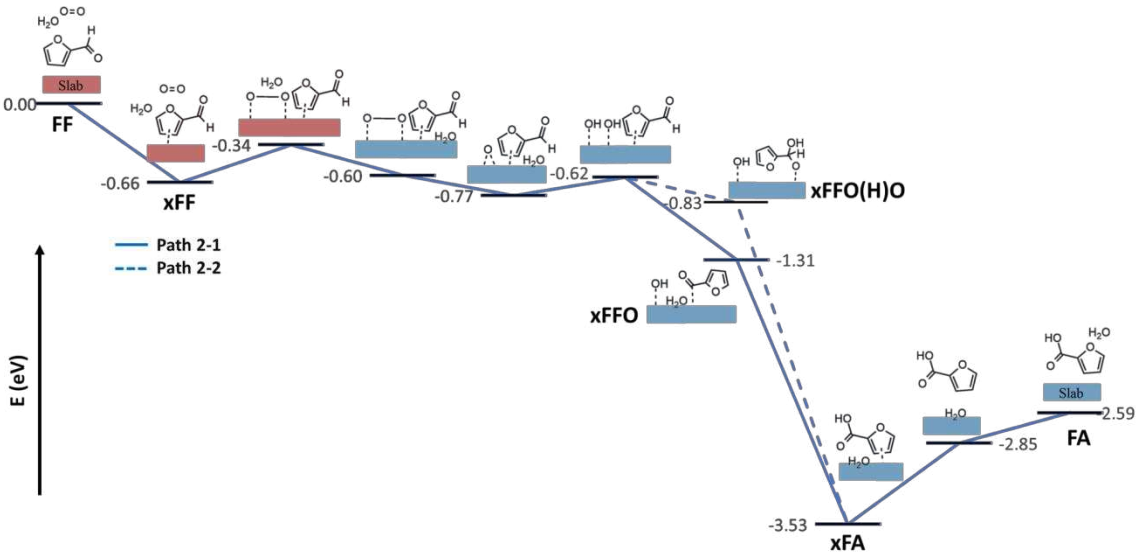

Figure 4- 8 *The oxidation reaction energy profile for converting furfural to furoic acid with the participation of water on Au (111) using the electronic energies (in eV) computed, showing C-H (Path 2-1) and C-O (Path 2-2) oxidation pathways. Note that the red slab indicates steps similar to when there was no water participation, while the blue slabs signify the steps peculiar to only when there was water participation. FF is furfural, x is catalyst surface, FA is furoic acid, FFO is furan oxide, and FFHdiO is furan hydrogen dioxide. All surface species are singly mono-adsorbed (not co-adsorbed) on a slab.*

All the elementary reaction steps were exothermic except a few steps (as shown in Figure 4- 8). These elementary steps include oxygen gas (O_2) adsorption, water (H_2O) oxidation, furoic acid (FA), and water (H_2O) desorption. These identified endothermic elementary steps, where participation of water (H_2O) was accounted were similar to the ones obtained for the oxidation of furfural in the absence of water participation on the Au (111) slab, except for the water (H_2O) oxidation and desorption.

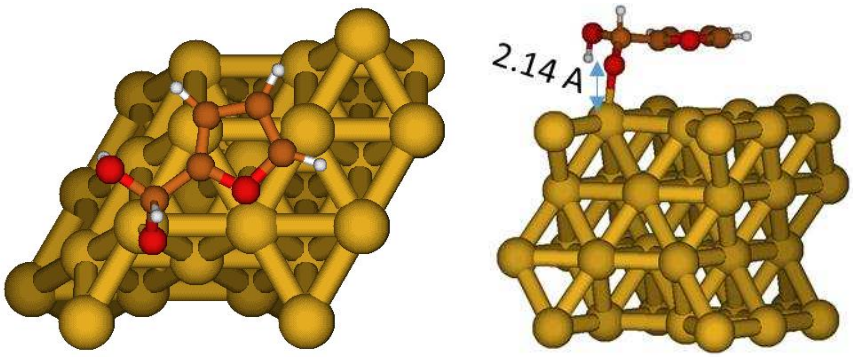

Figure 4-9 *Structural geometry of the resulting products of oxidizing furfural (FF) via the O-H oxidation routes: FFO(OH)H (distance from the surface, O-Au is 2.14A)*

The feasibility of oxidizing surface furfural (xFF) into surface furoic acid (xFA) on Au(111) slab in the presence of water via C-H bond breaking and C-O bond formation was further evaluated. The result presented in Figure 4- 8 indicates that oxidizing surface furfural (xFF) via C-O bond formation (E_{rxn} = -0.21 eV) to form intermediate furan carboxylate (xFFO(OH)H in Figure 4-9) was less exothermic than the one oxidized via C-H bond breaking (E_{rxn} = -0.69 eV) to create an intermediate furan oxide (xFFO in Figure 4-6). The high exothermicity of the C-H oxidation pathway in the presence of water (Path 2-1) favors the formation of furan oxide (xFFO), through which furoic acid (FA) is produced. The findings also agreed with Gu et al. report [2] confirming that C-H oxidation is more exothermic than C-O oxidation on Au(111). Another report by Yan et al. [24] also shows the oxidation of the C-H bond to be exothermic during the transition of CH_3CH_2O* into CH_3CHO* in their study on Pt and PtAu.

4.3.2 Influence of water in the oxidation of furfural to furoic acid on Au

Comparative analysis of the respective pathways for with or without water in the oxidation of furfural into furoic acid on Au (111) slab was further carried out. Figure 4- 10 displays a summary of the report obtained for evaluating water's influence on the common elementary steps in the oxidation mechanism (with or without water participation). Figure 4- 10 indicates that all the common steps were not affected except the initial step of oxidizing surface furfural (xFF) into furan oxide (xFFO), furan hydrogen dioxide (xFFHdiO), or furan carboxylate (xFFO(OH)H) intermediates. And the conversion of furan intermediates (xFFO or xFFO(OH)H) to surface furoic acid (xFA).

Following the earlier deduction in Section 4.3.1 that confirms the oxidation of furfural into furoic acid via the C-H oxidation pathway to be energetically feasible on Au(111) in the presence of water. We further search for insight into how the water influences the oxidation pathway. The investigation reveals that the participation of water

affected the exothermicity of the initial stage of the oxidation process. It shows that the participation of water improves the exothermicity of the C-H bond breaking (E_{rxn} = -0.69 eV) to yield furan oxide (xFFO) intermediate than when water participation was not considered (E_{rxn} = -0.54 eV) as shown in Figure 4- 10. The further oxidation of the furan oxide (xFFO) intermediate indicated that the formation of furoic acid (xFA) would be more feasible than other routes (for furan carboxylate (xFFO(OH)H) / furan hydrogen dioxide (xFFHdiO)) with or without water participation. The furoic acid (xFA) on Au(111) showed no difference in the presence/absence of water participation in reaction energies.

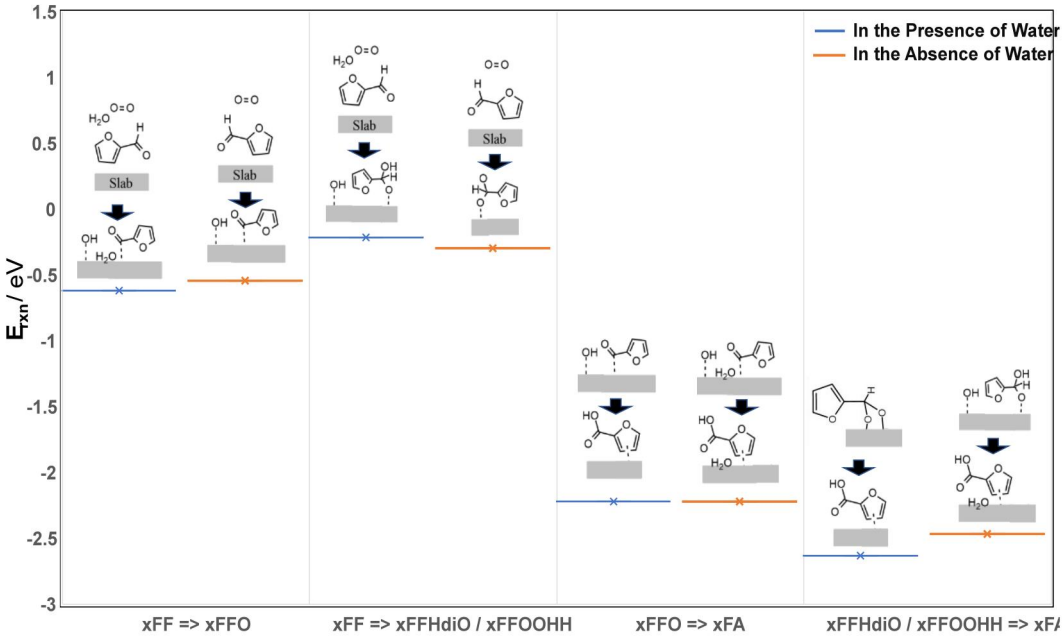

Figure 4- 10 The reaction energies for common reaction steps in the furfural oxidation with or without water participation (using computed electronic energies in eV). Note: The structures above are the initial step, and those below the lines are the final step across each change. FF is furfural, x is catalyst surface, FA is furoic acid, FFO is furan oxide, FFHdiO is furan hydrogen dioxide, FFOOHH is furan carbonate. All surface species are singly mono-adsorbed (not co-adsorbed) on a slab.

The analysis of the initial stage of the furfural oxidation to furoic was seen to have shown a significant difference due to the presence of the surface hydroxyl (OH, that is, the product of water oxidation) on the Au(111), which was absent for oxidation without water participation (Path 1-1). Similarly, the presence of surface hydroxyl

(xOH) on the Au(111) with/without water participation in the further oxidation of furan oxide (xFFO) to furoic acid (xFA) resulted in a similar effect obtained for their respective reaction energies. The impact of surface hydroxyl (xOH) on Au(111) on the other pathways (that is, C-O oxidation paths, Path 1-2 or 2-2) on their exothermicity and species stability is largely evident in Figure 4- 10.

4.3.3 Influence of adsorption energies on the furfural oxidation reaction mechanism

We further investigated the adsorption energies of some surface species such as oxygen, hydrogen, hydroxyl, water, furfural, and furoic acid for the Au (111) surface to understand that the energies influence the reaction energy profiles presented in the preceding section in Figure 4- 3, Figure 4- 7, and Figure 4- 10. The resulting energies collated for the adsorption of species on Au are shown in Table 4- 2.

Table 4- 2 *Adsorption energies of the selected key species involved in the oxidation of furfural into furoic acid. Note: X is Au; Eads(H) computed as 'E_{xH}-(E_X+0.5*E_{H2})'; Eads(O) computed as 'E_{xO}-(E_X+0.5*E_{O2})'; and Eads (OH) as minimum of 'E_{xOH}-X-0.5*E_{H2O}-0.25*E_{O2}', 'E_{xOH}-E_X-0.5*E_{H2}-0.5*E_{O2}', and 'E_{xOH}+0.5*E_{H2}-E_X-E_{H2O}'.*

Specie	Formula	Symbols	Adsorption site	Eads, eV
Oxygen gas	O_2	xO_2	Top	0.64
Hydrogen gas	H_2	xH_2	Top	-0.08
Water	H_2O	xH_2O	Top	-0.26
Furfural	$C_5H_4O_2$	xFF	FCC (parallel)	-0.66
Furoic acid	$C_5H_4O_3$	xFA	FCC (parallel)	-0.68
Oxygen atom	O	xO	FCC	0.15
Hydroxyl	OH	xOH	Bridge	-1.25
Hydrogen atom	H	xH	FCC	0.05

The adsorption energies collated in Table 4- 2 indicate that a weak adsorption strength was obtained for the binding of hydrogen gas (xH_2), water (xH_2O), furfural (xFF), furoic acid (FA), and hydroxyl (xOH). A more weaker adsorption strength was

obtained for other surface species, such as oxygen gas (xO_2), oxygen (xO), and hydrogen (xH).

Further analysis of the results in Table 4- 2 reveals that the stability of the oxygen (xO_2) gas on Au(111) would be difficult, but rather, its atom form (xO) would be more stable compared to its gas form. The adsorption effect is visible in Figure 4- 3 and Figure 4- 7 for oxygen adsorption and activation, indicating the preference of Au(111) to have xO than xO_2, unlike other metals like Pd and Pt, which shows better interaction with oxygen. Also, the strong adsorption strength reported for the binding of hydroxyl (xOH) species on Au (111) largely contributes to the improved stability of species involved in the oxidation of furfural to furoic acid (in the presence of water). A fairly stronger interaction was obtained for the furoic acid than the furfural, indicating the possibility of deeper oxidation on the slab. This finding for strong binding of furoic acid to Au(111) was similarly reported by Roman et al.[23], where it was indicated that it is easier desorbing furoic acid on Au(111) than Pt(111) which was more difficulty.

4.3.4 Exploration of possible competition pathways leading to undesired products

To gain more insight into the possibility of degrading furfural intermediate and furoic acid into undesired products, we explored several reaction routes as an approach or measure for understanding the selectivity of the furan oxide (xFFO) intermediates and surface furoic acid (xFA) for its desorption route.

4.3.4.1 Pathway selectivity for the intermediate species progression to desired products

The section of this report presented the evaluation of the selectivity for the path leading to the oxidation of furfural intermediate to produce furoic acid in the presence of water (since the earlier section has confirmed the C-H oxidation pathway with water to be more feasible).

Here we analyzed the feasibility of the routes leading to the formation of desired [that is, furan oxide (xFFO), furoic acid (xFA)] and the selected undesired species [that is, furan dioxide (xFFdiO), furan diol (xFFdiOH), furanol (xFFOH), and furan carboxylate (xFFO(OH)H)] that could lead to the formation of furoic acid (FA, the desired product) and undesired products, respectively. For each of the routes, the species in the presence of xO, xO_2, xH, xH_2, xOH, or xH_2O were explored. The most stable form for each selected species was used to examine the possibility of leading the reaction to desired or undesired pathways. The respective reaction energies for various pathways are presented in Figure 4- 11 (details of other cases explored that were less stable are shown in Table 4- 4).

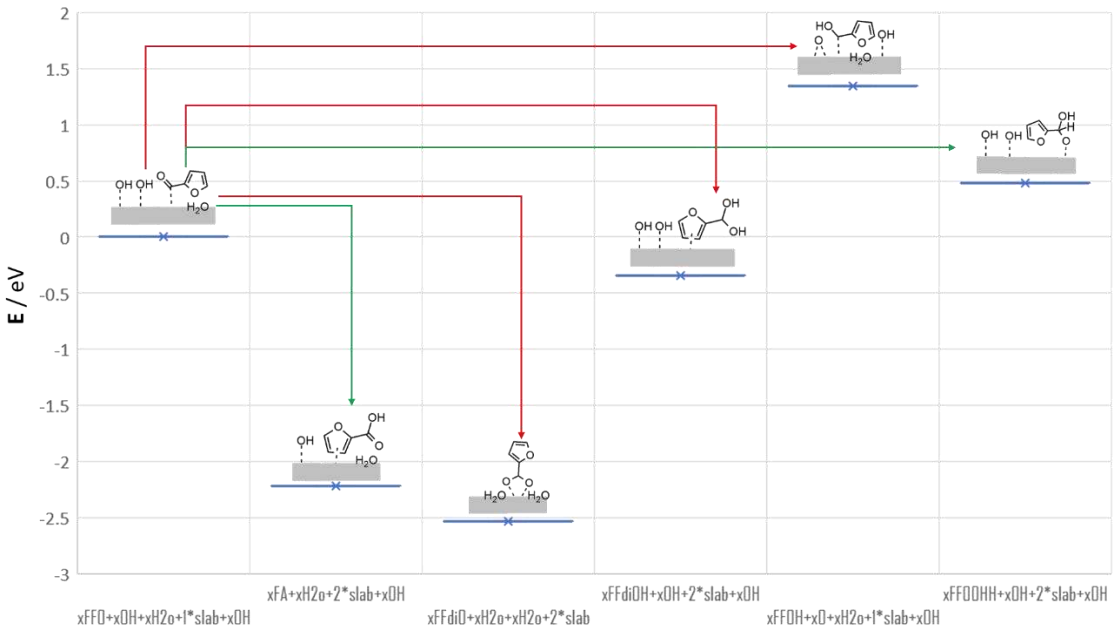

Figure 4- 11 *Furfural intermediate oxidation route selectivity for the furoic acid production using the electronic energies (in eV) computed. Note that red leads to undesired products, while green leads to desired products. Note that FF is furfural, x is catalyst surface, FA is furoic acid, FFO is furan oxide, FFHdiO is furan hydrogen dioxide, FFOOHH is furan carbonate, FFdiOH is furan diol, FFdiO is furan dioxide, FFOH is furan alcohol. All surface species are singly mono-adsorbed (not co-adsorbed) on a slab.*

The analysis of results presented in Figure 4- 11 obtained for the selectivity of furfural intermediate (furan oxide, xFFO) for the furoic acid (FA) production indicates that the

xFFO (an intermediate would not be thermodynamically feasible in transforming into furanol (xFFOH) and furan carboxylate (xFFO(OH)H). However, due to their exothermic reaction energies, other pathways leading to the production of furan diol (xFFdiOH), furoic acid (xFA), and furan dioxide (xFFdiO), were found to be thermodynamically feasible. These findings indicate that furan diol (xFFdiOH) and furan dioxide (xFFdiO) would be the primary competitors with the desired product (that is, xFA). The xFFdiO was the most substantial competition pathway with the xFA. The xFFdiO would be obtainable from the furan oxide (xFFO) intermediate via the formation of the C-O bond and the breaking of the O-H bond. The availability of surface oxygen (xO) in a gold (Au) catalyst (that is, composed of the support and active agent) would favor the oxidation of the furan oxide (xFFO) intermediate to undesired intermediate (xFFdiO) against the formation of furoic acid (xFA). This surface oxygen (xO) could like be responsible for the lower yield reported for the oxidation of furfural into furoic acid in the presence of Au on some catalyst support (that is, highly oxygenated following the Mars–Van Krevelen Mechanism[25,26]). Report from experimental studies earlier indicated that the oxidation of furfural (FF) into furoic acid (FA) on Au using HT support (71% furoic acid[27], 100% furoic acid[28]) show better yield than one obtained for the use of Au/VPP (vanadyl pyrophosphate, with 38% maleic acid yield) [27] . This variation in their yield and selectivity can be well understood to be a function of the surface hydroxyl (xOH) or oxygen (xO) availability on their support. This was because HT (hydrotalcite) is primarily surrounded by OH functional groups 25,27, unlike VPP, which is covered mainly by O [27] . Going by our theoretical study indicates that the sufficiency of surface oxygen (xO) on Au(111) would aid the degradation leading to the formation of furan dioxide (xFFdiO) intermediate, where Au/VPP [27,28] has more exposure xO, especially from its support, unlike Au/HT[27] that has more of xOH from its support.

4.3.4.2 Pathway selectivity for the furoic acid desorption over undesired products

Further evaluation of the possible reaction routes that could compete with the desorption of furoic acid on a gold (Au(111)) slab was reported in Figure 4- 12. Similar to the analysis made for the furan oxide (xFFO, one of the intermediates in furfural oxidation), we also explore the chance of the selected pathways to compete with the desorption of furoic acid (FA) from Au(111). The selected competing pathways evaluated lead production of furan ketone (xFFO), furan alcohol (xFFOH), furan dioxide (xFFdiO), furan diol (xFFdiOH), furan triol (xFFtriOH), and furan carboxylate (xFFO(OH)H) instead of furoic acid (FA).

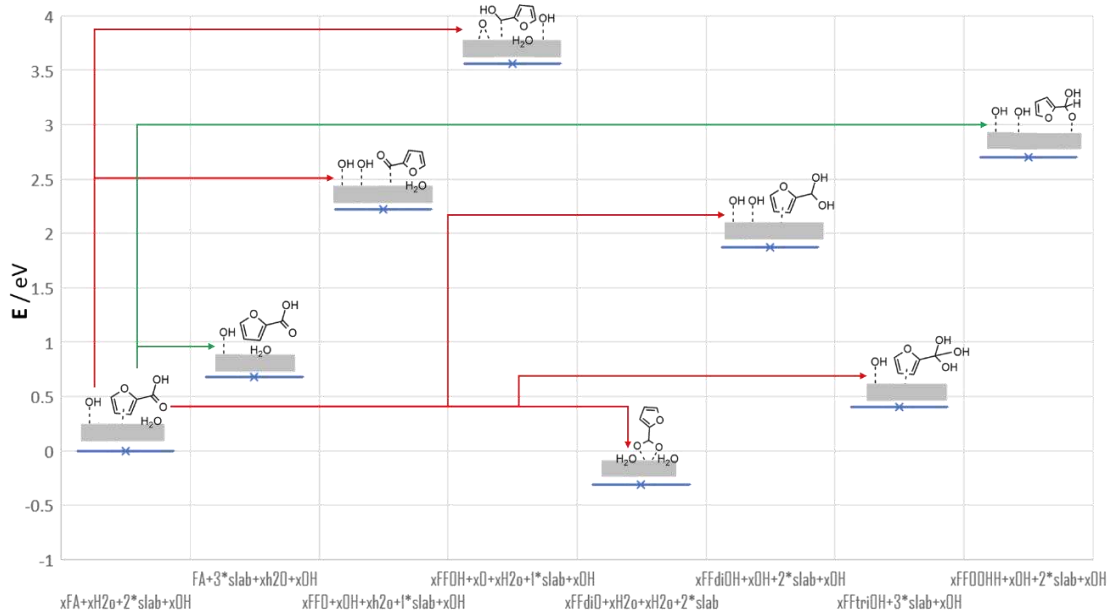

Figure 4- 12 Furoic acid desorption route selectivity for the furoic acid production using the electronic energies (in eV) computed. Note that red leads to undesired products, while green leads to desired products. Note that FF is furfural, x is catalyst surface, FA is furoic acid, FFO is furan oxide, FFHdiO is furan hydrogen dioxide, FFOOHH is furan carbonate, FFtriOH is furan triol, FFdiO is furan dioxide, FFOH is furan alcohol. All surface species are singly mono-adsorbed (not co-adsorbed) on a slab.

The analysis of the selectivity profile presented using the various reaction pathways' reaction energies is shown in Figure 4- 12. The result indicates that the formation of furan ketone (xFFO), furan alcohol (xFFOH), furan triol (xFFtriOH), and furan carboxylate (xFFO(OH)H) would be less feasible due to their higher positive reaction energies relative to the desired route (FA desorption route). In comparison, other

pathways leading to the production of furan dioxide (xFFdiO) and furan triol (xFFtriOH) showed better reaction energies comparable to the one obtained for FA desorption. This confirms the formation of the furan dioxide (xFFdiO in Figure 4-14) and furan triol (xFFtriOH in Figure 4-13) during the oxidation of furfural into furoic acid to be more competitive with the desorption of FA from Au(111). The most severe pathway competing with the furan ketone (xFFO) intermediate oxidation and furoic acid desorption on Au (111) was found to be one leading to the formation of furan dioxide (xFFdiO) intermediate due to the higher exothermicity of its pathway. The identified threat of xFFdiO formation during the oxidation process, agreed with the report of Roman et al. 15, predicted the possibility of deeper oxidation holding in the electro-oxidation of xFF into xFA on Au(111). The use of catalyst support that can generate oxygen (xO) for oxidation of xFFO into xFFdiO on Au influences the lower FA yield reported by Bruno [27] for using Au/VPP but favor a higher yield for the use of Au/HT due to the generation of xOH from the support instead of xO from the support. The pathways can be prevented or hindered via sufficient availability of hydroxyl during oxidation processes.

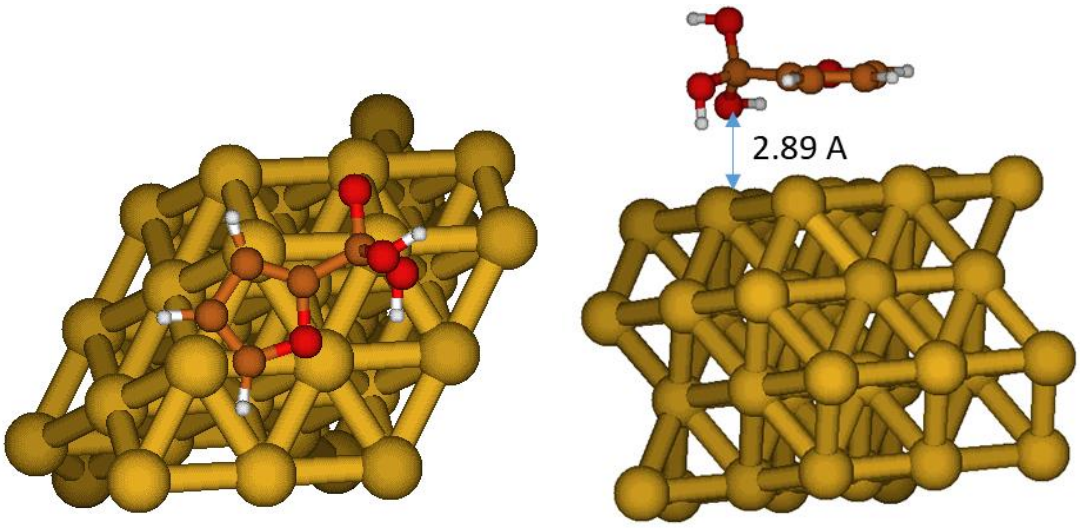

Figure 4-13 *A structural geometry for the formation of furan triol, xFF-tri-OH (with a distance from the surface, O-Au is 2.89 A) as a possible side products.*

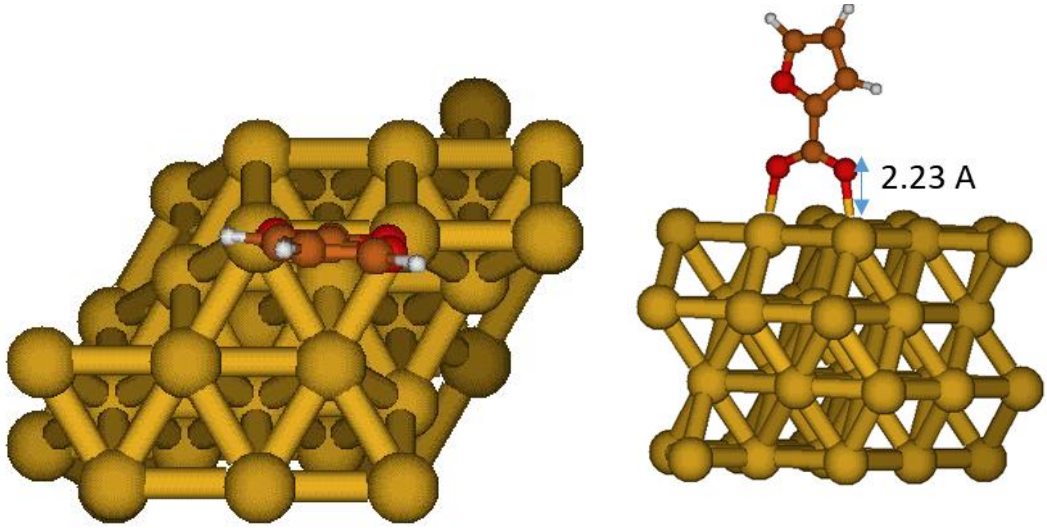

Figure 4-14 *A structural geometry for the formation of furan dioxide, xFFdiO (with a distance from the surface, O-Au is 2.23 A) as a possible side products.*

The breaking of the O-H bond from a furoic acid (xFA) leading to the production of furan dioxide (xFFdiO) has been a significant threat competing with the oxidation of the furfural (FF) into furoic acid (FA) and desorption of furoic acid (FA) from the Au (111) slab. Redesigning the Au catalyst to favor more of the C-H bond breaking than the breaking of the O-H bond would aid in preventing the degradation of this intermediate into an undesired one and improve the yield. The report of Gu et al. [2] shows that the deployment of oxidation in a basic environment could facilitate the desorption of furan dioxide or carbonate (xFFdiO in Figure 4-14) formation from Au, unlike the case of using a neutral environment which would be difficult and could favor deactivation of the catalyst. Otherwise, the surface furan dioxide or carbonate would require to be protonated before it can be easily desorbed on Au.

4.4 Conclusions

A computational study investigating the mechanism involved in the oxidation of furfural into furoic acid with or without water participation was successfully carried out, including an exploration of the possible processes leading to degradation on the Au (111) slab. It has been confirmed that the oxidation of furfural into furoic acid on

Au in water is highly beneficial. It showed better stability and a much more exothermic reaction pathway than the other pathway without water participation.

The energetically feasible reaction mechanism obtained from this study for the oxidation of the furfural into furoic acid is the one held on Au (111) in the presence of water participation via the C-H oxidation pathway. This pathway includes steps such as serial adsorption of furfural (FF), oxygen (O_2), and water (H_2O); activation of oxygen; water oxidation; initial oxidation of furfural into an intermediate (furan ketone, xFFO, by C-H bond breaking); further oxidation of the earlier intermediate (xFFO, by the formation of C-O bond with OH to furoic acid, xFA); then, serial desorption of furoic acid (FA) and water (from the Au (111) slab).

More results from this study confirm that breaking the O-H bond and making surface oxygen (O) from some catalyst supports have been the biggest threats to the degradation of the furfural intermediate and surface furoic acid species on an Au (111) slab. This study, therefore, suggests that redesigning the Au catalyst to favor C-H bond breaking, hinder the breaking of the O-H bond, and ease the desorption of furoic acid would aid in preventing the degradation activities, improving the yield and selectivity for their desired reaction path and products. It would work better if there were enough water to make hydroxyl (to get rid of or stop surface oxygen atoms from being available), to use a base, or to choose a catalyst support that does not make oxygen (O) but makes hydroxyl (OH) during oxidation on Au. It would aid in preventing degradation activities on Au during the synthesis of furoic acid.

4.5 List of references cited

1. Qiu, Y., Zhang, J., Jin, J., Sun, J., Tang, H., Chen, Q., Zhang, Z., Sun, W., Meng, G., Xu, Q., Zhu, Y., Han, A., Gu, L., Wang, D., & Li, Y. (2021). Construction of Pd-Zn dual sites to enhance the performance for ethanol electro-oxidation reaction. *Nature Communications 2021 12:1*, *12*(1), 1–9. https://doi.org/10.1038/s41467-021-25600-9

2. Gu, Q., Sautet, P., & Michel, C. (2018). Unraveling the Role of Base and Catalyst Polarization in Alcohol Oxidation on Au and Pt in Water. *ACS Catalysis*, *8*(12), 11716–11721. https://doi.org/10.1021/ACSCATAL.8B03494/SUPPL_FILE/CS8B03494_SI_001.PDF

3. Monyoncho, E. A., Steinmann, S. N., Sautet, P., Baranova, E. A., & Michel, C. (2018). Computational screening for selective catalysts: Cleaving the CC bond during ethanol electro-oxidation reaction. *Electrochimica Acta*, *274*, 274–278. https://doi.org/10.1016/J.ELECTACTA.2018.04.102

4. Pereira, A. O., & Miranda, C. R. (2014). Atomic scale insights into ethanol oxidation on Pt, Pd and Au metallic nanofilms: A DFT with van der Waals interactions. *Applied Surface Science*, *288*, 564–571. https://doi.org/10.1016/J.APSUSC.2013.10.074

5. Karanjit, S., Bobuatong, K., Fukuda, R., Ehara, M., & Sakurai, H. (2013). Mechanism of the aerobic oxidation of methanol to formic acid on Au8−: A DFT study. *International Journal of Quantum Chemistry*, *113*(4), 428–436. https://doi.org/10.1002/QUA.24056

6. Belletti, G. D., Colombo, E., Cabana, N., Quaino, P., & Collins, S. (2022). Mechanistic Investigation of Methanol Oxidation on Au/TiO2: A Combined DRIFT and DFT Study. *Topics in Catalysis 2022 65:7*, *65*(7), 915–925. https://doi.org/10.1007/S11244-022-01620-7

7. Liu, S., Jin, P., Zhang, D., Hao, C., & Yang, X. (2013). Reaction mechanism for methanol oxidation on Au(1 1 1): A density functional theory study. *Applied Surface Science*, *265*, 443–451. https://doi.org/10.1016/J.APSUSC.2012.11.026

8. Chang, C. R., Long, B., Yang, X. F., & Li, J. (2015). Theoretical Studies on the Synergetic Effects of Au-Pd Bimetallic Catalysts in the Selective Oxidation of Methanol. *Journal of Physical Chemistry C*, *119*(28), 16072–16081. https://doi.org/10.1021/ACS.JPCC.5B03965/SUPPL_FILE/JP5B03965_SI_001.PDF

9. Caglar, A., Düzenli, D., Onal, I., Tezsevin, I., Sahin, O., & Kivrak, H. (2020). A comparative experimental and density functional study of glucose adsorption and electrooxidation on the Au-graphene and Pt-graphene electrodes. *International Journal of Hydrogen Energy*, *45*(1), 490–500. https://doi.org/10.1016/J.IJHYDENE.2019.10.163

10. Amaniampong, P. N., Karam, A., Trinh, Q. T., Xu, K., Hirao, H., Jérôme, F., & Chatel, G. (2017). Selective and Catalyst-free Oxidation of D-Glucose to D-Glucuronic acid induced by High-Frequency Ultrasound. *Scientific Reports*, *7*(1), 1–8. https://doi.org/10.1038/srep40650

11. de Jong, E., Visser, H. A., Dias, A. S., Harvey, C., & Gruter, G. J. M. (2022). The Road to Bring FDCA and PEF to the Market. *Polymers*, *14*(5), 943. https://doi.org/10.3390/POLYM14050943

12. Research and Data. (2020). *2,5-Furandicarboxylic Acid (FDCA) Market | Size & Analysis*. https://www.reportsanddata.com/report-detail/2-5-furandicarboxylic-acid-fdca-market

13. Grand View Research. (2014). *Furandicarboxylic Acid Market Size, Share & Trends Analysis Report By Application (PET, Polyamides, Polycarbonates, Plasticizers, Polyester Polyols), By Region, And Segment Forecasts, 2015 - 2020*. https://www.grandviewresearch.com/industry-analysis/fdca-industry

14. NIST. (2022). *2-furoic acid*. NIST Chemistry WebBook, SRD 69. https://webbook.nist.gov/cgi/cbook.cgi?ID=C26447289&Units=SI&Mask=4EF

15. NIST. (2022). *Furfural*. NIST Chemistry WebBook, SRD 69. https://webbook.nist.gov/cgi/cbook.cgi?ID=C98011&Mask=2

16. NIST. (2022). *Oxygen*. NIST Chemistry WebBook, SRD 69. https://webbook.nist.gov/cgi/cbook.cgi?ID=C7782447&Mask=1

17. Avramescu, F., & Isagescu, D. A. (1978). Heats of combustion of mono- and difurfurylidene acetone. *Rev. Roum. Chim.*, *23*, 655–659.

18. Miller, P. (1936). The free energy of furfural and some of its derivatives. *Iowa State Coll. J. Sci.*, *10*, 91–93.

19. Landrieu, P., Baylocq, F., & Johnson, J. R. (1929). Etude thermochimique dans la serie furanique. *Bull. Soc. Chim. France*, *45*, 36–49.

20. Parks, G. S., Mosley, J. R., & Peterson, P. V. , Jr. (1950). Heats of combustion and formation of some organic compounds containing oxygen. *J. Chem. Phys.*, *18*, 152.

21. Chase, M. W. , Jr. (1998). NIST-JANAF Themochemical Tables, Fourth Edition. *J. Phys. Chem. Ref. Data, Monograph 9*, 1–1951.

22. Gong, L., Agrawal, N., Roman, A., Holewinski, A., & Janik, M. J. (2019). Density functional theory study of furfural electrochemical oxidation on the Pt (1 1 1) surface. *Journal of Catalysis*, *373*, 322–335. https://doi.org/10.1016/J.JCAT.2019.04.012

23. Román, A. M., Agrawal, N., Hasse, J. C., Janik, M. J., Medlin, J. W., & Holewinski, A. (2020). Electro-oxidation of furfural on gold is limited by furoate self-assembly. *Journal of Catalysis*, *391*, 327–335. https://doi.org/10.1016/J.JCAT.2020.08.034

24. Yan, S. Y., Huang, Y. R., Yang, C. Y., Liu, C. W., Wang, J. H., & Wang, K. W. (2018). Enhanced activity of ethanol oxidation reaction on PtM (M=Au, Ag and Sn): The importance of oxophilicity and surface oxygen containing species. *Electrochimica Acta*, *259*, 733–741. https://doi.org/10.1016/J.ELECTACTA.2017.11.024

25. Ross, J. R. H. (2019). The Kinetics and Mechanisms of Catalytic Reactions. In *Contemporary Catalysis* (pp. 161–186). Elsevier. https://doi.org/10.1016/B978-0-444-63474-0.00007-2

26. Doornkamp, C., & Ponec, V. (2000). The universal character of the Mars and Van Krevelen mechanism. *Journal of Molecular Catalysis A: Chemical*, *162*(1–2), 19–32. https://doi.org/10.1016/S1381-1169(00)00319-8

27. Bruno, R. (2016). *Selective oxidation of furfural and 5-methyl furfural under green conditions*. http://amslaurea.unibo.it/13421/1/Tesi LM Bruno Reghizzi_RW_BR.pdf

28. Roselli, A., Carvalho, Y., Dumeignil, F., Cavani, F., Paul, S., & Wojcieszak, R. (2020). Liquid Phase Furfural Oxidation under Uncontrolled pH in Batch and Flow Conditions: The Role of In Situ Formed Base. *Catalysts*, *10*(1), 73. https://doi.org/10.3390/CATAL10010073

29. Baskaran, T., Christopher, J., & Sakthivel, A. (2015). Progress on layered hydrotalcite (HT) materials as potential support and catalytic materials. *RSC Advances*, *5*(120), 98853–98875. https://doi.org/10.1039/C5RA19909C

4.6 Supplementary Information for Chapter 4

4.6.1 Supplementary information on the results of furfural oxidation

Table 4- 3A *The reaction energies for common reaction steps in the furfural oxidation with or without water participation. Note that FF is furfural, x is catalyst surface, FA is furoic acid, FFO is furan oxide, FFHdiO is furan hydrogen dioxide, FFOOHH is furan carbonate.*

Elementary Reaction Step	Notations	Reaction Energies, eV		
		With Water (using -OH)	Without Water (Using -O)	Difference
Oxidation of xFF into xFFO	xFF => xFFO	-0.69	-0.54	0.15
Oxidation of xFF into xFFHdiO or xFFOOHH	xFF => xFFHdiO/xFFOOHH	-0.21	-0.30	0.09
Oxidation of xFFHdiO or xFFOOHH to xFA	xFFHdiO/xFFOOHH => xFA	-2.70	-2.46	0.24

Table 4- 4B *The reaction energies for common reaction steps in the furfural oxidation with no difference for with or without water participation. Note that FF is furfural, x is catalyst surface, FA is furoic acid, FFO is furan oxide, FFHdiO is furan hydrogen dioxide, FFOOHH is furan carbonate.*

Elementary Reaction Step	Notations	Reaction Energies, eV
Oxygen adsorption	O_2 => xO_2	0.32
Oxygen activation	xO_2 => 2xO	-0.17
Furfural adsorption	FF => xFF	-0.66
Furoic acid desorption	xFA => FA	0.68
Oxidation of xFFO to xFA	xFFO => xFA	-2.22

Table 4- 5 *Furfural intermediate selectivity route possibilities evaluated. Note that FF is furfural, x is catalyst surface, FA is furoic acid, FFO is furan oxide, FFHdiO is furan hydrogen dioxide, FFOOHH is furan carbonate, FFdiO is furan dioxide.*

Step	E / eV	Remark
xFFO+xOH+xH+xOH+xOH	-705.82	Less stable
xFFO+xOH+xH_2O+1*slab+xOH	-707.41	Most stable
xFA+xH+xOH+slab+xOH	-708.04	Less stable
xFA+xH_2O+2*slab+xOH	-709.63	Most stable
xFA+xH+xO+xH+xOH	-706.59	Less stable
xFA+xH_2O+2*slab+0.5*xH_2O+0.25*xO2g	-709.62	Less stable
xFFdiO+xH+xH+xOH+xOH	-706.75	Less stable
xFFdiO+xH+xH2o+1*slab+xOH	-708.34	Less stable
xFFdiO+xH_2O+xH_2O+2*slab	-709.94	Most stable
xFFdiOH+xOH+2*slab+xOH	-707.76	Most stable

xFFOH+xO+xH+xOH+xOH xFFOH+2*xOH+1*slab+xOH xFFOH+xO+xH_2O+1*slab+xOH xFFOH+0.5*xO2g+xH_2O+1.5*slab+xOH	-704.47 -705.92 -706.07 -705.90	Less stable Less stable Most stable Less stable
xFFOOHH+xOH+2*slab+xOH	-706.93	Most stable

Table 4- 6 *Furoic selectivity route possibilities evaluated. Note that FF is furfural, x is catalyst surface, FA is furoic acid, FFO is furan oxide, FFHdiO is furan hydrogen dioxide, FFOOHH is furan carbonate, FFtriOH is furan triol, FFdiO is furan dioxide*

Step	E / eV	Remarks
xFA+xH+xOH+slab+xOH xFA+xH_2O+2*slab+xOH xFA+xH+xO+xH+Xoh xFA+xH_2O+2*slab+0.5*xH_2O+0.25*xO2g	-708.03 -709.63 -706.59 -709.62	Less stable Most stable Less stable Less stable
FA+2*slab+xH+xOH+xOH FA+3*slab+xH_2O+xOH FA+1*slab+2*xH+xO+xOH FA+2*slab+xH+xO+xH_2O	-707.36 -708.95 -705.91 -707.51	Less stable Most stable Less stable Less stable
xFFO+xOH+xH+xOH+xOH xFFO+xOH+xH_2O+1*slab+xOH	-705.82 -707.41	Less stable Most stable
xFFOH+xO+xH_2O+1*slab+xOH xFFOH+0.5*xO2g+xH_2O+1.5*slab+xOH xFFOH+2*xOH+1*slab+xOH xFFOH+xO+xH+xOH+xOH	-706.07 -705.90 -705.92 -704.47	Most stable Less stable Less stable Less stable
xFFdiO+xH+xH+xOH+xOH xFFdiO+xH+xH_2O+1*slab+xOH xFFdiO+xH_2O+xH_2O+2*slab	-706.75 -708.34 -709.94	Less stable Less stable Most stable
xFFdiOH+xOH+2*slab+xOH	-707.76	Most stable
xFFtriOH+3*slab+xOH	-709.23	Most stable
xFFOOHH+xOH+2*slab+xOH	-706.93	Most stable

4.6.2 Geometrical Structures of Other Species in Degradation Study

In this section, we present the geometrical structures of other species in evaluating the oxidation of furfural into furoic acid not presented in the main discussion earlier. Note that the red atom is oxygen, white atom is hydrogen, yellow atom is gold, and black atom is carbon.

Table 5- 7 *Geometrical structures of the other species are present in evaluating the degradation route.*

Geometry	Description
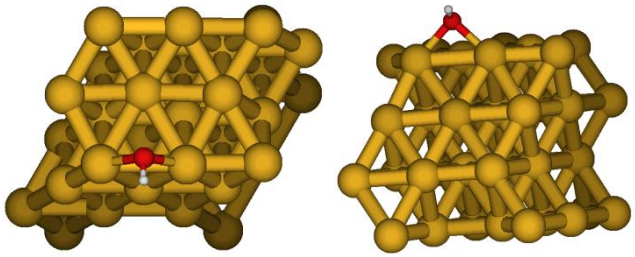	**xOH** (most stable) on Au (111) in hollow FCC position on the metals with a distance (O-Au) of 2.25A.
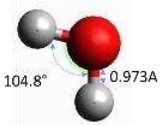	**Water** (most stable) in a gas phase (unadsorbed form) with bond length and angle (H-O-H).
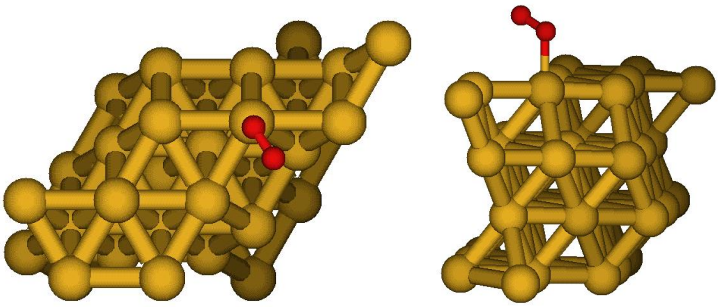	surface oxygen gas, xO_2 (with a bond distance (O-Au) of 2.27A)
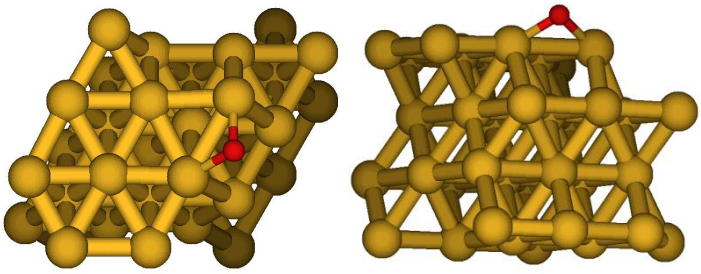	surface oxygen atom, xO with a bond distance (O-Au) of 2.14A.

Investigating HMF Oxidation Mechanism & Pathways Promoting Degradation in FDCA Synthesis on Au

5 Investigating HMF Oxidation Mechanism & Pathways Promoting Degradation in FDCA Synthesis on Au

Chapter 5 Investigating HMF oxidation mechanism & pathways promoting degradation in FDCA synthesis on Au

5.1 Overview

In line with earlier reports presented in Chapter 2 (where the reports of existing works are reported), we established that degradation of species on metals during base-free oxidation of HMF has posed a significant threat to the yield of FDCA. This challenge has resulted in lowering the yield of FDCA and poor selectivity on some metals, including gold (Au), on which we focus our studies.

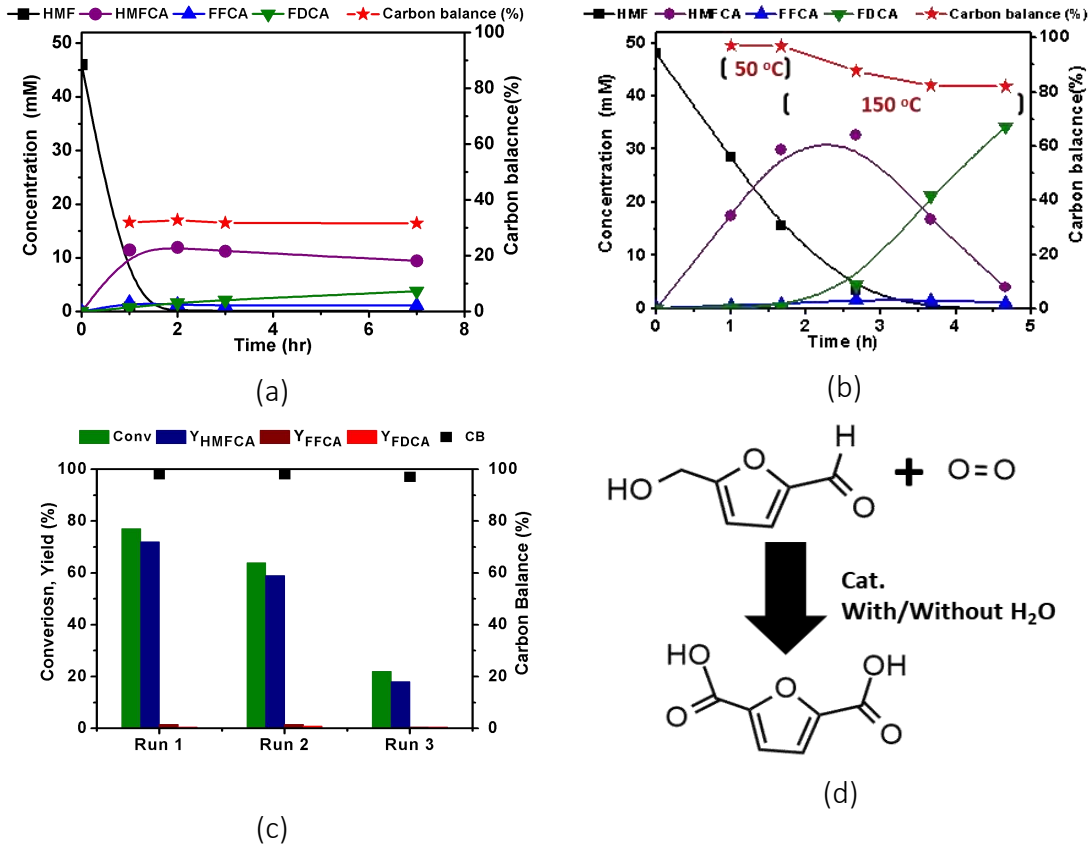

Figure 5- 1 Concentration-time plot for species (HMF, HMFCA, FFCA, and FDCA yield with carbon balance report carried out at the conditions ($P(air)_0$ = 20 bar, $m_{Au/ZrO2}$ = 33 mg, n_{HMF}/n_{Au} = 500, $C_{0\,(HMF)}$ = 45 m M, n_{OH}/n_{HMF} = 3, 1wt% Au/ ZrO2 SZ-61192: PVA:Au = 1.2). Note that (a) top-left (T=110°C), (b) top-right (T=50°C for 7h, and latter change to T=150°C), (c) bottom-middle (T=50°C, 2h) information [1], and (d) a simplified chemical equation for the HMF oxidation to FDCA.

The degradation activity on Au was evident in one of the recent reports collated by one of our experimental partners' laboratory studies[1]. Their report shows a low yield (with some imbalances in the carbon, as shown in Figure 5- 1 (a)) for using pure Au/ZrO_2 support (at 110^oC) in the oxidation of HMF into FDCA in the presence of water. The pathway(s) promoting the degradation (leading to about 70 % carbon loss) is yet to be clearly identified. However, our experimental partner has deployed several strategies to identify the source and route promoting the observed degradation. One of their attempts (in Figure 5- 1(b)) was to explore starting with a lower temperature (50^oC) and then switching to a higher temperature (150^oC) after 2h (when HMF has almost been converted into HMFCA). With such a strategy, no visible carbon loss within the first 2h of the reaction, and a carbon loss of about 20% was observed within the next 3h, as shown in Figure 5- 1(b). The strategy of switching from low to high temperatures reduces the amount of carbon loss observed earlier (at 110 ^oC) by about 50%. Our study, therefore, finds it essential to unravel the pathways promoting the degradation observed from an experiment study reported in Figure 5- 1.

So, to understand the mechanism promoting the degradation of the species involved in the oxidation of HMF into FDCA on Au using the DFT calculation method:

1. We first explored the mechanism involved in the oxidation of HMF into FDCA on the solid catalyst (Au) in the presence of water to understand if it follows an aldehyde or hydroxyl oxidation pathway.
2. We investigated several degradation routes feasible for producing undesired products on the Au slab. We choose to focus on species experimentally reported to have been seen degrading during their studies, including HMF and HMFCA.

5.2 Computational Methodology

We evaluated the reaction energies of various reaction routes (or pathways) using thermodynamic analysis to identify the most energetically feasible pathway or route. The approach was used both in the study of oxidation and degradation pathways. Details on the computational method for the reaction energies are presented earlier in Chapter 3.

Moreover, all the computational details used in computing the respective energies for species involved in the study using the DFT method are also presented earlier in Chapter 3. Exception for a few specifications peculiar to this chapter. The peculiar specifications for this chapter include the 4x4 atoms supercell used as its slab in the study with four layers (Au-Au inter-atomic distances of 2.93 Å). The 2D Brillouin zone integration was performed at the gamma point. The total height of the periodic supercell was set at 23.92 Å, which takes 70 % of the supercell height to be a vacuum above the metal slab.

5.3 Results and Discussions

Here, the results obtained for our investigation of the oxidation and degradation pathways during the production of FDCA from HMF on Au in the presence of water are presented. In agreement with the earlier conclusion in Chapter 4 on the promotion of oxidation in the presence of water on Au, we resolved to constrain this section to be mainly on the use of aerobic oxidation, which has already been established. This was similar to Gu et al.[2], which showed that the presence of water on Au in the base-free oxidation of ethanol was found to be favorable.

In addition, Section 5.3.1 report the findings made for exploring the mechanisms involved in the oxidation pathways investigated, while the later Section 5.3.2 present

our search for the degradation routes energetically promoting the production of undesired products in the presence of water.

5.3.1 Mechanism involved in oxidizing HMF to FDCA on Au

Using the experience gained from the survey of the existing experimental and theoretical studies for oxidizing HMF into FDCA, we proposed a mechanism shown in Figure 5- 2 for understanding the activities involved in oxidation processes on a metal catalyst in the absence/presence of water. The mechanism shows two different oxidative pathways we computationally evaluated in our studies. This pathway includes one that produces FDCA via the aldehyde oxidation route (involving the production of HMFCA as an intermediate) and the other pathways via the hydroxyl oxidation route (involving the production of DFF as an intermediate).

The oxidation of the HMF in the absence of water gets, initiated with the activation of oxygen (O_2) gas to give surface oxygen (O) species on the Au catalyst, was found to be less favorable. This was similar to the earlier report (Chapter 4) for furfural oxidation into furoic acid, which validates the presence of water to have been more favorable for using a gold (Au) catalyst. Due to that deduction established earlier in Chapter 4 for the benefit of water presence on Au during the oxidation, the section would majorly present findings made for HMF to FDCA on Au in the presence of water only. In addition, the mechanism involved in the oxidation of water to yield hydroxyl (xOH) on Au (111) has been established in Chapter 4.

5.3.1.1 General overview of the mechanism analyzed for the oxidation of HMF to FDCA

The oxidation of HMF is initiated with the presence of surface hydroxyl (xOH) species obtained from the oxidation of water via the feeding of water and oxygen gas on Au (111), as shown in Figure 5- 2.

The oxidation of the HMF began with the adsorption of HMF to the Au (111) slab. The next step was the oxidation of adsorbed HMF (that is, xHMF) into intermediate species (xDFF or xHMFCA) via hydroxyl or aldehyde oxidation pathways, respectively. The resulting intermediate species (xDFF or xHMFCA) were further oxidized into xFFCA via oxidation of the aldehyde (xDFF) and hydroxyl (xHMFCA), respectively. FFCA was then oxidized via its aldehyde functional group to the formed xFDCA (adsorbed FDCA) on Au (111).

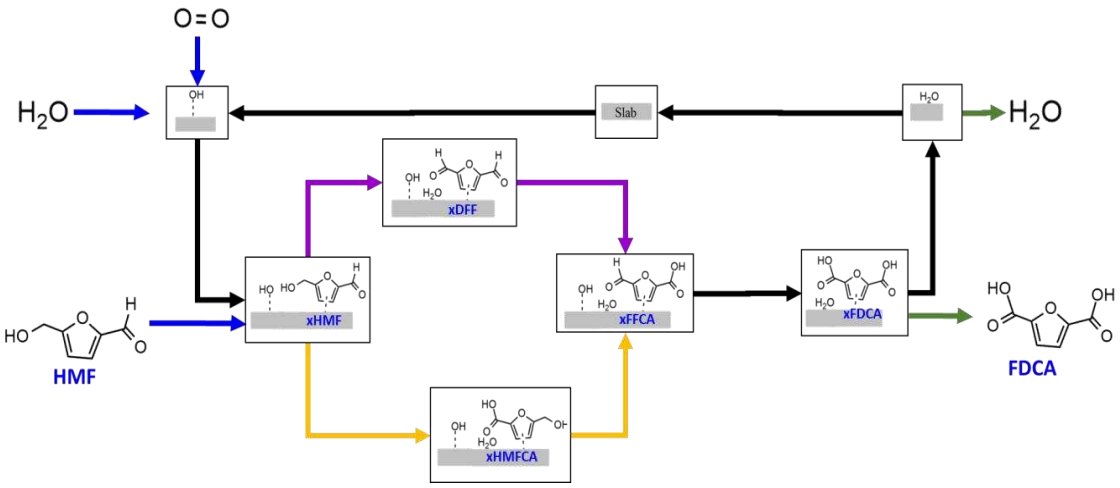

Figure 5- 2 Scheme for the oxidizing HMF to FDCA over Au (111) catalyst. Note that the line with purple is the hydroxyl oxidation pathway, yellow is the aldehyde oxidation pathway, blue is the adsorption pathway, green is the desorption pathway, and black is the other conversion processes. All surface species are singly mono-adsorbed (not co-adsorbed) on a slab.

The desorption of xFDCA leads to the production of FDCA. In oxidation, the respective hydrogen atom abstracted from the species at any step bonds with xOH to form surface water which is expected to be oxidized to generate more xOH in the presence of oxygen gas.

5.3.1.2 Analysis of the oxidation mechanism for the conversion of HMF to FDCA

A Gibbs reaction energy profile collected from the study is presented in Figure 5- 3 at 110 °C. Analysis of the reaction energy profile indicated that all the steps involved in the oxidation mechanism were exergonic and spontaneous except for the HMF adsorption, which was shown to be slightly endergonic (G_{rxn} = 0.26 eV) and

exothermic (H_{rxn} = -0.92 eV, TdS = 1.81 eV) due to its positive Gibbs reaction energy and negative Enthalpy. The slightly positive Gibbs reaction energy obtained for HMF adsorption could be due to the limitation of effectiveness in adsorption entropy when degree of freedom is lost during conversion from the gas phase to surface species. However, the TdS(1.81 eV at 110 °C) result reveals the role a temperature rise would play in aiding its adsorption. The formation of surface hydroxyl (xOH) on Au (111) was highly exergonic (G_{rxn} = -1.46 eV). In addition, the exergonicity of xOH formation step would feasibly aid in driving the energy requirement for HMF adsorption on Au (111).

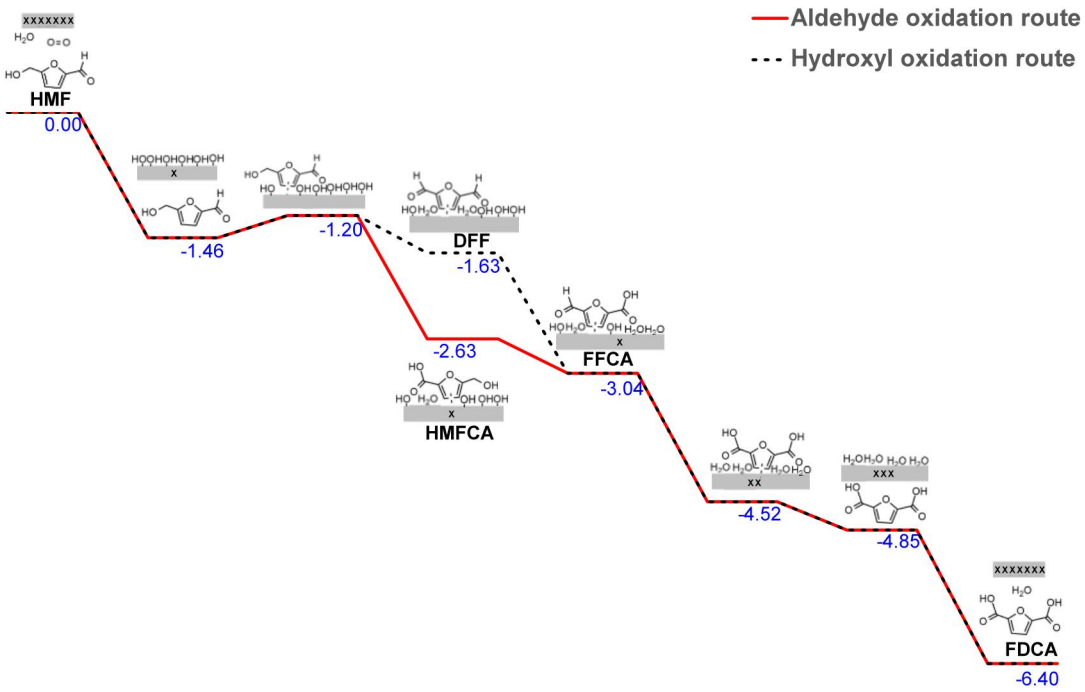

Figure 5- 3 Gibbs reaction energy profile (in eV) for the oxidation of the HMF into FDCA over Au (111) at 1 bar and 110°C. Note that the straight line is the hydroxyl oxidation pathway (i.e., HMFCA route), and the broken line is the aldehyde oxidation pathway (i.e., DFF route). X represents the number of empty slabs modeled in the analysis. All surface species are singly mono-adsorbed (not co-adsorbed) on a slab.

The aldehyde oxidation pathway (in Figure 5- 3) involving the conversion of xHMF to xHMFCA via its aldehyde (HCO) group in the presence of xOH was further analyzed. This pathway involves the breaking of the C-H bond (on aldehyde) and the formation of C-O with one of the xOH(s) to form xHMFCA (in Figure 5- 4) on Au. The distance of xHMFCA from Au slab (with shortest distance of 2.63 Å) in Figure 5- 4 confirms the adsorption mode or interaction to be Van der Waals interaction otherwise known as

physisorption. And the eliminated H atom later bonds with xOH species to form surface water (xH_2O). The reaction energy, G_{rxn} obtained for transforming xHMF into xHMFCA, was found to be -1.43 eV using the energy profile. In further transforming xHMFCA into xFFCA on Au, its (i.e., xHMFCA) hydroxyl (OH) group was oxidized by breaking the O-H and C-H bonds, with the formation of C=O. This resulted in more water formation via H bonding with OH species. These changes result in the formation of xFFCA. Reaction energy, G_{rxn} of -0.41 eV, was obtained for transforming xHMFCA into xFFCA on Au. The first (xHMF to xHMFCA) and second (xHMFCA to xFFCA) oxidation were exergonic and spontaneous. The result showed that the first oxidation (with G_{rxn} = -1.43 eV that oxidizes aldehyde function to carboxylic acid) step was more exergonic than the second (with G_{rxn} = -0.41 eV that oxidizes alcohol function to aldehyde). This path's higher exergonicity (G_{rxn} = -1.43 eV) was similar to the high conversion rate accounted for by Wan et al.[5] for transforming aldehyde function of HMF to carboxylic acid in HMFCA in their study. It also reveals why our experimental partner results (in Figure 5- 1(c), especially one for the regeneration test) showed high evolution of HMFCA in their product distribution during the FDCA synthesis using Au.

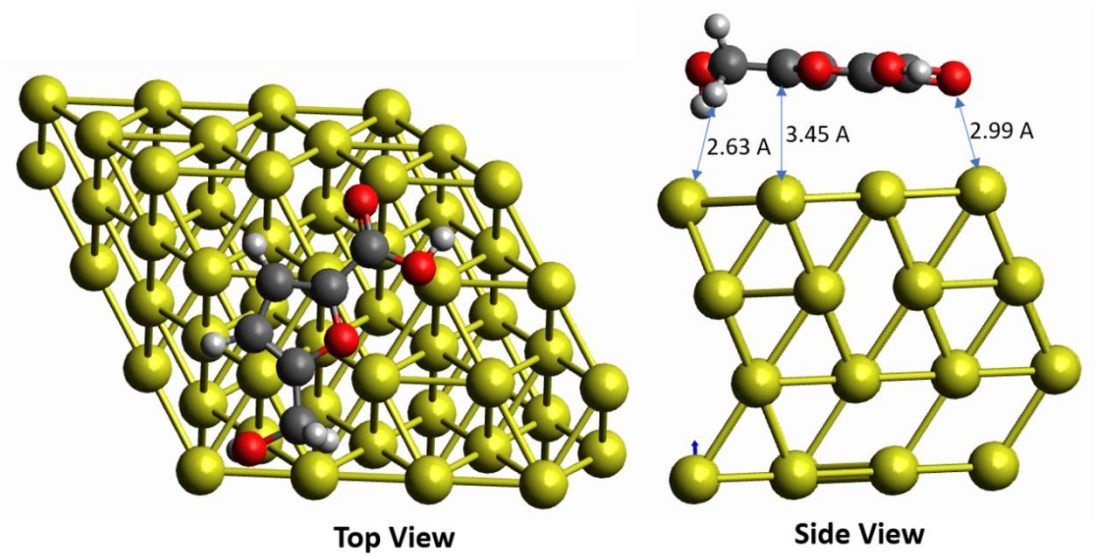

Figure 5- 4 *Optimized structure of the HMFCA chemisorbed on Au(111). The left image is the top view, while side view of the structure is the right image.* ***Note*** *that the red atom is oxygen, white atom is hydrogen, yellow atom is gold, and black atom is carbon. All surface species are singly mono-adsorbed (not co-adsorbed) on a slab.*

In contrast, we also analyzed the hydroxyl oxidation pathway that oxidizes the xHMF via its hydroxyl (OH) group in the presence of xOH on the Au (111) to yield xDFF. The pathway is composed of the O-H and C-H bonds breaking and forming a C=O bond. This results in water formation (from bonding H with OH specie on the surface) and xDFF (shown in Figure 5- 5). The study confirms the mode of xDFF adsorption on Au to be Van der Waals interaction otherwise known as physisorption. The conversion process that led to xDFF showed reaction energy, G_{rxn} of -0.43 eV. Similar to xHMFCA, the xDFF further oxidizes to xFFCA. In this further step, one of the xDFF aldehydes (HCO) groups oxidizes to yield xFFCA. The oxidation step involves breaking the C-H bond (from xDFF) and forming the C-O bond (with surface xOH specie). The reaction energy, G_{rxn}, for the formation of xFFCA and water (via the bonding of H with OH on the surface) from xDFF on Au was found to be -1.41 eV. The first (alcohol function of xHMF to aldehyde in xDFF) and second (aldehyde function of xDFF to carboxylic acid in xFFCA) oxidation were exergonic. However, the first oxidation step showed a lower reaction energy than the second one, which shows a lower conversion rate in the report of Wan et al.[3].

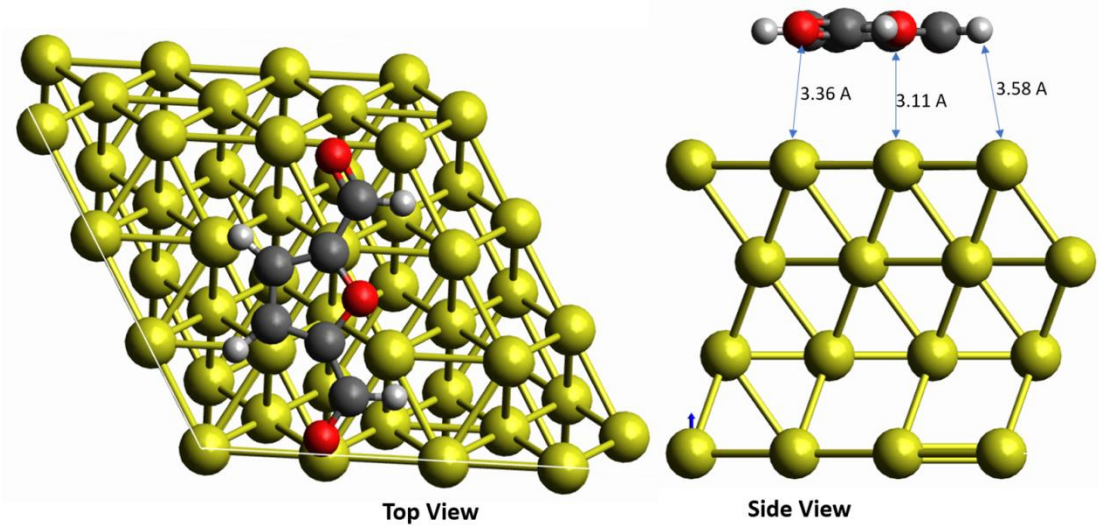

Figure 5- 5 *Optimized structure of the DFF chemisorbed on Au(111). The left image is the top view, while side view of the structure is the right image.* ***Note*** *that the red atom is oxygen, white atom is hydrogen, yellow atom is gold, and black atom is carbon. All surface species are singly mono-adsorbed (not co-adsorbed) on a slab.*

A thermodynamic feasibility evaluation (or comparative analysis) of results (in Figure 5- 3 at 1 bar and 110 ^{o}C) obtained for the two pathways for transforming xHMF into xFFCA on Au shows that the aldehyde oxidation path (xHMF to xFFCA via xHMFCA) would be energetically feasible. The validation of the aldehyde oxidation pathway was due to its higher reaction energy obtained for the first oxidation step (aldehyde function of xHMF to carboxylic acid in xHMFCA, G_{rxn} = -1.43 eV) than the hydroxyl pathway (alcohol function of xHMF to aldehyde in xDFF, G_{rxn} = -0.43 eV). This implies that the reaction energy of the aldehyde path was 3.3 times more exergonic than the hydroxyl path in their first oxidation step. It is predicts that aldehyde oxidation route would be faster than hydroxyl route in accordance with BEP relationship (which indicates a linear direction relationship of reaction energies and barriers). And the higher stability of the xHMFCA relative to xDFF further validates the feasibility of the aldehyde pathway. The comparative analysis of the two pathways using thermodynamics confirms that the aldehyde oxidation pathways are feasible. Our findings for validating the aldehyde oxidation pathway for the oxidation of HMF into FFCA agreed with an experiment report [3], which reveals a higher conversion rate for aldehyde function of HMF to carboxylic acid in HMFCA (31 umol/cat-g/sec) than alcohol function of HMF to aldehyde in DFF (5 umol/cat-g/sec) on Au. Similarly, the experimental findings by Megia-Sayago et al. [4] for the use of Au agreed with the feasible pathway (aldehyde oxidation pathway) identified in our study, despite their usage of the base. Our finding further agreed with our experimental results[1] (in Figure 5- 1(c) profiles), which shows the evolution of HMFCA without any visible profile for DFF production using Au catalyst.

The xFFCA (obtained from the aldehyde oxidation) is further oxidized into xFDCA via its aldehyde (HCO) group. This stage involves the breaking of the C-H bond (from xFFCA) and the formation of the C-O bond (with xOH species on Au slab) to give a new

molecule with two carboxylic acid functional groups, better known as FDCA (the desired product). The conversion of xFFCA to xFDCA was also exergonic (G_{rxn} = -1.49 eV).

Moreover, the desorption of FDCA (G_{rxn} = -0.33 eV, H_{rxn} = 0.87 eV at 110 °C) from the Au (111) slab was found to be favorable due to its negative reaction energy. This implies that FDCA desorption would be spontaneous. Despite being slightly endergonic, it would easily get desorbed from the Au(111) with a rise in temperature & entropy (TdS) effect, similar to the earlier discussion on adsorption. Although, the endergonic nature of the FDCA desorption could expose it to degradation into an undesired product. In addition, it would lead to the formation of undesired precursors for producing undesired products[5,6].

The analysis of the mechanism involved in the oxidation of HMF into FDCA on Au in the presence of water was successfully identified. This was validated to have followed the order of adsorption water on the Au slab (due to its ease and exothermic nature). Followed by the adsorption of oxygen gas which later got the water (xH_2O) oxidized into hydroxyl (OH) on Au. Then, the adsorption of HMF on Au. It then first oxidation of aldehyde function of xHMF to carboxylic acid in xHMFCA. Next was the second oxidation step, alcohol function of xHMFCA to aldehyde in xFFCA. The aldehyde function of xFFCA is then oxidized to carboxylic acid in xFDCA and water. Desorption of FDCA was the later step. The mechanism obtained agreed with one proposed from some experimental studies[3,5] on the process.

Furthermore, the reaction energies, G_{rxn}, obtained for the steps were found to be in the order: xFFCA to xFDCA (-1.49 eV) > xHMF to xHMFCA (-1.43 eV) > xHMFCA to xFFCA (-0.40 eV) > xFDCA to FDCA (-0.33 eV). Excluding the adsorption and desorption steps, the oxidation of xFFCA's aldehyde functional group to xFDCA and xHMF's aldehyde functional group to xHMFCA was the set of fast reaction steps, while the

oxidation of xHMFCA's alcohol functional group to xFFCA was the slowest steps in the mechanism. Being a series reaction that is dependent on the other to yield another, it implies that there would be the production of more HMFCA due to its higher Gibb reaction energy (-1.43 eV for oxidizing xHMF's aldehyde functional group to xHMFCA) due to the lower reaction energy (-0.40 eV for oxidizing xHMFCA's alcohol functional group to xFFCA) obtained for the step converting it to FFCA. With a low conversion rate of xHMFCA's alcohol functional group to xFFCA, it is expected the record a lower FDCA yield, despite showing the highest reaction energy (-1.49 eV for oxidizing xFFCA's aldehyde functional group to xFDCA) in the oxidation mechanism. Our findings reveal why higher selectivity and yield were reported for HMFCA in our Lille experimental partner [1] results (in Figure 5- 1 obtained at 50 and 150 ^{o}C), showing faster conversion of HMF to HMFCA than FDCA desorption.

Our deductions were also in agreement with other experimental reports like one investigated by Ferraz et al.[5] for Au/SiTi, which shows the selectivity for HMFCA as the highest (~54 % at 12 h, ~53 % at 24 h) while FDCA was the lowest (~3 % at 12 h, 4 % at 24 h) at 100 ºC and 1 bar. Although, the author[5] further reported a good selectivity for FFCA (38-40 %). The experimental report of Davis et al.[7] also agreed with our findings, confirming a higher selectivity of 95 and 84 % for HMFCA with a lower selectivity (<3%) for FDCA in the presence of Au/C and Au/TiO_2. Another experimental study reported by Wan et al.[3] for Au/CNT also confirms a high selectivity for HMFCA (16 %) and low selectivity for FDCA (1.4 %). FFCA showed 8.3 % selectivity in their study at 100 ºC, 5 bar for 12 h. In addition, a theoretical analysis of the FDCA synthesis from HMF by Lu et al. [8] (using Co_3O_4 (111) and electrochemical method) and Yaqi Liu et al. [9] (using Pt(111) slab) confirmed the step oxidizing HMFCA's alcohol functional group into FFCA to have been the rate-determining step (RDS) for FDCA

production, which agreed with our findings for Au (111) that reveal the same step as the slowest step. Moreover, the study of Yaqi Liu et al. [9] further catalyst facet also influences the RDS of the reaction.

5.3.2 Exploration of pathways leading to HMF & HMFCA degradation over oxidation

The existing experimental report has associated Au's poor selectivity for FDCA with the presence of degradation activities which were not clear experimentally. However, it was certain that the degradation was held due to the imbalance observed for carbon [1,5] . However, this section presents our findings for the routes promoting degradation activities that must have resulted in the production of side products based on our theoretical investigation. We gained insight into the possible degradation routes in the FDCA production on Au by comparing the degradation routes with oxidation routes leading to the production of FDCA. The reaction energies of the respective routes were computed and used to validate or invalidate their influence on the selectivity of Au for the FDCA production route.

In the study, we primarily investigate the degradation routes present in the oxidation of HMF and HMFCA on Au (111), in line with the experimental report in Figure 5- 1(a-c). Other species (presented in the Supplementary Information) involved in the reaction do not show any feasible degradation routes except for the formation of furan (during the oxidation of some intermediates and desorption of FDCA), which is better controlled or managed in a basic environment (that is, experimental condition deployed by partner), unlike neutral environment. This enables our research to unravel the details of the factors contributing to the carbon loss and catalyst deactivation reported by our partner [1] in their experiment, where degradation is suspected to have held during the conversion of HMF to FFCA before the production of FDCA on Au.

Our investigation of the degradation possibilities in the synthesis of FDCA over Au was structured into different stages as follows:

1. Degradation activities competing with HMF oxidation (to HMFCA) , and
2. Degradation activities competing with HMFCA oxidation (to FFCA) in the FDCA production.

This approach would aid in unraveling the major routes posing a threat to FDCA synthesis that often contribute to the experimentally observed carbon loss in the production. The study mainly takes focus on oxidation activity with water participation, in agreement with the deduction reported for the HMF oxidation in previous section (5.3.1) and Chapter 4 of this report.

5.3.2.1 Exploring the degradation routes in the oxidation of HMF into HMFCA on Au

In understanding the feasibility of the various degradation routes in converting HMF to HMFCA, we looked into the pathway leading to the oxidation of HMF to desired products. The pathway includes breaking the C-H bond from the xHMF's aldehyde group to give an intermediate for the production of HMFCA. And other possible degradation pathways that could lead to undesired products or routes were explored across the path shown in Figure 5- 6.

In this exploration, we have several breaking and formations of bonds involving C-H, C-C, and C-O. The various pathways (oxidation and degradation path) explored in the study are presented in Figure 5- 6. The oxidation of 1-mole xHMF in the presence of 3-mole xOH (from oxidation of 1.5-mole xH_2O and 0.75-mole xO_2) with 1-mole empty slab via different routes includes:

1. Breaking of the C-H bond on the aldehyde functional group of HMF (H-CO)
2. Breaking of the C-H bond on the furan ring of the HMF-aldehyde side (H-RingCO(H)) and the HMF-hydroxyl side (H-RingCH_2OH)

3. Scission of the C-C bond on the aldehyde (C-CO(H)) and the hydroxyl (C-CH_2OH) functional groups of HMF

4. Ring Opening via the C-O bond of the HMF furan

5. Desorption of HMF (unconverted) from the Au (111) slab

The results obtained for analyzing the various routes' reaction energies were also presented in Figure 5- 7, showing the most feasible reaction pathways for both oxidation and degradation routes.

Among the various degradation routes investigated for xHMF during oxidation to xHMFCA indicates that the breaking of the C-C bond (that is, C-CH_2OH and C-CO(H)) and ring-opening would be less feasible due to their higher Gibbs reaction energies compared to other routes (as shown in Figure 5- 7). The different routes which were more feasible include the breaking of C-H bonds from furan rings and the desorption of HMF from Au (111). Moreover, the hydrogen abstraction (that is, C-H bond breaking from the furan ring) was found to be more severe from the furan ring side close to aldehyde than others (from the hydroxyl side of the ring).

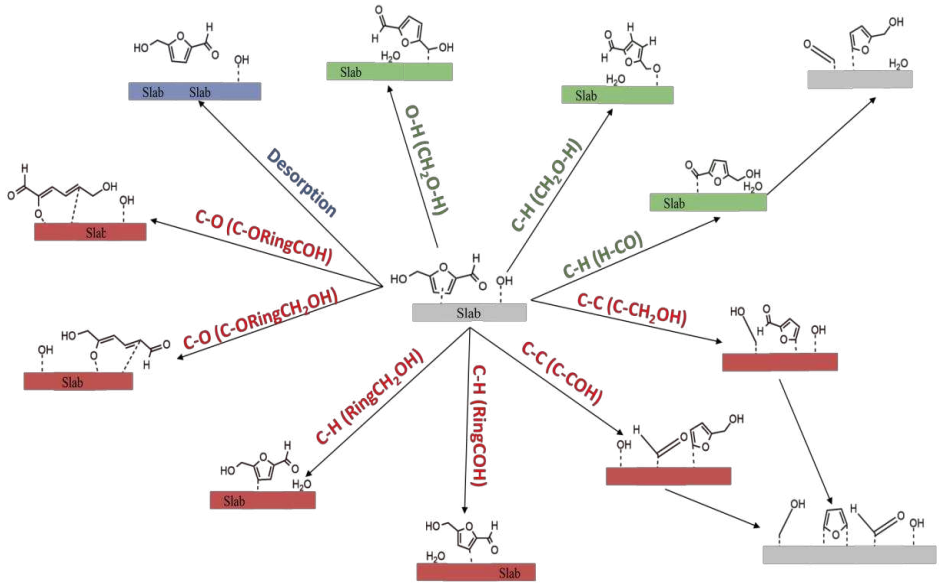

Figure 5- 6 Scheme revealing possible degradation pathways in the transition of HMF to the intermediates over a heterogeneous catalyst. Note that red is the undesired pathway, blue is the fairly good pathway, and green is the desired pathway (HMF on slab is at the middle). All surface species are singly mono-adsorbed (not co-adsorbed) on a slab.

Our studies also reveal that most of the degradation routes evaluated were endothermic except for the HMF desorption route. The HMF desorption would make high conversion of HMF difficult due to its ease of desorbing from the surface, but it would not be responsible for the lower carbon balance observed in the study of the process.

However, a few of the identified endothermic degradation routes in Figure 5- 7 can feasibly compete with the oxidation route due to their lower reaction energies. The route is hydrogen abstraction from the furan ring by breaking the C-H bond on Au (111). In a nutshell, the feasible degradation routes (or competition routes) with the oxidation of HMF to yield FDCA were found to be the breaking of the C-H bond in the furan ring and HMF desorption. At a lower temperature, the furan ring C-H bond breaking and HMF desorption would be less feasible than the oxidation routes. At the same time, the higher temperature would improve degradation routes feasibility for the oxidation of HMF on Au (111).

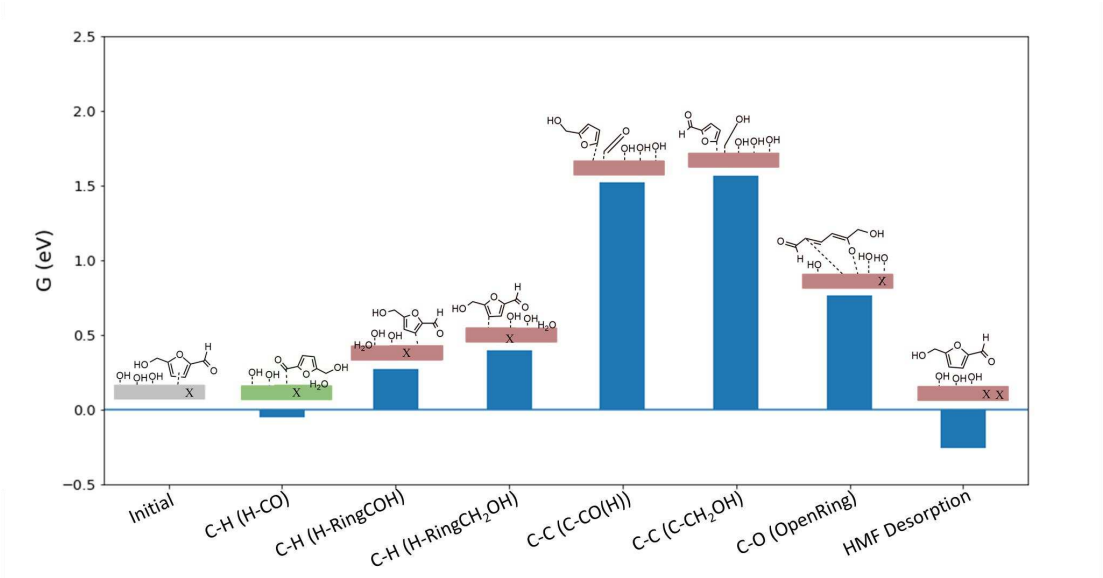

Figure 5- 7 Reaction energies and scheme revealing possible degradation pathways in the transformation of HMF to the HMFCA intermediates over Au catalyst at 1 bar and 110°C. Note that red is the undesired pathway, gray is the initial form before the chemical change, green is the desired pathway, X is a 1-empty catalyst slab, and all bonded species that have a dashed line or are placed on the slab. All surface species are singly mono-adsorbed (not co-adsorbed) on a slab.

Comparing our results with the experimental results [1] reveal answers for why HMF would best oxidize favorably with less degradation at a lower temperature than the higher temperature on Au. This was because the furan ring C-H bond breaking would be highly feasible at the higher temperature, leading to the production of undesired products and intermediates shown in Figure 5- 1 with a low carbon balance at more elevated temperatures on Au.

5.3.2.2 Exploring the degradation routes in the oxidation of HMFCA into FFCA on Au

We further explored the degradation routes involved in oxidizing HMFCA to FFCA. To do that, we explored two oxidative pathways for oxidizing HMFCA to yield FFCA. The two pathways in HMFCA were due to its hydroxyl branch that needs to be oxidized to produce an aldehyde functional group (FFCA). These pathways include O-H and C-H bond breaking to turn the hydroxyl group of the HMFCA into an aldehyde one. So, in this study, we analyze which of the bond breaking precedes the other in the oxidation (that is, O-H to C-H or C-H to O-H bond breaking) using the reaction energies. After this, we focused our investigation on the preceding feasible oxidative pathway, which was comparatively investigated to see how other degradation pathways could compete with it to yield undesired products, which were visible in the experimental result for the carbon balance (Figure 5- 1).

Pathways that include bond breaking and formations involving C-H, C-C, and C-O, similar to the ones investigated for HMF, were also explored here for HMFCA. The various pathways (oxidation and degradation path) explored in the study are presented in Figure 5- 8. The possible degradation routes include:

1. Breaking of the C-H bond from the rings;
2. C-C scission of carboxylic acid (C-CO(OH)), and hydroxyl (C-CH_2OH);
3. Furan ring opening;

4. Breaking of the O-H bond from carboxylic acid (OCO-H);
5. HMFCA desorption (unconverted); and
6. Other pathways are the routes that can only favor the oxidation of HMFCA to FFCA.

The analysis of the results presented in Figure 5-9 confirms the oxidation of the HMFCA initially via the breaking of the O-H bond of the hydroxyl (OH) group to be more feasible than the C-H bond breaking of the same group (that is, O-H to C-H bond breaking route). This implies that the later step would oxidize via the C-H bond. Our findings that reveal that O-H bond breaking would precede in the oxidation of HMFCA to FFCA before C-H bond breaking agrees with the trend of the reaction energies obtained by Gu et al. [2] for breaking of O-H (-0.17 eV) and C-H (-1.87 eV) in the oxidation of ethanol to yield aldehyde over AuPt alloy.

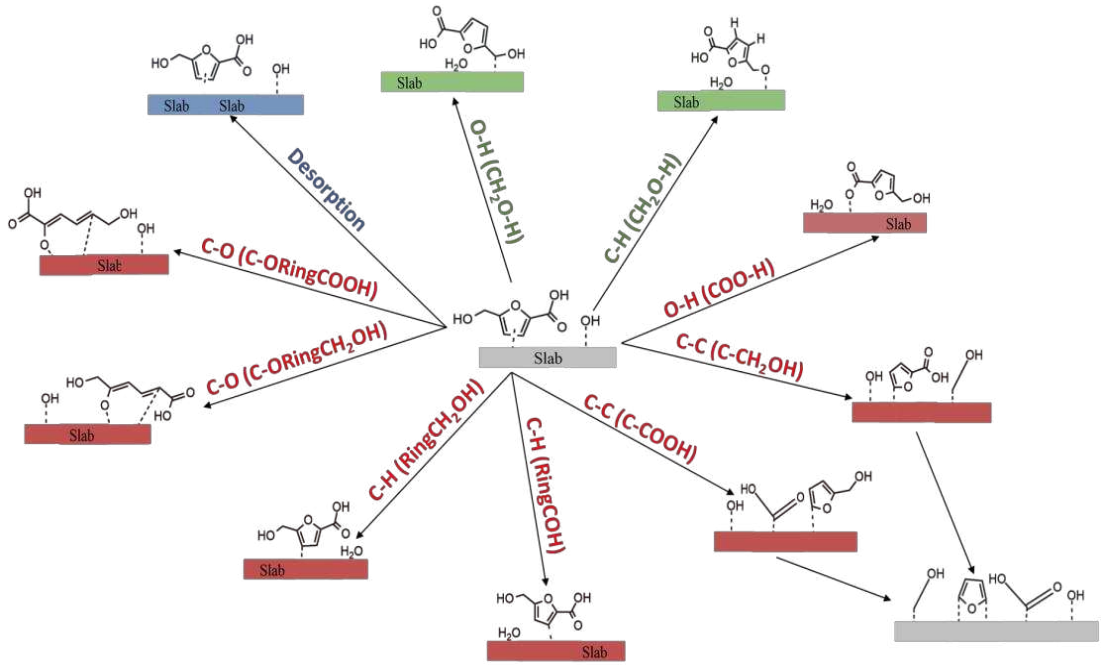

Figure 5-8 Scheme revealing possible degradation pathways in the transition of HMFCA to its intermediate or degraded forms over a heterogeneous catalyst. Note that red is the undesired pathway, blue is the fairly good pathway, and green is the desired pathway. All surface species are singly mono-adsorbed (not co-adsorbed) on a slab.

Our analysis of all the degradation pathways investigated for this transformation reveals that all the routes were endothermic except for the HMFCA desorption and

the feasible oxidation pathway, which was exothermic (to give intermediate). Route desorbing HMFCA from the Au(111) slab would retard the amount of HMFCA available for further oxidation to yield FDCA. The exergonic nature of the HMFCA desorption reveals why a high yield of HMFCA is often observed in the experimental results Figure 5- 1(a & c) reported by our partner[1]

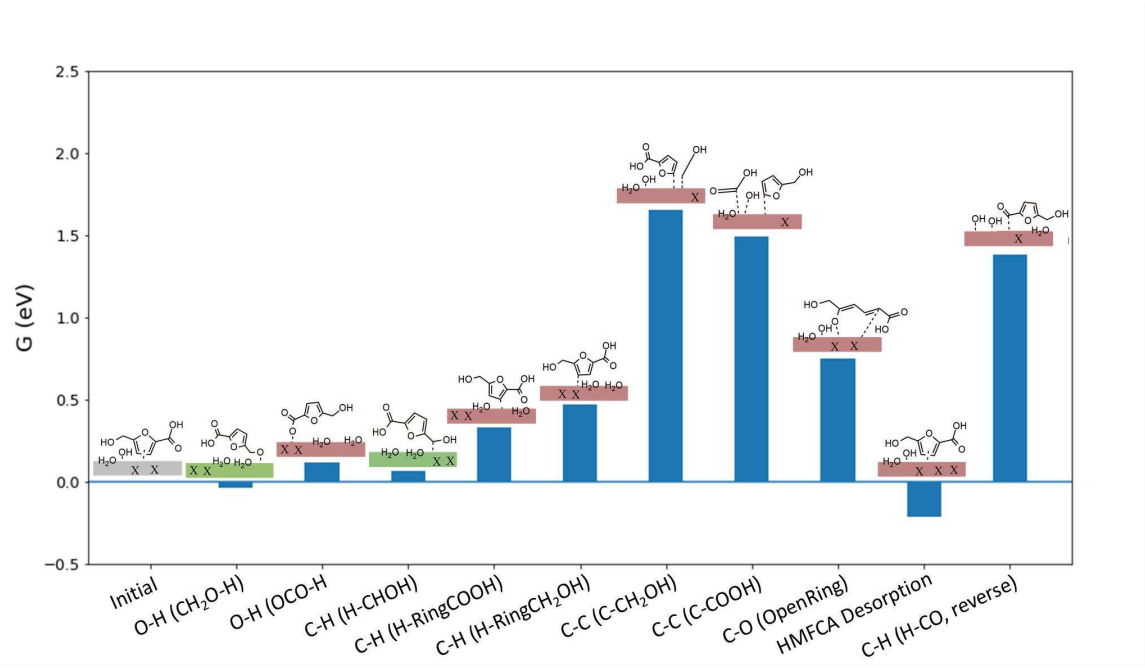

Figure 5- 9 *Reaction energies and scheme revealing possible degradation pathways in converting HMFCA to the FFCA-intermediates over Au catalyst. Note that red is the undesired pathway, gray is the initial form before the chemical change, green is the desired pathway, X is a 1-empty catalyst slab, and all bonded species that have a dashed line or are placed on the slab. All surface species are singly mono-adsorbed (not co-adsorbed) on a slab.*

Further analysis of the endergonic pathways shows that the C-C scission and the ring opening were highly endergonic. In contrast, the breaking of the O-H and C-H bond from the carboxylic acid functional group (to form carboxylates) and furan rings (to form other undesired products/intermediates), respectively, which shows a small endergonicity (below G_{rxn} < 0.5 eV), among the degradation pathways. The review of Gui et al. [2] report further establishes role of basic environment in promoting the formation and ease desorption of carboxylic acid as alternative to the degradation (aid catalyst poisoning) leading to carboxylate (due to its high surface stability) obtained for a neutral environment. So, in agreement with the existing literature,

deployment of basic environment in the oxidation of HMF on Au(111) would help in averting furan carboxylate formation. However, the C-H bond breaking from the furan rings remains a major feasible degradation route competing with the oxidation of HMFCA on Au(111) to progress the production of FDCA. The degradation route must have also contributed to the lower carbon balance observed in the experimental results collated by our partner[1] in Figure 5- 1, based on our study.

In a nutshell, the thermodynamics analysis of the various pathways shows that HMFCA would feasibly get oxidized via the breaking of the O-H bond but also the breaking of the C-H bond to yield FFCA on Au(111). The formation of furan carboxylate via O-H bond breaking (from carboxylic acid), furan ring opening, and HMFCA desorption were the identified feasible degradation routes. In accordance with Gui et al.[2], the use of basic environment would in preventing possibly poison that furan carboxylate lead to and also facilitate the conversion of carboxylate to carboxylic acid.

5.3.3 Comparative analysis of degradation routes using reaction and activation energy

To better understand where the degradation was higher, whether it was during the oxidation of HMF or HMFCA on Au(111), we compare the two together. The comparison was made for oxidizing HMF's aldehyde functional group to HMFCA intermediate and HMFCA's alcohol functional group into FFCA intermediate. Focus is given to routes that show Gibbs reaction energies less than 0.5 eV (that are more significant) in both the first and second steps of oxidizing HMF and HMFCA on Au. Comparison of the degradation intensity in the oxidation of HMF/HMFCA via:

1. The analysis of reaction energy, G_{rxn}, and
2. The analysis of activation energy, G_{act}.

The two parameters were used in ascertaining where degradation is more intense thermodynamically and kinetically. Other data for pathways with higher reaction energies is presented in the Supplementary Information of this Chapter.

5.3.3.1 Analysis of HMF/HMFCA degradation intensity on Au using Reaction Energy

Here, we compared the degradation routes feasible during the oxidation of HMF and HMFCA on Au using the Gibbs reaction energies. Figure 5- 10 graphically compares the different significant pathways in the oxidation of HMF and HMFCA during the production of FDCA on Au.

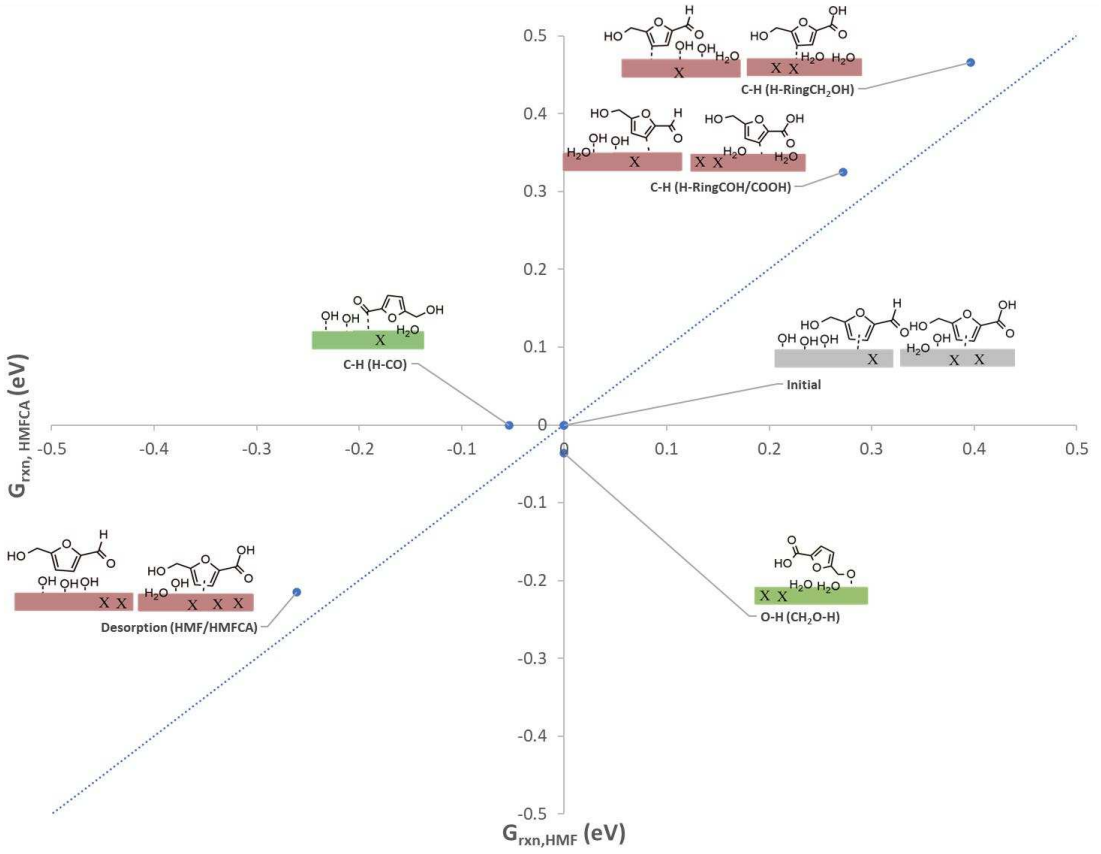

Figure 5- 10 *Compares the different significant degradation pathways in 1st stage of oxidizing HMF/HMFCA to the intermediate. Note that red is the undesired pathway, gray is the initial before the chemical change, green is the desired pathway, X is a 1-empty catalyst slab, and all bonded species that have a dashed line or are placed on the slab. A case where two slabs denote slab-1 for HMF and slab-2 for HMFCA. All surface species are singly mono-adsorbed (not co-adsorbed) on a slab.*

The result showed the reaction energies obtained for the routes with the most significant effects which include HMF/HMFCA desorption and hydrogen abstraction (that is, C-H bond breaking) from the furan ring of HMF/HMFCA. We plot the Gibbs

reaction energies of HMFCA against the ones for the HMF (in Figure 2- 10). Cases where certain degradation points in the Figures fall below the line would imply that such degradation is more intense in HMFCA, but then it falls above the line, which would mean that HMF degradation is more intense.

The comparative analysis of the reaction energies for the degradation indicates that all the degradation points in Figure 5- 10 were above the line, which signifies that the degradation across the identified routes were more intense during the oxidation of HMF to HMFCA than the oxidization of HMFCA to FFCA. And the strength of the feasible degradation routes was found to be in order: HMF/HMFCA desorption > furan ring C-H bond breaking via ringside with COH/COOH > furan ring C-H bond breaking via ringside with CH_2OH/CH_2OH as shown in Figure 5- 10.

Despite the fact established in the preceding discussion that degradation is more intense during the oxidation of HMF than that of HMFCA, it is important also to note that a comparison of the oxidation reaction energies reveals that oxidation of HMF to HMFCA is easier than the one of HMFCA to FFCA on Au (111). This was graphically visible in Figure 5- 10, where one with the most negative reaction energies is confirmed to be an easier process.

The deduction further agrees with the existing experimental and theoretical reports[7–9] that have shown that the step converting HMFCA to FFCA controls the reaction rate due to its slower rate of converting FFCA, which has often favored the desorption of HMFCA from Au (111). This was evident in the results in Figure 5- 1(a), where a lower HMF conversion and high yield of HMFCA were reported by our experimental partner[1] in their analysis.

5.3.3.2 Analysis of HMF/HMFCA degradation intensity on Au using Activation Energy

We further evaluated the intensity of the degradation in the oxidation of HMF and HMFCA to HMFCA and FFCA with the participation of water, respectively (from the kinetic point of view) using activation energy, also known as the energy barrier. From which, findings from the analysis of the respective activation energies in Figure 5- 11 indicated that the degradation route across the HMFCA was found to be of higher barrier (0.81 eV) compared to HMF (0.71 eV) on Au (111).

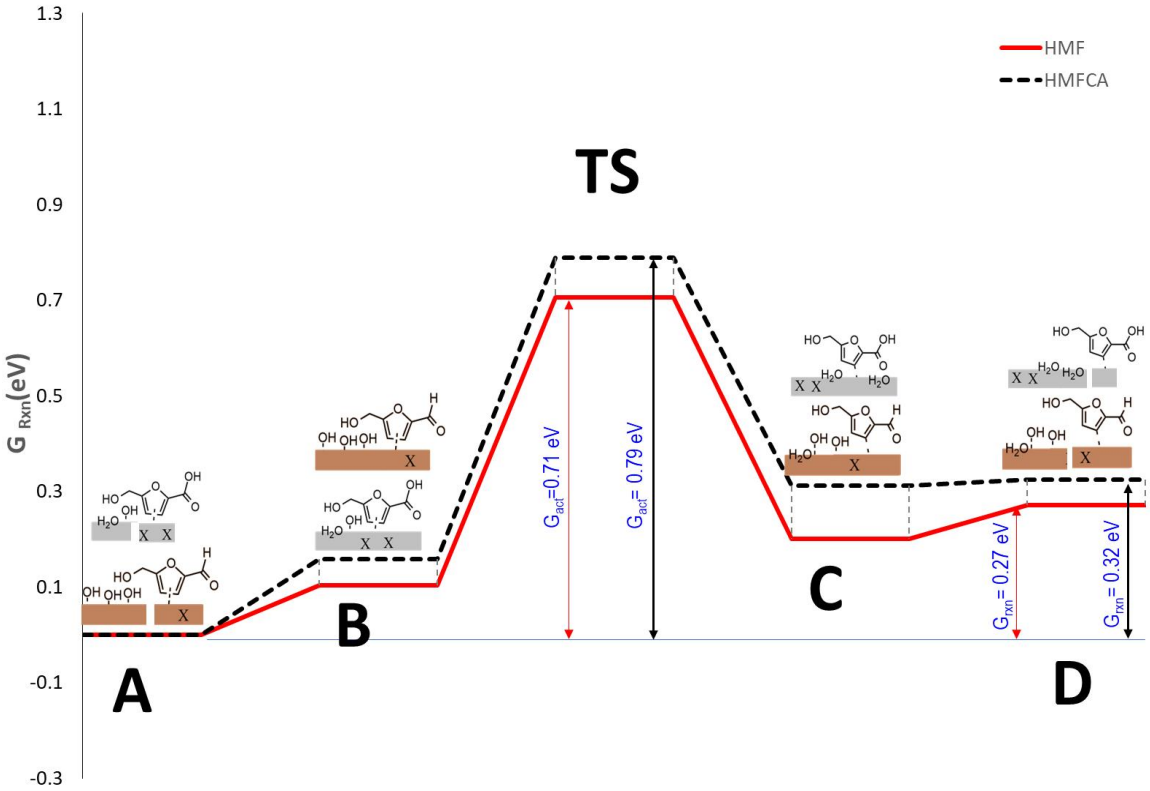

Figure 5- 11 *Gibbs Free Energy Profile of the Degradation on HMF (red) and HMFCA (black). A and D represent the modeling of the mono-adsorption mode (no interaction of adsorbates), while B and C denote the co-adsorption mode (with interaction of adsorbates). The slab with red color denoted the HMF routes, while the grey stands for the HMFCA routes. X represents the number of empty slabs modeled in the analysis.*

The results imply that it would be easier for the degradation to hold during the oxidation of HMF to HMFCA on Au than that of HMFCA to FFCA. And the bulk of the undesired products associated with the low carbon balances reported in the experiment would be largely from the degradation of HMF with little from the HMFCA degradation. The energy profile further shows that mono-adsorption of species (on a

single slab each) was found to be more stable and favorable for the HMF and HMFCA (at A), while the resulting degradation products of HMF were more stable when co-adsorbed (at C). No significant difference was observed for the HMFCA degradation products at C and D in the energy profile (Figure 5- 11).

The energy barriers indicate that the degradation activity was more intense on HMF than on HMFCA. This deduction implies that the imbalance obtained in Figure 5- 1 for the experimental studies[1] is majorly the product of HMF degradation due to its lower energy barrier. It also show that the thermodynamic analysis showed a good agreement with kinetic analysis' output.

5.3.3.3 Analysis of Geometrical Structures for Species in HMF/HMFCA Degradation on Au

We further analyzed the structural geometries of the initial (IS), transition (TS), and final (FS) states of the degradation routes across the HMF and HMFCA to the degraded intermediate (from our DFT calculations). The geometries are in Figure 5- 12 for HMF and Figure 5- 13 for HMFCA.

In our study, we analyzed the HMF geometries collected in Figure 5- 12, presenting the pictorial representation of the breaking of H from C (on the furan ring) to bond with O (in the surface xOH). The review of the C-H bond distances across the three states (first, transition, and final) reveals 1.09 Å, 1.42 Å, and 2.28 Å for the IS, TS, and FS, respectively. And the O-H bond distances were found to be 2.28 Å, 1.19 Å, and 0.98 Å for the IS, TS, and FS, respectively. The results imply that the C-H and O-H bond gets longer and shorter, respectively, across IS to FS, confirming the transfer of H to O in xOH on the slab to form a water molecule.

Additional analysis of the HMF transition state geometry structure on Au (111) reveals that xOH better interacts with the H on the furan ring C atom when a position in a bridge position is compared to the top position, as shown in Figure 5- 12.

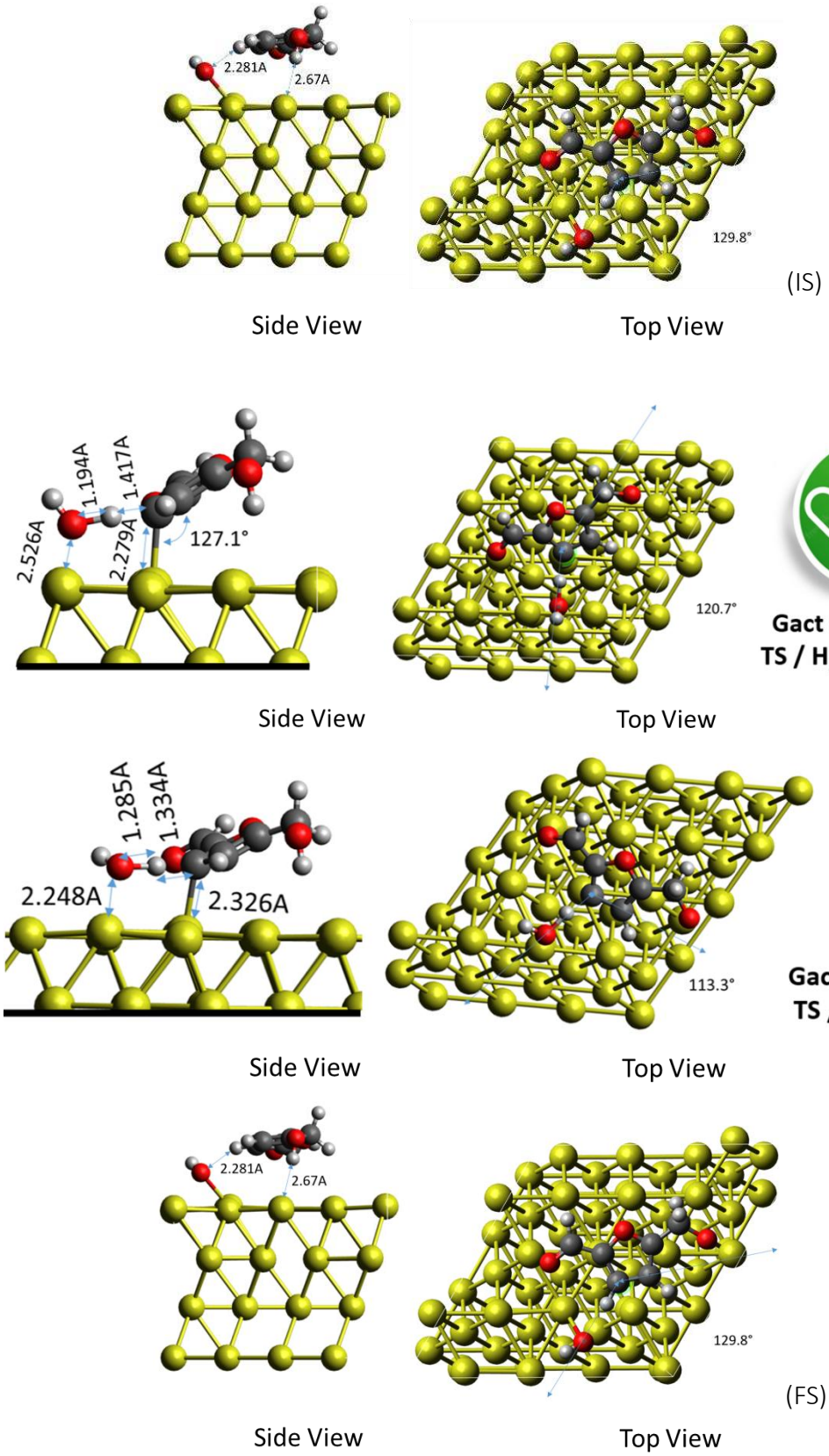

Figure 5-12 Geometries for the initial (IS), transition (TS), and final state (FS) for the most feasible HMF degradation route on Au (111), showing distances and angles in the structures (using the BLUE arrow lines). Note that the O-H = 0.977 Å, and C-H (where degradation is holding) = 1.091 Å. Note that the red atom is oxygen, white atom is hydrogen, yellow atom is gold, and black atom is carbon. All surface species are co-adsorbed on a slab.

A comparative analysis of the O-H-C transition state show an O-H and H-C bond distance was 1.19 and 1.42 Å (when water is at the bridge position); and 1.29 and 1.33 Å (when water is at the top position). Outside the fact that TS with water@bridge (G_{act} = 0.71 eV) in Figure 5- 12 show a lesser energy barrier than the TS with water@top (G_{act} = 0.74 eV), the formation of O-H bond length to yield water was found to be shorter for TS with water@bridge than TS with water@top.

In the degradation of HMFCA, we analyzed the geometries collected for HMFCA in Figure 5- 13, displaying the abstraction of H from C (on the furan ring) to bond with O (in the surface xOH). The investigation of the C-H bond distances across the three states reveals 1.09 Å, 1.43 Å, and 2.32 Å for the IS, TS, and FS, respectively. And the O-H bond distances were found to be 3.92 Å, 1.18 Å, and 0.99 Å for the IS, TS, and FS, respectively. The results similarly show that the C-H and O-H bond gets weaker and stronger, respectively, across IS to FS, confirming the abstraction of H to bond with O in the surface xOH to form a water molecule.

Evaluating the HMFCA transition state (TS) geometry structure reveals that xOH better interacts with the H on the furan ring C atom when positioned in a bridge position compared to the top position, as shown in Figure 5- 13. A comparative analysis of the O-H-C transition in the degradation of HMFCA on Au(111) shows an O-H and H-C bond distance was 1.18 and 1.43 Å with water@bridge; and 1.28 and 1.34 Å with water@top. The TS with water@bridge (G_{act} = 0.79 eV) in Figure 5- 13(TS) was more energetically stable with lesser barrier than the TS with water@top (G_{act} = 0.81 eV) and formed a stronger bond towards the formation of water@bridge in Figure 5- 13(TS) than the one formed on top. So, the degradation of HMF and HMFCA were generally more exergonic (or facilitated) and lower barrier when water is at bridge position than top position.

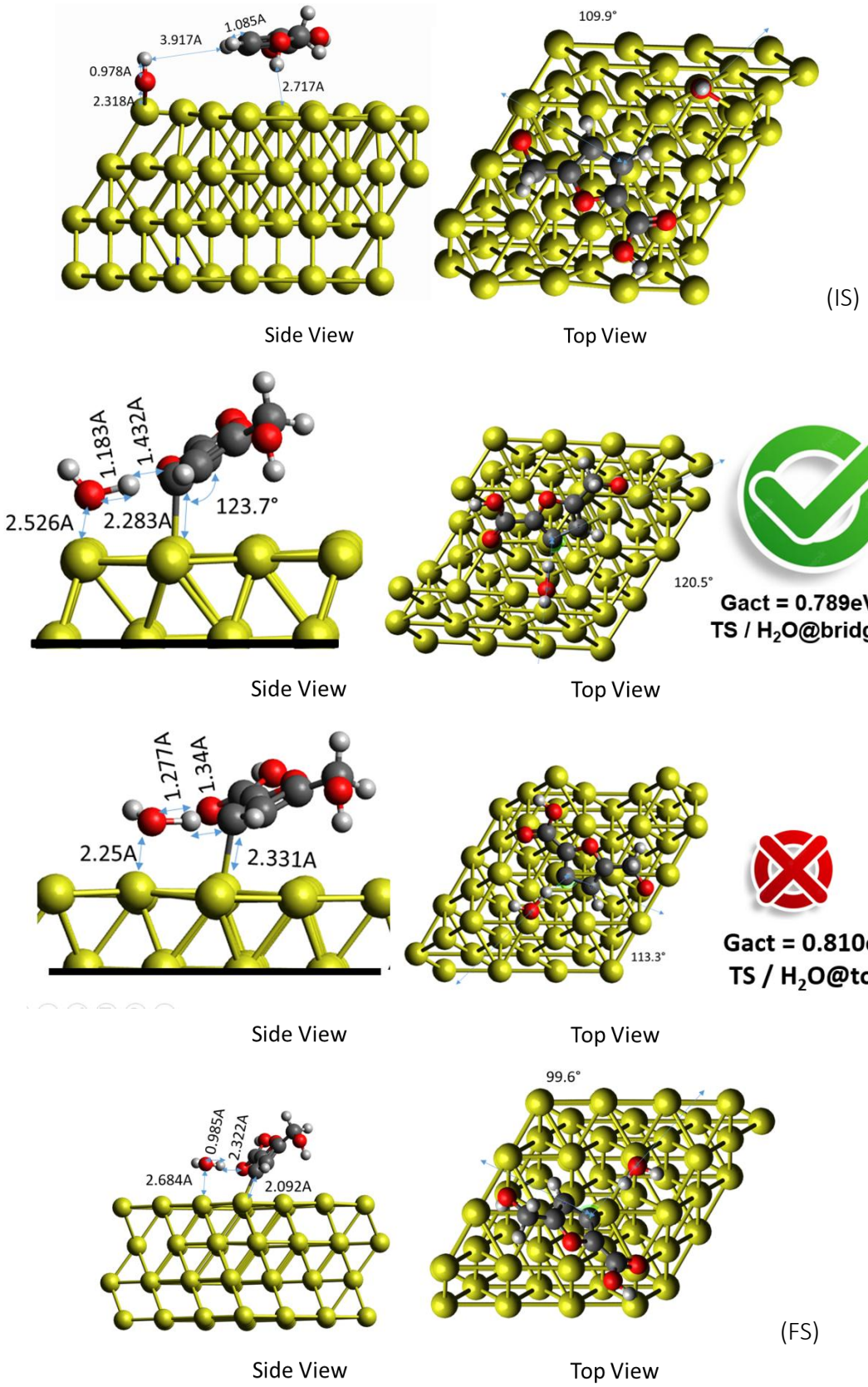

Figure 5- 13 *Geometries for the initial (IS), transition (TS), and final state (FS) for the most feasible HMFCA degradation route on Au (111), showing distances and angles in the structures (using the BLUE arrow lines). Note that the O-H = 0.977A, and C-H (where degradation is holding) = 1.084A.* ***Note*** *that the red atom is oxygen, white atom is hydrogen, yellow atom is gold, and black atom is carbon.All surface species are co-adsorbed on a slab.*

The analysis of the HMF and HMFCA degradation on Au(111) confirms that they both preferred forming the water on the bridge than the top, showing a stronger bond toward the formation of water (O-H) than the C-H bond. Moreover, the degraded furan-based intermediates formed were found to have shown shorter bond length (C-Au is 2.28 Å [HMF] and 2.87 Å [HMFCA]) with Au(111) when water@bridge than while a longer bond length (C-Au is 2.33 Å [HMF] and 2.33 Å [HMFCA]) was obtained for a case of when water@top. It was also deduced that the degraded product obtained from HMF was stronger than that of HMFCA, evident with the shorter bond length obtained for C-Au (HMF) as 2.28 Å.

Findings from the analysis of the geometrical structures of the species in the degradation do agree with the energy barrier trend obtained for the HMF (0.71 eV) and HMFCA (0.79 eV) (in Section 5.3.3.2). It was also confirmed that HMF degradation is largely responsible for the carbon loss reported in the laboratory experiment[1] and other experimental reports due to the ease of degradation obtained for HMF compared to HMFCA.

5.4 Conclusions

A study of the mechanism involved in the oxidation of HMF into FDCA on a gold (Au) slab was successfully identified. Our study found the mechanism to commence with water oxidation to yield hydroxyl (xOH), which was easy and exothermic. It was proven that aldehyde oxidation (the HMFCA pathway) was the pathway for transforming HMF to FFCA. The xFFCA was then oxidized into xFDCA and water via the hydroxyl group pathway (of FFCA), starting with O-H bond breaking followed by C-H bond breaking to yield xFDCA. In a subsequent step, the xFDCA was desorbed to yield FDCA. Our analysis of surface reaction energies shows that the step oxidizing FFCA's aldehyde functional group to FDCA (-1.49 eV) is the fastest, followed by the step oxidizing HMF's aldehyde functional group to HMFCA (-1.43 eV), and the step

oxidizing HMFCA's alcohol functional group to FFCA (-0.40 eV) is the slowest. The study reveals that a slower rate of HMFCA to FFCA has resulted in a lower yield of FDCA and a higher yield of HMFCA, which agrees with the experiment report.

To shed more light on the carbon losses reported in the experiment results, we successfully explored different degradation routes across the HMF and HMFCA. From this, we knew that ring opening and cracking around aldehyde, hydroxyl, and acid functional groups were impossible because their routes' reaction energies were too high. However, hydrogen abstraction from the furan rings and desorption were the major routes identified to facilitate the degradation route leading to carbon losses reported in the experiment. Our comparison of the degradation intensity across HMF and HMFCA on Au (111) using reaction and activation energies confirms HMF to have sustained more degradation than the HMFCA on Au(111). The analysis of the geometrical structures obtained for the transition state (TS) further confirms that a higher degradation intensity was confirmed to have a hold during the oxidation of HMF than HMFCA on Au (111). The study agreed with the experimental report that showed high HMFCA yield and rapid degradation of HMF than HMFCA on Au catalyst.

Findings from the study would be valuable in facilitating better guidance (or direction) for the design of a more efficient catalyst for the oxidation of the HMF to produce a high yield of FDCA to retard degradation.

5.5 List of references cited

1. Ferraz, C. P., & Wojcieszak, R. (2022). *Experimental Study of HMF Oxidation into FDCA over Gold-nanoparticle*.
2. Gu, Q., Sautet, P., & Michel, C. (2018). Unraveling the Role of Base and Catalyst Polarization in Alcohol Oxidation on Au and Pt in Water. *ACS Catalysis*, *8*(12), 11716–11721. https://doi.org/10.1021/ACSCATAL.8B03494/SUPPL_FILE/CS8B03494_SI_001.PDF
3. Wan, X., Zhou, C., Chen, J., Deng, W., Zhang, Q., Yang, Y., & Wang, Y. (2014). Base-free aerobic oxidation of 5-hydroxymethyl-furfural to 2,5-furandicarboxylic acid in water catalyzed by functionalized carbon nanotube-supported au-pd alloy nanoparticles. *ACS Catalysis*, *4*(7), 2175–2185. https://doi.org/10.1021/CS5003096/SUPPL_FILE/CS5003096_SI_001.PDF

4. Megías-Sayago, C., Lolli, A., Bonincontro, D., Penkova, A., Albonetti, S., Cavani, F., Odriozola, J. A., & Ivanova, S. (2020). Effect of Gold Particles Size over Au/C Catalyst Selectivity in HMF Oxidation Reaction. *ChemCatChem*, *12*(4), 1177–1183. https://doi.org/10.1002/CCTC.201901742

5. Ferraz, C. P., Costa, N. J. S., Teixeira-Neto, E., Teixeira-Neto, Â. A., Liria, C. W., Thuriot-Roukos, J., Machini, M. T., Froidevaux, R., Dumeignil, F., Rossi, L. M., & Wojcieszak, R. (2020). 5-Hydroxymethylfurfural and Furfural Base-Free Oxidation over AuPd Embedded Bimetallic Nanoparticles. *Catalysts* , *10*(1), 75. https://doi.org/10.3390/CATAL10010075

6. Cao, M., Zhang, C., He, B., Huang, M., & Jiang, S. (2017). Synthesis of 2,5-furandicarboxylic acid-based heat-resistant polyamides under existing industrialization process. *Macromolecular Research*, *25*(7), 722–729. https://doi.org/10.1007/S13233-017-5070-4

7. Davis, S. E., Zope, B. N., & Davis, R. J. (2012). On the mechanism of selective oxidation of 5-hydroxymethylfurfural to 2,5-furandicarboxylic acid over supported Pt and Au catalysts. *Green Chemistry*, *14*(1), 143–147. https://doi.org/10.1039/C1GC16074E

8. Lu, Y., Liu, T., Yang, C., Dong, C.-L., Huang, Y., Li, Y., Zhou, B., Zhou, L., Wu, Y., Kong, Z., Yang, M., Wu, Y., Zhao, W., Zou, Y., & Wang, S. (2021). Unraveling the role of oxygen vacancy in the electrooxidation of 5-hydroxymethyfurfural on Co3O4. *Research Square*. https://doi.org/10.21203/RS.3.RS-685285/V1

9. Liu, Y., Ma, H. Y., Lei, D., Lou, L. L., Liu, S., Zhou, W., Wang, G. C., & Yu, K. (2019). Active Oxygen Species Promoted Catalytic Oxidation of 5-Hydroxymethyl-2-furfural on Facet-Specific Pt Nanocrystals. *ACS Catalysis*, *9*(9), 8306–8315. https://doi.org/10.1021/ACSCATAL.9B02115/SUPPL_FILE/CS9B02115_SI_001.PDF

5.6 Supplementary Information for Chapter 5

5.6.1 Other Data for Comparison of HMF and HMFCA degradation intensity

Information on the various degradation routes explored in our project is presented in this section (including both significant and less significant routes).

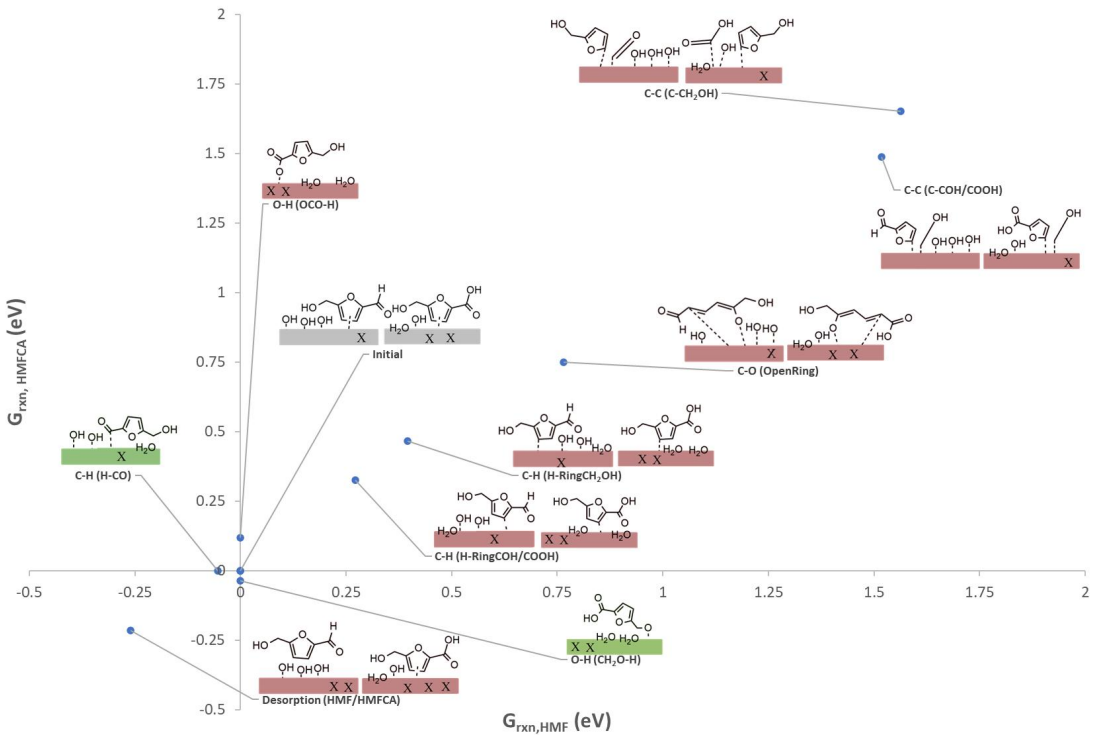

Figure 5- 14 Other details for other degradation routes, including the less significant ones. Gray slab denotes initial reaction state, red slab is degradation intermediate products (explored), and green slab is the oxidation intermediate products. All surface species are singly mono-adsorbed (not co-adsorbed) on a slab.

The comparison of HMF and HMFCA degradation routes on Au (111) is summarized in Figure 5- 14.

5.6.2 Geometrical Structures of Other Species in Degradation Study

In this section, we present the geometrical structures of other species in evaluating the degradation routes not presented in the main discussion earlier. It is shown in Table 5- 1 Geometrical structures of the other species are present in evaluating the degradation route. Table 5- 1. Additional information, like the transition state geometry structure for the case of having the water molecule on the BRIDGE position, was also presented therein and as other species like xHMF, xHMFCA, xOH, and xH_2O

on Au (111). Note that the red atom is oxygen, white atom is hydrogen, yellow atom is gold, and black atom is carbon.

Table 5- 1 Geometrical structures of the other species are present in evaluating the degradation route.

Geometry	Description
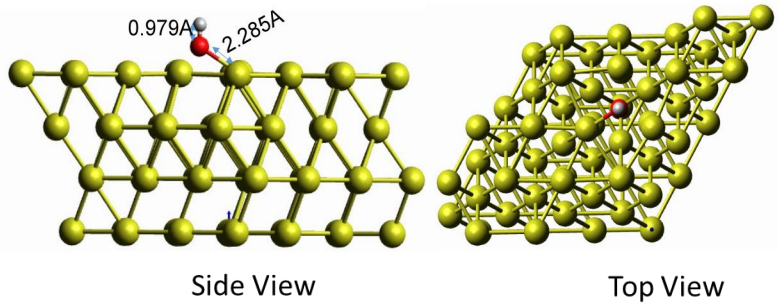	**xOH** (most stable) on Au (111) in hollow FCC position on the metals. The geometry displayed important distances in the structure.
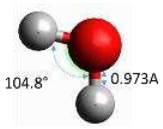	**Water** (most stable) in a gas phase (unadsorbed form) with bond length and angle (H-O-H).
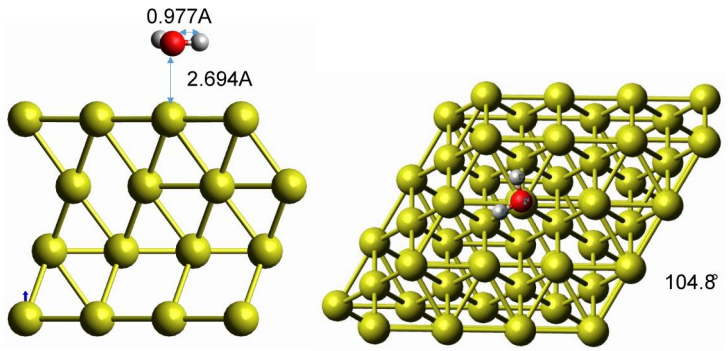	**Adsorbed water** on Au(111) with molecule adsorbed on TOP of the Au metal. The geometry displayed important distances and angle (H-O-H) in the structure.
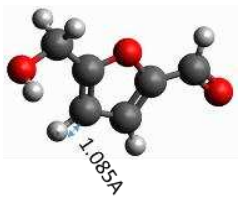	**HMF** (most stable), showing the bonding length of C-H where degradation with the highest reaction energy (least endothermic) was obtained.

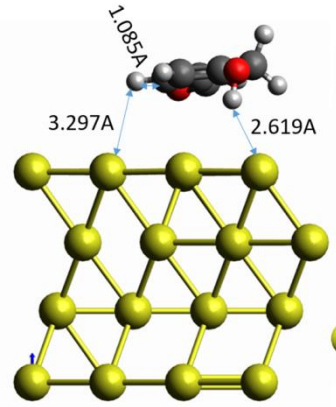 Side View 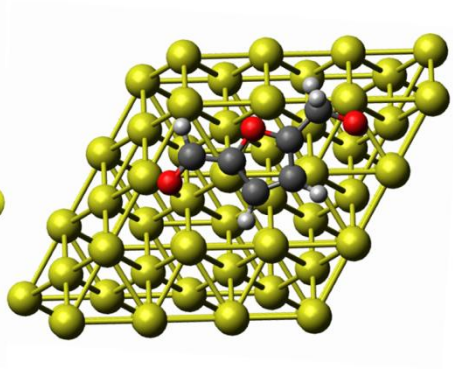 Top View	**xHMF** (most stable, before degradation) on Au(111) and important distances are displayed in the structure. It is the same as a component in step A in Figure 5- 11, excluding xOH.
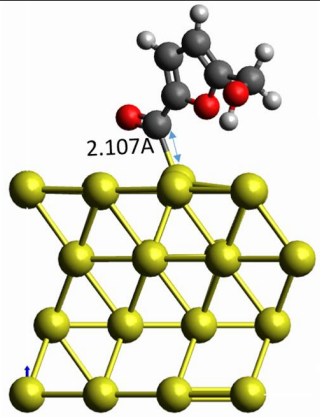 Side View 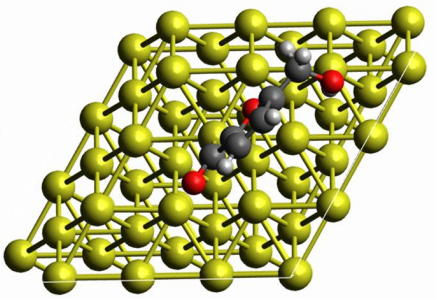 Top View	**xHMF oxidized product** (via H-C bond on the aldehyde) excluding surface water.
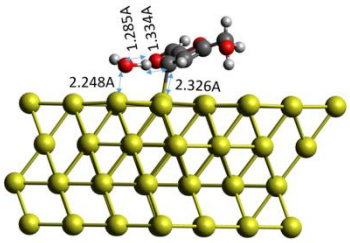 Side View 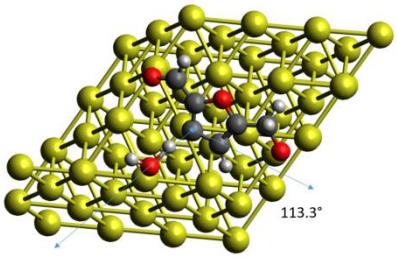 Top View	**TS for HMF degradation** (water@top), a case of when the degraded product is on TOP (most stable) and water (on TOP) on Au metal.
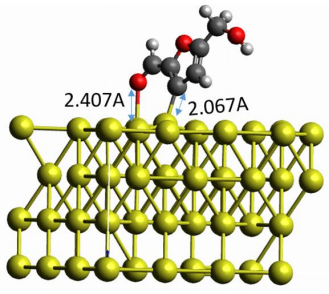 Side View 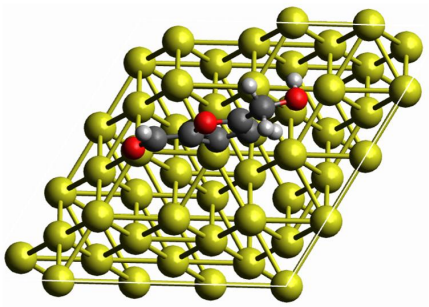 Top View	**xHMF** after degradation (via H-C bond on the furan ring) excluding surface water. It is also denoted as a component in step A in Figure 5- 11.

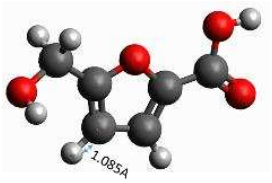	**HMFCA** (most stable), showing the bonding length of C-H where degradation with the highest reaction energy (least endothermic) was obtained.
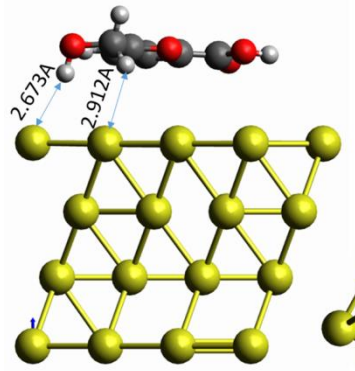 Side View 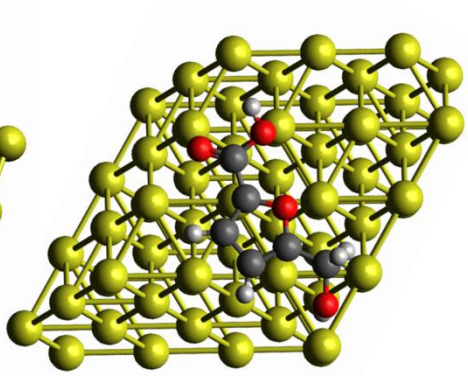 Top View	**xHMFCA** states before degradation (via H-C bond on the furan ring) excluding xOH. It is also denoted as a component in step A in Figure 5- 11.
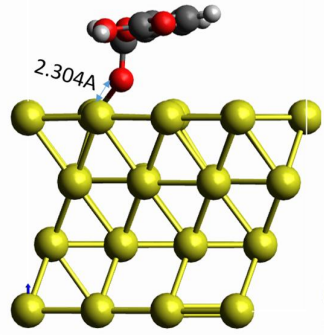 Side View 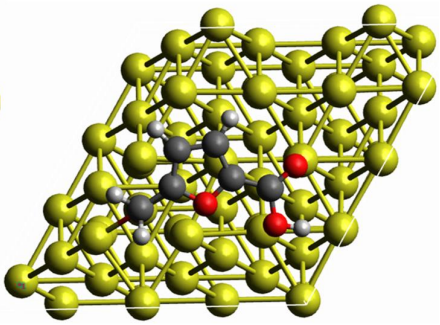 Top View	**xHMFCA oxidized product** (via H-O bond on the hydroxyl) excluding surface water .
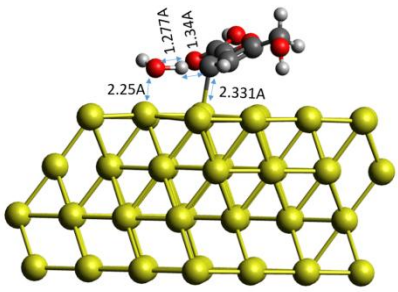 Side View 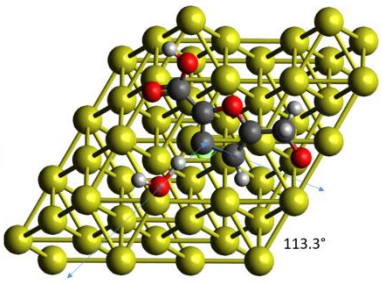 Top View	**TS for HMFCA degradation** (water@top), a case of when the degraded product is on TOP (most stable) and water (on TOP) on Au metal. The geometry displayed important distances in the structure.

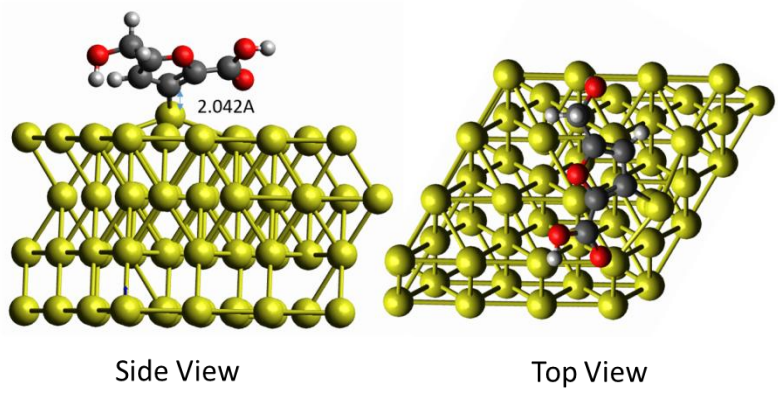	**xHMFCA degraded product** (via H-C bond on the furan ring) excluding surface water. It is also denoted as a component in step D in Figure 5- 11.

5.6.3 Reaction Expression for the Schemes Used in Evaluating Degradation Routes

This section presents a simplified reaction expression for the various degradation routes explored in our study. They are grouped into two, where the first was Table 5- 2, showing the degradation for HMF routes (during HMF oxidation to HMFCA).

Table 5- 2 *Scheme revealing possible degradation pathways in transforming HMF to HMFCA intermediates over Au catalyst. (Note that x is the catalyst slab/site, H is hydrogen, and R is the furan ring of the compounds).*

Category	Description	Reaction expression
Initial	Initial	xHMF+3*xOH+1*slab $xHOCH_2\_HRH\_HCO + 3xOH + x$
Oxidation	C-H (H-CO)	xHMF_deH_CO+xH_2O+1*slab+2*xOH $xHOCH_2\_HRH\_CO + xH_2O + 2xOH + x$
Degradation	C-H (H-RingCO(H))	xHMF_deH_ringCOH+xH_2O+1*slab+2*xOH $xHOCH_2\_HR\_HCO + xH_2O + 2xOH + x$

Degradation	C-H (H-RingCH_2OH)	xHMF_deH_ringCH_2OH+xH_2O+1*slab+2*xOH $xHOCH_2\_RH\_HCO + xH_2O + 2xOH + x$
Degradation	C-C (C-CO(H))	xHMF_CH_2OH+xCOH+3*xOH+0*slab $xHOCH_2\_HRH + xOCH + 3xOH$
Degradation	C-C (C-CH_2OH)	xHMF_COH+xCH_2OH+3*xOH+0*slab $x\_HRH\_HCO + xH_2COH + 3xOH$
Degradation	C-O (OpenRing)	xHMF_ringbreak+3*xOH+1*slab $xC_6H_6O_3 + 3xOH + x$
Degradation	Desorption HMF	HMF+3*xOH+2*slab $HOCH_2\_HRH\_HCO + 3xOH + 2x$

The second group in Table 5- 3 is the degradation routes evaluated for the HMFCA (during its oxidation into FFCA, which is expected to lead to FDCA) on Au (111).

Table 5- 3 *Scheme revealing possible degradation pathways in the transformation of HMFCA to FFCA-intermediates over Au catalyst. (Note that x is the catalyst slab/site, R is the furan ring of the compounds, and H is hydrogen).*

Category	**Description**	**Reaction expression**
Initial	Initial	xHMFCA+xOH+2*slab+xH_2O $xHOCH_2\_HRH\_COOH + xH_2O + xOH + 2x$
Oxidation	O-H (CH_2O-H)	xHMFCA_deH_CH_2O+2*xH_2O+2*slab $xOCH_2\_HRH\_COOH + 2xH_2O + 2x$

Degradation	O-H (COO-H)	xHMFCA_deH_COO+2*xH_2O+2*slab $xHOCH_2\_HRH\_COO + 2xH_2O + 2x$
Oxidation	C-H (H-CHOH)	xHMFCA_deH_CHOH+2*xH_2O+2*slab $xHOCH\_HRH\_COOH + 2xH_2O + 2x$
Degradation	C-H (H-RingCOOH)	xHMFCA_deH_ringCOOH+2*xH_2O+2*slab $xHOCH_2\_HR\_COOH + 2xH_2O + 2x$
Degradation	C-H (H-RingCH_2OH)	xHMFCA_deH_ringCH2OH+2*xH_2O+2*slab $xHOCH_2\_RH\_COOH + 2xH_2O + 2x$
Degradation	C-C (C-CH_2OH)	xHMFCA_COOH+xCH_2OH+xOH+1*slab+xH_2O $x\_HRH\_COOH + xH_2COH + xH_2O + xOH + 1x$
Degradation	C-C (C-COOH)	xHMFCA_CH_2OH+xCOOH+xOH+1*slab+xH_2O $xHOCH_2\_HRH + xCOOH + xH_2O + xOH + 1x$
Degradation	C-O (OpenRing)	xHMFCA_ringbreak+xOH+2*slab+xH_2O $xC_6H_6O_4 + xH_2O + xOH + 2x$
Degradation	Desorption HMFCA	HMFCA+xOH+3*slab+xH_2O $HOCH_2\_HRH\_COOH + xH_2O + 3x$
Degradation	C-H (H-CO, reverse)	xHMF_deH_CO+2*xOH+1*slab+xH_2O $xHOCH_2\_HRH\_CO + xH_2O + 2xOH + 1x$

Exploring Strategies for Re-Designing Au Catalyst for the Retardation of Degradation Rate in FDCA Synthesis

6 Exploring Strategies for Re-designing Au Catalyst for the Retardation of Degradation Rate in FDCA Synthesis

Chapter 6 Exploring Strategies for Re-designing Au Catalyst for the Retardation of Degradation Rate in FDCA Synthesis

6.1 Overview

The preceding chapter (Chapter 5) has unraveled the pathways promoting the degradation activities on the Au surface during the production of FDCA from HMF. The affected stages of the production (or synthesis) include the conversion of the HMFCA intermediate into HMFCA, FFCA into FDCA intermediate, and the desorption of FDCA. These affected stages have been reported to favor the production of HMF carboxylate, CO and small furan compounds, and FFCA carboxylate on Au, respectively.

It is, therefore, vital to computationally explore a range of strategies for redesigning the Au catalyst structure to aid in retarding the degradation activity on it. Here, we present the report of our findings for the exploration of the alloying effect on Au performance in retarding the degradation activity.

6.2 Computational Methodology

In the study, we investigated the viability of oxidizing water to yield hydroxyl (xOH) on new metals such as Pd(111) and Pt(111), similar to that of Au (111) using their Gibbs reaction energy (whose details are presented in Chapter 3) to understand if it would favor the oxidation of HMF into FDCA on the respective slabs. Moreover, the peculiar specifications for this chapter include the 4x4 atoms supercell used as its slab in the study with four layers (Au-Au, Pd-Pd, and Pt-Pt inter-atomic distances of 2.93, 2.80, and 2.81 Å, respectively). The 2D Brillouin zone integration was performed at the

gamma point. The total height of the periodic supercell was set at 23.92 Å, which takes 70 % of the supercell height to be a vacuum above the metal slab. Other generic computational details are presented in Chapter 3.

To gain insight for re-designing Au catalyst, we explore the feasibility of a singe-atom alloy (i.e., bimetallic) system approach in redesigning Au for improved performance. The Au-alloy system was modeled to have a ratio of 63:1 for the Au to the new metal. The selected new metals include platinum (Pt) and palladium (Pd). The study sampled different atom positions (that is, 16 positions) of the top layer of the Au slab in the study. An illustration of the slab is shown in Figure 6- 1 with the new metals in one of the positions evaluated on the top layer of the slab.

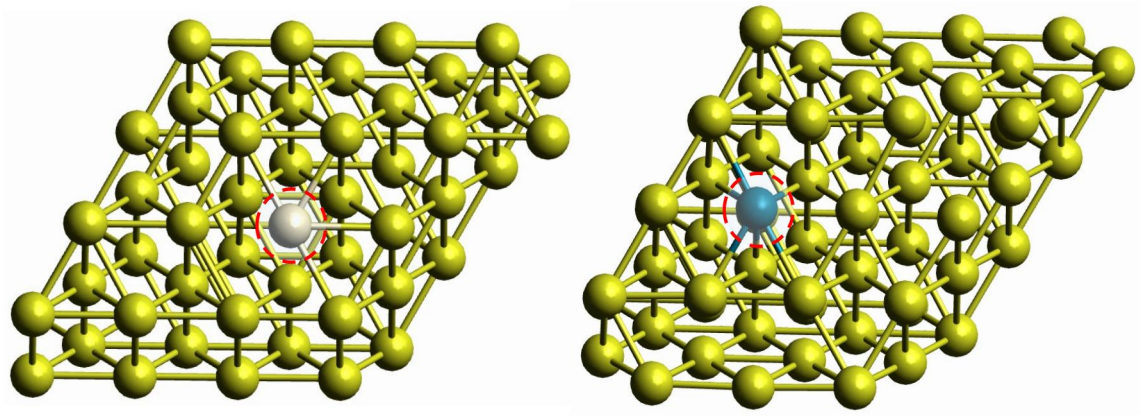

Figure 6- 1 *An illustration of the singe-atom alloy (111) slab, where the left image is the AuPt and the right image is the AuPd. The Au, Pt, and Pd are colored gold, milky-like, and blue, respectively, showing the top view of the structure. Note that the yellow atom is Au, gray atom is Pt, and blue atom is Pd; the broken line circle is indicate where Au was substituted with a new metal. The new metals (the promoters) are substituting a top Au atom of the Au (111) slab.*

The position with the most stable structure was the optimum for any concerned case or specie. We deployed the DFT method in the study using the computational details earlier presented in Chapter 5 for FDCA synthesis on Au. Energies computed were used to gain insight into the ease of the degradation activity on the various alloys using their reaction energies.

6.3 Results and Discussions

Here, we present the results obtained for our investigation of the impact of different metals (Pd and Pt) on the oxidation of water to yield hydroxyl (xOH) to ascertain the viability of the slab for the hydroxyl (xOH) production for the HMF oxidation process. Other analyses reported in this section include the HMF oxidation reaction mechanism and energy profiles simulated over Pd (111) and Pt (111). The findings made are also compared with Au(111). Desorption profiles for the various slabs (Au, Pd, and Pt) were also analyzed, as well as the alloying effect on the stability of the degradation product on the Au-based slab.

6.3.1 Influence of the metals in the oxidation of water to yield xOH: Au, Pd, and Pt

Here, we evaluated the impact of the Pd (111) and Pt (111) relative to Au (111) on the catalysis of the water oxidation for the formation of hydroxyl (xOH) on the respective slabs. The strategy presented in Figure 6-2 was deployed to understand the significance of the water present in the oxidation of the HMF on other metals (Pd and Pt) relative to Au (111), which has earlier been evaluated in Chapter 4.

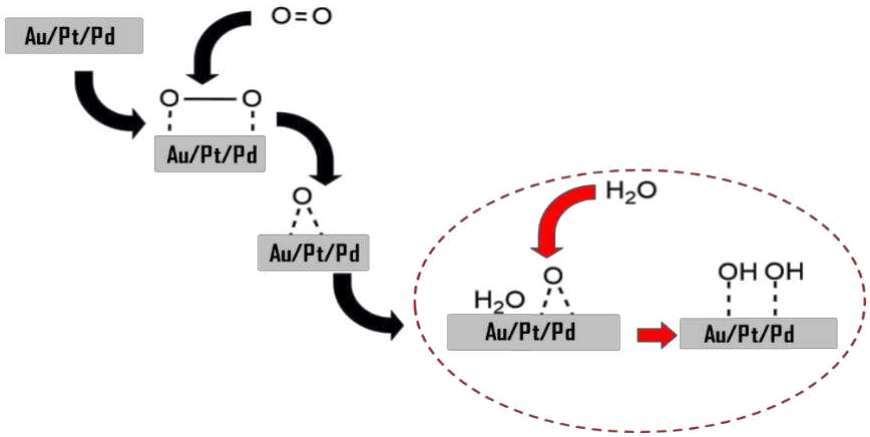

Figure 6-2 Strategy deployed in the analysis of water oxidation to yield hydroxyl (xOH) across different M(111) slabs (M = Au, Pd, and Pt). Note that the red circle indicates the aspect the analysis focused on (i.e., the feasibility of xOH formation on the slabs.

The result obtained from the analysis is presented in Figure 6-3, where it was shown that the oxidation of the water into xOH on Au (111) was found to be exothermic. In contrast, other slabs like Pd (111) and Pt (111) showed positive reaction energies. This

implies that the oxidation of the water molecule into xOH on Pd (111) and Pt (111) would be highly endergonic, while Au (111) is exergonic.

Our study reveals that the oxidation of HMF in the absence of water participation would be more favorable on Pd (111) and Pt (111). Unlike Au (111), which would be more favorable with the participation of water in oxidation process. The findings made for Au (111) in our study showed good agreement with a theoretical study by Liu [1] using PW19-GGA that reveals that shows a lower activation energy for the oxidation of water to '2xOH' (E_{act} = 0.46 eV [or 44.61 kJ/mol]) compared to 'xO+xH+xOH' (E_{act} = 2.65 eV [or 255.54 kJ/mol]). Similarly, a theoretical investigation carried out by Cao & Chen [2] using PW19-GGA agreed with our findings that confirm the impossibility or difficulty of oxidizing water to yield surface hydroxyl (xOH) on Pd (111) due to its barrier (E_{act} = 0.3 eV) that is a bit high with endothermic reaction energy compared to the path leading to formation surface oxygen atom (xO) (E_{act} = 0.1 eV). This implies that even though we used different theoretical methods (PBE-GGA) in our study, a similar deduction was reached for the viability of the process on Au (111) and Pd (111).

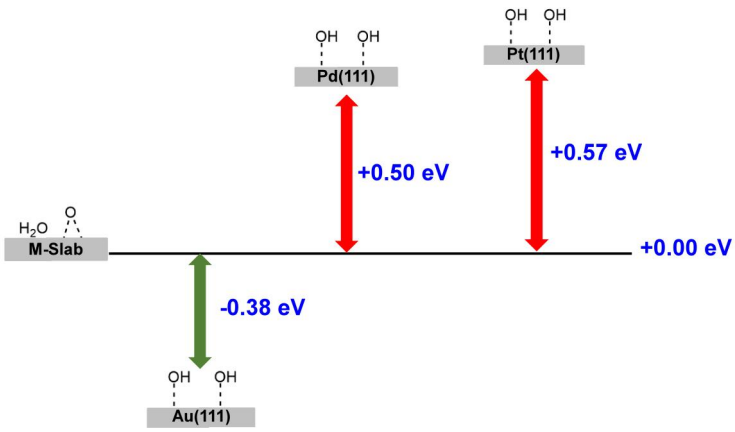

Figure 6-3 The Gibbs energy profile of water oxidation for hydroxyl (xOH) production. Note that the red arrow indicates the endothermic (unfavorable route), while the green arrow is the exothermic (favorable) route at 1 bar and 110 °C. M is the generic form of the slabs for Au, Pd, and Pt.

A further survey of existing report of Gu et al.[3] and other literature[4,5] on water oxidation on Pt (111) reveals that our deduction, which indicates that it is not feasible

on Pt (111) to yield xOH, showed good agreement with other literature. One of the literature includes a theoretical study (using PBE-GGA) by Ungerer et al.[5], which reveals that the molecular adsorption of water was more viable for Pt (111), unlike Pt (001) which adsorbed water dissociatively. This implies that Pt (111) did not favor the dissociation of water on its slab, unlike Pd (111). In agreement with our study findings, the work of Kiskinova et al.[4] also confirms the difficulty of oxidizing or dissociating water on Pt (111), and the author suggests the introduction of K to the Pt slab as a promoter to ease the generation of surface hydroxyl (xOH).

6.3.2 Analysis of the HMF oxidation mechanism on other metals: Pd and Pt

In line with the findings made in Section 6.3.1, where the participation of water in the oxidation of HMF on Pd and Pt were confirmed unfavorable. We find it essential to understand their own oxidation mechanism without the participation of water. This implies the activation of oxygen to surface oxygen atom (xO) unlike the case of Au(111) where water is participates. The general HMF oxidation mechanism employed in the analysis of the Pd(111) and Pt (111) slab without the participation of water is pictorially displayed in Figure 6- 4.

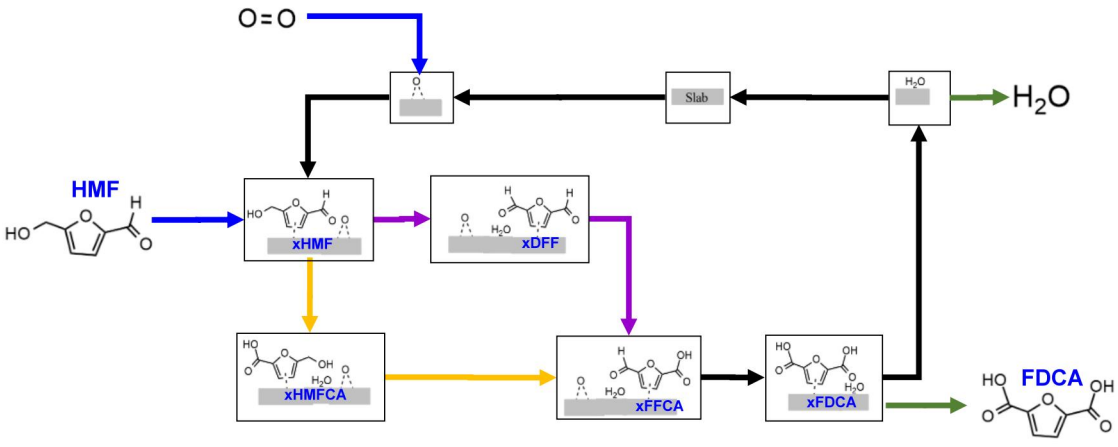

Figure 6- 4 A Simplified reaction mechanism for HMF oxidation on Pd(111) and Pt(111). Note that the line with purple is the hydroxyl oxidation pathway, yellow is the aldehyde oxidation pathway, blue is the adsorption pathway, green is the desorption pathway, and black is the other conversion processes. All surface species are singly mono-adsorbed (not co-adsorbed) on a slab.

The oxidation of HMF is initiated with the activation of oxygen gas to form surface oxygen atoms (xO). After which, HMF is adsorbed to the slab (111), and the adsorbed HMF (that is, xHMF) is then oxidized via the hydroxyl or aldehyde routes to yield xDFF (that is, adsorbed DFF) and xHMFCA (that is, adsorbed HMFCA), respectively. The intermediates (xDFF and xHMFCA) obtained via either route would then be further oxidized to yield xFFCA (that is, the adsorbed FFCA). The later steps include the oxidation of xFFCA to produce xFDCA with water formation and, lastly, the desorption of FDCA and water from the slab (111).

6.3.2.1 Analysis of the reaction energy profile for HMF oxidation mechanism Pd (111)

The analysis of the Gibbs reaction energy profiles (in Figure 6- 5) for the oxidation of HMF to FDCA on Pd (111) oxidation mechanism employed for the analysis of the Pd(111) with the reaction mechanism presented in Figure 6- 4 shows that all the elementary steps involved in this oxidation reaction were all exergonic exception of the FDCA desorption steps which was slightly endergonic. The exergonic nature of the various elementary reaction steps in the oxidation further reveals that the oxidation of HMF without the generation of xOH would be feasible, which agrees with the literature [2] which reports the infeasibility of oxidizing water on Pd (111) to yield surface hydroxyl (xOH).

Moreover, the trend of the Gibbs reaction energies, G_{rxn} for the elementary steps were in the order of O_2 to xO (-1.92 eV) > xHMF to xHMFCA (-1.53 eV) > xFFCA to xFDCA (-1.50 eV) > xDFF to xFFCA (-1.45 eV) > xHMF to xDFF (-0.87 eV) > xHMFCA to xFFCA (-0.79 eV) > HMF to xHMF (-0.50 eV) > xFDCA to FDCA (0.12 eV), according to the Figure 6- 5. The analysis reveals that the FDCA desorption showed the highest reaction energy, while the oxygen activation showed the least in general. The reaction energy indicates oxygen activation is highly spontaneous relative to other steps. It was easier to activate oxygen without water on Pd (111) than on Au (111).

The study further confirms the oxidation of the HMF via the aldehyde (xHMF to xHMFCA, G_{rxn} = -1.53 eV) route to be thermodynamically feasible compared to the hydroxyl (xHMF to xDFF, G_{rxn} = -0.87 eV) route due to the higher reaction energy obtained for the aldehyde routes. This implies that the HMF oxidation on Pd (111) would proceed via the aldehyde route to yield xHMFCA, followed by other later steps on its slab. The route confirmed in our study was found to agree with the experimental report of Davis et al.[6] and Sanabria et al.[7] which shows insignificant DFF selectivity and higher selectivity for HMFCA in their results in the presence of Pd/AC[6] and PdCl/AC[7], respectively.

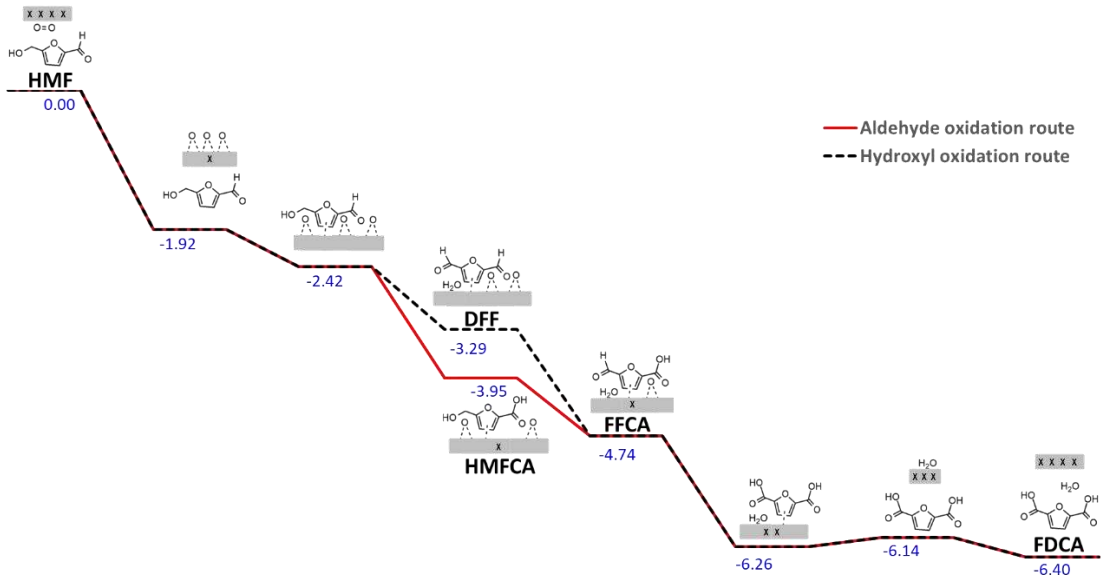

Figure 6- 5 Gibbs reaction energy profile (in eV) for the oxidation of HMF on Pd (111) at 1 bar and 110°C. Note that the straight line is the hydroxyl oxidation pathway (i.e., HMFCA route), and the broken line is the aldehyde oxidation pathway (i.e., DFF route). X represents the number of empty slabs modeled in the analysis. All surface species are singly mono-adsorbed (not co-adsorbed) on a slab.

In the exception of the adsorption, oxygen activation, desorption, and hydroxyl oxidation (xHMF to xDFF) routes, the trend of the surface reaction would be in the order of xHMF to xHMFCA (G_{rxn} = -1.53 eV) > xFFCA to xFDCA (G_{rxn} = -1.50 eV) > xHMFCA to xFFCA (G_{rxn} = -0.79 eV). The trend order indicates that oxidation of xHMF to xHMFCA was the easiest step while xHMFCA to xFFCA is the most difficult. In other words, the oxidation of HMFCA is said to be the slowest while HMF oxidation is the

fastest, which implies that the step oxidizing HMFCA to FFCA could be the rate-determining step (RDS) for the oxidation process, being the step with the lowest reaction energy (G_{rxn} = -0.79 eV). The higher yield and selectivity accounted for HMFCA for the use of Pd/AC, and PdCl/AC in the oxidation of HMF to FDCA in the experimental report by Davis et al.[6] and Sanabria et al.[7] confirms the conversion of alcohol function of HMFCA to aldehyde in FFCA happened at the slowest rate (rate-determining step) compared to other conversion steps in their experiment. This implies that the step is responsible for the low yield of FDCA in their studies and can be said to be RDS in their investigation, which agrees with our deductions. Our study shows that its was more easier to oxidize aldehyde function (that is, aldehyde function of xHMF to carboxylic acid in xHMFCA) than alcohol function oxidation (that is, alcohol function of xHMFCA to aldehyde in xFFCA) on Pd(111).

6.3.2.2 Analysis of the reaction energy profile for HMF oxidation mechanism Pt (111)

We further analyzed the reaction energy profile collated for Pt (111) use in Figure 6- 6, where all the elementary steps presented were largely spontaneous, excluding the oxidation of HMFCA's alcohol function to carboxylic acid in FFCA and desorption of FDCA, which is less spontaneous. The results indicate that the oxidation of HMFCA to FFCA and FDCA desorption would be slow during the oxidation catalytic cycle on Pt (111). Similar deductions have been made for the FDCA desorption on Pd (111), indicating that it was also less spontaneous but more spontaneous on Au (111). The viability or ease of desorbing FDCA from Pd and Pt can also be improved with the engineering of the surface reaction entropy and temperature, TdS.

Further analysis of the various oxidation routes presented in Figure 6- 6 confirms that the aldehyde oxidation route (G_{rxn} = -2.15 eV) would be more feasible compared to the hydroxyl oxidation route (G_{rxn} = -0.77 eV) due the stability and exergonicity of the aldehyde oxidation routes. The deduction was similar to the findings made for Au

(111) and Pd (111) in this study, which indicates the reaction would proceed from xHMF to xHMFCA, then xHMFCA to xFFCA. In an experimental study by Davis et al.[6], their findings show a good agreement with our deduction for the reaction route, showing insignificant selectivity for DFF evolution and higher selectivity for HMFCA in the presence of Pt-supported by activated carbon. Similar to the report of Sanabria et al.[7] (using PtCl/AC) and Da Silva et al.[8] (using Pt/ZrO_2), which also showed higher selectivity for the aldehyde (HMFCA) oxidation route with insignificant selectivity of the hydroxyl (DFF) route.

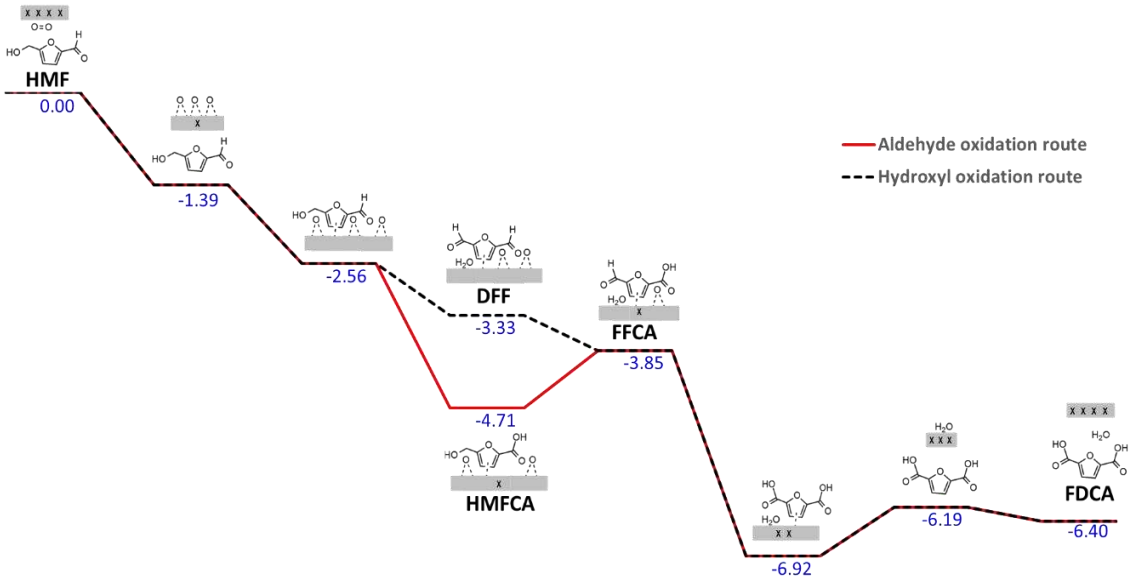

Figure 6- 6 *Gibbs reaction energy profile (in eV) for the oxidation of HMF on Pt (111) at 1 bar and 110°C. Note that the straight line is the hydroxyl oxidation pathway (i.e., HMFCA route), and the broken line is the aldehyde oxidation pathway (i.e., DFF route). X represents the number of empty slabs modeled in the analysis. All surface species are singly mono-adsorbed (not co-adsorbed) on a slab.*

Excluding the adsorption, desorption, oxygen activation, and hydroxyl oxidation (xHMF to xDFF) routes, the order of the reaction energies was found to have followed the trend: xFFCA [aldehyde] to xFDCA [carboxylic acid] (G_{rxn} = -3.07 eV) > xHMF [aldehyde] to xHMFCA [carboxylic acid] (G_{rxn} = -2.15 eV) > xHMFCA [alcohol] to xFFCA [aldehyde] (G_{rxn} = 0.86 eV). In our study, we assume that the reaction kinetics followed the same pattern as the reaction energies. The trend order indicates that oxidation of xFFCA [aldehyde] to xFDCA [carboxylic acid] was the fastest reaction step,

while xHMFCA [alcohol] to xFFCA [aldehyde] is the slowest and most difficult. The findings made imply that the step oxidizing alcohol function of HMFCA to carboxylic acid in FFCA on Pt (111) could be the rate-determining step (RDS) for the oxidation process, due to the lowest reaction energy (G_{rxn} = -0.79 eV) accounted for the reaction step, which agreed with the experiment in the literature[6–8]. The report from Da Silva et al.[8] further demonstrated how using a basic environment could help speed up the RDS of the HMF oxidation to yield more FDCA. And thermodynamic sink shown in the energy profile for the oxidation of the HMF to HMFCA and HMFCA to FFCA on Pt (111) could possible lead to deactivation due to the endothermic nature of the path oxidizing the HMFCA's alcohol function to aldehyde function in FFCA.

6.3.2.3 Comparative analysis of the HMF oxidation across the metals

The comparative analysis of the oxidation energy profile across all the metal slabs reveals that HMFCA was generally more stable than DFF. The oxidation of HMF via the aldehyde routes was generally more exergonic than the hydroxyl oxidation route, which agreed with the experimental reports of Davis et al.[6] and Sanabria et al.[7]

Analysis of the energy profiles reveals that the oxidizing alcohol function of xHMFCA to aldehyde in xFFCA was found to be the slowest step across all the metal slabs like Pt (111) and Pd (111) in this Chapter and Au (111) in Chapter 5. However, the fastest steps in the oxidation mechanism across the metal slabs were found to be the oxidation of FFCA (xFFCA to xFDCA) on Au (111), HMF (xHMF to xHMFCA) on Pd (111), and FFCA (xFFCA to xFDCA) on Pt (111). It is, therefore, essential to engineer ways of improving the rate of the oxidizing HMFCA into FFCA on metal slabs.

6.3.3 Impact of Alloying Effect on Oxidation and Degradation Intensity

In this section, we try to explore the influence or impact of alloying Au(111) with a single new metal. From this, three different cases of catalysts were modeled. The cases (that is, single-atom alloy metals) include AuAu(111) (which is the same as

Au(111) in the previous Chapter as a pure form of Au catalyst), AuPd(111), and AuPt(111). Each of the case's impacts was evaluated in the selectivity of oxidation/degradation of HMF and HMFCA to gain insight into redesigning Au-based catalysts to retard or avert the activities of degradation routes. In this analysis, we assume that oxidation of the HMF on AuX(111) alloys (where X = Au, Pd, Pt) would be feasible with the participation of water to have hydroxyl (xOH) on the slab. This was due to the large proportion of Au on the alloy slab (Au:X is 63:1), and Au oxidizes best in with water participation unlike other metals.

6.3.3.1 HMF oxidation and degradation

Here, we explored the influence of alloying the Au with a new single metal atom on the pathway identified for the degradation of HMF and HMFCA on Au (111) in Chapter 5. The study unraveled the impact of the single-atom alloy cases on the Au selectivity for the oxidation route leading to the formation of FDCA. In the study, we deployed a ratio of 63:1 for Au metals to the new ones in modeling our single-atom alloy cases. For each case of the alloy systems explored, the most stable position for the new metal on the topmost layer was identified and used for analysis. The results collected from the study are presented in Figure 6- 7.

The selectivity of the Au-based alloys for the oxidation activities was found to be in the order of AuPt(111) > AuPd(111) > AuAu(111) using $G_{Rxn/Oxid}$, and degradation activities was in the order of AuAu(111) > AuPd(111) > AuPt(111) using $G_{Rxn/Degrad}$. The study reveals that the degradation of HMF would be less on AuAu(111) compared to other forms of its alloy, while the oxidation of HMF on the AuPd(111) and AuPt(111) would be more rapid compared to its pure form (Au).

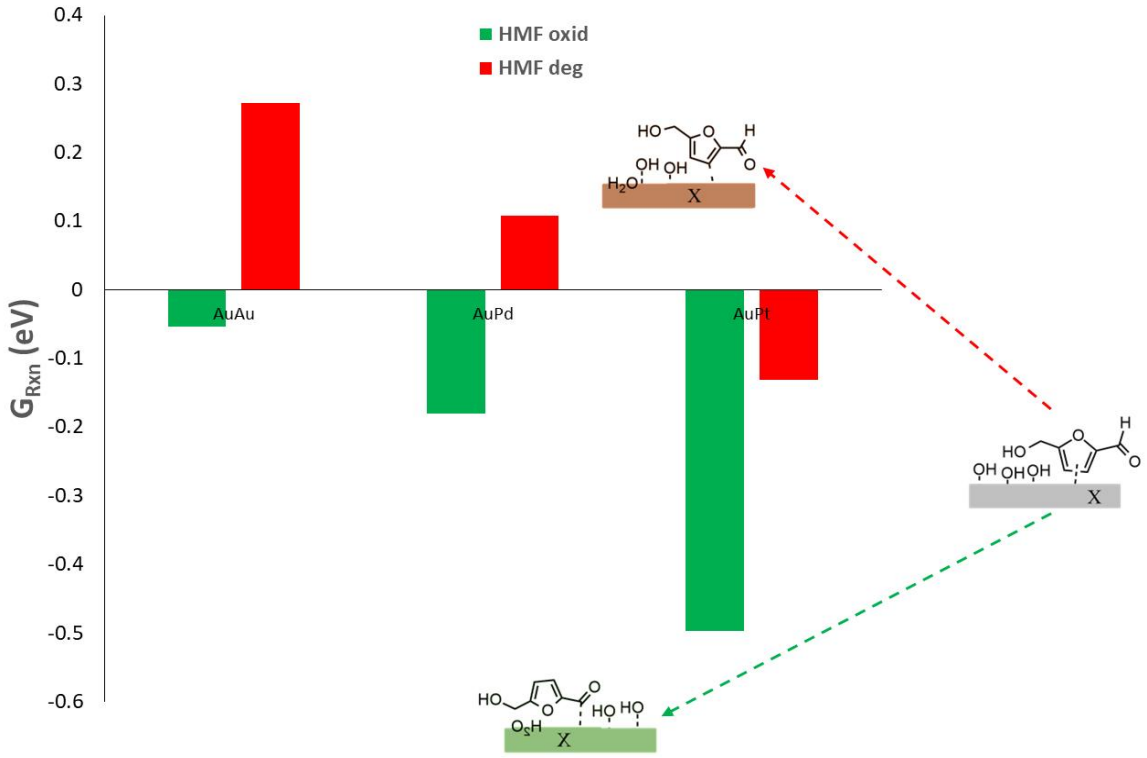

Figure 6- 7 Influence of the alloying effect on the HMF degradation and oxidation activity, computed at 110 ºC and 1 bar. The GREEN bars stand for Gibbs reaction energies for oxidizing HMF's aldehyde functional group and the RED bars stand for Gibb reaction energies for degrading HMF via the C-H bond of the furan ring on AuAu(111), AuPd(111), and AuPt(111). All surface species are singly mono-adsorbed (not co-adsorbed) on a slab.

Moreover, the evaluation of the route stability (that is, reaction energy gap for routes) was found to be in the order of AuPd(111) < AuAu(111) < AuPt(111) using $G_{Rxn/Degrad} - G_{Rxn/Oxid}$. The analysis of oxidation activity intensity relative to the degradation activities (that is, $G_{Rxn/Degrad} - G_{Rxn/Oxid}$) confirms AuPt(111) as one with the least viable degradation activities due to the wide reaction energy gap obtained for two routes in Figure 6- 7, where oxidation route was largely exothermic while degradation was much lesser. The higher exothermic route for HMF oxidation activity shown relative to the degradation route indicates a significant rise in AuPt(111) selectivity for producing FDCA compared to undesired products, compared to others (AuAu(111) and AuPd(111)), which would aid in avoiding the carbon loss accounted for in the experiment[9].

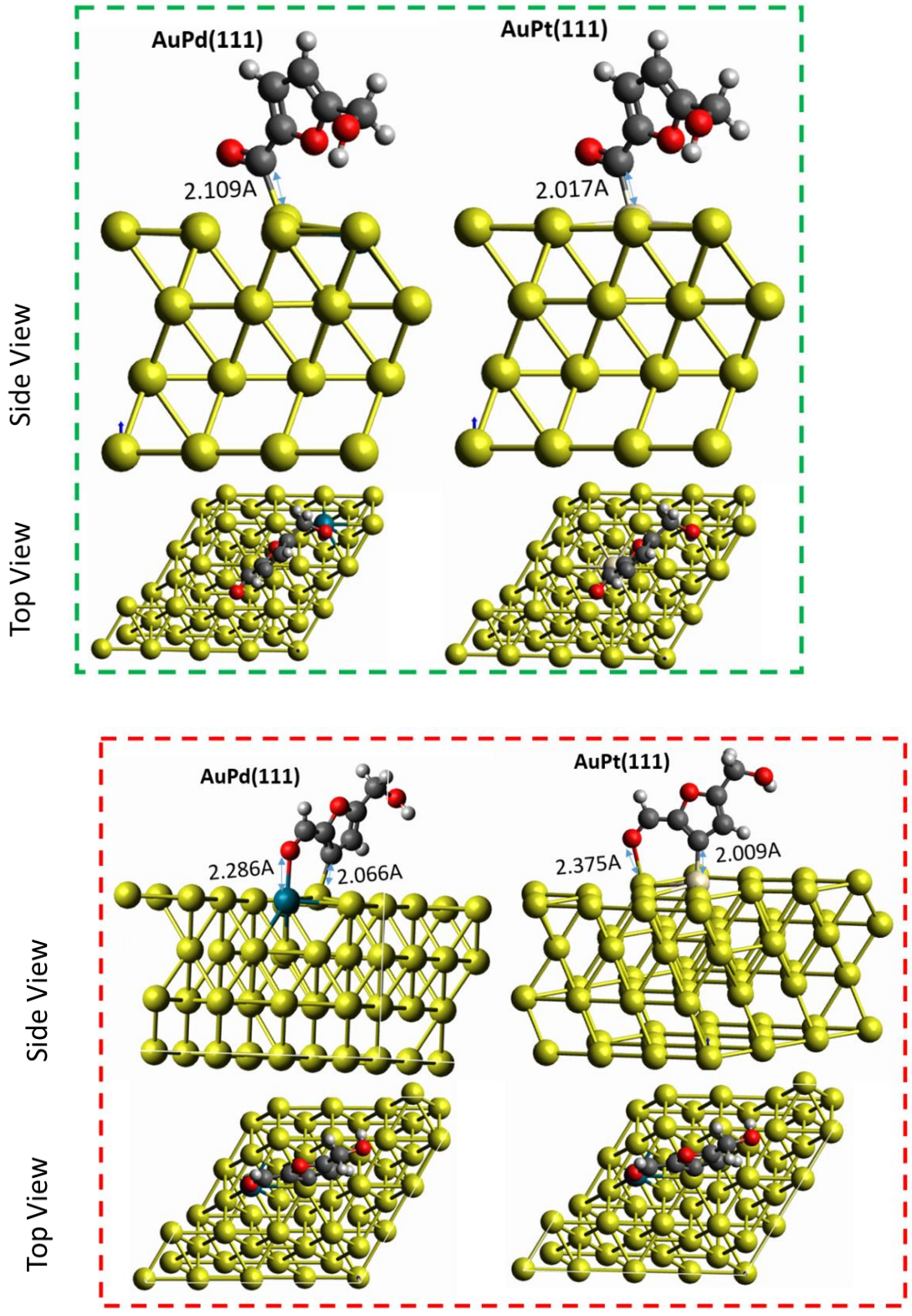

Figure 6-8 Structural geometry for the oxidized (GREEN) and degraded (RED) HMF species on the different slabs with important bond lengths. Note that the black atom is C, small while atom is H, yellow atom is Au, gray atom is Pt, and blue atom is Pd; the broken line circle is indicate where Au was substituted with a new metal. All surface species are singly mono-adsorbed (not co-adsorbed) on a slab.

Figure 6-8 further reveals that the HMF oxidized product strongly bonded on AuPt (111) than AuPd (111) due its shorter bond length (2.017 Å) with the AuPt (111) slab indicating the slab favoring more oxidation activity compared to AuPd(111). In a nutshell, the bond length for the alloys shows good agreement with their Gibbs reaction energies for the selectivity of HMF oxidation, whereas AuPt (111) shows the best selectivity for oxidation activity due to its shorter bond length (C-Au). Our prediction of AuPt alloying impact on the catalysis of HMF oxidation agreed with existing report of the use of the alloy in oxidation of other biomass derivatives like glucose[10] and others[11,12].

Analysis of the results in Figure 6-7 reveals the impact of the alloying effect on the selectivity of the Au catalyst for the promotion of the oxidation route and retardation of the degradation routes. The study reveals that the introduction of palladium (Pd) and platinum (Pt) improves the selectivity of the Au catalyst for oxidation activities better than its pure form. The Au alloy was predicted to have shown a higher selectivity for the oxidation activities, which aids in retarding the degradation activities.

6.3.3.2 HMFCA oxidation and degradation

The approach deployed for analysis of alloy impact on HMF in Section 6.3.3.1 (presented in its earlier paragraph) was similarly used for HMFCA. Findings made for the study of the alloying effect on the HMFCA, as shown in Figure 6-9. The ease of oxidizing HMFCA to FFCA was in the order of AuPd (111) > AuPt (111) > AuAu (111), and the ease of hindering degradation of HMFCA was found to be in the order of AuAu(111) > AuPd(111) > AuPt(111).

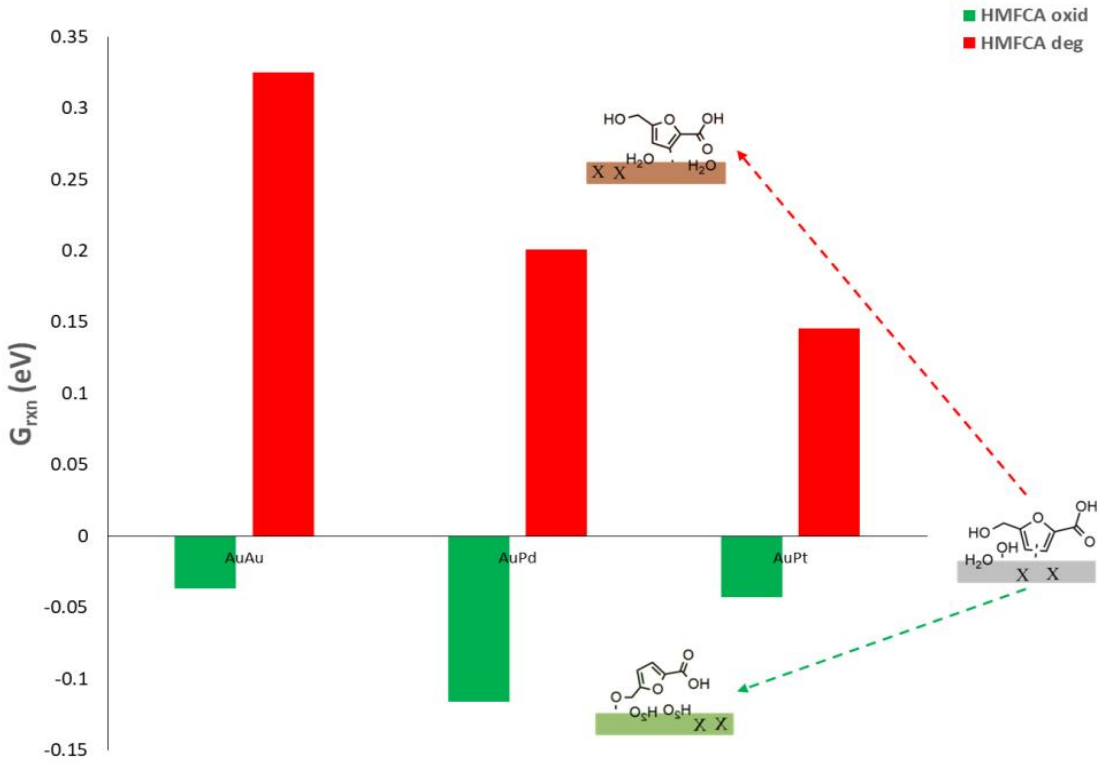

Figure 6- 9 The alloying effect on the HMFCA oxidation and degradation selectivity, computed at 110 ºC and 1 bar. The GREEN bars stand for Gibbs reaction energies for oxidizing HMFCA's alcohol functional group and the RED bars stand for Gibbs reaction energies for degrading HMF via the C-H bond of the furan ring on AuAu(111), AuPd(111), and AuPt(111). All surface species are singly mono-adsorbed (not co-adsorbed) on a slab.

The results indicate that the least endothermic degradation route for HMFCA was on AuPt(111), but AuAu(111) shows a better endothermic pathway for hindering the degradation activity. Although, our simulation for the AuAu(111) shows less exothermic reaction energy for HMFCA oxidation. Figure 6- 10 also indicates that the affinity of the HMFCA degraded product for AuPt(111) was stronger than AuPd(111) due to the short bond length (2.027 Å) obtained for AuPt alloy (especially at the C-Au bond, where the H was abstracted). The bond lengths obtained across the slab shows a good correlation with the Gibbs reaction energies on the alloy in Figure 6- 10. The findings were in good agreement with the literature[12] that shows adding Pd and Pt to Au improves the selectivity for oxidation activity.

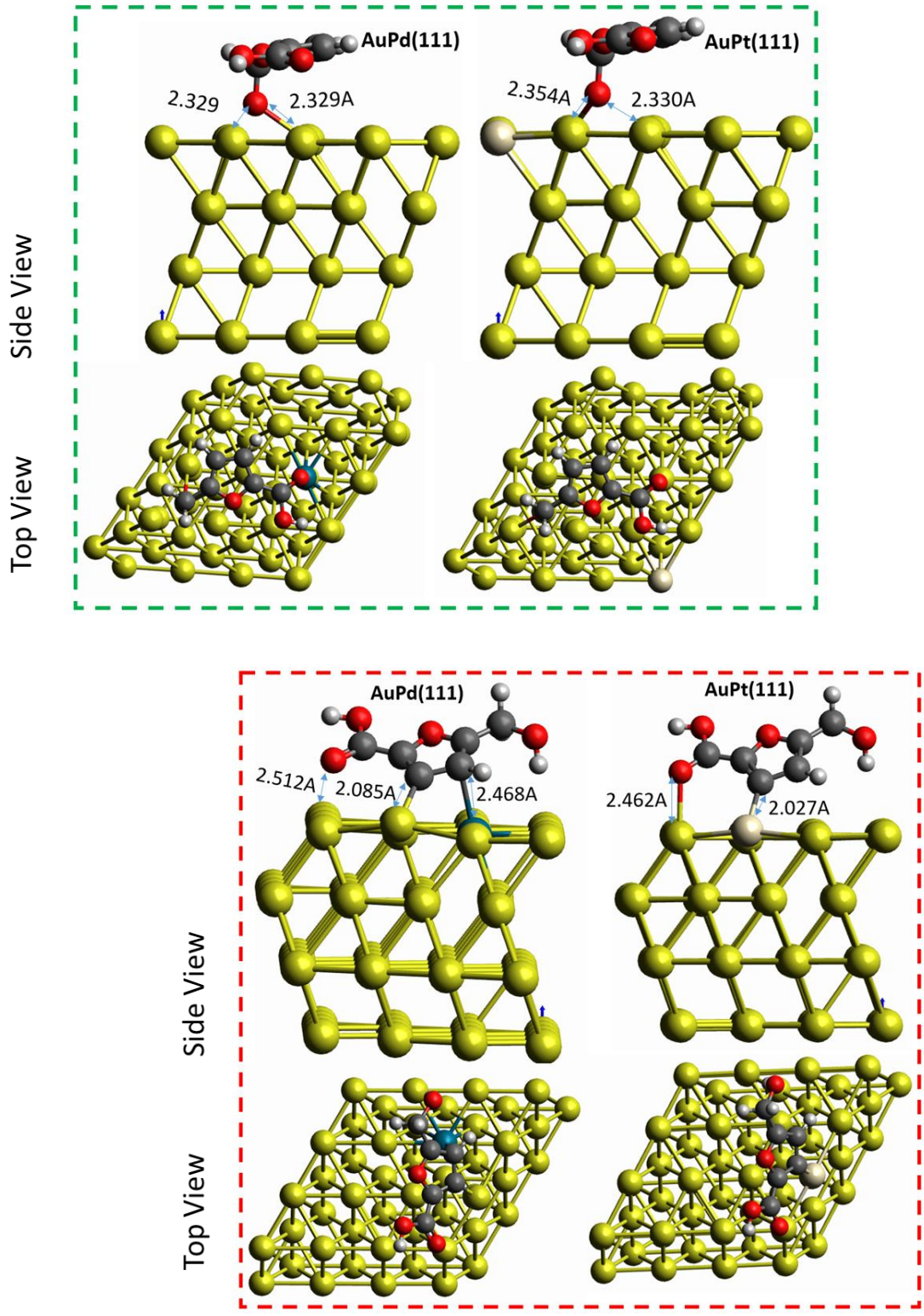

Figure 6- 10 Structural geometry for the degraded (in RED) and oxidized (in GREEN) HMFCA species on the different slabs with important bond lengths.Note that the black atom is C, small while atom is H, yellow atom is Au, gray atom is Pt, and blue atom is Pd; the broken line circle is indicate where Au was substituted with a new metal. All surface species are singly mono-adsorbed (not co-adsorbed) on a slab.

In a nutshell, the degradation of HMFCA is least feasible on AuAu (111) compared to other alloys. And the oxidation of HMFCA was found to be more exothermic on AuPd

(111) compared to AuAu (111) and AuPt (111). Although, the pure form and its alloys were all found to have shown an exothermic reaction energy for the oxidation of HMFCA on their slab.

6.3.3.3 Overall analysis of the AuAu(111), AuPd(111), and AuPt(111) on HMF and HMFCA

The unalloyed form of the Au (111) was found to have shown the least degradation route with better selectivity due to its wide reaction energy gab obtained for the use of AuAu(111), making it difficult for HMFCA degradation to override the oxidation activity unlike other alloys selectively. The study confirms a better selectivity for the HMFCA oxidation route compared to other alloys but shows a poor selectivity for the HMF oxidation route than its degradation compared to the other alloys.

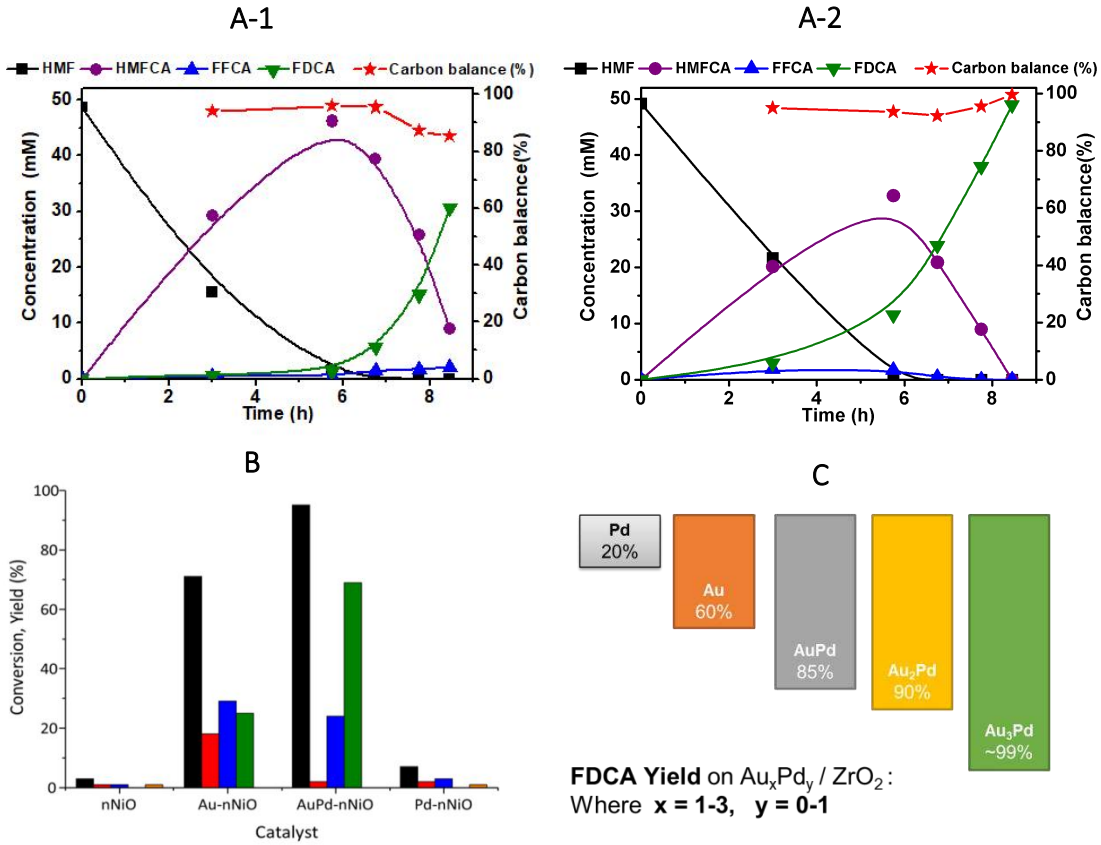

Figure 6- 11 (A)Experimental results of unalloyed (on A-1, Catalyst = 1wt% Au/ ZrO_2 SZ-61156: PVA:Au = 1.2) and alloyed Au (on A-2, Catalyst = 0.5wt% Au-0.5wt% Pd/ ZrO_2 SZ-61192) catalyst in HMF oxidation, accounting for the concentration of species (HMF, HMFCA, FFCA, and FDCA) yield with carbon balance carried out at the conditions ($P(air)_0$= 20 bar, $m_{Au/ZrO2}$ = 33 mg, n_{HMF}/n_{Au} = 500, $C_{0\,(HMF)}$ = 45 m M, n_{OH}/n_{HMF} = 3, T = 50°C for 7h, and latter change to T = 150°C) information [9]. (B) Another result for HMF oxidation on Au, AuPd and Pd catalyst supported on nNIO, collected at 90 °C, 10 bar O_2, 6 h, HMF/metal = 100, where BLACK is HMF conversion, RED is HMFCA yield, BLUE is FFCA yield, GREEN is FDCA yield, ORANGE is DFF, by Bonincontro et al.[14] (C) Our experimental partner's new results.

However, the alloying of the Au with Pd to form AuPd (111) was found to have improved the oxidation activity leading to the formation of FDCA with more degradation than the pure AuAu (111). The findings made implies that alloying the Au (111) with Pd would aid in improving the oxidation of HMFCA into FFCA, which has been proven to be difficult in our study and existing reports in the literature[6,8] due to its slower rate of conversion to FFCA. The findings agreed with our partner's experimental results[9] in Figure 6- 11A.

Other experimental works in the literature, like Wan et al.[13] (96% FDCA yield using AuPd/CNT), and Bonincontro et al.[14] (95% FDCA yield using AuPd/nNiO in Figure 6- 11B), also agreed with our simulation prediction, which confirms that adding Pd to the Au results in an improved yield and selectivity for FDCA. This was due to the enhanced/accelerated activity of the HMFCA oxidation (that is, HMFCA to FFCA), which was the rate-determining step (RDS). And the small carbon losses shown in the species evolution plot in the experimental results collected by our partner[9] in Figure 6- 11 can be said to be a product of unhindered or un-eliminated degradation activities (which could be from either HMF or HMFCA). The RDS (HMFCA to FFCA) shown in our studies reveals that the unease path of converting HMFCA to FFCA relative to its desorption from Au(111) has resulted to the high of HMFCA seen in Figure 6- 11 for the experiments (using Au/ZrO_2 in A and Au/nNiO in B). In the two experiments, the alloying of Au(111) with Pd improves the conversion of HMFCA to FFCA (being the RDS) which improves the yield of FDCA in Figure 6- 11 using AuPd/ZrO_2 and AuPd/nNiO.

Our study further unravels that the introduction of Pt to Au (111) should significantly improved the selectivity of the catalyst for the formation of FDCA due to the highly significant reaction energy obtained for the oxidation of HMF compared to the degradation route, which was relative of much lower reaction energy. This highly

exothermic reaction energy obtained for the HMF oxidation activity would significantly render degradation activity (reported in Chapter 5 as the primary contributor to the carbon loss) less significant and competitive. Based on our prediction, the AuPt (111) is expected to improve the FDCA yield and selectivity, similar to how it influences glucose oxidation to favor tartaric acid selectively on AuPt/TiO_2 [10] and the oxidation of glycerol to favor glyceric acid production on AuPt/AC[15]. This implies that there would be a much better carbon balance and selectivity for the path leading to the production of FDCA. Adding Pt to Au showed a slight improvement in HMFCA oxidation activities.

6.4 Conclusions

A study of water oxidation to form hydroxyl was successfully carried out on Au (111), Pd (111), and Pt (111) using a DFT calculation. The study confirms that the water oxidation would not be favorable across all the metals investigated, except for the use of Au (111), which was favorable due to the exothermic reaction energy obtained for it. Moreover, the analysis reveals that oxidation of the HMF in the presence of water would not be energetically favorable for Pd (111) and Pt (111).

Further study of the HMF oxidation mechanism over Pd (111) and Pt (111) in the absence of water reveals that the oxidation of HMF across the two metals was initiated via the aldehyde oxidation route (also called the HMFCA route). Moreover, the slowest reaction step (also known as the most challenging step) was the oxidation of HMFCA (that is, xHMFCA to xFFCA) on both metals. The findings do agree with the existing experimental reports.

The prediction for AuPt (111) reveals that the degradation activity was significantly slower in the oxidation of HMF than in the oxidation of HMFCA. On the other hand, the effect of AuPd (111) to slow down degradation was stronger when HMFCA was

oxidized than when HMF was, but not as strong as AuPt (111) for HMF. However, adding Pt to Au (111) significantly improves the selectivity of Au for HMF oxidation activity better than it does for HMFCA oxidation activity. In comparison, the introduction of Pd resulted in enhanced activity for the oxidation of HMFCA compared to HMF. Although, the intensity (or exothermicity) of the oxidizing HMF (on AuPt) was found to be largely more significant than that of the HMFCA (on AuPd).

Our results suggest that the Pt can be used to redesign the Au catalyst by alloying them to form a bimetallic (AuPt) alloy. The innovation is a strategy for retarding the rate of HMF degradation, which has been established in Chapter 5 of our study to have been intense relative to other routes. Alternatively, both Pt and Pd can be employed in redesigning the Au catalyst by alloying them to form a trimetallic (AuPtPd) alloy as another strategy for taking advantage of retarding HMF degradation, improving selectivity for HMF oxidation activity (via AuPt), improving HMFCA oxidation activity (via AuPd); and achieving lesser HMFCA degradation (via AuAu).

6.5 List of references cited

1. Liu, R. (2013). Adsorption and dissociation of H2O on Au(1 1 1) surface: A DFT study. *Computational and Theoretical Chemistry*, *1019*(1), 141–145. https://doi.org/10.1016/J.COMPTC.2013.07.009

2. Cao, Y., & Chen, Z. X. (2006). Theoretical studies on the adsorption and decomposition of H2O on Pd(1 1 1) surface. *Surface Science*, *600*(19), 4572–4583. https://doi.org/10.1016/J.SUSC.2006.07.028

3. Gu, Q., Sautet, P., & Michel, C. (2018). Unraveling the Role of Base and Catalyst Polarization in Alcohol Oxidation on Au and Pt in Water. *ACS Catalysis*, *8*(12), 11716–11721. https://doi.org/10.1021/ACSCATAL.8B03494/SUPPL_FILE/CS8B03494_SI_001.PDF

4. Kiskinova, M., Pirug, G., & Bonzel, H. P. (1985). Adsorption and decomposition of H2O on a K-covered Pt(111) surface. *Surface Science*, *150*(2), 319–338. https://doi.org/10.1016/0039-6028(85)90649-1

5. Ungerer, M. J., Santos-Carballal, D., Cadi-Essadek, A., van Sittert, C. G. C. E., & de Leeuw, N. H. (2019). Interaction of H2O with the Platinum Pt (001), (011), and (111) Surfaces: A Density Functional Theory Study with Long-Range Dispersion Corrections. *Journal of Physical Chemistry C*, *123*(45), 27465–27476. https://doi.org/10.1021/ACS.JPCC.9B06136/ASSET/IMAGES/LARGE/JP9B06136_0009.JPEG

6. Davis, S. E., Zope, B. N., & Davis, R. J. (2012). On the mechanism of selective oxidation of 5-hydroxymethylfurfural to 2,5-furandicarboxylic acid over supported Pt and Au catalysts. *Green Chemistry*, *14*(1), 143–147. https://doi.org/10.1039/C1GC16074E

7. Sanabria, L., Lederhos, C., Quiroga, M., Cubillos, J., Rojas, H., & Martinez, J. J. (2017). Pt y Pd soportado en carbón activado para la oxidación de 5-hidroximetilfurfural a ácido 2,5-furanodicarboxílico. *Ingenieria Y Competitividad*, *19*(2), 36–42. https://doi.org/10.25100/iyc.v19i2.5291

8. da Silva, E. D., Gonzalez, W. A., & Fraga, M. A. (2016). Aqueous-phase oxidation of 5-hydroxymethylfurfural over Pt/ZrO2 catalysts: Exploiting the alkalinity of the reaction medium and catalyst basicity. *Green Processing and Synthesis*, *5*(4), 353–364. https://doi.org/10.1515/GPS-2016-0010/MACHINEREADABLECITATION/RIS

9. Ferraz, C. P., & Wojcieszak, R. (2022). *Experimental Study of HMF Oxidation into FDCA over Gold-nanoparticle*.

10. Liu, M., Jin, X., Zhang, G., Xia, Q., Lai, L., Wang, J., Zhang, W., Sun, Y., Ding, J., Yan, H., & Yang, C. (2020). Bimetallic AuPt/TiO2Catalysts for Direct Oxidation of Glucose and Gluconic Acid to Tartaric Acid in the Presence of Molecular O2. *ACS Catalysis*, *10*(19), 10932–10945. https://doi.org/10.1021/ACSCATAL.0C02238/SUPPL_FILE/CS0C02238_SI_001.PDF

11. Hutchings, G. J. (2014). Selective oxidation using supported gold bimetallic and trimetallic nanoparticles. *Catalysis Today*, *238*, 69–73. https://doi.org/10.1016/J.CATTOD.2014.01.033

12. al Rawas, H. K., Ferraz, C. P., Thuriot-Roukos, J., Heyte, S., Wojcieszak, R., & Paul, S. (2021). Influence of Pd and Pt Promotion in Gold Based Bimetallic Catalysts on Selectivity Modulation in Furfural Base-Free Oxidation. *Catalysts*, *11*(10), 1226. https://doi.org/10.3390/CATAL11101226

13. Wan, X., Zhou, C., Chen, J., Deng, W., Zhang, Q., Yang, Y., & Wang, Y. (2014). Base-free aerobic oxidation of 5-hydroxymethyl-furfural to 2,5-furandicarboxylic acid in water catalyzed by functionalized carbon nanotube-supported au-pd alloy nanoparticles. *ACS Catalysis*, *4*(7), 2175–2185. https://doi.org/10.1021/CS5003096/SUPPL_FILE/CS5003096_SI_001.PDF

14. Bonincontro, D., Lolli, A., Villa, A., Prati, L., Dimitratos, N., Veith, G. M., Chinchilla, L. E., Botton, G. A., Cavani, F., & Albonetti, S. (2019). AuPd-nNiO as an effective catalyst for the base-free oxidation of HMF under mild reaction conditions. *Green Chemistry*, *21*(15), 4090–4099. https://doi.org/10.1039/C9GC01283D

15. Bianchi, C. L., Canton, P., Dimitratos, N., Porta, F., & Prati, L. (2005). Selective oxidation of glycerol with oxygen using mono and bimetallic catalysts based on Au, Pd and Pt metals. *Catalysis Today*, *102–103*, 203–212. https://doi.org/10.1016/J.CATTOD.2005.02.003

6.6 Supplementary Information for Chapter 6

6.6.1 Other Geometrical Structures for the Other Species in the Chapter's Studies

Table 6- 1 Geometrical Structure of the species in the Chapter's study. presenting the other structure not presented in the main chapter.

Table 6- 1 *Geometrical Structure of the species in the Chapter's study. Note that the black atom is C, small while atom is H, yellow atom is Au, gray atom is Pt, and blue atom is Pd.*

Geometrical Structure	Description
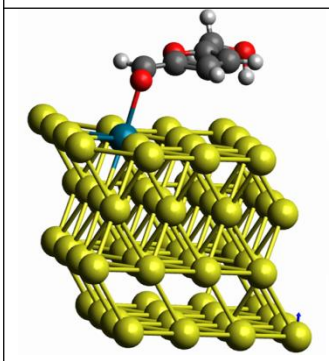 Side View 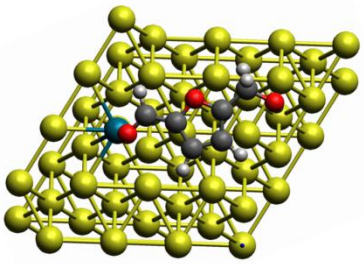 Top View	HMF adsorbed on AuPd(111)
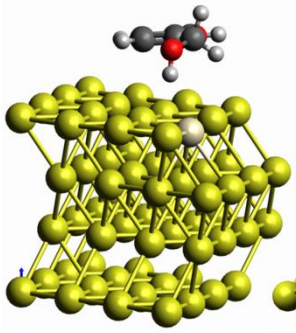 Side View 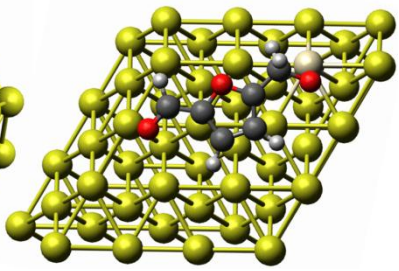 Top View	HMF adsorbed on AuPt(111)
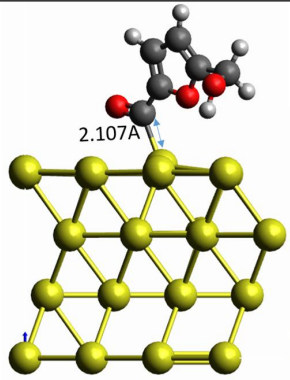 Side View 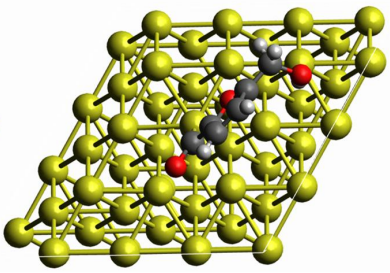 Top View	HMF Oxidization Intermediate Product on AuAu(111)

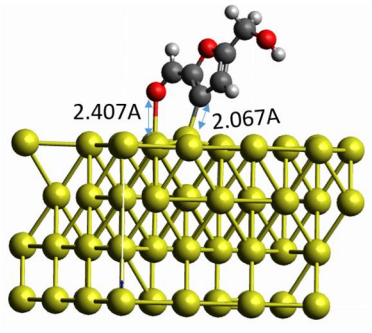 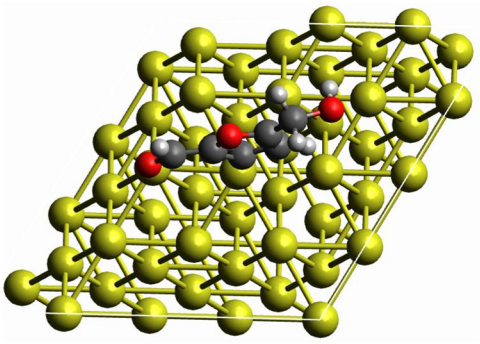 Side View Top View	HMF Degraded Intermediate on AuAu(111)
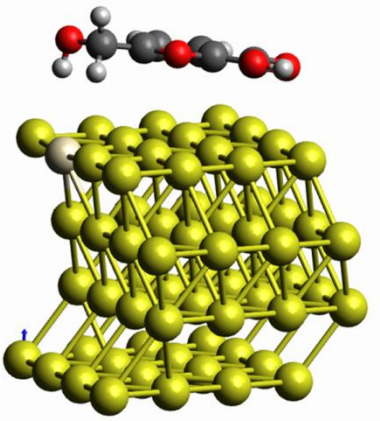 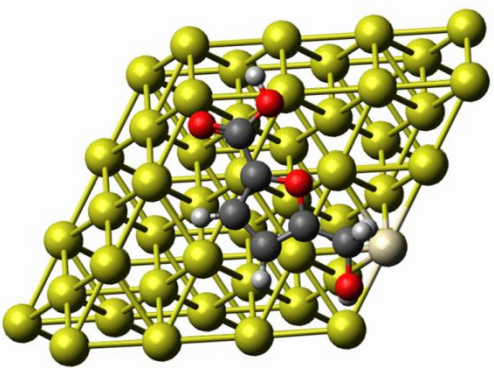 Side View Top View	HMFCA adsorbed on AuPt(111)
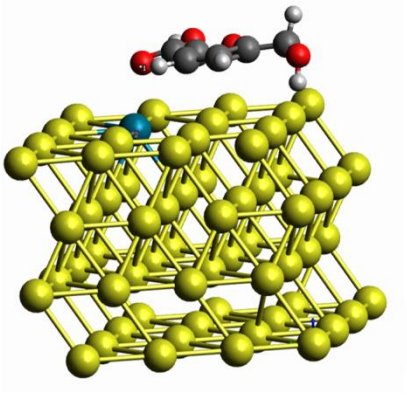 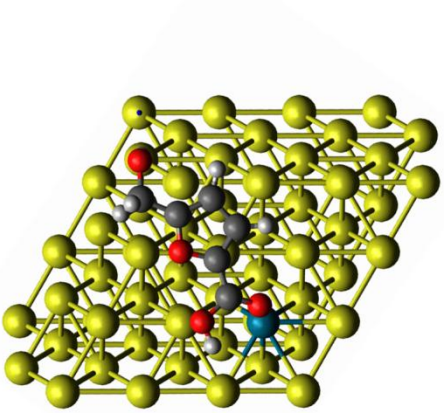 Side View Top View	HMFCA adsorbed on AuPd(111)

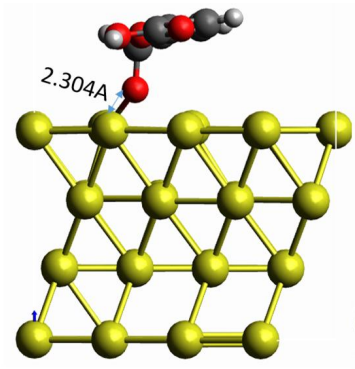 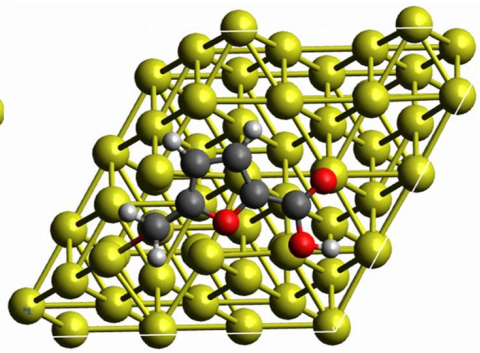 Side View Top View	HMFCA Oxidization Intermediate Product on AuAu(111)
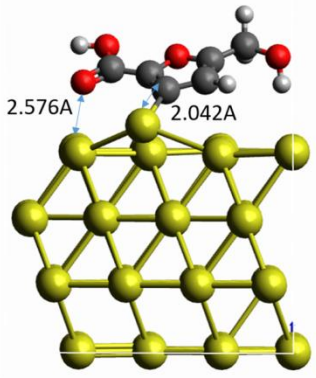 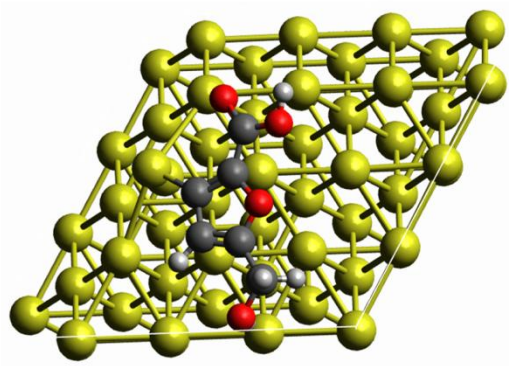 Side View Top View	HMFCA Degraded Intermediate on AuAu(111)

Summary & Further Studies

7 Summary & Further Studies

Chapter 7 Summary & Further Studies

7.1 Summary of Key Findings

This study successfully deployed the computational approach using periodic density functional theory (DFT) calculations in the simulation, analysis, and redesign of the catalyst for the prevention or retardation of degradation activities experimentally observed in the oxidation of furfural and HMF to FDCA over gold (Au). In addition, we successfully explored ways of engineering the performance of a gold (Au)-based catalyst using alloying strategies, where Au-based alloys, AuX (where X = Au, Pd, and Pt), were investigated in the search for one with higher selectivity for oxidation activities leading to FDCA production than one leading to degradation activities (which lead to high carbon loss); as a measure for hindering or retarding the degradation activities of the catalyst. In a VASP package, periodic DFT calculations were run with density-dependent dispersion correction (dDsC).

In the first part of our study, we looked at the conversion of furfural to furoic acid on Au(111). We found that when water was present on Au(111) and participated in the reaction, it was much more exothermic and beneficial than when it did not participate. It was also confirmed that the most energy-efficient way to start oxidation on Au (111) in the presence of water is through the C-H oxidation pathway (which leads to furan ketone, xFFO), followed by steps like oxidation of the xFFO intermediate (by forming a C-O bond with OH to make furoic acid, xFA), and furoic acid (FA) desorption. The research also confirms that breaking the O-H bond and making surface oxygen (O) from some catalyst supports are major threats to the degradation of the furfural intermediate and surface furoic acid species on an Au (111) slab. Based on the study's results, we think that redesigning the Au catalyst to help break C-H bonds, stop O-H bonds from breaking, and make it easier for furoic acid to get rid of itself would help

stop the degradation activities and increase the yield and selectivity for their desired reaction path and products. The presence of enough water to generate hydroxyl (xOH) for the elimination of surface oxygen atoms, the use of a base, or the selection of a catalyst support that does not generate oxygen (O) but hydroxyl (OH) during oxidation on Au would be more efficient. It would stop degradation promotion caused by some catalyst support reduction activities.

In the second study, we used the knowledge we had gained about the impact of water on Au(111) from the furfural oxidation study to constrain the study of HMF oxidation to take place in the presence of water. From this, the oxidation of water to yield hydroxyl (xOH) was found to be easy and exothermic. Moreover, the HMF oxidation route was confirmed to be via the aldehyde oxidation pathway (i.e., the HMFCA path). It also reveals that a slower rate of oxidizing alcohol function of HMFCA to the aldehyde in FFCA has led to a lower FDCA yield and a higher yield of HMFCA, which agrees with experimental reports. In our search for degradation sources., we established the infeasibility of ring opening and cracking holding around the aldehyde, hydroxyl, and acid functional groups due to their relatively high reaction energies obtained for their routes. Hydrogen abstraction from the furan rings was the primary route identified, promoting the degradation activities leading to the carbon losses reported in the experiment. Our study reveals that HMF is more prone to degradation than the HMFCA on Au(111), using Gibbs reaction energies, activation barriers, and the geometrical structures obtained for the analysis.

In the later study, our comparative analysis of the metals (Au, Pd, and Pt) in the oxidation of water to form hydroxyl (xOH) shows that it was not favorable for all the metals investigated, except for the use of Au(111), which shows exothermic reaction energy. So, it would be more energy-efficient for Pd(111) and Pt(111) to oxidize HMF without the participation of water. Further analysis of the HMF oxidation mechanism

over Pd(111) and Pt(111) reveals that the oxidation across the two metals was more favorable via the aldehyde oxidation route. Furthermore, it was confirmed that the step of oxidizing the alcohol function of HMFCA to the aldehyde function of xFFCA was the slowest step for both metals, which is in line with what has been found in experiments. In our exploration for a better strategy for redesigning the Au catalyst, we showed that alloying Pt with Au(111) significantly improves the selectivity of Au for HMF oxidation activity better than it does for HMFCA oxidation activity. In comparison, the introduction of Pd resulted in enhanced activity for the oxidation of HMFCA compared to HMF. Although, the intensity (or exergonicity) of the oxidizing HMF (on AuPt) is largely more significant than that of the HMFCA (on AuPd). The study suggests that Pt can be used to redesign the Au catalyst by alloying them to make a bimetallic (AuPt) alloy as a strategy for slowing down the rate of HMF degradation, as shown in Chapter 5 of our study. Alternatively, the combined use of Pt and Pd in redesigning the Au catalyst by alloying them to form trimetallic (AuPtPd) material can be considered. The strategy uses AuPt to slow down the breakdown of HMF and improve the selectivity of HMF oxidation activity, AuPd to make HMFCA oxidation activity better, and AuAu to slow down the breakdown of HMFCA.

7.2 Perspectives for Further Studies

The best way of deploying the use of the AuPt and AuPd collectively in the oxidation of HMF into FDCA can be explored. For purpose of understanding which of the following strategies presented in Figure 7-1 would be more effective for optimizing the FDCA yield with good process energy efficiency and economic viability. The first strategy is a process design with two reactors, a recovery unit (Sep) for unconverted HMF, and two pumps for maintaining pressure values. The second (one in the middle in Figure 7-1) has a process design similar with the first strategy except for the absence of recovery unit (Sep) and a pump. Whereas, the third strategy employs the

use of single reactor with two different catalyst bed, where the first bed was for the AuPt and second bed was for AuPd. The idea of having first bed in a single reactor (or first reactor bed in a two-reactors process) loaded with AuPt was because its facilitate oxidation of HMF to HMFCA and prevent degradation of HMF. In contrast, the AuPd facilitate the oxidation HMFCA into FDCA.

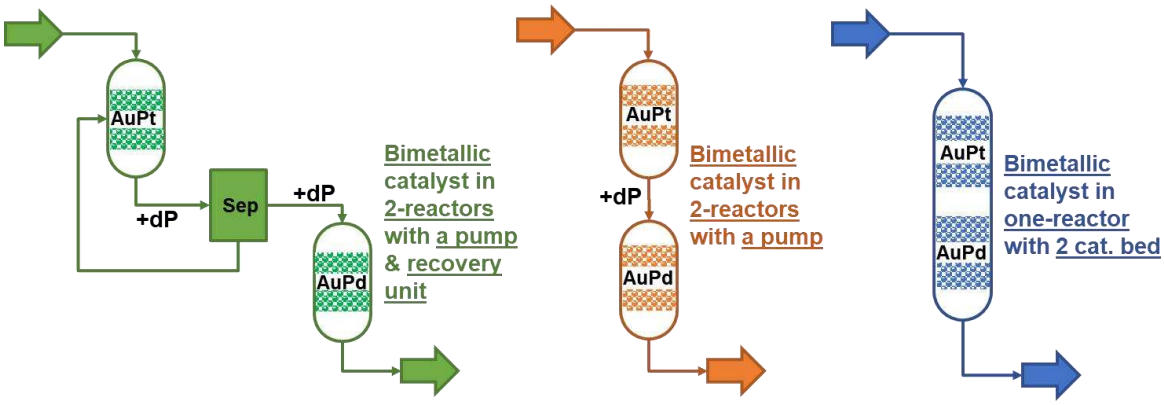

Figure 7-1 *Possible process design for a combined deployment of AuPt and AuPd in the oxidation of HMF to FDCA.*

Some existing experimental studies have shown that the catalyst support has, in some cases, influenced the surface reaction via the release of oxygen from the support structure, which often leads to leaching and some undesired side reactions (degradation). It was reported to occur on reducible support materials. More research can be done to understand how the reducible support influences the catalysis of the furfural and HMF oxidation, potentially providing a better way to avoid the undesired activity initiated by the reduction process in the catalyst support material.

The impact of solvent and coverage effects on the catalysis of the Au-based catalyst in the oxidation of furfural and HMF into FDCA can be considered in further studies, for the purpose of unraveling how they could influence the catalysis of selected metals, like Au, Pt, Pd, and many others.

To meet the growing market demand for FDCA, which is used to make different valuable materials, it is vital to find better materials for catalyzing the carboxylation of

furoic acid (as shown schematically in Figure 7-2) as an alternative source whose yield can be compared to that of HMF oxidation. A heterogeneous catalytic approach is under-explored in this process compared to other methods. These approaches include homogeneous catalysis using palladium chloride and enzymatic catalysis using *P. thermopropionicum* (PHmfF). Using the computational approach to gain insight into the impacts of heterogeneous catalysts in improving the production yield would be necessary.

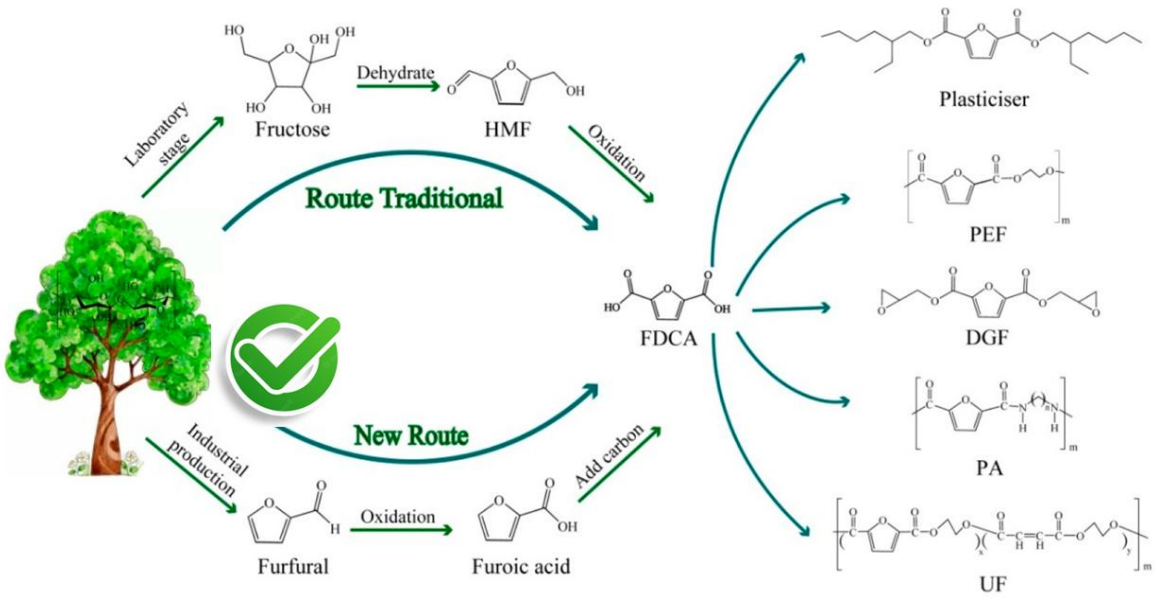

Figure 7-2 *A new route for FDCA production to consider in the further studies via the use of furfural.*

Exploration of all the reaction reaction barriers by micro-kinetic simulation in search of further insight into how reaction condition, catalyst loading, type of reactor, and species evolution (with changing independent variables like temperature, time, and others) affect the processes studied using DFT simulation would be essential. It would further help bridge some experimental results with the theoretical ones. We can have theoretical results in form-like product distribution, conversion, yield, selectivity, and turn-over-frequency (TOF) similar to the experiment, unlike other descriptors used in DFT simulation.

Abstract

(In English): Hydroxymethyl furfural (HMF) and furfural (FF) have been identified as key bio-refinery platforms for the synthesis of new materials. The conversion of these platform molecules into intermediates increasingly relies on heterogeneous catalysis rather than the enzymatic approach in recent years. One of these catalytic processes is the oxidation of HMF and FF to 2,5-furan dicarboxylic acid (FDCA) and furoic acid (FA), using O_2 as oxidant and supported gold catalysts. However, oxidation faces degradation challenges when using heterogeneous catalysts, leading to low yield and poor selectivity for FDCA and FA. In this thesis, we proposed a redesign strategy of the Au catalyst to retard the degradation activities reported in the oxidation of biomass derivatives (HMF and FF) on Au. Our study uses a theoretical approach based on the periodic density functional theory. First, we showed that the activation of O_2 when working in a liquid water environment is metal dependent: OH forms on Au, while O forms on Pt and Pd. Then, the oxidation and degradation pathways of HMF and FF on Au were identified by computing the stability of possible surface intermediates. This study shows that the alcohol function is more difficult to oxidize than the aldehyde function in HMF and this step is probably the rate-determining step. Regarding degradation, the furan ring's C-H is the most sensitive to oxidation compared with other routes examined. Analysis of the same reaction on Pt and Pd shows the mechanism to be the same, with greater stability of intermediates leading to higher activity but also higher degradation. Finally, the effect of alloying on Au catalysis was evaluated, showing that AuPd alloy improves the kinetics, while AuPt alloy improves HMF oxidation selectivity and delays degradation activity. Our study suggests alloying Pt and Au to retard HMF degradation, the main threat. Alternatively, alloying Pt and Pd with Au to form a trimetallic alloy would improve kinetics and retard HMF degradation.

Keywords / *Mots-clés*: Heterogeneous Catalysis, Reaction Engineering, Green Chemistry, Oxidation, Degradation, Selectivity.

Résumé

(In French): L'hydroxyméthyl furfural (HMF) et le furfural (FF) ont été identifiés comme des plateformes clés de bio-raffinage permettant la synthèse de nouveaux matériaux. La conversion de ces molécules plateformes en intermédiaires repose de plus en plus sur la catalyse hétérogène plutôt que l'approche enzymatique ces dernières années. L'un de ces procédés catalytiques est l'oxydation du HMF et du FF en acide 2,5-furane dicarboxylique (FDCA) et en acide furoïque (FA), en utilisant O_2 comme oxydant et des catalyseurs d'or supportés. Cependant, contrôler finement l'oxydation est difficile et ces procédés souffrent généralement de dégradation lors de l'utilisation de catalyseurs hétérogènes, conduisant à un faible rendement et une mauvaise sélectivité pour le FDCA et le FA. Dans cette thèse, nous cherchons à proposer une stratégie de reconception du catalyseur Au pour retarder les activités de dégradation rapportées dans l'oxydation des dérivés de la biomasse (HMF et FF) sur Au. Nous utilisons une approche théorique basée sur la théorie fonctionnelle de la densité périodique. Tout d'abord, nous avons montré que l'activation de O_2 lorsque l'on travaille dans un environnement d'eau liquide dépend du métal : OH se forme sur Au, tandis que O se forme sur Pt et Pd. Ensuite, les voies d'oxydation et de dégradation de HMF et FF sur Au ont été identifiées en calculant la stabilité des intermédiaires de surface possibles. Cette étude montre que la fonction alcool est plus difficile à oxyder que la fonction aldéhyde dans le HMF et cette étape est probablement l'étape cinétiquement déterminante. En ce qui concerne la dégradation, les liaisons C-H du cycle furane du HMF sont les plus sensibles à l'oxydation par rapport aux autres voies examinées. L'analyse de la même réaction sur Pt & Pd montre que le mécanisme est le même, avec une plus grande stabilité des intermédiaires conduisant à une plus grande activité mais aussi à une dégradation plus importante. Enfin, l'effet d'alliage sur la catalyse Au a été évalué, ce qui montre que l'alliage AuPd améliore la cinétique, tandis que l'alliage AuPt améliore la sélectivité de l'oxydation du HMF et retarde l'activité de dégradation. Notre étude suggère d'allier Pt et Au pour retarder la dégradation du HMF, la principale menace. Sinon, l'alliage de Pt et Pd avec Au pour former un alliage trimétallique améliorerait la cinétique et retarderait la dégradation du HMF.

Mots-clés: *Catalyse hétérogène, Ingénierie des réactions, Chimie verte, Oxydation, Dégradation, Sélectivité.*

Speciality / Spécialité:

Reaction Engineering, Computational Heterogeneous Catalysis and Theoretical Chemistry
Ingénierie de la Réaction, Catalyse Hétérogène Computationnelle et Chimie Théorique

Host Laboratory / Laboratoire D'accueil:

Laboratoire de Chimie - UMR 5672, ENS de Lyon - Universite de Lyon, France.

International Joint Supervision & Collaboration Partner Institution:

Ahmadu Bello University, PTDF Catalysis Research Centre, Chemical Engineering Department, Zaria, Nigeria.